TRANSACTIONS

Series A

Journal of ENGINEERING FOR POWER

October 1959

Divisions: POWER • GAS TURBINE POWER • NUCLEAR ENGINEERING • FUELS OIL AND GAS POWER • **Research Committees:** FURNACE PERFORMANCE FACTORS CORROSION AND DEPOSITS FROM COMBUSTION GASES • BOILER FEEDWATER STUDIES • HIGH TEMPERATURE STEAM GENERATION • CONDENSER TUBES PROPERTIES OF STEAM • **Committees on:** AIR POLLUTION CONTROLS • SOLAR ENERGY APPLICATION • **And:** POWER TEST CODES COMMITTEES

THE AMERICAN SOCIETY OF MECHANICAL ENGINEERS

TRANSACTIONS
OF THE ASME
Series A

EDITORIAL DEPARTMENT

OFFICERS OF THE ASME

PUBLICATIONS COMMITTEE

REGIONAL ADVISORY BOARD

Journal of
ENGINEERING FOR POWER

VOLUME 81 • SERIES A • NUMBER 4

October 1959

CONTENTS

361 **The Aerodynamic Approach to Furnace Design**
J. H. Chesters

371 **Use of Flow Models for Boiler-Furnace Design**
R. W. Curtis and L. E. Johnson

380 **Use of Models for Studying Pulverized-Coal Burner Performance**
G. C. Whitney

383 **Basic Principles of Combustion-Model Research**
A. A. Putnam and E. W. Ungar

389 **A New Performance Criterion for Steam-Turbine Regenerative Cycles**
J. Kenneth Salisbury

403 **Power Test Code Thermometer Wells**
J. W. Murdock

417 **Flow-Induced Noise in Heat Exchangers**
A. A. Putnam

423 **The Effect of Fuel Types and Admission Method Upon Combustion Efficiency**
H. N. McManus, Jr., W. E. Ibele, and T. E. Murphy

428 **Torsion of a Prismatical Bar Whose Section Is a Crescent**
F. Sisto

433 **The Transient Response of Gas-Turbine-Plant Heat Exchangers—Regenerators, Intercoolers, Precoolers, and Ducting**
A. L. London, F. R. Biancardi, and J. W. Mitchell

449 **Stresses in Hollow Cylinders Due to Asymmetrical Heat Generation**
Harry Kraus and George Sonnemann

TRANSACTIONS OF THE ASME
Series D

Journal of
BASIC ENGINEERING

Vol. 81 • Series D • No. 3

CONTENTS FOR SEPTEMBER, 1959

275 Static and Dynamic Control Characteristics of Flapper-Nozzle Valves, by T.-Y. Feng. (58—A-160)
285 Some Measurements of Boundary-Layer Growth in a Two-Dimensional Diffuser, by J. F. Norbury. (58—A-196)
297 The Skewed Boundary Layer, by E. S. Taylor. (58—A-113)
305 On the Nature of Stall, by S. J. Kline. (58—A-170)
321 Optimum Design of Straight-Walled Diffusers, by S. J. Kline, D. E. Abbott, and R. W. Fox. (58—A-137)
332 Labyrinth-Seal Leakage Analysis, by W. Zabriskie and B. Sternlicht. (58—A-118)
341 Centrifugal Manometer, by J. F. Kemp. (58—A-111)
349 The Aerodynamic Design of Two-Dimensional Turbine Cascades for Incompressible Flow With a High-Speed Computer, by H. N. Cantrell and J. E. Fowler. (58—A-141)
362 An Analysis of Axial Compressor Cascade Aerodynamics, Part I, by G. L. Mellor. (58—A-83)
379 An Analysis of Axial Compressor Cascade Aerodynamics, Part II, by G. L. Mellor. (58—A-84)
387 Loss and Stall Analysis of Compressor Cascades, by Seymour Lieblein. (58—A-91)
401 Stall Prediction in Gas-Turbine Engines, by R. J. Lubick and L. E. Wallner. (58—A-133)
409 A Survey of Stall Propagation—Experiment and Theory, by H. W. Emmons, R. E. Kronauer, and J. A. Rockett. (58—A-150)
417 Modulation Phenomena in Stall Propagation, by J. A. Rockett. (58—A-152)
426 Studies of Jet Compression—I, Apparatus and Methods. Results With Air at Room Temperature, by H. J. Hoge, S. S. Eichacker, and D. L. Fiske. (58—SA-13)

TRANSACTIONS OF THE ASME
Series E

Journal of
APPLIED MECHANICS

Vol. 81 • Series E • No. 3

CONTENTS FOR SEPTEMBER, 1959

TECHNICAL PAPERS

319 On Supersonic Wind Tunnels With Low Free-Stream Disturbances, M. V. Morkovin. (59—APM-10)
325 Velocity and Temperature Fluctuation Measurements in a Turbulent Boundary Layer, D. S. Johnson. (58—A-81)
337 Density Variation Effects in Stepped-Thrust Bearings, C. F. Kettleborough. (59—APM-19)
341 Response of a Nonlinear String to Random Loading, T. K. Caughey. (59—APMW-4)
345 Response to Van Der Pol's Oscillator to Random Excitation, T. K. Caughey. (59—APMW-5)
349 A Perturbation Solution of the Equations of Motion of a Gyroscope, Robert Goodstein. (59—A-5)
353 Vibration of Beam-Mass Systems With Time-Dependent Boundary Conditions, T. C. Yen and S. Kao. (59—APM-22)
357 Dynamic Loading Tests of an Aircraft-Type Beam, E. A. Ripperger and W. R. Barton
367 Viscous Damping in Flexural Vibrations of Bars, M. K. Newman. (59—APMW-8)
377 Natural Modes and Their Stability in Two-Degree-of-Freedom Systems, R. M. Rosenberg and C. P. Atkinson. (58—A-57)
386 On Finite Bending of Pressurized Tubes, Eric Reissner. (59—APM-5)
393 Instability and Folding Deformation of a Viscoelastic Medium in Compression, M. A. Biot. (59—APMW-21)
401 Stress Distribution in Semi-Infinite Strip Subjected to Concentrated Load, P. S. Theocaris. (59—APM-17)
407 Postbuckling Behavior of Rectangular Plates With Small Initial Curvature, Noboru Yamaki. (58—A-59)
415 New Theory of Elastic Sandwich Plates—One-Dimensional Case, Yi-Yuan Yu. (59—APM-23)
422 On Invariant Perforation in an Infinite Strip, Chih-Bing Ling. (59—APM-20)
432 Thermal Stresses in Moderately Thick Elastic Plates, B. E. Gatewood. (59—APM-7)
437 Analysis of Plane Stress in Polar Co-ordinates, H. D. Conway. (59—APM-1)
440 The Stress Function of a Radial Strain, F. Goded. (59—APM-25)
442 Determination of Safe Loads of Beams Subjected to Twisting and Bending Moments, P. G. Hodge, Jr., and R. Sankaranarayanan. (59—APM-26)

DESIGN DATA AND METHODS

448 Factors of Stress Concentration Due to Elliptical Fillets, M. M. Frocht and D. Landsberg.

BRIEF NOTES

451 Creep of Elastic Belt on a Pulley, G. V. Tordion. 452 Modification of Rayleigh's Principle for Calculating Beam Frequencies, F. M. Lewis. 454 Yield Point Load of an Annular Plate, P. G. Hodge, Jr. 455 Analysis of Indeterminate Structures by Displacement Method, P. H. Denke and C. K. Wang. 456 Internal Damping of Thermal Origin in Thin Wires, P. Srinivasan. 457 Lateral Buckling of Tapered Narrow Beam, L. H. N. Lee. 458 Stresses in Infinite Wedges Tapered in Width and Thickness, H. D. Conway. 460 Minimization of Spring Torque, T. Vreeland, Jr. 461 Steady-State Response of Linear Vibration Systems, M. E. Gurtin. 462 Further Understanding of Shakedown Theorems, Melvin Zaid. 462 Series Solution for Ellipsoidal Shells, Robert Schmidt.

DISCUSSION

465 Discussion of previously published papers by E. L. Reiss; G. N. Hatsopoulos and J. H. Keenan; F. A. McClintock; F. M. White, B. F. Barfield, and M. J. Goglia; M. M. Abbassi; Eli Sternberg and W. T. Koiter; M. J. Schilhansl

BOOK REVIEWS

475

TRANSACTIONS OF THE ASME
Series B

Journal of
ENGINEERING FOR INDUSTRY
Volume 81 • Series B • Number 3

CONTENTS FOR AUGUST, 1959

187 Factors Influencing the Performance of Grinding Wheels, by E. J. Krabacher. (58—SA-40)
201 Vibrations of Flexible Precision Grinding Spindles, by R. S. Hahn. (58—A-97)
207 The Effect of Process Variables on Extrusion Pressures of Lead, by J. Frisch and E. G. Thomsen. (58—A-109)
217 Approximate Solutions to a Problem of Press Forging, by S. Kobayashi and E. G. Thomsen. (58—A-140)
228 Theory and Experiment of Press Forging Axisymmetric Parts of Aluminum and Lead, by S. Kobayashi, R. Herzog, J. T. Lapsley, Jr., and E. G. Thomsen. (58—A-154)
239 A Three-Dimensional, Tool-Life Equation—Machining Economics, by B. N. Colding. (58—A-123)
251 Some Observations on the Shearing Process in Metal Cutting, by S. Kobayashi and E. G. Thomsen. (58—A-139)
263 Observations on the Angle Relationships in Metal Cutting, by D. M. Eggleston, R. Herzog, and E. G. Thomsen. (58—A-138)

TRANSACTIONS OF THE ASME
Series C

Journal of
HEAT TRANSFER
Vol. 81 • Series C • No. 3

CONTENTS FOR AUGUST, 1959

175 Heat Transfer Between Concentric Rotating Cylinders, by I. S. Bjorklund and W. M. Kays. (58—A-99)
187 Full-Scale Human-Body-Model Thermal Exchange Compared With Equational Condensation of Human Calorimetric Data, by L. P. Herrington. (58—A-181)
195 The Emissivity and Absorptivity of Parachute Fabrics, by J. P. Hartnett, E. R. G. Eckert, and R. Birkebak. (58—A-125)
202 An Experimental and Analytical Study of Vortex-Flow Temperature Separation by Superposition of Spiral and Axial Flows—Part 1, by J. E. Lay. (58—SA-71)
213 An Experimental and Analytical Study of Vortex-Flow Temperature Separation by Superposition of Spiral and Axial Flows—Part 2, by J. E. Lay. (58—A-90)
223 Analysis of the Aerodynamic Heating for a Re-Entrant Space Vehicle, by M. J. Brunner. (59—Av-5)
230 A Photographic Study of Boiling in the Absence of Gravity, by R. Siegel and C. Usiskin. (59—Av-37)
237 Some Radiator Design Criteria for Space Vehicles, by J. P. Callinan and W. P. Berggren. (59—Av-29)
245 Optimization of a Conventional-Fuel-Fired Thermoelectric Generator, by B. W. Swanson and E. V. Somers. (59—SA-14)

Technical Briefs

249 Heat Transfer From a Rotating Disk to Fluids of Any Prandtl Number, by E. M. Sparrow and J. L. Gregg.
251 An Approximate Treatment of Unsteady Heat Conduction in Semi-Infinite Solids With Variable Thermal Properties, by K.-T. Yang and Albin Szewczyk.

The Aerodynamic Approach to Furnace Design

J. H. CHESTERS

Assistant Director of Research, The United Steel Companies, Ltd., Research and Development Department, Swinden Laboratories, Moorgate, Rotherham, Yorkshire, England

Flow patterns and mixing in actual furnaces can be best appreciated by starting with free jets and proceeding via jets in simple envelopes to jets (cold or alight) fed with surrounding air streams and impacting on surfaces. The fuel stream in an open-hearth furnace behaves initially as a free jet, entraining the relatively low velocity air around it, but on hitting the bath it splashes and runs forward and up the side walls. The gases reaching the roof eject flux droplets and then divide, part recirculating to meet the oncoming air and part joining the main flow to the exit. Future progress requires more knowledge of droplet dynamics, and demands more symmetrical flow, control of recirculation, or radical changes.

Introduction

It was not until 1945 that a systematic study was begun of flow patterns in models and furnaces and their relation to mixing, flux deposition, temperature distribution, and refractory wear. The story of the early developments has been told in a paper on "The Growth of an Idea" [1],[1] whose main object was to show that rapid progress can best be achieved by wholehearted co-operation, which in turn demands willingness to give generously of information without guarantee of return. It was also stressed that long-term studies demand a fundamental approach, since otherwise even such an elementary thing as recirculation remains unexplained and, therefore, uncontrolled.

During the last decade a large number of research groups have started work in this field and a substantial literature is now available. Whereas the initial hope was to get a rough idea of furnace conditions from models, it has been shown that given sound similarity, data quantitatively applicable to actual furnaces can be obtained. This can be illustrated by recent publications on open-hearth [2] and reheating furnaces [3]. The similarity conditions are by no means simple, but the general relationships, as summarized for example by Johnstone and Thring [4], are now fairly well established.

Flow Pattern

Furnaces are basically refractory boxes into which streams of fuel are injected. A first essential to understanding flow pattern and mixing in such systems is, therefore, a study of the behavior of free jets in air.

(a) Free Jets. A great deal has been written on this subject and each paper tends to modify earlier conclusions. The essential features, however, have been set out by several authors, e.g., Hinze and Van Der Hegge Zijnen [5], who studied "the radial and axial distribution of time-mean values of velocity, temperature, and gas concentration in a turbulent jet issuing from a round orifice into quiescent ambient air." They found that, for distances greater than 8-orifice-diameters downstream, the shape of the jet was that of a cone, whose origin was an infinitely small aperture located a fraction of a diameter upstream from the orifice. The general picture, including the normal or Gaussian type distribution curves for the various cross sections, is illustrated in Fig. 1.

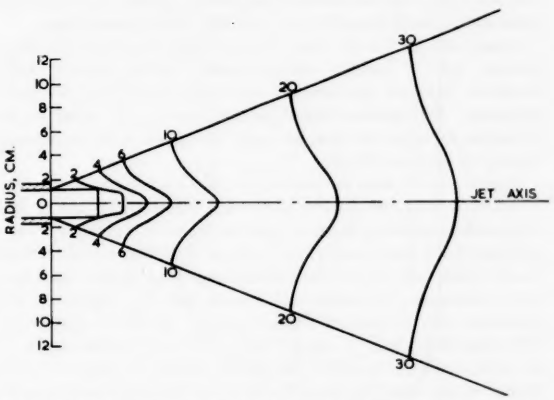

Fig. 1 Radial velocity distribution in free jet. (After Taylor, Grimmett, and Comings.)

Hinze and Zijnen [5] found that the velocity U_m at a distance x from the orifice was given by

$$\frac{U_m}{U_0}\,\frac{x + 0.6d}{d} = 6.39 \qquad (1)$$

It will be noted that this brings in a correction of $0.6d$ for the shift in the apparent origin. Similar formulas have been given by Taylor, Grimmett, and Comings [6], and also by Squire [7], the constants obtained varying somewhat with the assumptions made.

The radial distribution of velocity is given by Hinze and Zijnen [5], as

$$\frac{U}{U_m} = \frac{1}{(1 + \eta^2/8a_0)^2} \qquad (2)$$

[1] Numbers in brackets designate References at the end of paper.

Contributed by the Research Committee on Furnace Performance Factors and presented at the Annual Meeting, November 30–December 5, 1958, New York, N. Y., of The American Society of Mechanical Engineers.

Note: Statements and opinions advanced in papers are to be understood as individual expressions of their authors and not those of the Society. Manuscript received at ASME Headquarters, July 10, 1958. Paper No. 58—A-72.

Nomenclature

x = distance along axis from orifice
y = radial distance from the jet axis
a = distance of apparent jet origin from orifice
$\eta = y/x + a$
d or d_0 = nozzle diameter
U_m = velocity on jet axis
U = velocity at a point off axis
U_0 = velocity at nozzle
L = axial deflection of jet
T_0 = initial temperature of jet fluid
T_a = temperature of surrounding gas
C_m = jet fluid concentration
a_0, K_1, and K_2 = constants

which describes a Gaussian distribution. If the experimental value for a_0, viz., 0.00196, is introduced, this becomes

$$\frac{U}{U_m} = \frac{1}{(1 + 64\eta^2)^2} \tag{3}$$

It will be seen from Fig. 1 that a portion of the jet profile remains uniform for a certain distance from the nozzle—this is the "potential core," in which the velocity remains equal to the discharge velocity.

The definition and measurement of jet angle are difficult and as a result there are great variations in the figures quoted. One of the devices introduced to give precision is that of the half-jet angle, defined as that at which the velocity on a given profile is equal to one half the velocity on the jet axis. Incidentally the jet angle as computed from concentration or temperature profiles is greater than that computed from velocity profiles, showing that mass and temperature diffuse more rapidly than momentum.

Keagy and Weller [8] give data for freely expanding inhomogeneous jets of helium, nitrogen, and carbon dioxide, shot vertically into air through a sharp-edged orifice of 0.128-in. diameter. The cross-sectional profiles were again found to be Gaussian in type but the jet angle increased with decreasing density of the nozzle fluid.

Where jets are fired horizontally, or have a horizontal velocity component, and the density of the jet differs from that of the surrounding medium, account must be taken of buoyancy. Furnacemen have long known that a flame shot into a cold furnace tends to lift, but that as the surroundings heat up the buoyancy effect decreases. It is also well known that the amount of lift increases with decreasing flame velocity. A recent survey by Gray and Robertson [9] shows that the axial deflection L varies inversely with the square of the initial velocity U_0 and is related to the initial temperature of the jet T_0 and that of the surrounding gas T_a by the following equation:

$$L \propto \frac{x^2}{U_0^2 d_0}, \frac{T_0 - T_a}{T_a} \tag{4}$$

In open-hearth furnaces operating at top temperature, where T_0 would be replaced by flame temperature, and with high-velocity jets, e.g., steam-atomized oil, $T_0 - T_a$ is so small and U_0^2 so large that the deflection is negligible. With low velocities, however, the buoyancy lift may be quite significant. For example, in a reheating furnace with a 6-in-diam port, the lift at a distance of 15 ft from the port, with initial velocities of 50 and 25 ft per sec, was found to be about 8 in. and 32 in., respectively.

(b) Jets in Boxes. The combustion chamber in many furnaces can be considered as being essentially of shoe-box shape, with given length-breadth-height ratios. The location of the flame varies greatly, but the simplest case would be that of a flame fired centrally and normal to one face. A first impression of the flow pattern in such a system can be gained by means of two-dimensional models. Thus a square section chamber, fired through one face, could be represented by the pattern shown in Fig. 2(*a*), and one fired diagonally by the pattern shown in Fig. 2(*b*). Even a preliminary examination of such patterns—obtained by sprinkling bakelite dust on water in a shallow tray—reveals certain main characteristics. Thus with central firing the jet proceeds across the square until it hits the opposite side, most of the high-speed flow thereafter being on the walls. It is further observed that flow with this design may well be asymmetrical, tending toward one side or the other according to the precise conditions existing at the moment. In contrast diagonal injection [Fig. 2(*b*)] yields a stable and symmetrical pattern. With both arrangements the entrainment at the root of the jet can be clearly seen, together with relatively dead areas on either side of the main jet. Experimentation suggests that the flow pattern in solid shapes

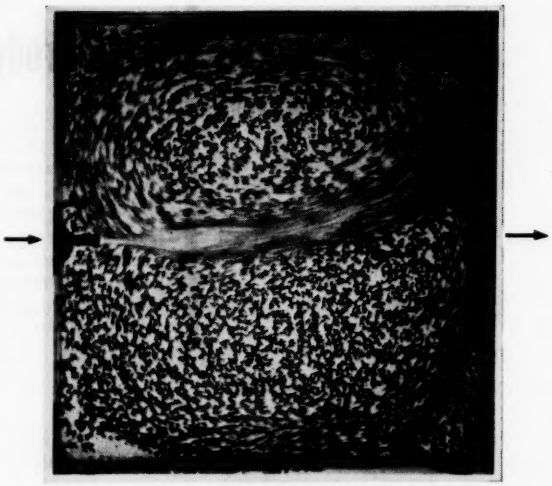

(a) Jet through center of side

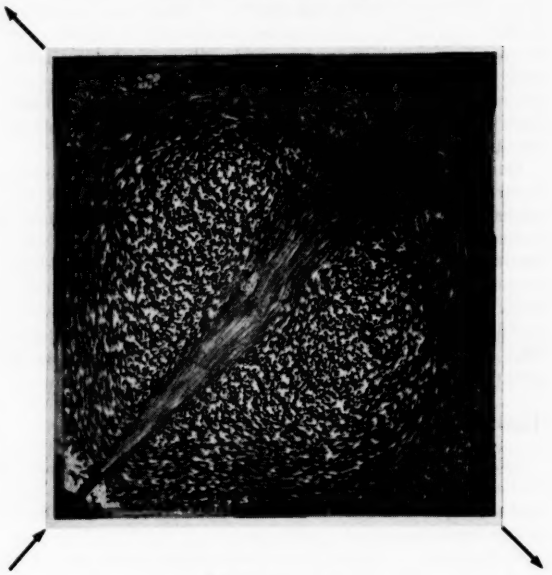

(b) Jet diagonally

Fig. 2 Flow pattern in square. Entry and exit points shown by arrows.

formed by revolution of the two-dimensional pattern, or by sideways translation of it, can be predicted with fair reliability from the two-dimensional data. Thus Fig. 2(*b*) if extended sideways might represent the combustion chamber of a corner-fired boiler having only one row of flames in operation, while rotation about the jet axis would show the pattern expected in a double cone-type vessel fired through one apex. A number of solids of revolution, based on two-dimensional studies already reported [10], have been tested as water models, while the cone obtained by a rotating triangle, has been examined not only as a water model but in the form of a conical brick box fired through the apex with an actual flame. The conclusion from this and subsequent experience supports the suggestion that flow pattern predictions from two and three-dimensional water models are applicable to actual furnaces.

Particularly interesting to the furnace operator is the result ob-

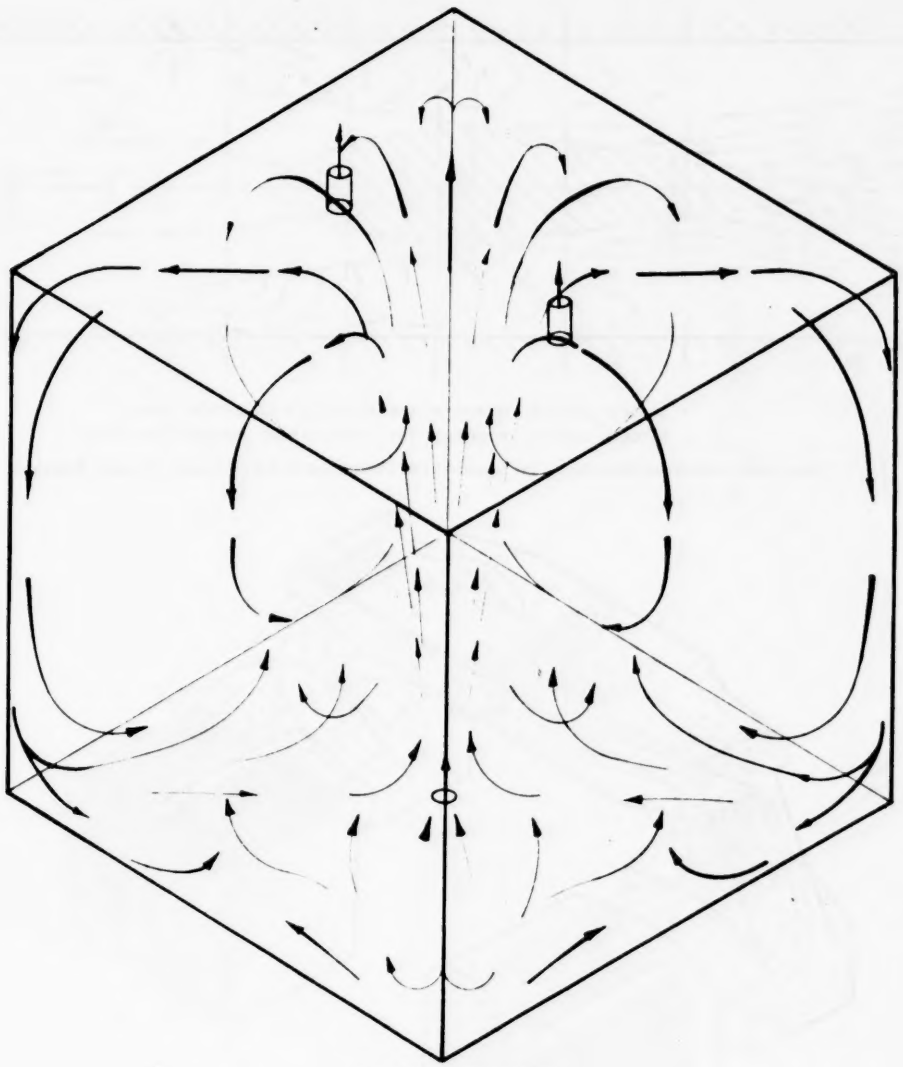

Fig. 3 Flow pattern in cube

tained when a jet is fired normally through the center of one face of a cube (see Fig. 3). It will be seen that the initial stream takes the form of a cone which impacts on the opposite wall and then spreads out in all directions. The recirculation motivated by entrainment at the root of the jet tends to be greatest at the four edges parallel to the jet, presumably because these are furthest from it and, therefore, less subject to drag. On reaching the face from which the jet emerged, the flow again spreads out over the end wall and this time divides itself into four fairly distinct quarters prior to being entrained. This peculiarly geometrical partition can be clearly seen if tracer particles, e.g., polystyrene, are introduced and the flow pattern at a distance of, say, 1 in in front of the orifice made visible by means of a sheet of light. This pattern for the cube approaches fairly closely the basic pattern observed in many furnaces, the latter being a variant of it, due to such changes as elongation of the tunnel or asymmetry of the jet. The type of flow found in an elongated box, in which the jet is fired horizontally, is well known to those who have studied the flame research at Ijmuiden (see Fig. 4).

An important generalization from flow pattern studies is that once a high speed flame hits the wall of the chamber the remainder of the fast flow tends to be on the walls—a particularly unfortunate condition for the refractories, which are thus subjected to worse than average conditions both of temperature and flux concentration.

(c) Furnace Models. The difference between the shoe-box discussed earlier and the simplest design of open-hearth furnace lies essentially in

a) the inclination of the jet toward the base, and
b) the air entry and waste-gas exit conditions.

If a jet is shot parallel to the base and spread out to impact on it, the splash pattern consists of a drawn-out streak, the flow at the surface being virtually all in a forward direction. If on the other hand the jet hits a surface perpendicularly, the splash pattern is radial, the flow proceeding outward equally in all directions. In actual open-hearth furnaces, the angle between the jet and the liquid surface of the bath usually lies between 10 and 20 deg.

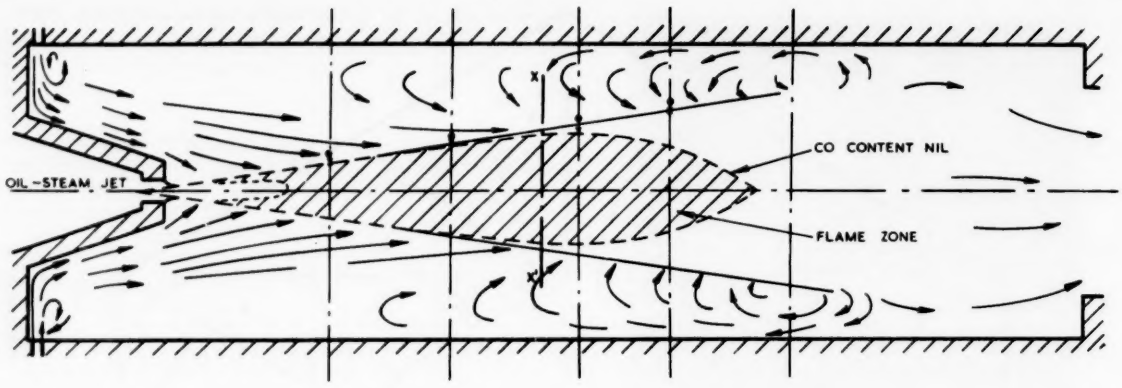
CO CONTENT NIL
OIL-STEAM JET
FLAME ZONE
x SUDDEN CHANGE POINTS IN THE O2 & CO2 DISTRIBUTION CURVES.
• SUDDEN CHANGE POINTS IN THE TEMPERATURE DISTRIBUTION CURVES.

Fig. 4 Flow pattern in Ijmuiden flame tunnel (as reported by R. Durand and G. Cohen de Lara, Neyrpric, Grenoble)

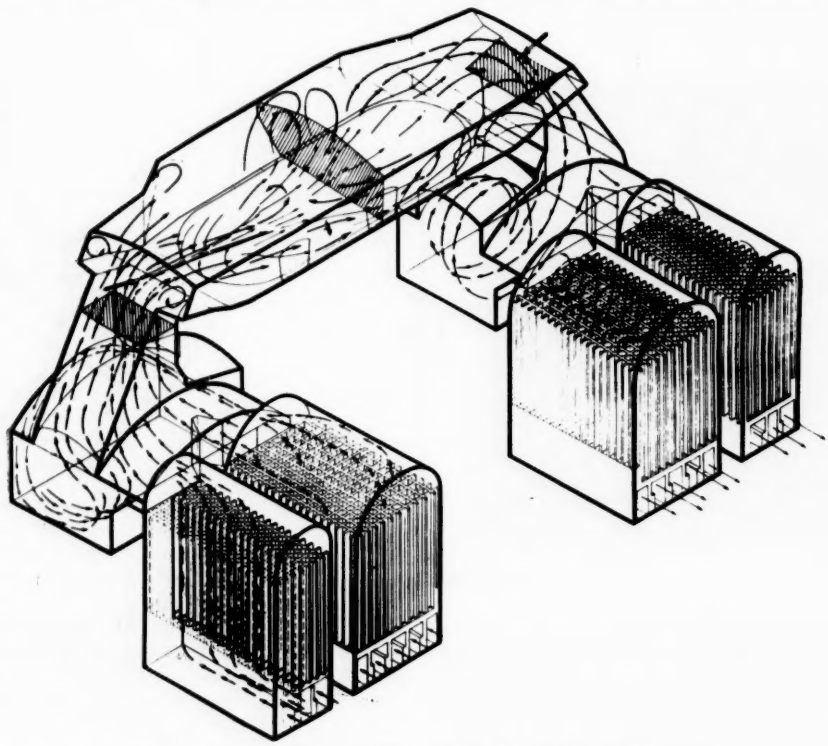

Fig. 5 Isometric sketch of flow pattern in model of single-uptake furnace

The result is an intermediate splash pattern, the fastest flow being forward, the slowest flow backward, and an intermediate but substantial amount sideways. This sideways component increases with the angle of impact and results, with a box-type structure, in run up the back and front walls and subsequent impact on the roof. In such a system the basic flow pattern (Fig. 5) shows a division of flow after impact with the roof, the part nearest the incoming end tending to return beneath the roof toward the root of the jet, while that further away continues in the same general direction below the roof, finally joining the main exit stream.

In the simplest designs the air enters the furnace vertically upward through a slot at the incoming end, whose axis is perpendicular to the length of the furnace. The waste gases leave by a similar slot at the other end. The incoming air streams past the burner barrel, or narrow part of the flame, to impact on the roof and then run along it, generally to a point about one third along the furnace length. At this stage it meets the recirculating return flow and turns downward to be entrained by the jet stream. If, therefore, a plot is made, either in a water model or an actual furnace, of flow conditions beneath the roof, it will be found that in the first and last thirds of the roof it is generally forward,

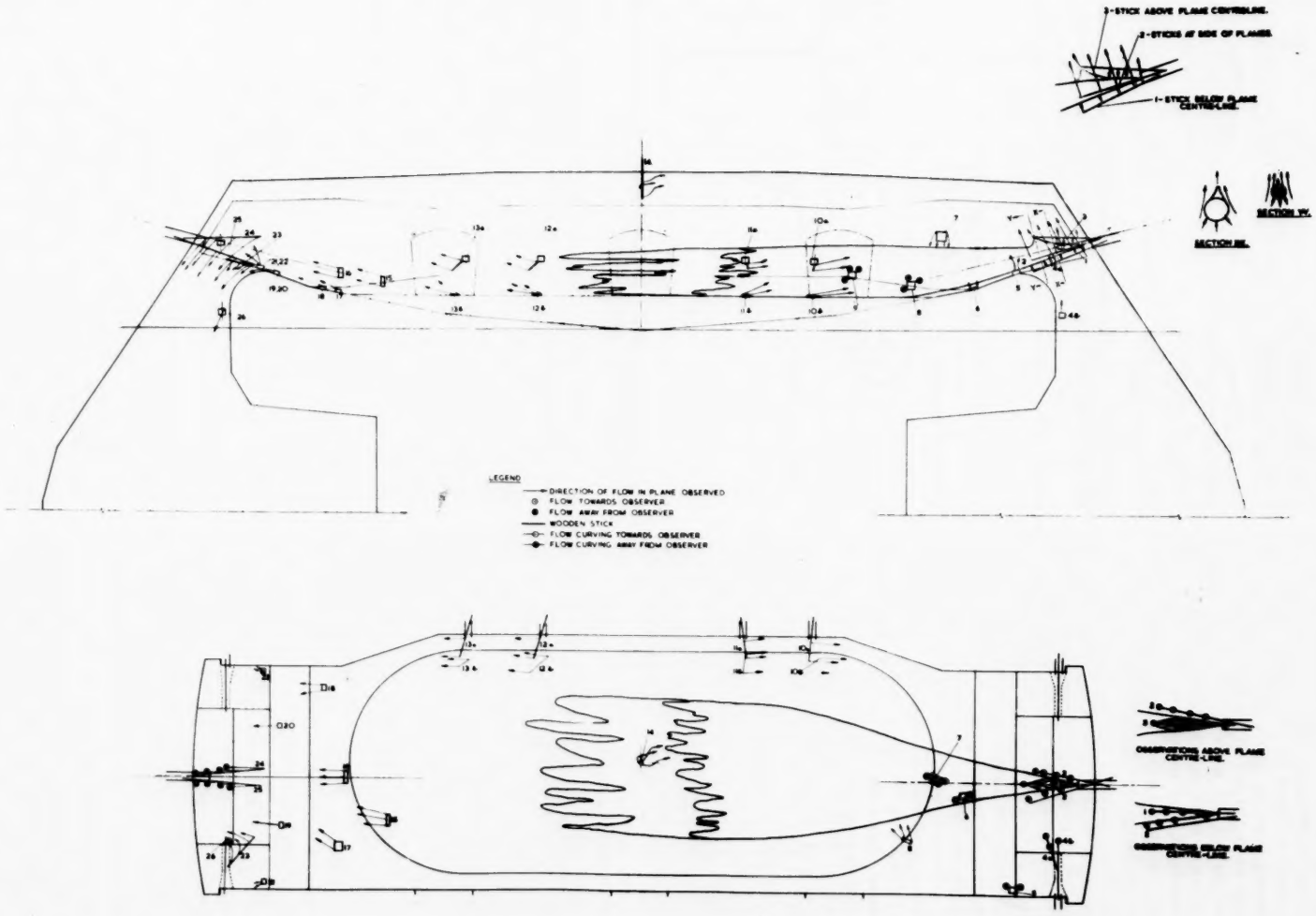

COMPOSITE PLOT OF FLOW PATTERN OBSERVATIONS, K FURNACE, TEMPLEBOROUGH, (JULY 1950.)

Fig. 6 Flow pattern of actual single-uptake furnace, for comparison with Fig. 5

while in the central third it proceeds in a reverse direction to that of the flame proper. The precise pattern is of course influenced by many variables, e.g., jet thrust, and entry and exit conditions. As will be seen later increasing the ratio of momentum in the air stream with respect to that of the fuel, tends to suppress recirculation and should, therefore, reduce return flow beneath the roof. Similarly the amount of run up the walls, which tends to be inclined toward the exit end, increases with the steepness of burner angle. Where an actual furnace rather than a symbolic design is being considered, a precise water model is built in Perspex, generally at 1/24th actual scale The conditions that must be obeyed to give similarity have been discussed fairly fully in earlier papers [3*b*, 11].

Study of a considerable number of such designs, including those of single, double, and even triple uptake furnaces, shows a remarkable similarity in general flow pattern, though numerous differences in detail. A change from single to double burners, for example, results in twin splash patterns on the bath and in a widely variable amount of run up the walls, depending on the inclination between the two burners. With single burner furnaces flow asymmetry is frequently marked even where the chamber itself is completely symmetrical, but considerable improvement can be obtained by displacing the burner toward the front wall.

(d) Actual Furnaces. Space does not permit detailed discussion of the intermediate stage, viz., hot models. Strange though it may seem, it is more difficult to achieve similarity between the hot models and working furnaces than between the latter and cold models. The explanation of this observation is far from simple but is connected, for example, with the fact that both cold models and actual furnaces tend to work at substantially uniform temperature, whereas far bigger differences are often found in hot models, due both to the large weight of brickwork compared with the size, and the fact that one-way firing tends to result in a comparatively cold entry end unless very hot preheated air is available.

(*i*) *Open-hearth furnace above stage level.*

Numerous cross checks have now been made between models and furnaces, both of flow pattern in general and of flow conditions at particular points. The most detailed is probably still that reported in 1951 [12] for a sloping-ended single-uptake furnace. This latter was probably the first furnace ever to be designed aerodynamically on the basis of a model and it was, therefore, particularly encouraging to find that the flow pattern (Fig. 6), as determined by means of wooden rods, or pieces of wood inserted in steel tubes, was in close agreement with that predicted. The principal objective with this design was the protection of the roof by impacting on to it, at less than the normal right-angle, a fast stream of clean air. The roof lives obtained, including a shop record, suggested that this objective was achieved, though the particular design was subsequently abandoned in favor of one more easily built and maintained. The latest comparison was published in Iron and Steel Special Report No. 59 [2*a*], which, although primarily concerned with combustion and heat transfer, also includes comparisons of flow pattern and mixing pattern in model and furnace. Both this investigation and studies by other workers confirmed beyond doubt the existence in actual furnaces of the substantial recirculation observed in both air and water models of open-hearth furnaces.

(*ii*) *Open-hearth furnace below stage level.*

An excellent comparison of flow conditions in model and furnace has recently been reported by Jones and Brion [13] of the Bethlehem Steel Company. Their report starts with a comparison of flow in downtakes, where the velocity contours—as measured by pitot tubes—are remarkably similar, showing not only a similar distribution but also similar absolute values. Still more

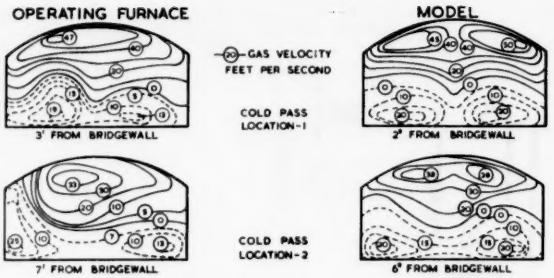

Fig. 7 Waste-gas velocity pattern in cold pass "gas chamber." (After R. J. Jones and D. F. Brion.)

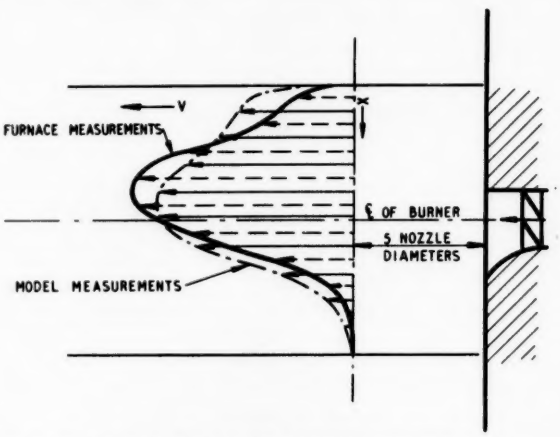

Fig. 8 Velocity distribution from turbulent burner—comparison of model and plant scale data. (After H. Boenecke.)

surprising in the agreement obtained (Fig. 7) between the operating furnace and model in the fantail and hot pass of the "gas chamber." That such checks are not absolute is hardly surprising, since absolute similarity is not even theoretically possible. They are, however, so good that if the cause of a particular condition in a furnace is acceptable in terms of model observations, and changes can be made in the model to improve matters, such modifications can be confidently recommended for the actual furnace—a vital fact in view of the large sums of money frequently involved. Work of this type has led to aerodynamics being now an everyday tool in many steelworks, and responsible for many changes that would never have been made in the absence of such techniques. Thus excessive wear in uptakes has often been tackled in the past by increasing the cross-sectional area, but aerodynamic studies suggest, and experience tends to confirm, that *average* velocities may have little connection with wear—a shift outward of the end wall merely resulting in wear at a lower and less accessible position.

(*iii*) *Soaking pits and reheating furnaces.*

Several workers are now applying aerodynamics in this field, our own studies having been recently reviewed by Gray and Robertson [3*a*]. More recently Boenecke [14] has described his work on cyclone burners in soaking pits. These include detailed comparisons between velocity traverses made in air models, soaking pits operated cold, and soaking pits at full temperature, the extent of agreement achieved (Fig. 8) being most encouraging. Encouraged by the success of such work Boenecke has gone on to compare static pressure measurements taken along a two-zone reheating furnace, with similar measurements made in a particu-

larly elegant air model. The degree of agreement was again found to be most encouraging.

(*iv*) *Glass tank furnaces.*

Kruszewski, et al., in two recent papers [15*a*, *b*] described the results of model work on glass tank furnaces, but unfortunately did not provide many data on operating units. It is, however, encouraging to see that the areas of wear found with full-scale glass tanks are those that might have been predicted from the flow pattern studies.

Mixing

(a) Free Jets. It has been shown that a relation exists between the reciprocal of the concentration of the jet fluid $1/C_m$ and the diameter of the nozzle d_0 and the distance x from it, that is similar in character to that controlling velocity. The relation can be expressed as

$$\frac{1}{C_m} = K_1 \cdot \frac{x}{d_0} + K_2 \qquad (5)$$

Sunavala, Hulse, and Thring [16] found values of 0.22 and -1.5 for the constants K_1 and K_2, respectively, but point out that with a similar equation derived from the work of Hinze and Zijnen [5] the corresponding constants were $K_1 = 0.19$ and $K_2 = +0.15$. These equations refer to the general slope of the curve and not the section immediately in front of the orifice. The fact that Forstall and Gaylord [17] obtained similar results with jets of water in water may be reassuring to those who still find it difficult to believe that the flow of gases in furnaces can be simulated by means of water models.

(b) Jets in Boxes. Hulse, McInerney, and Sarker [2*a*] have shown that when a free jet hits a plane the rate of mixing decreases immediately and quite substantially. On the other hand, the passage of a free jet over a rising air stream, as experienced in single-uptake open-hearth furnaces, makes little difference to mixing rate. Similar effects were observed in an air model of an actual furnace, but here it was found that the mixing rate was further decreased on impact, due presumably to the presence of the side walls and roof. Most encouraging is the observation that the mixing rate, as observed in an actual open-hearth furnace, is very similar to that predicted from air model studies.

Still more recently Cohen de Lara and Curtet [18] have reported their work at Grenoble on recirculation in square and round tunnels, and compare their results with those obtained previously by Thring and Newby [11]. They show that it is possible to predict from theory—both qualitatively and quantitatively—the extent of recirculation in circular tunnels, and arrive at the extremely interesting conclusion that it is controlled by the relative momenta in the central "fuel" jet and the surrounding "air." This conclusion may ultimately have a marked effect on furnace design since it suggests that, for example, decreasing uptake size for a given air flow might well reduce recirculation and therefore the damage to refractories.

(c) and (d) Furnace Models and Actual Furnaces. The most complete comparison so far reported is that given in Iron and Steel Institute Special Report 59 [2*a*], where air models, using hot air as the jet fluid, were employed to study the effect of such factors as burner angle and position on mixing pattern. It was shown, for example, that even where the furnace chamber itself is symmetrical the mixing pattern may be strongly asymmetrical, due to uneven velocity distribution within the air uptake. Although this limitation should ultimately be removed by attention to entry conditions, it has been shown that much improved symmetry can be achieved meantime by displacing the single burner toward the front wall or inclining it a few degrees in the same direction.

Another important conclusion from this work was that recirculation is quite substantial, being of the order of 50 per cent of the forward flow. In view of this it may well prove to have an important effect on heat transfer. A comparison of mixing on the flame axis shows it to be somewhat less in the furnace than in the model under the similarity conditions in use at the time. Since this work was reported, a more detailed study has been made by Holden [2*b*], in which improved similarity criteria are recommended. Another aspect of the problem, viz., dwell time, has been studied by Peirce and Thring [19], in this case for pulverized fuel boilers.

In spite of the progress reported, much remains to be done, in particular the relation between flow and mixing patterns must be tied up more specifically than at present with heat transfer along and across the furnace. A substantial step in this direction has already been made by Thring and Smith [20], their theory having been applied with quite encouraging results in comparing actual and theoretical heat transfer in an open-hearth furnace [2*a*]. It is already proving of practical value in the selection of variables for future trials, enabling, as it does, the probable gain from such radically different factors as oxygenation and increased oil-flow rate to be predicted.

Flux Deposition

Even with the best available design, the combustion chamber of an open-hearth furnace has a life of only three to six months if driven at an economic rate. The cost of maintaining the structure runs at about three dollars per ton of steel made—a substantial proportion of the total conversion figure. This, together with the effect on furnace availability, makes the minimization of refractory wear a major objective of aerodynamic design. Although a knowledge of flow and mixing patterns provides a useful start, a third major factor, viz., flux deposition, must be considered. Unfortunately droplet (or particle) dynamics falls in an underdeveloped country, only approximate answers being available to most of the questions the furnace designer would like to ask. It can, however, be stated as a result of a preliminary examination of the literature [21], including certain recent reports of the National Advisory Committee for Aeronautics [22] and a limited number of experiments of our own, that the deposition of iron oxide droplets on furnace walls, tends to increase with:

a) The concentration of droplets in the gas stream;

(Pitch-creosote firing leads to greater fume concentration than oil firing and also to heavier droplet deposition and refractory wear.)

b) The coarseness of the fume;

(The droplet size is known to vary over a wide range—from $^1/_2$ mm to an aerosol.)

c) The velocity of the gas stream and the droplets carried by it;

(This may explain in part the improvement reported by increasing roof height, which in turn will tend to reduce the velocity of the recirculating gases.)

d) Decreasing radius of turn.

(This explains the heavy wear observed at right-angle bends, e.g., at the top of the back and front walls and the entry to the downtakes. It also suggests the general desirability of "streamlining.")

More quantitative and directly applicable data being required, an attempt is being made to obtain them by means of a small wind tunnel, in which droplets can be injected. Although this work is still at an early stage, it can be stated from such studies, and from more extensive work done with sintered alumina probes pushed through holes in roofs [23*a*, *b*], that many surprises are in store. From these are arising new ideas as to how flux deposition and therefore wear can be reduced. It has, for example, been

shown that iron oxide deposition on silica roofs varies from zero up to more than 1 lb per sq ft per hr, and that the high-deposition regions are also the regions of worst wear, though other factors, such as temperature and the presence of reducing gases, clearly affect the issue. Strangely enough the wear on basic brick roofs also appears to be a function of iron oxide pickup, even though the mechanism of failure is by slabbing rather than gradual solution.

Until more is known about the origin and size distribution of iron oxide droplets in furnaces, model studies are liable to be misleading, but even at the present stage useful information is being collected in models having a sticky interior surface and using aluminum dust, balsa dust, or polystyrene particles, to simulate iron-oxide droplets. With large tilting furnace models [2*a*], the best checks have been obtained using sulfur dioxide as a tracer, the gas being liberated from the bath surface to simulate fume rising from the charge. The rate of arrival of this gas at the roof surface was measured by means of filter papers dipped in starch iodate solution, which turn brown and then purple as sulfur dioxide is absorbed.

That more fundamental data are needed has been demonstrated by recent studies on the use of moving air curtains for the protection of refractories [24]. Both laboratory and furnace tests showed that fine fume and coarse droplets impacting at right-angles and at a speed of about 12 ft per sec on a moving air curtain of up to 100 ft per sec, can penetrate it quite readily—the fume by eddy diffusion and the droplets by virtue of their inertia. Although it has been shown that such devices can be employed to protect critical positions in the refractory structure, a great deal more work is required before such techniques can be fully applied.

Future Developments

The greatest need would appear to be a design specification. In the absence of this the following objectives are put forward with a view to promoting discussion:

(*i*) *The achievement of symmetrical flow and mixing within the furnace chamber.*

Conditions in most single burner furnaces are far from symmetrical and could well be improved by changes in entry conditions and burner position. Similar improvements could be achieved with twin-burner furnaces, which possess the additional advantage of improving bath coverage and therefore, it is assumed, heat transfer.

(*ii*) *The control of recirculation.*

Opinion in British furnace design circles is hardening in favor of reducing recirculation, both because it leads to refractory wear and because it is thought to reduce heat transfer. It is hoped to obtain quantitative data on the latter point by means of hot models deliberately modified to encourage and discourage recirculation. Another alternative would appear to be the use of multiple burners, which demand less total momentum for a given flame length.

(*iii*) *Radical changes in design.*

Although numerous attempts to break away from the design originally conceived by Siemens have failed, due, for example, to instability of flow pattern [24], the pressure from rival processes, and in particular pneumatic methods based on tonnage oxygen and large arc furnaces, may well lead to radical changes, such as have, for example, been suggested by Glinkov [25], who recently described a furnace fired simultaneously from both ends and arranged for continuous withdrawal of waste gases followed by recuperation. The more radical the change from existing design, the greater will be the need for a preliminary study of the aerodynamics if excessive wear or poor heat transfer is to be avoided.

Acknowledgments

In conclusion I should like to express my thanks to The United Steel Companies Limited, and particularly to Mr. F. H. Saniter, Director of Research, for permission to publish this paper. I should also like to thank my colleagues in the department, particularly those in the Furnace Design and Fuel Sections, who have been responsible for much of the work described.

References

1 J. H. Chesters, "The Growth of an Idea—Illustrated by Research on Flow Patterns in Open-Hearth Furnaces," *Iron and Coal Trades Review*, vol. 166, 1953, pp. 179–187.

2*a* S. W. Pearson, M. W. Thring, and J. H. Chesters, "Combustion and Heat Transfer in an Open-Hearth Furnace," Iron and Steel Institute Special Report No. 59, 1956.

b A. Hogg, C. Holden, and R. G. Siddall, "The Use of Aerodynamic Models in the Study of Industrial Furnaces," Seventh International Symposium on Combustion, Oxford, England, 1958 (in press).

3*a* F. A. Gray and A. D. Robertson, "The Investigation of Fluid Flow Problems by Model Techniques," *Journal of The Institute of Fuel*, vol. 29, no. 189, 1956, pp. 428–436.

b N. P. Bacon, "Experiments With Furnace Models," Proceedings of the Joint Symposium on Scaling-Up of Chemical Plant and Processes, London, England, 1957, pp. S99–S108.

4 R. E. Johnstone and M. W. Thring, "Pilot Plants, Models, and Scale-up Methods in Chemical Engineering," McGraw-Hill Series in Chemical Engineering, 1957.

5 J. O. Hinze and B. G. Van Der Hegge Zijnen, "Transfer of Heat and Matter in the Turbulent Mixing Zone of an Axially Symmetrical Jet," *Applied Science Research*, vol. **A1**, 1948, pp. 435–461.

6 J. F. Taylor, H. L. Grimmett, and E. W. Comings, "Isothermal Free Jets of Air Mixing With Air," *Chemical Engineering Progress*, vol. 47, no. 4, 1951, pp. 175–180.

7 H. B. Squire, "Jet Flow and Its Effects on Aircraft," *Aircraft Engineering*, vol. 22, 1950, pp. 62–67.

8 W. R. Keagy and A. E. Weller, "A Study of Freely Expanding Inhomogeneous Jets," Symposium on Heat Transfer and Fluid Mechanics Institute, Berkeley, Calif., June, 1949, p. 89.

9 F. A. Gray and A. D. Robertson, "Deflection of Hot Jets Due to Buoyancy," *Journal of The Institute of Fuel*, vol. 29, no. 189, 1956, pp. 424–427.

10 J. H. Chesters and A. R. Philip, "Open-Hearth Furnace Models—Part I, Flow Patterns in Ducts," *Journal of The Iron and Steel Institute*, vol. 162, 1949, pp. 385–391.

11 M. W. Thring and M. P. Newby, "Combustion Length of Enclosed Turbulent Jet Flames," Fourth Symposium (International) on Combustion, The Williams & Wilkins Co., Baltimore, Md., 1953, pp. 789–796.

12 J. H. Chesters, "Flow Patterns in Open-Hearth Furnaces," *Open Hearth Proceedings, AIME*, vol. 34, 1951, pp. 282–310.

13 R. H. Jones and D. F. Brion, "Gas Flow in an Open Hearth Model," AIME Conference, New York, N. Y., February, 1958 (in press).

14 H. Boenecke, "Flow Pattern and Model Studies on Industrial Gas Burners," VDI Colloquium on Flow and Combustion in Freudenstadt, October, 1957, preprint.

15*a* H. R. S. Jack, S. Kruszewski, and D. A. Richardson, "Combustion and Heat Transfer in Glass Tanks," Joint Conference on Combustion, ASME and IME, Boston, Mass, June, 1955, and London, England, October, 1955.

b S. Kruszewski, "Application of New Techniques in the Design of Furnaces," Third International Congress on Glass, Venice, Italy, 1953.

16 P. D. Sunavala, C. Hulse, and M. W. Thring, "Mixing and Combustion in Free and Enclosed Turbulent Jet Diffusion Flames," *Combustion and Flame*, vol. 1, no. 2, 1957, p. 179.

17 W. Forstall and E. W. Gaylord, "Momentum and Mass Transfer in a Submerged Water Jet," *Journal of Applied Mechanics*, vol. 22, TRANS. ASME, vol. 77, 1955, pp. 161–164.

18 G. Cohen de Lara and R. Curtet, "The Study of Recirculation in Diffusion Flame Furnace Models," Third Conference on Flames, Paris, France, February, 1958, preprint.

19 T. J. Peirce and M. W. Thring, "Distribution of Residence

Times in a Model of a Pulverized Fuel Boiler," Institute of Fuel, Conference on Pulverized Fuel, Paper No. 3, November, 1957.

20 M. W. Thring and D. Smith, "An Improved Model for the Calculation of Heat Transfer in the Open Hearth Furnace," *Journal of The Iron and Steel Institute*, vol. 179, part 3, 1955, pp. 227–230.

21*a* M. Glauert, "A Method of Constructing the Paths of Raindrops of Different Diameters Moving in the Neighbourhood of (1) a Circular Cylinder, (2) An Aerofoil Placed in a Uniform Stream of Air, and a Determination of the Rate of Deposit of the Drops on the Surface and the Percentage of Drops Caught," Aeronautical Research Committee Reports and Memoranda No. 2025, 1940.

b C. N. Davies, "The Sedimentation of Small Suspended Particles," The Institution of Chemical Engineers and the Society of Chemical Industry, Road and Building Materials Group, Symposium on Particle Size Analysis, Supplement to *Trans. Institution of Chemical Engineers*, vol. 25, 1947, pp. 25–39.

c P. H. Gregory, "The Deposition of Airborne Particles on Trap Surfaces," *Nature*, vol. 166, serial no. 4220, 1950, p. 487.

d P. G. W. Hawksley, "The Physics of Particle Size Measurement, Part I—Fluid Dynamics and the Stokes Diameter," The British Coal Utilisation Research Association, *Monthly Bulletin*, vol. 15, no. 4, 1951.

e H. Chilton, "Catching Droplets and Particles: Methods of Separation From Gas Streams," *Times Science Review*, No. 9, Autumn, 1953, pp. 17–18.

f K. Stewart, "The Condensation of a Vapour to an Assembly of Droplets or Particles," *Trans. Faraday Society*, vol. 52, part 2, February, 1956, pp. 161–173.

22*a* R. J. Brun and H. W. Mergler, "Impingement of Water Droplets on a Cylinder in an Incompressible Flow Field and Evaluation of Rotating Multicylinder Method for Measurement of Droplet-Size Distribution, Volume-Median Droplet Size, and Liquid-Water Content in Clouds," NACA TN 2904, 1953.

b P. T. Hacker, R. J. Brun, and B. Boyd, "Impingement of Droplets in 90° Elbows With Potential Flow," NACA TN 2999, 1953.

c R. J. Brun and R. G. Dorsch, "Impingement of Water Droplets on an Ellipsoid With Fineness Ratio 10 in Axysymmetric Flow," NACA TN 3147, 1954.

d P. T. Hacker, P. G. Saper, and C. F. Kadow, "Impingement of Droplets in 60° Elbows With Potential Flow," NACA TN 3770, 1956.

e J. P. Lewis and R. S. Ruggeri, "Experimental Droplet Impingement on Four Bodies of Revolution," NACA TN 4092, 1957.

23*a* M. J. McInerney, "Iron-Oxide Deposition in Open-Hearth Furnaces" (Letter to the Editor), *Journal of The Iron and Steel Institute*, vol. 179, part 3, 1955, p. 248.

b J. H. Chesters, "The Climate of the Open-Hearth Furnace," *Iron and Steel*, vol. 30, no. 3, 1957, pp. 87–93 and 125–129.

24 J. H. Chesters, C. Holden, and A. D. Robertson, "Protection of Refractories by Moving Air Curtains," *Journal of The Iron and Steel Institute*, vol. 185, part 2, 1957, pp. 177–200.

25 M. A. Glinkov and G. I. Demin, "Russian Recirculatory Steelmaking Furnace," Russian Symposium on Use of Oxygen in Metallurgy, Moscow, U.S.S.R., 1957. State Publishing House for Scientific Literature on the Ferrous and Light Metal Industries.

DISCUSSION

M. A. Mayers[2]

The papers by Dr. Chesters and Mr. Abbott represent a revival of interest in a tool which has been available, but has been largely neglected in combustion developments.

The usefulness of this kind of investigation is brought home to me by the example quoted by Dr. Chesters of the stabilization of the double vortex produced on either side of a jet entering a plenum on a diameter. During World War II, I was engaged in the development of a gas turbine combustor.[3] The first prototype produced such a stable vortex pair, but subsequent versions, in many cases, showed the type of alternating instability which the author described in Fig. 2(*b*). We were unable to learn how to stabilize the vortex pair, although the advantages in decreased combustion volume and improved cleanness were very great. The author's results, if they had been available, would have shown one way, ndd suggested several others, by which we might have accomplished this objective.

I wish to take issue with the author on the desirability of eliminating recirculation. I believe my disagreement with him arises from a difference in application. In the combustor development mentioned, we found that it was essential to establish a high and stable rate of recirculation. Only by this means can the rapid ignition necessary for high volume rates of combustion be obtained.

Another purpose for which we may hope model techniques may be used is to develop the control of ash flow and deposits in power boilers. Mr. E. G. Bailey used to say that our combustion problems in power boilers were not properly problems in combustion, but of ash disposal. This technique may provide a better means than we have had before of investigating and controlling the flow and deposition of ash and slag in such boilers.

K. C. McCutcheon[4]

The use of properly designed cold or hot models in design of, or improving the design of, furnaces in this country is not common practice. It is coming into more general use in Great Britain and on the Continent. A great deal of it is done in connection with the work of the International Flame Research Committee.

The author has given a good résumé of the work which has been reported on some of the work that has been done. He points out that there is a lot of money spent on furnace repairs that can be saved by eliminating wear by improved design.

What he did not mention, although he knows it, is that, by correcting faulty design, it will also be possible to increase over-all production rate, and decrease fuel consumption. There is more money to be saved.

Doing the work with models can also save money, and accomplish results more quickly. In most plants the operators and masonry men are continually changing slopes, areas, wall thicknesses, burners, and the like, in order to improve conditions. This is expensive and too often is not followed up, and mistakes are repeated. Work properly done on a model can quickly determine what has a chance of success in a furnace.

The author is describing a modern technique which should be used more often. The practice is one which could readily be done in outside research laboratories. There is need for more work on the plant aspects of the problem, as well as on the fundamentals.

I want to congratulate the author for a very interesting paper, and recommend it for study to fuel men, operators, and design engineers, to the end that the practice be adopted and put into general use.

Author's Closure

I would agree with Mr. Mayers that whether recirculation is desirable depends on the particular application. In jet-engine flame tubes it is undoubtedly useful, because the recirculating gases promote rapid evaporation of the cold oil droplets injected into a relatively cold container. With the open-hearth furnace the brickwork temperatures are so high that, to quote a jet-engine designer, the oil would burn even if put in with a hose. Furthermore flame stability is rarely a problem with open-hearth furnaces. Considerable thought has been given by a number of research workers in Great Britain to the possible effects of recirculation and there is an increasingly strong opinion not only that it is responsible for much of the damage to roofs but that it tends to lower flame temperature and therefore heat transfer. We hope to check these suggestions on hot models (approx. $^1/_5$th full scale) in the near future, using designs in which recirculation is first encouraged and then discouraged.

We believe that model techniques will eventually tell us a good deal about droplet or particle deposition, but work in this field is likely to be mainly qualitative until the laws of drop dynamics

[2] Sanderson & Porter Engineers, New York, N. Y. Mem. ASME.

[3] M. A. Mayers and W. W. Carter, "The Elbow Combustion Chamber," TRANS. ASME, vol. 68, 1946, pp. 391–398.

[4] Consultant, Armco Steel Corporation, Ashland, Ky.

are better understood. This field is one in which co-operative effort might advantageously be extended, the possibilities of application ranging from disease propagation by sneezing to furnace design and gas cleaning.

I am glad that Mr. McCutcheon raised the faster driving issue, for it is here that our work in aerodynamics is paying its biggest dividend. Recent trials have shown the possibility of operating furnaces at 33 per cent faster rates than normal without appreciable increase in refractories costs and a potential decrease in fuel consumption per ton. If the open-hearth furnace is to remain competitive with large arc furnaces and the new oxygen steelmaking processes, it must be driven faster and the possibility of doing so economically depends in the main on improvements in aerodynamic design and refractories. So far most of this work has been concerned with the above-stage part of the open-hearth furnace, but as driving rates increase regenerator capacity often proves inadequate. Aerodynamic studies have already shown the possibility of improvements in gas flow distribution, both on the air and waste gas cycles, with increases of as much as 50 deg C (90 F) in the air preheat levels. In conclusion it might be said that the relevance of aerodynamic research to furnace design no longer requires proof. What is necessary is its systematic application both to old and new designs.

R. W. CURTIS

Research Engineer,
The Babcock & Wilcox Company,
Research Center, Alliance, Ohio

L. E. JOHNSON

Test Engineer,
The Babcock & Wilcox Company,
Research Center, Alliance, Ohio

Use of Flow Models for Boiler-Furnace Design

This paper discusses, from a practical viewpoint, the use of scale models to study flow-distribution problems encountered in the design of boiler furnaces. Some of the types of models used by the authors' company and the methods of testing each type are described. A brief discussion of model design is presented. An example of how flow models were used to aid in the design of the furnace arrangement for a specific unit is described.

Much of the work in boiler and furnace design concerns the determination of the shape and size of ducts, pipes, and enclosures that will produce efficient flow of air, gases, and fluid fuels to and through the system. It is now well recognized that the flow-distribution patterns of furnace gases affect the efficiency of combustion, the heat transfer to furnace surface, the amount and location of furnace and superheater fouling, and the rate of deterioration of furnace and superheater surface due to corrosion, erosion, wastage, and so on. Except for simple configurations, the prediction of these flow patterns is impractical or impossible by ordinary analytical methods and, even though it might be possible to write differential equations for certain flow conditions, it is not always possible to solve them. The use of scale flow models is an excellent method for solving flow problems.

A considerable amount of literature is available on the general theory and design of models, and a number of articles have been written concerning the use of models to solve specific problems. Relatively few of these, however, relate specifically to furnace design. This paper deals primarily with the use of models by the authors' company to solve flow problems encountered in boiler-furnace design. It includes a description of the types of models used, methods of testing each type, the particular advantages and applications of each type, and, as a specific example, the use made of models in establishing the furnace arrangement for the first commercial supercritical-pressure steam generator now installed and operating at the Philo Plant of the Ohio Power Company.

Types of Models

The many types of flow models may be classified in several ways: According to the working fluid, such as air, water, or gas, or according to the geometry, such as two dimensional or three dimensional. Gas models may be classified according to temperature, such as cold (room temperature), hot (prototype operating temperature), and warm (somewhere between room temperature and prototype operating temperature). Water models may be either open-channel or closed. A specific model can be a combination of these various classifications, such as a two-dimensional, open-channel water model, or a three-dimensional, warm-gas model, and so on. The type of model chosen will depend on the type of unit to be tested and the kind of information that is desired.

Two-Dimensional, Open-Channel Water Models. To obtain a quick, qualitative, visual analysis of the flow pattern in any unit where flow is essentially the same in parallel adjacent planes, a two-dimensional, open-channel water model is used, Fig. 1. This type of model is usually made of clear plastic to facilitate visual observation. It is essentially a shallow open tray in the shape of a side, plan, or front section of the prototype, depending on the principal direction of flow. The scale is usually in the range of $^1/_{64}$ to $^1/_{12}$ of the full-size unit (corresponding to the drawing scales of $^3/_{16}$ in. to 1 in. per ft). Water flows through the model by gravity, the depth being maintained by a perforated-plate closure at the exit. To make the flow pattern visible, the model is illuminated from below by fluorescent lights through opal glass, and a tracer is added to the water.

This tracer may be in the form of a dye added continuously in one or more small streams or in a single pulse, or it may be in the form of solid particles, such as ground black pepper, sprinkled on the surface of the water. To obtain permanent records of the flow pattern, movies are taken of the model while the dye is being added; or still pictures, when a solid tracer is used. On the still pictures the particles photograph as streaks which show the location of eddies and the areas of high and low velocities, Fig. 2.

The advantages of this type of model are that it is inexpensive and easy to build and that testing is relatively simple and quick. Its disadvantages are that results are qualitative only and that flow in only two dimensions is indicated. In some cases, the fact that velocities are limited may reduce the Reynolds number so that dynamic similarity to the prototype is not maintained.

Two-Dimensional, Closed Water Model. This type of model is used when quantitative results are desired. Fig. 3. It is similar to the open-channel model except that a cover is placed on the model and water is added under pressure to increase the velocity and

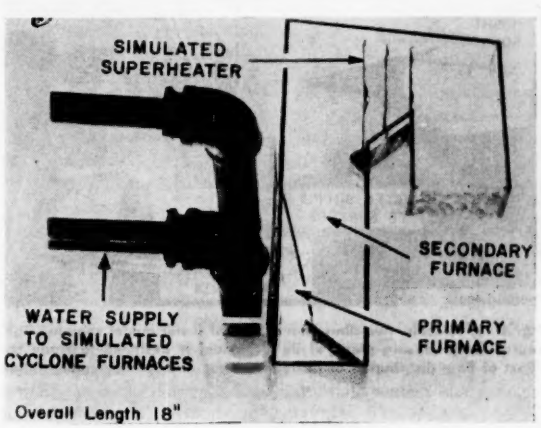

Fig. 1 1/48-scale, two-dimensional, open-channel water model representing side section of a cyclone-fired boiler

Contributed by the Research Committee on Furnace Performance Factors and presented at the Annual Meeting, New York, N. Y., November 30–December 5, 1958, of The American Society of Mechanical Engineers.

Note: Statements and opinions advanced in papers are to be understood as individual expressions of their authors and not those of the Society. Manuscript received at ASME Headquarters, August 1, 1958. Paper No. 58—A-120.

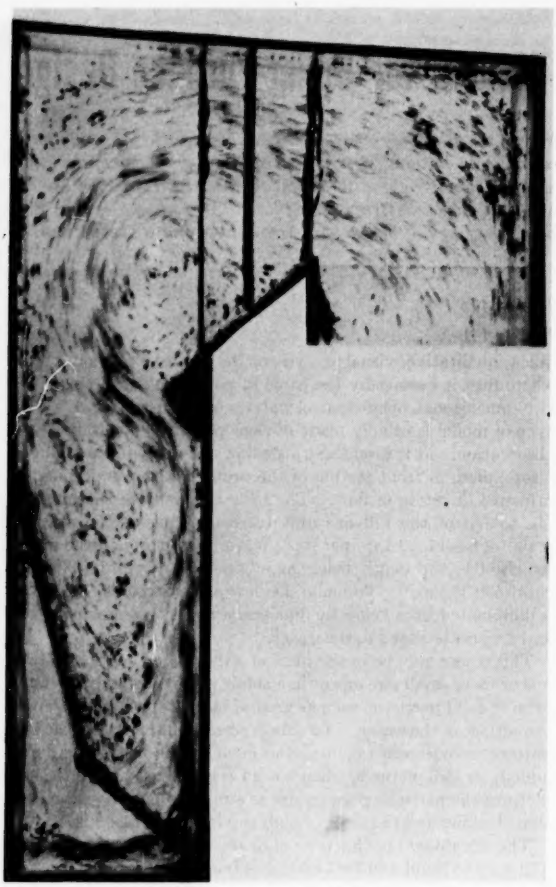

Fig. 2 Flow tracer pattern produced in the model shown in Fig. 1

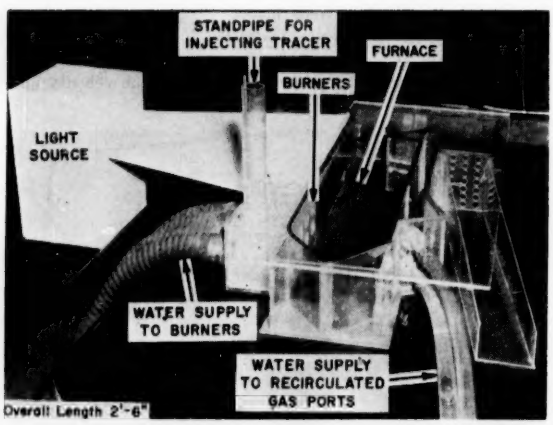

Fig. 3 1/48-scale, two-dimensional, closed water model showing light source for producing plane of light. Model is designed to study the effect of flow distribution of recirculated gas and furnace configuration

Fig. 4 Flow traces produced in the upper portion of the furnace of the model shown in Fig. 3

thus improve dynamic similarity. To obtain accurate quantitative measurements of flow patterns, a probe is used to determine velocity vectors.

Approximate quantitative analyses of the flow distribution may be obtained by adding to the water flowing through the model a solid granular tracer having a specific gravity of 1.00, and illuminating the model with a plane of light at the plane in which it is desired to determine the flow pattern. If a still picture is taken, the particles entering the illuminated plane will show as streaks which indicate the magnitude and direction of the velocity vectors, Fig. 4.

Visual analysis of the flow pattern also may be accomplished by introducing tracers such as dye or particles. The results obtained by this method are often of greater value than quantitative results because a visualization of the flow distribution through the entire unit may be realized instead of measured values in localized areas.

Three-Dimensional Water Models. To determine the complete flow pattern, three-dimensional water models are used, Fig. 5. This type of model is built so that all three dimensions are to

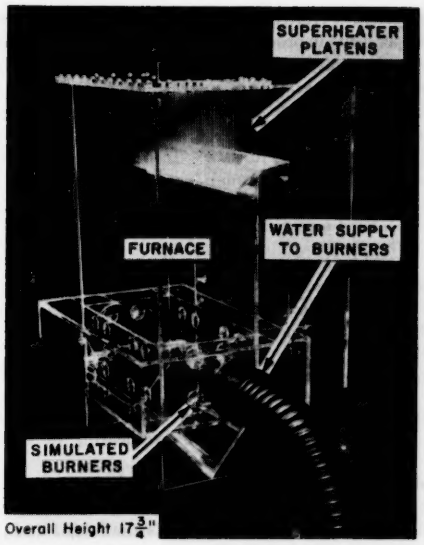

Fig. 5 1/48-scale, three-dimensional, water model of oil and gas-fired boiler

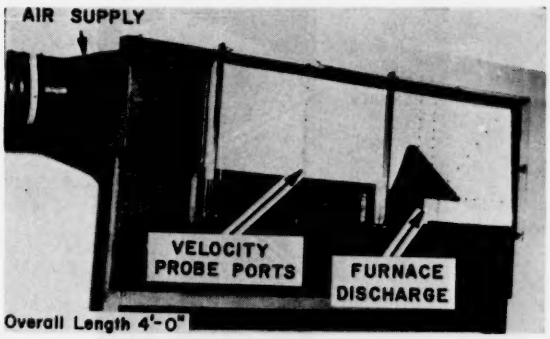

Fig. 6 Two-dimensional air model used to study effect of upper furnace configuration on flow distribution

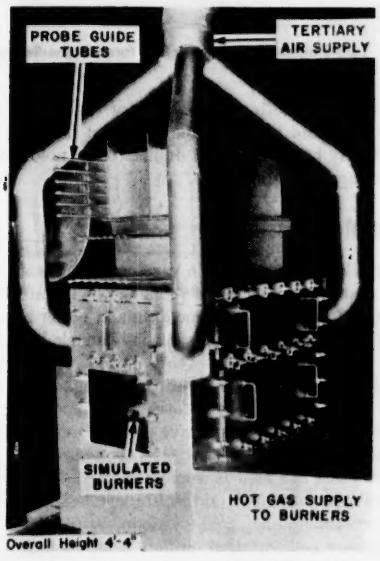

Fig. 7 Three-dimensional warm-gas model used to check furnace-gas flow distribution and mixing of tertiary air in a new design of boiler

scale (usually in the range of $1/64$ to $1/12$). It is usually made of clear plastic to facilitate visual analysis. Flow patterns can be determined by means of a velocity probe.

Models of this type are also used to study mixing of two or more streams of fluids. A concentrated brine (NaCl) solution is added to one of the streams to increase the electrical conductivity of the water to about 10 times its normal value. Samples of water are collected from the location in the model at which it is desired to determine the extent of mixing. The electrical conductivity of the sample will indicate the amount of brine it contains, and this in turn is used to evaluate the mixing effectiveness up to that location.

Air Models. Cold air models are sometimes used to obtain quantitative measurements of flow distribution; two-dimensional models to obtain flow in two dimensions; and three-dimensional models where fully three-dimensional patterns are required. Models of this type may be built of wood except for one side which is covered with transparent plastic. The side opposite the plastic is provided with ports through which velocity probes can be inserted at locations where it is desired to take measurements. A two-dimensional air model is shown on Fig. 6. A modified Fecheimer tube [1][1] is used to determine the direction and magnitude of the velocity at the desired points. In some instances an approximate quantitative measure of distribution of furnace residence time has been obtained by taking a large number of velocity readings.

Gas Models. Warm, three-dimensional gas models are used to obtain accurate quantitative measurements of flow distribution and to study problems of mixing such as that encountered in the use of recirculated gas (often referred to as "tempering gas") to temper the gases entering the superheater. These models are built of steel plate in the size range of $1/24$ to $1/8$ scale, Fig. 7. Air at room temperature is used to simulate the recirculated gas. The main gas stream is in the temperature range of 800 to 1200 F, the temperature being selected so that the density ratio of recirculated gas to furnace gas in the model is the same as would be encountered in the prototype. At several locations provisions are made for inserting a velocity probe to determine flow distribution, and a temperature probe to determine mixing effectiveness.

Model Design

Generally speaking, for accurate results, models should have both geometric and dynamic similarity. In some cases a meticulously close conformity of model and prototype is necessary. However, in the case of furnace models we have found that this is not required and, in cases where combustion takes place in the prototype furnace, it is impossible to attain without having heat release in the model. In these cases compensation for lack of combustion and the accompanying expansion of gases may be obtained by making the burner larger than the scale of the rest of the furnace [2]. In practice, a velocity traverse is taken at the discharge of a full-size operating burner, and a simulated burner that will produce the same flow pattern is installed in the model.

Investigators have shown that flow patterns, mixing, and dynamic pressure losses are essentially independent of Reynolds number above a value of about 10,000 [3]. Therefore, as long as the flow is well up in the turbulent-flow region, the Reynolds number on the model can be considerably less than in the prototype

[1] Numbers in brackets designate References at end of paper.

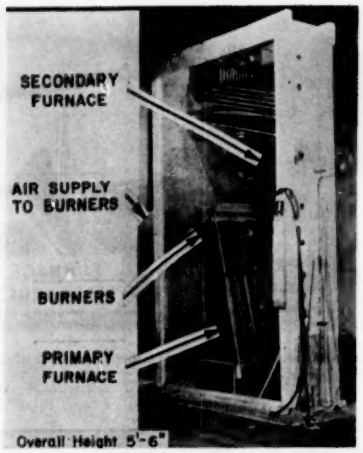

Fig. 8 Two-dimensional air model for furnace gas-flow studies

without seriously affecting the validity of the results, unless the model is to be used to determine frictional pressure drop. In this case it may be necessary to duplicate Reynolds numbers to assure accuracy.

History of Model Testing

Scale models have been used in various branches of engineering for many years. As long as 85 years ago, William Froude used scale models of ships to determine drag and power requirements. The use of scale models of planes in wind tunnels by aeronautical engineers has been highly developed and widely publicized. Practically all branches of engineering now make extensive use of models or pilot plants to solve otherwise impossible problems. Only in relatively recent years have models been widely used to solve problems in furnace design.

About 20 years ago models were being used to some extent by the authors' company as an aid in furnace design. In 1938, for example, two-dimensional, cold-air models were used to study the effect of furnace configuration on flow patterns in furnaces, Fig. 8. These models were built of wood except for one side which was glass. Tube banks were simulated by wires of the proper diameter. Flow distribution was determined by velocity probes inserted through holes in one side and the rear of the furnace. Confirming indications of flow direction were obtained by inserting a rod, with a string tied to the end, through holes in one side of the model.

A more comprehensive example is described by Lane and Morrison for the series of tests run in 1945 to determine the effects of windbox and air-duct design on the furnace performance of a boiler designed for Southwark Station of the Philadelphia Electric Company [4].

In the past 5 years there has been a progressive increase in the use of models and in the improvement of techniques by the authors' company, so that now it is standard practice to check all new designs of furnaces. A group has been organized at the Research Center for the sole purpose of conducting flow studies, not only of furnaces but of other components involving flow problems which cannot be solved by conventional analytical means.

Use of Models in Design of Philo Unit

The use of models in the design of the supercritical-pressure steam generator at the Philo Plant of the Ohio Power Company has been mentioned briefly in a previous paper [5]. This unit was designed to use a relatively large percentage of recirculated gas (70 to 80 per cent) in order to keep the furnace size to a minimum which would permit installation in an existing building.

Design Considerations. The major considerations to be worked out with the aid of models were the shape of the furnace, the arrangement of heat-transfer surface, and the method of introducing recirculated gas into the furnace. In order for the recirculated gas, in conjunction with the small furnace, to do an effective job of cooling the hot furnace gas before entering the convection pass it was considered essential that:

1 The recirculated gas be mixed thoroughly with the hot furnace gas before entering the convection pass.

2 The gas-flow distribution through the furnace be such that most effective use is made of furnace surface.

3 The gas-mass-flow upset entering the convection pass be kept to a reasonable minimum.

These considerations would be necessary to prevent slagging in the convection pass and local overheating of superheater tubes.

Model Test Procedure. Two-dimensional open-channel water models at $^1/_{24}$ scale were used extensively to explore various furnace arrangements. For these tests the height and depth of the furnace were built to scale, but the width, represented by the height of the walls on the model, was only $1^1/_2$ to 3 in. instead of the 17 in. that would have been needed if built to scale. Water in sufficient quantity was used to assure turbulent flow in the model. The flow pattern was made visible by sprinkling ground black pepper on the surface of the water, and permanent records were obtained by taking photographs (using $^1/_5$ to $^1/_{10}$ sec exposure). In spite of the fact that these models were only two-dimensional, a good general indication of the effectiveness of mixing recirculated gas in the furnace was obtained by adding dye to the water simulating the recirculated gas and observing its diffusion as it passed through the furnace.

The first proposed furnace arrangement is shown in Fig. 9. The water-model tests indicated that mixing would be satisfactory but that the gas-mass-flow upset entering the convection pass would be excessive. Fig. 10 shows the flow distribution obtained using the solid tracer. The flow was concentrated at the bottom of the convection pass, with some reverse flow at the top. Several variations of this general arrangement were tried with little improvement in the gas-flow upset.

Other arrangements were then tested. Some of these accomplished good mixing but had high mass-flow upset, while others did the opposite. In some arrangements the furnace pressure drop was excessive. The arrangement shown in Fig. 11 appeared to solve all of these problems satisfactorily.

To obtain quantitative values for flow distribution and the effectiveness of mixing, a $^1/_6$-scale warm-gas model of this arrangement was built, Fig. 12. It was constructed mainly of steel plate. Natural gas was fired in the air ducts leading to the simulated cyclone furnaces to raise the temperature to approximately 1075 F to simulate the 3000-F gases leaving the primary furnace in the prototype. Air from the fan discharge at about 100 F was used to simulate the 800-F recirculated gas. The quantity of air flow was such that velocities in the model were about equal to those in the prototype. Reynolds numbers were about $^2/_3$ of those in the prototype. The model had provisions for inserting velocity and temperature probes for determining flow distribution and mixing. Preliminary tests indicated that, with the proper design of recirculated gas ports, the gas-mass-flow upset entering the convection pass would be acceptable.

The next step was to determine the number, size, shape, and location of recirculation gas ports necessary to obtain good mixing of recirculated gas with the gas discharged from the cyclones. To test the performance of various port arrangements, temperature

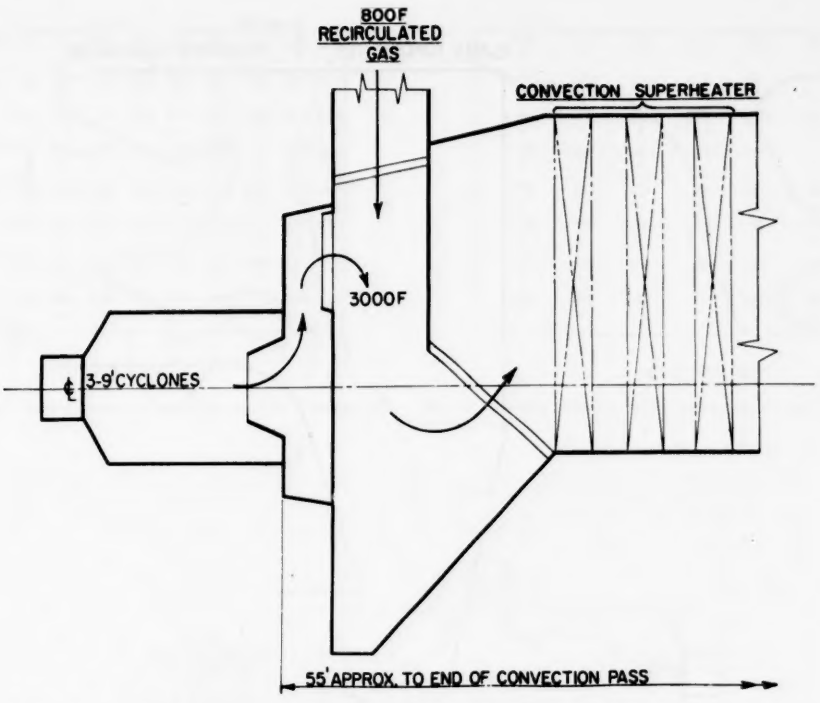

Fig. 9 Side section of proposed furnace arrangement for Philo super-critical-pressure steam generator

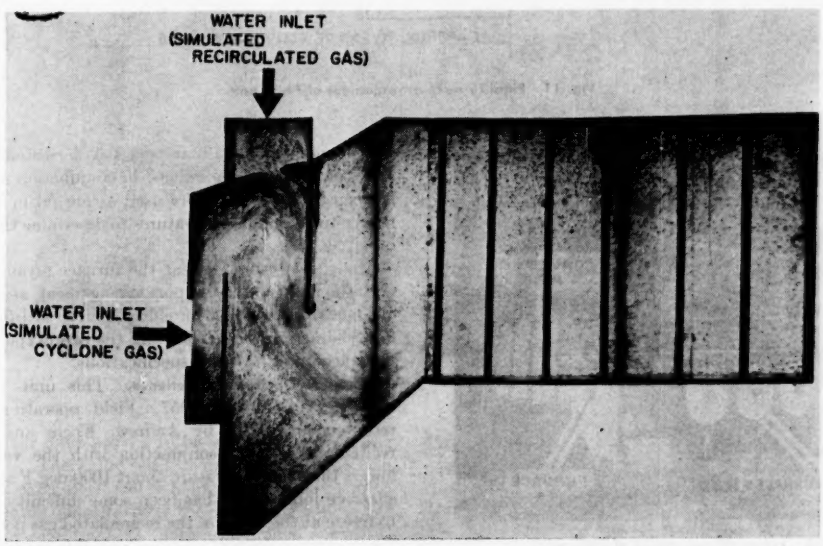

Fig. 10 Flow pattern of proposed furnace arrangement determined by two-dimensional, open-channel water model

and velocity traverses were taken at the furnace outlet (section A-A in Fig. 11), as well as at several other planes throughout the furnace, and were evaluated on the basis of the most uniform patterns.

Model Test Results. Temperature and velocity patterns using the final arrangement of 10 rectangular ports are shown in Figs. 13 and 14. Because the model operates at relatively low temperatures and with little or no heat transfer, the temperature patterns obtained on the model cannot be used directly to predict the temperature patterns in the prototype. They do, however, show the effectiveness of mixing. The magnitude of gas-temperature unbalance in the prototype due to incomplete mixing can be estimated by multiplying the temperature unbalance in the model by an appropriate factor to correct for the difference in temperatures between the model and the prototype. For this test the factor is approximately 2.5. Corrections also must be made for the

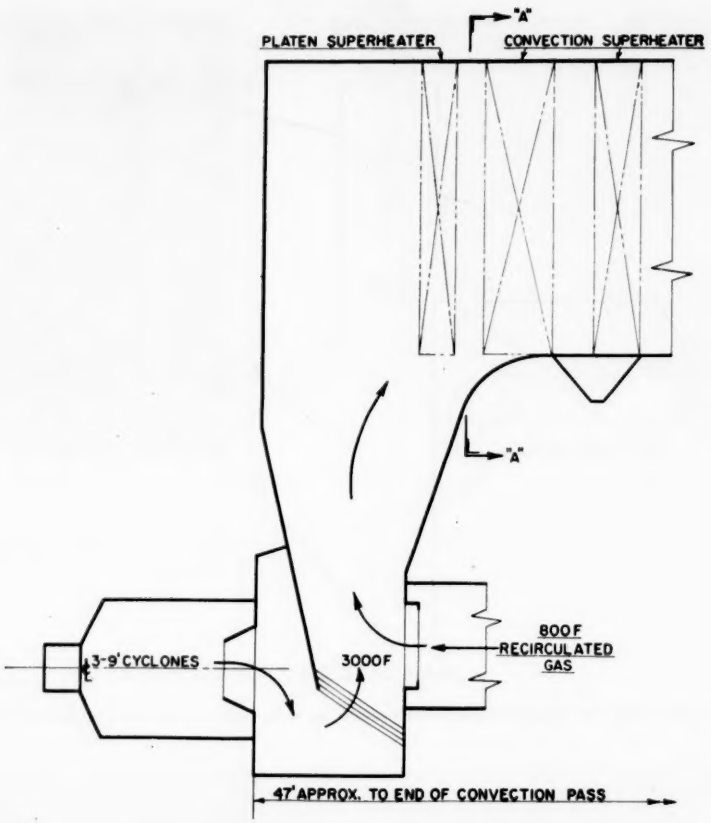

Fig. 11 Final furnace arrangement of Philo unit

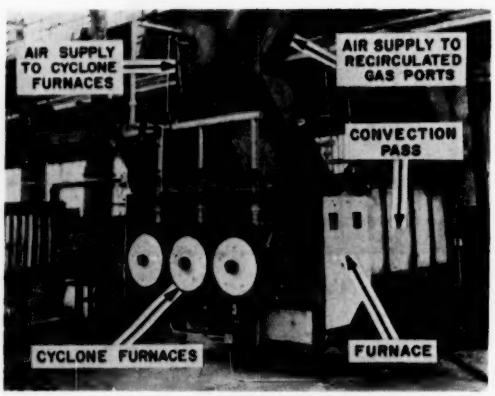

Fig. 12 1/6-scale gas model of Philo unit

effects of heat transfer on temperature patterns. The velocity distribution through the furnace, in conjunction with empirical rules based on engineering data derived from extensive tests of operating units, was used for this purpose. In general, these results show that temperatures near the side walls are low and that the temperature distribution is affected by furnace residence time. Gases with high velocity combined with a short path through the furnace will leave the furnace at a higher temperature than gases taking a longer path or with lower velocity.

The velocities plotted in Fig. 14 are relative velocity components perpendicular to section A-A, corrected to give an average value of 1.00. These values, in conjunction with the corrected temperature pattern, were used as an aid in calculating superheater-tube metal temperatures to determine the type of material required.

Model tests showed that the furnace arrangement of Fig. 11 with the recirculated-gas port arrangement, as determined by the gas-model tests, would produce entirely satisfactory furnace-gas flow characteristics. Therefore the prototype unit, Fig. 15, was built according to these specifications.

Prototype Operating Experience. This unit went into service at Philo in March, 1957. Field operating experience was reported previously by Andrew, Koch, and Pirsh [6]. The recirculated gas, in conjunction with the very small furnace, lowers the gas temperature about 1000 deg F and is doing a most effective job. There has been some difficulty with slag tending to freeze at the edges of the recirculated gas ports, thereby reducing the area of the port openings, but this condition has never been serious enough to force a shutdown. Methods of keeping the ports wide open are being investigated.

The fact that this new design of boiler has had such a good operational record, particularly from a standpoint of furnace performance, is evidence of the value of the information obtained from the use of flow models in the design stage.

Conclusion

The use of models in designing the furnace for the supercritical-pressure steam generator at Philo is only one example of the many

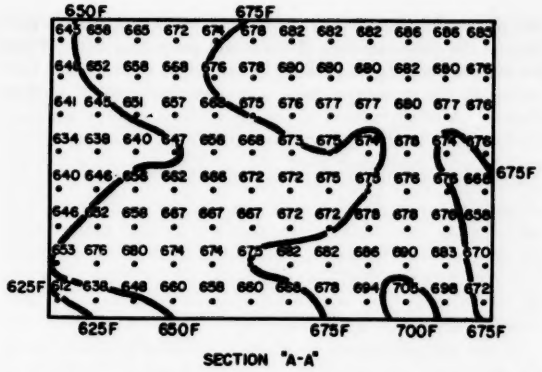

Fig. 13 Temperature pattern entering convection pass of 1/6-scale gas model of Philo unit

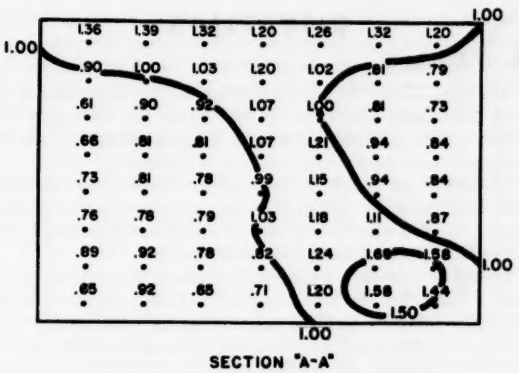

Fig. 14 Velocity pattern entering convection pass of 1/6-scale gas model of Philo unit

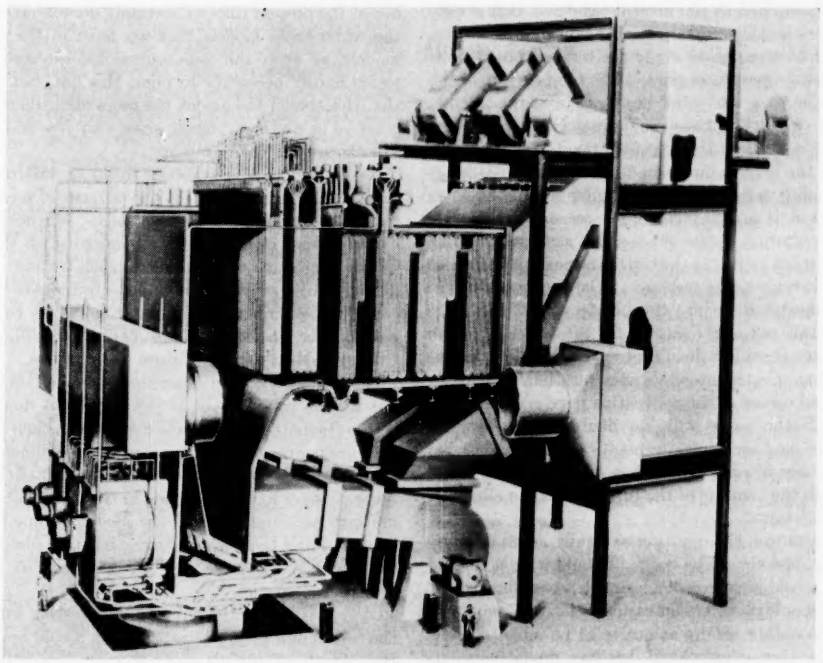

Fig. 15 Philo supercritical-pressure steam-generator unit

jobs for which models have proved to be valuable in providing design information. There are still many aspects requiring further study. For example, it will be helpful to develop a simple method for determining quantitatively the effects of gas-flow distribution on furnace performance. Specifically, such a method should provide data on furnace heat absorption and behavior of ash and slag. At present we can only estimate these effects by empirical rules based on previous experience.

The results obtained from the use of model tests over the past 20 years have increased our confidence in the value of this method of studying the flow problems involved not only in furnace design but in other components as well. For this reason the use of models to study flow problems of all types is increasing and we expect it to continue to be an important contribution to the design of efficient boiler furnaces.

References

1 Ralph Poole, "Aerodynamics for the Heating and Ventilating Engineer," *The Heating and Ventilating Engineer and Journal of Air Conditioning*, 1946, pp. 455–460.

2 R. E. Johnstone and M. W. Thring, "Pilot Plants, Models, and Scale-Up Methods in Chemical Engineering," McGraw-Hill Book Company, Inc., New York, N. Y., 1957, pp. 202–212.

3 Ibid., p. 199.

4 R. A. Lane and E. L. Morrison, "Southwark Station Boiler Air-Flow Model Tests and Operation Results," TRANS. ASME, vol. 71, 1949, pp. 941–950.

5 W. H. Rowand, "Developing the First Commercial Supercritical-Pressure Steam Generator," *Power*, vol. 98, September, 1954, pp. 73–80.

6 J. D. Andrew, Jr., P. H. Koch, and E. A. Pirsh, "Operating Experience With the First Commercial Universal Pressure Steam Generator for the Philo Plant," presented March 27, 1958, at the American Power Conference, Chicago, Ill.

DISCUSSION

M. J. Archbold[2]

The authors are to be commended for the large amount of work they have done prior to and during the writing of this article. Their company is also to be commended for the interest and willingness to do this type of research.

In the first paragraph of the paper, the authors have indicated that they recognize the gas-flow problems involved in furnace design, and it is their feeling that the use of scale-flow models will help materially in solving these problems.

From the viewpoint of the utility engineer, it is indeed gratifying to learn that the manufacturers and their engineers recognize these problems and that they are taking steps toward their solution. A few engineers have felt for some time that neither the utility industry nor the manufacturer have fully appreciated that the problem existed. As we go to larger units, small errors in design become exceedingly costly throughout the lifetime of the equipment. It is my feeling that only the surface of this problem has been scratched at the present time and that a very large amount of work is still necessary to obtain optimum designs.

We recently had an occasion to study the temperatures at the rear end of a pendant superheater pass. The temperature of the gas at the top of the pass was 400 F higher than at the bottom. By looking at Fig. 2, you will note the large cyclonic roll of the gas produces a high velocity at the top of the pendant superheater pass and a flow in the reverse direction at the bottom. It is believed that in actual practice, there is a similar roll of the gases and if this is the case, it supplies part of the reason for this wide difference in temperature. It also gives a clue as to why fouling of the superheater tubes begins at the top of the pass and proceeds downward as the service hours increase. The projection of the slope of the superheater floor into the furnace must be a large factor in starting this roll of the gases. In the upper left-hand corner of the furnace there is a dead spot with the roll of the gas probably proceeding in a counterclockwise rotation. Likewise, up in the right-hand corner of the convection pass, a dead spot is indicated in which the gases will, no doubt, roll backward. These points mentioned are certainly points which the designer someday will probably recognize and when he does, he no doubt will want to change the contour of the furnace so as to eliminate these undesirable features.

When building a model, the question naturally arises concerning what type of model should be built. Should it be a cold air two-dimensional, a cold air three-dimensional, a two-dimensional water model, or should a three-dimensional hot-gas model be used? In order to obtain results as nearly as possible to actual field conditions, a three-dimensional hot-gas model certainly should be a very excellent approach to the problem. Each one of these has its place in design work and it is only the designer who will know what tool he wishes to use and for what part of the design he wishes to use it. For our work it was found that the two-dimensional smoke-table testing of certain portions of the duct layouts permitted us to eliminate some of the poor designs before making up the three-dimensional model. This saved us a considerable amount of costly revamping and testing of the three-dimensional model and hence was a time and money saving procedure.

It has been my belief that the nearer you get to the conditions under which the equipment will actually be operated in your model testing, the closer you will get to the true answer.

The work which has been done in the Commonwealth Edison Company has not been on the furnace, but has been in connection with that portion of the steam generating unit immediately following the economizer. Two-dimensional, three-dimensional, and water-table models have been built for testing certain portions of the colder sections of the steam generating unit. From the start of building and testing of the model to the actual field testing of the prototype itself, a considerable amount of time elapses. A small amount of testing of the prototype has been done and, in a number of instances, we have found that the models gave us an exceptionally good clue as to what to expect in the performance of the prototype. On one very recent job, a number of the sections of the duct work immediately ahead of and also following the dust collector were tested in a smoke table. After the designs were changed, a three-dimensional model was built. It is gratifying to report that this particular installation is working exceptionally well and we feel that we have learned a considerable amount from these models.

In one particular instance where a water-table model set-up had been used, the prototype, which was designed in accordance with the indications brought out in the model testing, did not perform nearly as well as was anticipated. We probably should not allow one instance to shake our confidence in a method of testing, but at the present time we certainly do not have the confidence in the water-table models that we have in the three-dimensional models, or even the two-dimensional smoke-table models. It seems hardly necessary to point this out, but we are convinced that the smaller the model, the more meticulous the model maker must be in its construction, since very few and very small errors can change the entire picture.

As rapidly as it is practical to do so, instruments and equipment are being obtained for the purpose of measuring the actual velocities in our later installations. Whenever possible, these measurements are made prior to starting up the boilers. If the proper equipment is available for such testing, and if the work is done by people who understand the purpose of the testing, then a considerable amount of information can be collected which will either alter the design and call for modifications, or which will guide the design on future installations.

On another job, two-dimensional smoke-table tests were made, but in this instance the prototype is not doing as well as had been anticipated. Cold field checks were then made and velocity measurements taken, and a small three-dimensional model was made up. This model made use of some rather basic changes and these changes have been made in the field in accordance with the information obtained from the model. Time has not permitted field checking these last changes, but this case is recited in order to more fully illustrate the steps necessary for correction of poor flow characteristics.

It should be pointed out that field testing consists of operating the forced and induced draft fans on a cold boiler and in holding the velocity of the air going through the setting at a predetermined value. In some cases, the velocity has matched the velocity of the gases in actual operation. In other cases, we have used velocities approximating one half of the actual gas velocity. At the present time, we are not certain just what velocities should be used. The instruments which are used in these tests are hot wire anemometers and, by actually entering the ducts and the equipment, velocity traverses at various locations are made. By using titanium tetrachloride, a visible plume can be produced which will give the observer an excellent check on the direction and turbulence of the gases. Not only can this chemical be used in the prototype, but it can also be used quite effectively in the three-dimensional model studies and should prove quite effective also in certain phases of two-dimensional model studies. However, in the two-dimensional model studies we have used kerosene fumes exclusively.

Once again I would like to emphasize the need for greater use of model studies in the design of power plant equipment. Proper distribution of air and gas are vital to optimum operation of practically all steam generating components. This is a big

[2] General Mechanical Engineer, Commonwealth Edison Company, Chicago, Ill. Mem. ASME.

problem and one which needs full co-operation by all parties involved.

William T. Reid[3]

From a practical standpoint, water models fill a real need in visualizing flow in complex circuits. They can be adapted readily to a wide variety of problems, and they are relatively inexpensive and easy to construct. Air and gas models are basically more difficult to assemble and operate, yet, as the authors show, they have been applied successfully in analyzing flow distribution in fairly complicated designs. Although the authors have used velocity probes and temperature probes to investigate the completeness of mixing and the direction and magnitude of the velocity vectors in such gas models, other techniques are available for simplified systems where no physical interference with gas flow is permissible.

An example of such a technique is the schlieren method, where optical tricks are played to visualize gas flow. The principle depends on the refraction of a beam of light with a sharply defined edge, a second edge serving to produce light and dark areas in the image depending upon whether the beam passing through the schlieren field was refracted above or below the edge. By this technique, a silhouette is obtained of solid objects in the schlieren field, while gradients in the index of refraction of gases in the field show up as images in varying tones between black and white on a gray background. The result is to give an excellent visualization of the gas pattern.

The schlieren image can be produced by a constant light source, in which case still or motion pictures can be taken to record the images. From motion pictures taken at as high a rate as desirable, individual eddies or gas patterns can be followed to give a fair indication of velocity. By spark photographs with a duration of a few microseconds or less, the extent of turbulence can be nicely determined.

Although the schlieren field is two-dimensional, rotationally symmetric gas patterns, as for gas expanding freely from a nozzle, can be investigated. For example, quantitative measurements of a gas expanding freely from a nozzle have been made by calibrating a photographic record of the jet with a schlieren photograph of a gas-filled soap bubble in the same field. The mathematical procedures are somewhat involved, but the scheme has merit where physically sampling the gas stream is undesirable or impractical.

Because the schlieren method shows only the occurrence of gradients in the index of refraction, it is incapable of indicating whether such gradients result from temperature differences or from compositional differences. Temperaturewise, a good system can distinguish between gas streams differing by as little as 7 deg F. Differences in the molecular weight of gases of only a few per cent similarly can be seen. However, when temperature and composition both change, the schlieren image cannot separate the two variables. It does have great merit nonetheless in isothermal systems, and where the same gas is being observed at different temperatures. It would seem to have great merit in boiler-furnace studies in such fields as turning vanes or obstructions in ducts, air-flow past deposits, turbulence behind tube banks, or for burner studies.

Only a few laboratories have schlieren equipment, a somewhat surprising fact in view of the wide utility of the method for visualizing gas flow. Small-size schlieren systems, on the order of an inch or two in diameter, can be set up in a few minutes with such simple equipment as a slide projector, a good photographic objective with an opening the size of the wanted schlieren field, and two razor blades. Larger systems use parabolic mirrors in place of lenses; fields as large as 36 inches in diameter have been used. A more practical system can be built around 12-in-diam mirrors. This should be amply large to cover most model work concerned with boiler furnaces. Such a schlieren system, complete with mirrors, both continuous and spark-discharge light sources, and other auxiliaries, can be built for less than $10,000.

[3] Assistant Technical Director, Battelle Memorial Institute, Columbus, Ohio. Mem. ASME.

Authors' Closure

The authors wish to thank both Mr. Archbold and Mr. Reid for their valuable comments on the use of flow models.

We agree with Mr. Archbold that the results obtained from certain types of models can be misleading if proper care is not taken both in the design of the model and the interpretation of the test results. This is true of any model, but especially of the two-dimensional open-channel water models where the free-surface effects can influence the indicated flow pattern through a unit, especially if the unit contains sharp bends or large changes in cross-sectional area which change the fluid velocity. In these cases, two-dimensional closed models have proven more reliable.

We agree with Mr. Reid that the schlieren system is a good technique for visualiy observing flow patterns in a model, although as yet we have felt no need for introducing this complication in our determinations of flow distribution. We have found that the use of dye and solid-particle tracers for visual qualitative analyses and the use of velocity and temperature probes for quantitative analyses have given excellent results. There are other techniques of visual flow analysis which we have considered but have not used because we feel they offer no significant advantages over our present testing techniques. These include, in addition to the schlieren system which Mr. Reid describes, streaming double refraction for water models, the shadowgraph technique, and the interferometer for air and gas models.

In closing, we wish to re-emphasize the point made by Mr. Archbold concerning the importance of designing all power-plant equipment, including boiler furnaces, to provide proper distribution of air, fuel, gas, water, and steam through the unit. The use of scale models has been proven to be an economical method of optimizing the design of many of these components.

G. C. WHITNEY

Research Department,
Foster Wheeler Corporation,
New York, N. Y.

Use of Models for Studying Pulverized-Coal Burner Performance

DURING the past decade we have greatly increased our use of small scale models in the testing and developing of various pulverized fuel system components. Illuminated plastic and steel models operating with air and graded wood dust offer many advantages.

(1) Visibility is excellent providing quick, reliable, visual, evaluation of experimental changes.

(2) Model changes can be made quickly and inexpensively. This makes it economically feasible to try a wide range of ideas from which a much smaller group can be selected for more complete investigation.

(3) Many times it is physically impossible as well as economically impractical to arrange full scale tests. In pulverized coal work it has been impossible to get enough illumination or enough penetration of vision to be able to make observations.

Our first model investigation involved the construction of one-eighth scale wood and plastic models of the primary air and coal portion of a pulverized coal burner with external illumination. Graded hardwood dust with no plus 30 mesh or more than 10 per cent minus 200 mesh material was used instead of coal. Visibility was excellent and the qualitative results of one of the models were indicative of a satisfactory solution of the distribution problem.

The results of a model test are only of value if they can be correlated with the performance of the actual equipment. In this case the correlation involved variations in air temperature, dust density, size, and particle shape, as well as dimension. Fortunately a three-step program of evaluating these factors could be arranged.

The first step involved the wood-dust-and-air evaluation of an internally illuminated plastic-and-steel full-size model of a primary coal body of one of our smaller pulverized-coal burners. This model was tested in the apparatus shown in Fig. 1. Significant features of this model arrangement can be noted as:

1 Burner body—note that all secondary-air functions have been eliminated to permit better observation. The inner sleeve is clear plastic and fitted with fluorescent tubes. The rear plate is also made of clear plastic.

2 Plenum chamber simulating a furnace. Internal illumination and observation doors are provided.

3 Air is removed from the plenum chamber through the rotating dust separator.

4 Dust-free air is measured in an orifice meter.

5 Separated dust is removed from the plenum chamber by a calibrated variable-speed screw conveyer.

6 Dust is re-entrained in clean air.

7 The fan pumps the mixture of air and dust to the burner inlet.

8 The flexible section of conduit may be adjusted to vary dust disposition entering the burner.

Burner bodies similar in everything but scale to the original one-eighth-scale models were observed in this apparatus. For equal Reynolds number in the conduit and the same air-dust ratios the behavior pattern of the dust was the same for both sizes of models.

Operation with this test arrangement indicated that the wood-dust distribution of the full-size model of the burner body of a small burner was essentially the same (at comparable Reynolds numbers) as the previously observed wood-dust distribution and behavior in one-eighth-scale models of the large coal burners.

Having established that the wood-dust models behaved predictably over a scale range of roughly four to one, the second step was to compare the effect of changing from wood dust and cold air to coal and preheated air. As part of the first step we had operated burner-body models which were the same dimensionally as the primary air-and-coal body which was installed in our plant heating boiler. This is a single-burner furnace and the flame shape and coal-dust distribution could be fairly easily observed. These comparisons showed essentially similar maldistribution of coal dust.

As a further comparison we installed an operating burner body which incorporated the modifications which our wood-dust tests had indicated would give uniform coal-dust distribution regardless of approach-conduit configuration. Operation of this burner immediately indicated almost perfectly symmetrical flame shape, very uniform dust distribution at the tip of the burner, and excellent ignition stability. Subsequent operation of this burner

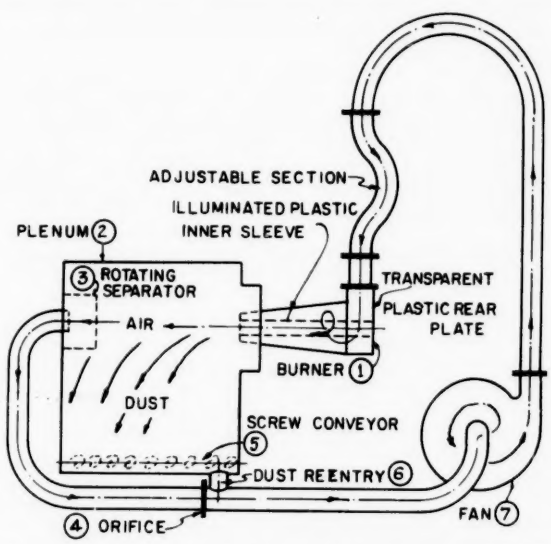

Fig. 1 Schematic arrangement of the test apparatus for wood-dust-and-air evaluation of an internally illuminated plastic-and-steel full-size model of the primary coal body of a small pulverized-coal burner

Contributed by the Research Committee on Furnace Performance Factors and presented at the Annual Meeting, New York, N. Y., November 30–December 5, 1958, of THE AMERICAN SOCIETY OF MECHANICAL ENGINEERS.

NOTE: Statements and opinions advanced in papers are to be understood as individual expressions of their authors and not those of the Society. Manuscript received at ASME Headquarters, July 31, 1958. Paper No. 58—A-95.

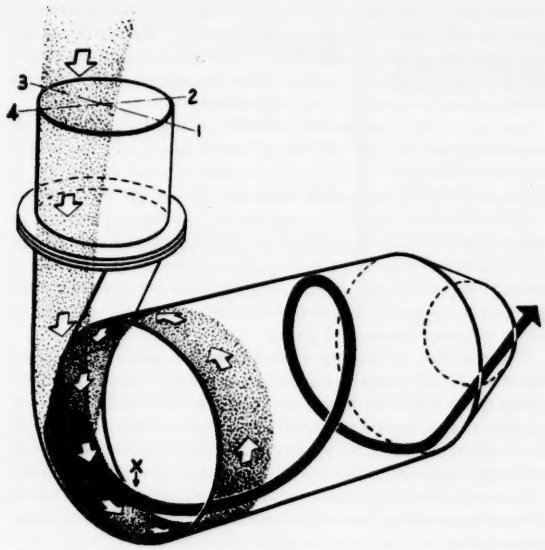

Fig. 2 Schematic of the critical proportions of the original, unsatisfactory standard primary coal body. All coal leaves the volute in a narrow band at *X* and proceeds as a standing rope or spiral to the outlet. No arrangement of baffles or hurdles could disperse it.

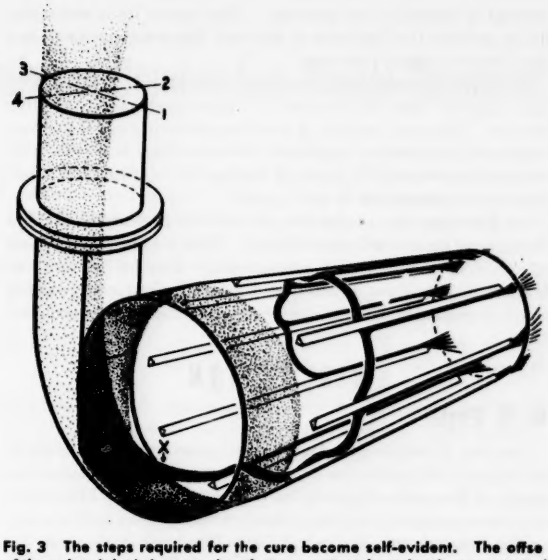

Fig. 3 The steps required for the cure become self-evident. The offset of the volute inlet is increased so that no matter where dust is concentrated in the approach conduit a not too unfavorable approach angle results, minimizing the tendency for dust to settle out at reduced ratings. Multiple random baffles have been grouped into continuous axial bars, and the cylinder-and-cone combination modified into a single continuous cone.

developed a turn-down ratio of nearly six to one with favorable raw-coal conditions and better than three to one at all times.

The third and final step was a field installation of one of these new designs of burner bodies in a large-size burner. The location selected was one that had given a great deal of trouble from coking and unsymmetrical flame shape. These troubles were immediately eliminated and we have had no reports of difficulty. This design has been standardized for several years and the performance of all burners has been uniformly good regardless of approach-conduit configuration variations.

It can be seen that the course of this development from problem to model, to model solution, to problem solution was necessarily time consuming. Each step had to be very carefully checked to assure that model problems of scale, media, temperature, and so forth, were properly evaluated. Since trial-and-error methods over a period of many years had produced no general solution, there appeared to be no other approach available. Fortunately, since the comparison criteria have been established, it has been possible to proceed more directly with the use of models in several other related problems.

It may be of interest to describe what was observed in the first and last of the many models which were tried out. Fig. 2 shows schematically the critical proportions of the original, standard, primary coal body. The first and most important observation was that no matter what the distribution of the dust in the conduit entering the burner, all of the dust was immediately centrifuged against the perimeter of the scroll and made from three to six complete rotations within the volute before entering the burner body proper. All coal leaving the volute inlet leaves in a narrow band at *X* and proceeds as a "standing rope" or spiral to the outlet. The amount of lead of this spiral determines the angle at which this "rope" leaves the burner, varies with inlet conditions, and can be changed readily. With coal concentrated in the region between 1 and 4, the dust splatters against the bottom of the volute, thus losing energy, and is more liable to settle out in the volute inlet. When this happens, the rotation is destroyed, and settling out continues until complete stoppage occurs or a high-velocity passage develops and maintains itself with very poor dust distribution at the tip of the burner. Of course with multiple burners connected to a single distributor, stoppage is the more probable end result. When dust is concentrated at other areas of the inlet (say 2 and 3) there is less "spattering" and less tendency to settle out in the volute at reduced ratings. Many attempts were made to disperse the standing rope. Actually the only thing that worked was a low baffle at right angles to the motion of the rope. Unfortunately the rope re-formed almost immediately. Succeeding baffles continued the dispersion until the conical section was reached. Here the rope re-formed and no arrangement of baffles or "hurdles" could disperse it.

Once the pattern of performance was spelled out, the steps required for cure became almost self-evident as shown in Fig. 3. The offset of the volute inlet was increased so that no matter where dust is concentrated in the approach conduit it will approach the volute at a not too unfavorable approach angle. This greatly minimizes the tendency for dust to settle out at reduced ratings. The multiple random baffles described in the foregoing for Fig. 2 have, for convenience, been grouped into continuous axial bars. The cylinder-and-cone combination of Fig. 2 is modified into a single continuous cone. It has been found that the length of the conical section itself is not critical. However, the position of the ends of the axial bars with respect to the ends of the conical section is quite important.

The effect of the bars is to take the standing rope and break it down into equal streaks which are elements of the cone. These streaks seem to be maintained and equalized by the continuing rotation of the primary air. If the bars are continued to the tip of the cone the streaks can be clearly observed well out into the furnace. If the bars are stopped off short of the tip these streaks become dispersed.

These are the basic principles of proportioning which have been applied to several sizes of burner with, thus far, very successful results. Unanticipated secondary advantages have also resulted from the improvement in coal distribution. With consistently uniform dust distribution it has become possible to reduce the

amount of secondary-air rotation. This makes for a less bushy flame, reduces the incidence of side-wall flame impingement, and also lowers windbox pressures.

Subsequently, similar techniques have been used to investigate and improve the performance of pulverized-coal-distributing devices. Here the problem is to deliver as nearly equal portions of air and coal from an exhauster to two or more burners. This program is presently in the field testing and confirmation stage. Material improvement is anticipated.

We have also used models very extensively in studying the flow characteristics of new burner designs. This has been particularly effective in the study of secondary-air distribution between burners in a common windbox and means for reducing required windbox pressures without aggravating the distribution problem.

DISCUSSION

M. D. Engle[1]

The use of models for studying and improving the design of pulverized-coal burners as reported in this paper is another example of the value of models for improving design. The author is to be congratulated on the research work reported in this paper.

The Pennsylvania Power and Light Company, with which the writer is associated, is fortunate in having had a practical demonstration of the improvement in the Foster Wheeler pulverized-coal burner which resulted from this work. At our Martins Creek Steam Electric Station the previous design of burner was originally installed for No. 1 boiler, a 1,200,000-lb-per-hr, 1450-psig, 950-F unit. Shortly after it was placed in service, the burners were changed to the new design and the improvement was marked.

A pulverized-coal burner can be likened to a carburetor as used for liquid fuels. It is the mechanism for properly distributing the coal particles in the air required for combustion in such a manner that each and every particle of coal is supplied with the proper amount of air in a manner that will promote rapid and complete combustion. Just why is this so important? Why is it so desirable to have the best design of burner? It might be interesting to list a few of the improvements which result from a better burner:

1 Higher boiler efficiency resulting from lower combustible lost in the flue dust.

2 Less slag deposit on furnace walls and on boiler, superheater, reheater, and economizer tubes and in the air heater.

3 The ability to burn a wider range of coals.

4 Fewer pounds of dust discharged from the chimney each hour.

5 Less soot and slag blowing.

6 Higher boiler availability resulting from fewer outages to hand-clean slag and to repair areas eroded by flue dust and soot blowers.

7 Wider range of operation with a stable flame.

8 Lower cost of ash and dust-handling. Less quantity to handle, lower maintenance, and less storage area required.

Some of the advantages of a better burner design have been enumerated to emphasize that a better design of pulverized-coal burner is not a matter of small consequences. The combined advantages can really be tremendous. The better design developed fully justifies the great effort put forth by such research engineers as the author to produce a better product.

And so it is with almost all products. A model enables the research engineer to find out things which are nearly impossible with the prototype. We should use models more extensively in our research and development work and we will get ahead faster.

Models have played a tremendous part in the spectacular development of the many types of atomic reactors and components which have been designed and built for many purposes. Many models are being used in the research and development work going on today to find out the facts which ultimately will give us a new source of economical power.

If the author of this paper would prepare another paper, for one of our future power meetings, giving the story on the improvements made with the commercial burners as a result of this research work, as compared with the previous designs, it would be an excellent addition to our technical literature on combustion and might very well point the way toward further improvements.

The paper certainly makes a strong argument for the use of laboratory tested models as a practical and economical way to improve design.

C. R. Marshall[2]

Each of the two 600,000-lb-per-hr boilers at our Riverside Steam Plant is fired with six 30-in. Foster Wheeler burners. Two of the six constitute an upper row of burners and the remaining four burners provide a lower row. Originally all of the burners were of the standard cylinder-and-cone design. "Coking" trouble, resulting from the use of certain coals which become sticky at relatively low temperatures, caused burning out of both inner and outer sleeves in spite of frequent burner lancing. Seven of nine failures were on the upper row of burners. This was attributed to two factors; namely, (*a*) higher temperatures in the upper part of the furnace, and (*b*) approximately 6 ft of the coal conduit was enclosed in the hot-air ductwork.

The two top burners on each boiler were changed to the continuous cone-and-axial-bar type of burner body and greatly improved performance resulted. The flame is uniform and stable and the load range of the burners is increased.

Since installing the new type bodies we have not experienced a burnout or evidence of overheating on these burners, although occasional trouble still occurs on those of the original design.

Author's Closure

The final judgment on the merits of a program of research and development comes from actual operation. Reports on failures or even suspected failures are prompt and voluminous. A suspected success is often only to be inferred from a sharp falling off in the number of complaints. The author is very grateful to Messrs. Engle and Marshall for their positive evidence on what appears to be a comparatively successful development.

[1] Pennsylvania Power and Light Company, Allentown, Pa. Fellow ASME.

[2] Assistant General Superintendent of Power Production, Northern States Power Company, Minneapolis, Minn.

A. A. PUTNAM

Assistant Division Chief,
Battelle Memorial Institute,
Columbus, Ohio
Mem. ASME

E. W. UNGAR

Principal Mechanical Engineer,
Battelle Memorial Institute
Assoc. Mem. ASME

Basic Principles of Combustion-Model Research

The use of models to study problems encountered in the design of commercial and industrial combustion equipment is less well known than the use of their counterparts for aeronautical, hydraulic, erosion, and similar studies. The basic assumptions upon which cold-flow modeling of combustion systems is carried out, the application of modeling to various combustion problems, and the type of results that should be expected from the application of modeling techniques are discussed.

THE use of models in scientific research is well known. One may cite the examples of wind tunnels used to study flight problems, models of river beds used to study erosion of soil and proper placement of levees, the use of water channels to study ship models, and the recent use of hypersonic shock tubes and tunnels to study the hypersonic-flight regime. Less well known is the use of models to study problems encountered in the design of commercial and industrial combustion equipment. Yet, as wide a range of factors is covered in these studies as in those previously cited. Combustion efficiency and stability are of interest. Pressure losses, flow patterns, erosion, and deposition patterns attract much attention. Heat transfer by conduction, convection, and radiation are all important.

With one basic technique, that of modeling a combustion unit, being used to obtain information relative to such a variety of subjects, it is well to inquire as to the actual limits of the technique. Such an inquiry is the more important when it is realized that it is extremely easy to show by rigorous reasoning that, where a combustion process is involved, it is impossible to model a combustion unit with anything other than the actual unit run at the conditions of interest. Yet the fact that modeling techniques have been used for years, both in a predictive and a diagnostic sense, indicates that this line of reasoning is not entirely correct. It is therefore well to apply some measure of validity to the possible uses of modeling.

This paper first considers the basic assumptions upon which cold-flow modeling of combustion systems is carried out. Next, some applications of modeling to various combustion problems are considered. Finally, the type of results that should be expected from the application of modeling techniques are discussed.

The Basic Assumptions

Problems in combustion may usually be considered from two points of view—combustion physics and combustion chemistry. The reaction rates obtained in the reaction zone of a laminar flame or in a homogeneous combustor are limited by chemical process. Comparisons such as in Table 1 [1][1] show that these rates are far above the over-all rates obtained in various industrial and military combustion units. Thus basically the chemical reaction is not the controlling feature in industrial combustion; rather, the limitation is due to the physical process of properly mixing fuel, oxidant, and some product of the combustion. On this basis problems in combustion may be treated from the fluid-flow standpoint. The chemical reaction can be considered as a superimposed variable, and when it is necessary to consider it, various subterfuges are adequate. These include considering chemical reaction as heat sources and substituting concepts of burning velocity, and quenching distance, and ignition temperature for the chemical process that actually occurs. We may conclude then, that our combustor models will be basically models of the fluid-flow system; chemical reactions will usually be treated as of secondary importance.

Table 1 Typical reduced space-heating rates [1]

	Space heating rate, $Btu/ft^3hr/atm^2$
Residential oil-heating unit	10^4–10^5
Navy boiler	2×10^5
Turbojet	2×10^6
Ramjet	7×10^6
Homogeneous reactor	5×10^8
Laminar propane-air flame	6×10^8

Modeling, dimensional analysis, and similarities are all related topics and all based on the assumption that relations describing physical phenomena are dimensionally homogeneous. Modeling, in this paper, means the running of experiments on one size of unit to ascertain the results to be expected on another size unit. It will be noted that such a procedure is carried out, in essence, whenever pipe-friction factors are used in a design.

In dimensional analysis, the important variables of the system are gathered into independent dimensionless groups. The groups themselves are not unique in their make-up, but the total number of independent groups is fixed for a given problem. A set of groups is made for each dependent variable. Then, a knowledge gained from experiments of how the group containing the dependent term varies with changes in the independent groups permits the prediction of results for different prototype changes.

The authors of this paper consider similarities to be dimensional analysis plus the use of equations describing the actual phenomenon. At the minimum, the use of similarity procedures will lead to no better results than dimensional analysis. More common is the case where similarity makes it possible to choose a more advantageous form of the dimensionless groups in the set. Going even further, theoretical dimensionless equations describing a phenomenon might be carried to a final solution after imposing the necessary boundary conditions. It is expected that in this instance the theoretical dimensionless terms relating the various dimensionless groups might vary from those obtained by experiment, but only by a small amount. In any case, carrying a solution this far should indicate the best co-ordinate system for plotting data in a simple manner.

Some philosophizing might be interjected at this point. When

[1] Numbers in brackets designate References at end of paper.

Contributed by the Research Committee on Furnace Performance Factors and presented at the Annual Meeting, New York, N. Y., November 30–December 5, 1958, of THE AMERICAN SOCIETY OF MECHANICAL ENGINEERS.

NOTE: Statements and opinions advanced in papers are to be understood as individual expressions of their authors and not those of the Society. Manuscript received at ASME Headquarters, July 16, 1958. Paper No. 58—A-73.

dimensionless groups are close to 1, using "close to" in a very loose sense, they are expected to have an important effect on the dependent dimensionless group. On the other hand, when they are far from 1, the effect is either expected to be small or it is expected that some regrouping of terms should take place. An excellent example is the case of flow in pipes. For large Reynolds number, the friction factor is little affected by Reynolds number and depends principally on pipe roughness. For intermediate Reynolds number of about 2000, which is "about" 1 (although on the large side from a strict point of view), Reynolds number has an important influence on friction factor. Far below 2000, we encounter the case where, as the Reynolds number rapidly gets smaller, one dependent dimensionless group, the friction factor, rapidly gets larger. It is well known that the product of Reynolds number and friction factor is a constant, in fact 64, in the region of low Reynolds number in viscous flow. Whether realized or not, considerations of this sort are in the back of our minds when we design and interpret model tests.

In designing a piping system, it is not necessary to obtain the friction factors for a pipe of the same length-to-diameter ratio as contemplated in the design, and likewise it is not always necessary to scale a model geometrically. However, there is a question as to how to avoid difficulties when geometric scaling is not preserved. The suggested procedure is to carry out the modeling in two steps. In the first step, it is assumed that the model is of the same over-all size as the prototype. In this step, the changes in dimensional scale that are to be made are considered. The experimenter assures himself that the changes that are contemplated will still permit the attaining of the desired result on this full-scale model. In the second step, this full-scale model is considered to be scaled down in size, to the final size desired for the model.

Two conditions often occur in model studies that lead to another sort of assumption. This assumption is that data presented in the form of dimensionless groups can be extrapolated, especially if they are plotted on log-log co-ordinates. This assumption may partially be based on a failure to recall the summation signs in Buckingham's proof of the π theorem. However, it is only justifiable on the basis of experience.

The first of the two conditions mentioned occurs when the principal independent variable or variables cannot be varied in the model over the range of values to be encountered in the prototype. Then, the dependent group is assumed to be related to the independent group by some simple mathematical relation as, for example,

$$G_d = G_{i1}^{a_1} G_{i2}^{a_2} \ldots G_{in}^{a_n},$$

in which the values of a are then determined on the basis of the available data, and used to extrapolate to the new range. If the study is carried out in a relatively new field, the experimenter will hesitate to extrapolate G_i by more than a factor of about 3, and then only if range of value of G_i is not near 1. On the other hand, if the experimenter is familiar with the field, he may feel no qualms over an extrapolation by factors of 10 to 100, especially if the corresponding value of a as determined from the data is in agreement with established information.

In the second condition to be considered, the important independent dimensionless groups can be matched between model and prototype. However, the less important dimensionless groups cannot be. In some instances, changes in the boundary conditions of the model can be made to preserve the value. More often, the effect of change is ignored as being unimportant to the problem. However, it should be pointed out that the same precautionary consideration should be used herein as considered earlier in this paper.

Applications of Modeling

Although generalizing and philosophizing about modeling techniques is of importance to our understanding of the basic assumptions, an understanding of the details of application can only come from consideration of specific systems. The following discussion uses two areas of work to illustrate the points considered of importance. These areas concern isothermal modeling of combustion systems and an associated problem of deposition in a combustor.

The Isothermal Model. An isothermal model is one in which no combustion takes place and no heat is added by an energy source. The advantages of such a model are ease of construction and modification, and the ease with which measurements may be obtained. A one or two-fluid system may be utilized in the model. If a one-fluid system is utilized, then a tracer is added to one of the fluids and concentration profiles are obtained. A related technique, isothermal in spirit only, is to use hot air as one fluid and measure the temperature profiles.

Thring [2] indicates three cases where the use of isothermal models is acceptable: (*a*) The fully turbulent system with a very small nozzle discharging into a large chamber in which there is slowly moving air; (*b*) the system where the volume flows of fuel and air are of the same order of magnitude and the linear dimension of the fuel nozzle is comparable to the furnace width; and (*c*) the system where the flow is on the borderline of streamline and turbulent. In these three cases a good approximation of the flame geometry can be based on the results of isothermal flow tests. In other words, the fluid-flow considerations are more important than such factors as the burning rate of fuel droplets.

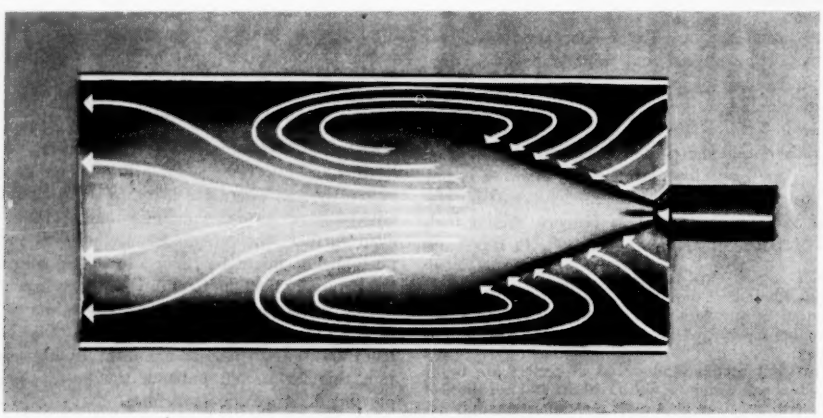

Fig. 1 The enclosed jet diffusion flame

The first of these cases can be illustrated by a consideration of the enclosed jet-diffusion flame. Such flames are common to boiler furnaces, open-hearth furnaces, residential oil-fired heating units, and some gas-turbine combustors. Thring and others have treated this case extensively [3]; the following discussion departs somewhat from their treatment, however.

Fig. 1 shows an enclosed jet-diffusion flame. As the fuel jet expands it mixes along the outside edge with the incoming air. In order to conserve momentum, the jet must aspirate a certain quantity of the surrounding fluid. If the quantity of air entering the combustor is limited, then as the jet gets close to the enclosing wall there is not enough surrounding air to conserve the jet momentum. Therefore, hot gases recirculate from downstream to supply the necessary quantity of the fluid flowing into the jet. This recirculation of fluid represents the major difference between a free jet and an enclosed jet.

A region exists along the edge of the jet where the fuel and combustion air mix in stoichiometric proportions to establish the mean flame front. It is desirable in model tests to establish the location of the zone which is equivalent to the stoichiometric proportions. It is also important to know the length of the flame. This length is approximated by some investigators as the distance along the jet axis between the nozzle and the concentration line at which the stoichiometric fuel to air ratio is obtained. A more reasonable practice however is to use a leaner mixture to account for the "unmixedness" of a turbulent flame [4]. These regions are not difficult to determine for a particular fuel from cold-flow tests if tracer gases are added to fluids simulating the fuel. The problem is to assure that the flow pattern is the same in the model and prototype, and that the rate of mixing is the same.

The first dimensionless group ordinarily considered in modeling is the Reynolds number. This number, often considered as indicating the ratio of inertial to viscous forces, was assumed large in this problem. Past experience indicates that, in this case, the intensity of mixing varies approximately with the flow rate, so that the over-all concentration pattern remains about the same with changes in Reynolds number. Thus we may neglect this group, at least temporarily.

A second dimensionless group to be considered is the ratio of mass input of fuel, or simulated fuel, to mass input of combustion air. This group should be held constant. And if it is reasonable to keep this group constant, it is also reasonable to maintain the ratio of total mass of gases aspirated by the nozzle fluid to the original mass of nozzle fluid. However, this latter ratio is a dependent dimensionless group which is beyond our direct control. We may or may not desire to measure it, but in any case, we must find the related and controlling primary dimensionless group or groups.

Considering the conservation of momentum between the cross-sectioned plane of the nozzle and the region where the jet strikes the wall,

$$\pi r_n^2 \rho_n V_n^2 = A \pi R^2 \rho_b \bar{V}^2,$$

where r_n is the nozzle radius, R is the radius of the jet, ρ_n is the density of the nozzle fluid, ρ_b is the density of the burned gases, V_n is the velocity of the nozzle fluid, $\bar{V}$ is the average velocity of burned gases, and A is a shape factor. Identifying the mass-flow rate of nozzle fluid by M_n, and the total mass-flow rate at the downstream cross section by M,

$$\frac{M_n^2}{r_n^2 \rho_n} = A \frac{M^2}{R^2 \rho_b}$$

Now, if one is to ensure that M/M_n is the same in model and prototype, then the dimensionless group $r_n^2 \rho_n / R^2 \rho_b$ should be constant.

Now consider the case where the model and prototype are of the same size, but isothermal modeling is to be used. Furthermore, consider that the region immediately surrounding the nozzle is not of interest, but that the main combustion region is of interest. Then the fluid that will be used in the nozzle should have the same density as the fluid in the region of interest; that is, $\rho_{n\,\text{model}} = \rho_b$. To maintain the necessary constancy of the dimensionless ratio,

$$r_{n\,\text{model}} = r_n \left(\frac{\rho_n}{\rho_{n\,\text{model}}} \right)^{1/2} = r_n \sqrt{\frac{\rho_n}{\rho_b}}.$$

This completes the first step in modeling, that of changing from prototype to full dimensional scale model. In the next step, the model can be altered up or down in size, as desired, and Reynolds number can be preserved if necessary. Ordinarily, however, one only makes certain the Reynolds number is well into the turbulent region.

The second system mentioned by Thring [2] is that in which the volume flows of the entering air and fluid stream are of the same order of magnitude, and the dimensions of the fuel nozzle and the furnace width are of the same order of magnitude. Mixing is considered to result from turbulence, and recirculation zones, if they do occur, are assumed to be unimportant. Sawai and his associates [5] considered this type of problem both analytically and experimentally. Analytically, the flame shape is a function mainly of the configuration of the combustor, the stoichiometric fuel-air rate, and the actual fuel-air ratio. Reynolds number is a secondary factor. Experimental results, both using a combustor, and using a 1/20-scale water model, appeared to confirm this deduction. It is interesting to note that a solution of caustic soda in water was used to simulate the fuel gas, and a solution of hydrochloric acid in water to simulate the air. The alkali solution was colored by phenolphthalein, and that point where the color vanished considered as indicating the flame front.

The third system mentioned by Thring [2] as being susceptible to cold-flow modeling is one in the borderline region between streamlined and turbulent flow. However, the experimenter must proceed cautiously in this case. Maintenance of Reynolds number in both the fuel and air-inlet regions and the main combustion zone appears to be important. However, some experimental variation of test conditions might show that the system is not as critical as expected. That necessary changes in the inlet areas, to preserve Reynolds number, might not have too much effect on the size of the combustion zone, has been indicated by some literature sources. For instance, in the study of overventilated laminar-diffusion flames conducted by Barr [6], a constant flow rate of butane was provided by means of a nozzle which was placed axially in a tube. A constant flow of air entered the combustion zone through the tube. The diameter of the nozzle was varied and the flame length measured. The ratio of nozzle diameter to the inner diameter of the surrounding air tube was varied from 0.133 to 0.643. For long flames, only a small decrease in flame length was observed. This observation probably results from the fact that the flame length, for a laminar flame, is dependent on the diffusion coefficient which is relatively constant. However, studies by Sawai [5] in the turbulent region indicate that an important factor for the flame shape is the ratio of velocities in shear-flow regions; preservation of the ratio preserves flame shape. This would seem to indicate that momentum considerations are important in the turbulent region, as was found for the case of the fuel jet.

Thus the following dimensionless group should be preserved in the problem now under discussion, in going from prototype to model:

Air-inlet Reynolds number: $D_1 V_1 \rho_1 / \mu_1 = D_{1m} V_{1m} \rho_m / \mu_m$

Fuel-inlet Reynolds number: $D_2 V_2 \rho_2 / \mu_2 = D_{2m} V_{2m} \rho_m / \mu_m$

Mass-flow-rate ratio: $D_1^2 V_1 \rho_1 / D_2^2 V_2 \rho_2 = D_{1m}^2 V_{1m} / D_{2m}^2 V_{2m}$

Momentum-flow-rate ratio: $D_1^2V_1^2\rho_1/D_2^2V_2^2\rho_2 = D_{1m}^2V_{1m}^2/D_{2m}^2V_{2m}^2$

The subscript m indicates the cold-flow model condition. The over-all Reynolds number is eliminated for simplicity. It could be added, using burned-gas velocity and kinematic viscosity.

A rearranging of terms results in a new set of dimensionless groups, consisting of either of the first two listed, and the following:

$$V_1/V_2 = V_{1m}/V_{2m},$$
$$D_1^2\rho_1/D_2^2\rho_2 = D_{1m}^2/D_{2m}^2,$$
$$\rho_1/\mu_1^2 = \rho_2/\mu_2^2.$$

This last group is of special interest, since it has no model term in it. It indicates that the modeling process can only be carried out when a special relation exists between the properties of the fuel and air. If this does not occur, one has the choice of ignoring the situation, or multiplying the two prototype Reynolds numbers by C_1, C_2 to obtain the model values, where

$$C_1/C_2 = \mu_1^2\rho_2/\mu_2^2\rho_1.$$

The particular division between C_1 and C_2 might be chosen on the basis of the experimenter's estimate of the criticality of the particular groups.

In addition to the isothermal combustion models discussed here, a system isothermal in kind but not exactly so has been developed by Spalding [7]. The same considerations as were involved here must be considered in this method, with the simulated fuel and the air assumed to be at the same temperature. However, by the use of electrical heating coils and thermocouples, the results that can be obtained are much more extensive than can be obtained with the simple cold-flow tests.

Fig. 2 is a sketch of a combustion model such as Spalding discussed. Heating coils simulate the combustion process. At the center of each coil, a thermocouple is installed to determine the gas temperature in the region. The walls of the model can be altered to study various configurations. To simulate the combustion in a system where fuel is injected separately from the air, rather than premixed with it, the air simulating the fuel is heated somewhat and the temperature profile is determined from the thermocouple readings. From this map of temperature, the fuel-air ratio as a function of location may be deduced. To each fuel-air ratio is assigned a heat input. Rather than try to simulate the chemical reaction rate as a function of temperature, a constant input of thermal energy is used when the temperature is in the range between the simulated flame temperature for the mixture ratio under consideration, and some lower temperature corresponding to about 0.7 of the maximum temperature increase. With air flowing through the section, the heaters are turned on in an arbitrary arrangement, and then adjusted so that all the proper ones are on, considering the temperature range indicated by the thermocouples. Making the changes indicated by change in firing rate permits the delineation of extinction limits; beyond the limits, the only stable heater settings are with all heaters off. At the other extreme, the preferred location from which to start ignition can be studied by turning on a single heater in the proper amount to simulate the input of ignition energy, and then turning on the remaining heaters as indicated by the temperature rise in their vicinity. The variations of flame shape can also be determined by noting which heaters are on.

It is clear that there are many assumptions involved in the use of this model. Furthermore, there are many factors which it cannot cover, such as pulsating or unstable combustion. Nevertheless, the use of this type of model as a tool in design appears quite promising, both for its original use in handling high-intensity combustors and use in modeling combustion in industrial and commercial furnaces and boilers.

Deposits. Downstream of the combustion zone, the problem of deposition of solids from the products of combustion, or of material picked up from a molten bath onto surfaces is sometimes encountered. Similar in nature may be the erosion effect where particulate material is scrubbed along the surface. There are actually three types of deposit systems which must be considered. One or all of these types may be important in any particular study. The three classes of systems to be considered are: (*a*) Small particles with diameters less than the free path of the gas molecules, (*b*) large particles with diameters appreciably greater than the free path of the gas molecules, and (*c*) particles in the intermediate range of sizes between (*a*) and (*b*). The similarity criteria for each of the three classes of deposit systems will be discussed in the order indicated. It should be mentioned that the modeling criteria which have been discussed previously must also still be considered.

Deposition of Small Particles. When the size of the particles which are depositing on a surface is less than the mean free path of the gas molecules, the particles are deposited by the mechanism

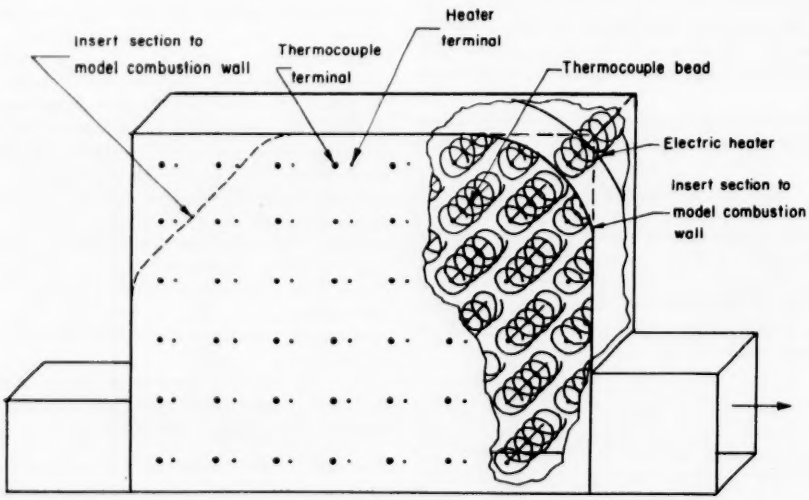

Fig. 2 Electrically heated combustion model [7]

of molecular diffusion. The deposit rate depends on the motion of the particle which is determined from the average velocity that the particle must attain in order to remain in thermal equilibrium with the carrier gas, and also depends on the particle concentration. This velocity is a function of only the particle mass and the gas temperature. Hence the important parameters to consider when modeling this system are: (*a*) The ratio of particle diameter to gas mean free path, (*b*) particle density, (*c*) gas temperature, and (*d*) particle concentration.

In modeling this type of system another method becomes usable; this is based on the fact that the mass-transfer rate by diffusion is related to the convective-heat-transfer rate through the ratio of the Prandtl to Schmidt numbers, taken to the $^2/_3$-power. This may be expressed symbolically as

$$\frac{M}{C} = \frac{q}{c_p(\Delta T)} \left(\frac{\mathrm{Pr}}{\mathrm{Sc}}\right)^{2/3}$$

where M is the mass-deposit rate, C is the free-stream concentration in volume of particulate per volume of gas, q is the heat-transfer rate, c_p is the specific heat, ΔT is the temperature difference, Pr is the Prandtl number, that is, the ratio of kinematic viscosity to thermal diffusivity, and Sc is the Schmidt number, that is, the ratio of kinematic viscosity to mass diffusivity. Hence measurement of the convective-heat-transfer coefficient may be sufficient to obtain the diffusion coefficient. The heat-transfer coefficient is, in many instances, an easier quantity to obtain experimentally than the diffusion coefficient.

Large Particles. Large particles must also remain in thermal equilibrium with the surrounding gas. However, the particle is now considerably larger than the free path of the gas molecules, hence, the particle is no longer moving in a discontinuous medium, composed of a large number of gas molecules, but is instead moving in a continuous fluid. The aerodynamic drag on the particle is obtained from Stokes' law [8]. The particle may deposit by a diffusion process or by inertial impaction.

If the mechanism of deposit of large particles is by diffusion from a turbulent stream, then the deposit rate and heat-transfer rate can be considered to be related as indicated by Reynolds analogy [9]. This is equivalent to equating to one the term $(\mathrm{Pr}/\mathrm{Sc})^{2/3}$ in the equation given for small particles. It follows that the terms which control heat transfer, such as Reynolds number and surface roughness, control mass transfer.

Large particles also may deposit by the mechanism of inertial impaction. The particles flowing in the stream have too much inertia to follow the stream as it turns around an obstacle. The stopping distance is the distance required for the particle to be stopped by viscous drag. This stopping distance may be computed for large particles, the initial velocity being equal to the free-stream velocity, and the drag being given by Stokes' Law. The most important similarity criteria then become the ratio of the stopping distance to the effective target radius, which is commonly referred to as the impaction parameter; of secondary importance is a parameter involving the Reynolds number with respect to the particle diameter. These groups may be expressed symbolically as [10]

$$K = \frac{\lambda_s}{D_t/2} = \frac{\rho_p D_p^2 U}{9\eta D_t}$$

and

$$\phi = \frac{\mathrm{Re}_p^2}{K} = 9\left(\frac{\rho_a}{\rho_p}\right)\mathrm{Re}_t$$

where K is the impaction parameter, λ_s is the particle-stopping distance, D_t is the target diameter, ρ_p is the particle density, D_p is the particle diameter, U is the fluid velocity in the free stream, η is the fluid viscosity, ϕ is a Reynolds number parameter which is characteristic of the target Reynolds number, Re is the Reynolds number, ρ_a is the gas density, and subscripts p and t refer to particle and target, respectively.

Intermediate-Size Particles. In the intermediate-size range, where the particles are starting to slip between gas molecules, the similarity criteria become more complex. Stokes' drag must be considered; hence, the Reynolds number with respect to the particle is of importance. However, the ratio of the particle diameter to the mean free path of the gas molecules is also of importance. As a result of all the similarity parameters to be satisfied for this size range, there is not much liberty that may be taken in modeling. Considering the present state of knowledge concerning this region, the model should use the same gas conditions and particle sizes as the prototype.

Concluding Remarks

The discussion that has been presented indicates that modeling can be of great help in designing or improving the operating performance of a prototype.

From a practical standpoint, if we are to go to the expense of designing a model and conducting an experimental program, we at least have a right to expect some reasonable representation of the results that would be obtained in a prototype. Depending on the refinement of the model and degree of care exercised in the research program, and the particular factors that are being investigated, we might expect only an indication of general trends with parameter changes, or, at the other extreme, data which will match within their scatter band similar data from a prototype.

To expand on this point a little, it is not always necessary to predict the exact values that might be encountered in a prototype. A typical example is where a prototype already exists and is running. It may be desired to make changes in the prototype to improve its performance. Thus, in the model, it would be sufficient to note the changes in performance brought about by changes in configuration or operating conditions. It would be expected that similar changes would cause similar performance change. Thus the model could be used in determining the optimum change in design of the prototype.

The second point given is also worth considering. Often more is expected in a comparison of model and prototype results than is expected in a comparison of two supposedly identical prototype units. It would appear that too often a model is made too perfectly. Especially in cold-flow models, the warpage, leaking, and other such factors that are expected to develop in prototypes are not present. Furthermore, misalignment of parts found in prototypes, and deviations from design, are not found in many models. It would appear profitable to pay more attention to the use of models to study the effects of expected deviation from design in prototypes.

A typical example often encountered in fluid-flow studies is the comparison of symmetrical and asymmetrical design. In such models, the symmetric system often appears to have many advantages. However, the investigator will know that asymmetrical systems are preferred in practice as giving better performance. Why? In one case, imposing expected production tolerances on the symmetric model gave the reason. The performance significantly deteriorated with deviations from symmetry which were far less than expected for production units.

If all these factors have been considered and investigated, then the remaining difference between model and prototype results are a consequence of differences in dimensionless groups of importance in the design. The amount of deviation is an indication of the actual importance of these factors.

References

1 W. H. Avery, "Space-Heating Rates and High-Temperature

Kinetics," "Fifth Symposium on Combustion," Reinhold Publishing Corporation, New York, N. Y., 1955, p. 86.

2 M. W. Thring, "Some Recent Developments in the Physics of Fuel Combustion," *British Journal of Applied Physics*, vol. 8, March, 1957, p. 89.

3 M. W. Thring and M. P. Newby, "Combustion Length of Enclosed Turbulent Jet Flames," "Fourth Symposium on Combustion," Reinhold Publishing Corporation, New York, N. Y., 1952, p. 789.

4 W. R. Hawthorne, D. S. Weddell, and H. C. Hottel, "Mixing and Combustion in Turbulent-Gas Jets," "Third Symposium on Combustion, Flame, and Explosion Phenomena," Williams and Wilkins, Baltimore, Md., 1949, p. 266.

5 I. Sawai, M. Kunugi, and H. Jinno, "Turbulent-Diffusion Flames," "Fourth Symposium on Combustion," Reinhold Publishing Corporation, New York, N. Y., 1952, p. 806.

6 J. Barr, "Length of Cylindrical Laminar-Diffusion Flames," *Fuel*, vol. 33, 1954, p. 51.

7 D. B. Spalding, "Analogue for High-Intensity Steady-Flow Combustion Phenomena," *Institution of Mechanical Engineers, Proceedings*, vol. 171, 1957, p. 383.

8 H. Schlichting, "Boundary-Layer Theory," McGraw-Hill Book Company, Inc., New York, N. Y., 1955.

9 Max Jakob, "Heat Transfer," John Wiley & Sons, Inc., New York, N. Y., 1949, vol. 1, chapter 24.

10 M. N. Golovin and A. A. Putnam, "The Inertial Impaction of Small Particles," Arnold Engineering Development Center, Contract AF 40(600)-710, January, 1958.

Bibliography

R. E. Johnstone and M. W. Thring, "Pilot Plants, Models, and Scale-Up Methods in Chemical Engineering," McGraw-Hill Book Company, Inc., New York, N. Y., 1957.

A. E. Weller and R. E. Thomas, "Similarities in Combustion," WADC TR 55-132, ASTIA Document No. AD-102523, October, 1955.

"The Use of Models for Investigating Open-Hearth-Furnace Design and Operation; Inactive Mixer Linings," Summary of the Proceedings of the 46th Steelmaking Conference, May 2 and 3, 1956.

A. Klinkenberg and H. H. Moody, "Dimensionless Groups in Fluid Friction, Heat, and Material Transfer," *Chemical Engineering Progress*, vol. 44, January, 1948, p. 17.

DISCUSSION

S. S. Penner[2]

The authors consider similarity procedures in combustion scaling and present physical arguments for a particular selection of dimensionless groups required in the modeling of representative problems. Although the set of dimensionless parameters required for the maintenance of complete similarity in flow systems with chemical reactions can be derived without difficulty,[3] practical applications always necessitate the judicious choice of a small number of dimensionless groups which are considered to be of overriding importance for the problem under study. The ultimate justification for this type of artistry must be an empirical demonstration of the utility of the derived scaling rules. The paper would be strengthened if the practical value of the correlation parameters were demonstrated in greater detail.

M. W. Thring[4]

The use of cold aerodynamic models for studying the mixing and flow patterns in various types of industrial flames is steadily increasing, and a careful study of methods of allowing for the change of density of the gases that occurs on combustion is extremely valuable. In addition to the examples mentioned in this paper, we have done a fair amount of work on the distribution of residence times of fuel particles determined by means of a cold-air model of the radiant combustion chamber of a large corner-fired, pulverized-coal, watertube boiler. Here we eventually used the first of the three similarity conditions corresponding to Case A of the paper; that is, we enlarged both the primary and secondary-air nozzles in relation to the rest of the combustion chamber so that our model was a model of a full-sized combustion chamber in which the fuel and air streams were regarded as going in, both having the correct jet momentum and both the correct mass flow, but having the density of the flame combustion products. The distribution of residence times was determined by inserting a quick pulse of very fine powder into one of the streams and then determining the distribution curve in time of light obscuration at the exit.

A great deal of work has been done with cold isothermal models of gas-turbine combustion chambers, and here again consideration of the flow pattern indicates that the air holes in the sides of the combustion chamber should be enlarged relatively in the model to the size that they would have if they were throwing their air in with the correct jet momentum and mass flow, but having the density of the combustion products. This is very important as a geometrically correct model will give much too high a penetration of the main stream by these side jets.

We are now going on to use the same model principle in studies of mixing and flow patterns with the type of pressure-jet oil flame without downstream air injection used in boilers and furnaces. Here again it will be necessary to replace the sheet of liquid oil by a gas stream entering through a narrow conical annulus which has the same forward and spin momentum as the oil stream and mass flow, while the combustion air going through the register around is also giving the correct forward and spin momentum and correct mass flow, but both of them are scaled to correspond to the flame density. We propose to study recirculation by putting the tracer, which in our case is nitrous oxide, into the model at a chosen point downstream and then measuring how much of it arrives at the root of the flame upstream and therefore provides flame ignition and stabilization.

Finally, it may be said, now that we have a fairly good idea of the similarity conditions as indicated in this paper, there is a very great need for a really comprehensive set of model studies of general systems corresponding in a simplified way to the types of flow pattern actually used in practice. We hope in my department to make some contribution to these comprehensive studies, but obviously it would be valuable to have several laboratories working in this field.

Authors' Closure

The authors appreciate the comments of Professors Penner and Thring, who are outstanding exponents of the use of dimensional analysis and modeling in their respective countries. It is the authors' good fortune that the need for confirming demonstrations of the similarity rules, as mentioned by Professor Penner, is met not only by three companion papers[5,6,7] but by the excellent examples given by Professor Thring. A recent article by Curtet[8] is also pertinent to problems of combustion modeling in which jet action is involved. Finally, it should be emphasized that proficiency and assurance in the use of modeling techniques comes only with practice. Thus, researchers entering the field of modeling should gain considerable familiarity with this technique before undertaking the more complicated aspects of modeling.

---

[2] Daniel and Florence Guggenheim Jet Propulsion Center, California Institute of Technology, Pasadena, Calif.

[3] S. S. Penner, "Chemistry Problems in Jet Propulsion," chapter 25, Pergamon Press Limited, London, England, 1957.

[4] Professor of Fuel Technology and Chemical Engineering, University of Sheffield, Sheffield, England.

[5] J. H. Chesters, "The Aerodynamic Approach to Furnace Design," published in this issue, pp. 361-370.

[6] G. C. Whitney, "Use of Models for Studying Pulverized-Coal Burner Performance," published in this issue, pp. 380-382.

[7] R. W. Curtis and L. E. Johnson, "Use of Flow Models for Boiler-Furnace Design," published in this issue, pp. 371-379.

[8] R. Curtet, "Confined Jets and Recirculation Phenomena With Cold Air," *Combustion and Flame*, vol. 2, 1958, p. 383.

J. KENNETH SALISBURY
Consulting Engineer,
Atherton, Calif. Fellow ASME

A New Performance Criterion for Steam-Turbine Regenerative Cycles

This paper presents an explanation and discussion of a heretofore unexploited criterion of the performance of the regenerative cycle. It is demonstrated that this simple criterion, the flow-weighted average extraction enthalpy, embodies in a single variable all of the effects of extracting steam for feedwater heating, and permits quick and direct estimation of the effect of any cycle change on heat rate. Thus the new variable is useful in both design and performance monitoring of the thermal cycle, as well as in estimating the improvement that is realized by regeneration.

IT IS THE PURPOSE of this paper to introduce a new concept of the regenerative cycle that utilizes a single variable as a criterion of the thermodynamic excellence of the feedwater-heating system for any given set of cycle boundary conditions. This variable is responsive to any change whatsoever that may occur within the heater system, and moreover quantitatively indicates the net effect on the heat rate. Since it is an over-all criterion, readily obtainable from relatively few data, it is believed that its applications are manifold in areas such as analysis of cycle designs, appraisal of the effect of changes, and monitoring of the performance of existing systems, for comparison with guarantees.

The variable, designated at H_e, is defined concisely as the flow-weighted enthalpy of extraction steam. It is, in effect, the "center of gravity" of the turbine extraction enthalpies. Its simplicity as a concept and the ease with which it may be determined in an actual power plant enhance its usefulness. It is probably true, in fact, that those who have worked with regenerative cycles have worked around the concept many times, without identifying it, or exploring its usefulness as a tool.

It is the primary purpose of this paper to present a clear, concise exposition of the H_e concept, rather than to develop all of the ramifications of its use. It is a secondary purpose to indicate a few of the quantitative relationships that have been developed in approaching the larger problem of complete performance monitoring.

Contributed by the Power Division and presented at the Annual Meeting, New York, N. Y., November 30–December 5, 1958, of THE AMERICAN SOCIETY OF MECHANICAL ENGINEERS.

NOTE: Statements and opinions advanced in papers are to be understood as individual expressions of their authors and not those of the Society. Manuscript received at ASME Headquarters, September 15, 1959. Paper No. 58—A-205.

PART 1
THE H_e CONCEPT

Consider the simplified system of Fig. 1. In this system the flow-weighted enthalpy of the extracted steam, that is the "effective extraction enthalpy," is designated as H_e. The entire heater system may be considered as a single thermodynamic entity, designated by the dash lines enclosing it. Since this is a thermodynamic system into and out of which energy is flowing,

Nomenclature

A = approximate value of Δ_{hs} [see Equation (22)], dimensionless
b = drain quantity, fraction of condensate flow
B = boiler flow from heater system in an actual cycle
C = condensate flow to heater system in an actual cycle
E = energy flow
f = extraction steam used energy as fraction of the total [see Equation (6)]
h_c = condensate enthalpy leaving the hot-well, Btu/lb
h_f = final feedwater enthalpy, Btu/lb
H_c = turbine exhaust enthalpy, Btu/lb
H_e = effective extraction enthalpy, Btu/lb
H_e' = pseudo-H_e
H_g = enthalpy of gland steam, Btu/lb
H_1 = throttle steam enthalpy or low-pressure heater extraction enthalpy, Btu/lb
H_L = enthalpy of steam leaving the system, Btu/lb
H_n = effective extraction enthalpy of all heaters above low-pressure heater, Btu/lb
k = drain-cooler effectiveness, dimensionless
K = constant [see Equation (56)], Btu/lb
L = approximate loss in heat rate [see Equation (31)], dimensionless
n = heater number, or exponent (see footnote 9), dimensionless
P = power, Btu/hr
PG = fractional improvement in heat rate due to regeneration, dimensionless
q = heat rejected, Btu/hr
Q = heat supplied, Btu/hr
r = heat rate, Btu/Btu
r_c = nonregenerative heat rate of a nonreheat system, Btu/Btu
r_n = regenerative heat rate of a nonreheat system, Btu/Btu
R_1 = enthalpy rise across low-pressure heater, Btu/lb
w = extraction flow per lb of condenser flow, dimensionless

Subscripts

bp = back pressure
c = condenser
d = drains
e = extraction or external
g = gland
hs = heater system
m = make-up
p = pump

Symbols

θ_x = fractional change in H_e' due to extraneous flow x, dimensionless
Δ = designation for increment
Δ_x = fractional change in heat rate due to change in component x, dimensionless
η = efficiency, dimensionless

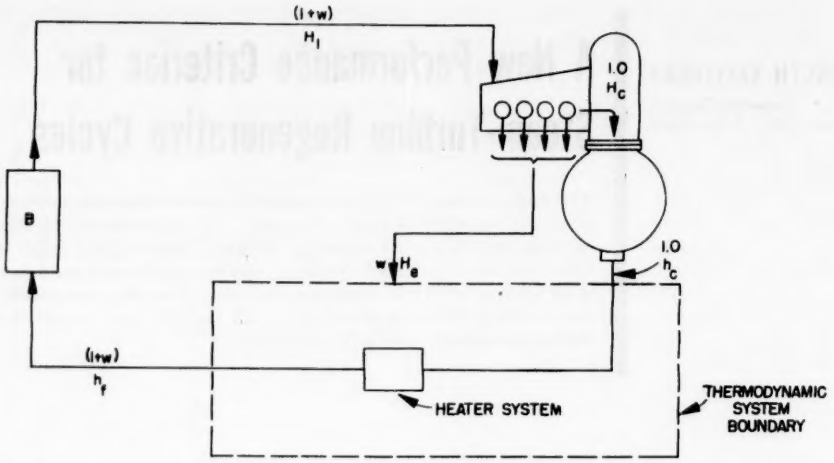

Fig. 1 Simplified regenerative cycle

the First Law of Thermodynamics may be applied. For the system shown, the steam conditions and final feedwater enthalpy h_f are fixed. Writing the First Law equation,

$$wH_e = (1 + w)h_f - 1(h_c) \tag{1}$$

Solving for H_e

$$H_e = \frac{h_f - \left(1 - \frac{w}{1 + w}\right) h_c}{(w/1 + w)} \tag{2}$$

in which it will be recognized that

$$\frac{w}{1 + w} = \frac{\text{extraction flow}}{\text{throttle flow}} = 1 - \frac{\text{condenser flow}}{\text{throttle flow}} \tag{3}$$

Note in Equations (2) and (3) that H_e depends on only two liquid enthalpy values, and on the ratio of condenser to throttle flow. That is, *H_e may be evaluated in this simplified system through knowledge of only four quantities, without any knowledge whatsoever of thermal phenomena that take place within the thermodynamic system.* It must be recognized, however, that the flow ratio is, itself, dependent on the thermal phenomena within the system and determines the value of H_e for given inlet and outlet enthalpy values. This property of H_e—its reflection of every aspect of the thermal system and representation thereof in a single enthalpy value—makes it valuable as a criterion of the excellence of the system and, in fact, as a complete and quantitative description of the effectiveness of the system in reducing heat rate.

Relationship Between H_e and Gain Due to Regeneration

To explain the relationship quantitatively requires a brief review of certain previously established concepts [1][1] of turbine cycle heat rate. For present purposes, to facilitate the explanation, a simple regenerative cycle, uncomplicated by reheat, will be used. The methods are also applicable, however, to the low-pressure portion of a reheat cycle, where most of the gain due to regeneration occurs.

The heat rate of a nonregenerative cycle depends only on the steam conditions (inlet pressure and temperature, and exhaust pressure) and the turbine efficiency. Occasionally the "theoretical nonextraction heat rate" is used. This quantity, for which tables may be made by using only the steam tables (see ref. [1], p. 288), is found by considering the turbine efficiency to be 100 per cent. When the theoretical nonextraction heat rate is divided by the turbine efficiency, the actual nonextraction heat rate is found. Thus

$$\text{Nonext. heat rate} = \frac{\text{Theoretical S.R.}\ (H_1 - h_c)}{\eta_t} = \frac{\text{Theor. nonext. heat rate}}{\eta_t} \tag{4}$$

When regenerative feedwater heating, through the use of staged heaters, is employed, the nonextraction heat rate is improved by a fractional amount, PG.[2] Thus

$$\text{Extraction heat rate} = \text{Nonext. heat rate}\ (1 - \text{PG}) \tag{5}$$

where PG may vary from very small values to approximately 0.15, depending on the excellence of design and performance of the heater system. It previously has been demonstrated [1] that PG is a function of numerous variables, such as the number and distribution of feedwater heaters, final feedwater temperature, and throttle pressure.

Despite the dependence of PG on many variables, it must be recognized that basically the gain in heat rate achieved by regenerative feedwater heating results from development of a fraction of the total power output by extraction steam, used to regeneratively heat the condensate stream, thus avoiding the rejection of latent heat in the condenser. Obviously, therefore, the greater the fraction of the total power produced by extracted steam, the greater will be the gain. If we fix the operating steam conditions and turbine efficiency, take the condenser flow to be unity, and let w be the total quantity of extraction per pound of condenser flow, it is quite obvious that we wish to make w large; it is not obvious that there may not be other pertinent effects, relating to the enthalpy at which the steam is extracted.

Because w and H_e clearly are related, since their product is the total energy input to the heater system, and because w is at least partially a criterion of the power produced by extracted steam, it seems apparent that H_e must affect the gain in heat rate achieved by regeneration. If we define a ratio f as:

$$f = \frac{H_1 - H_e}{H_1 - H_c} \tag{6}$$

[1] Numbers in brackets designate References at end of paper.

[2] This nomenclature derives from the use of G for the "theoretical gain," with an infinite number of ideal infinitesimal heaters, and P for the fraction ("percentage") of this gain achieved with a finite number of heaters in an actual cycle. Thus PG is the actual fractional gain.

it may, in fact, be shown[3] that the fractional gain in heat rate due to regeneration is given explicitly by

$$\text{PG} = 1 - \frac{\text{regenerative h.r.}}{\text{nonregen. h.r.}} = 1 - \frac{r_n}{r_c} = \frac{fw}{1+fw}\left(1 - \frac{1}{r_c}\right) \quad (7)$$

where

$$fw = \left(\frac{H_1 - h_f}{H_s - h_f} - 1\right)\left(\frac{h_f - h_c}{H_1 - H_c}\right) \quad (8)$$

Thus *PG is a function only of H_s and cycle conditions.* It is seen that the lower the value of H_s, the higher is the value of fw; by Equation (7), the higher the value fw, the greater the gain. Hence H_s is an *exclusive* criterion of the gain in heat rate, for given feedwater enthalpy h_f and steam conditions. The fractional gain may be found by using Equation (8) in Equation (7).

Use of H_s for Estimating Heat Rate. These relationships reveal an extremely useful method of approximating a regenerative cycle heat rate. Frequently the respective extraction enthalpy values may be found without difficulty. If the extraction openings are spaced properly, so that all of the required extraction flows are alike, the value of H_s will be the numerical average of the extraction enthalpies. Where the spacing is not so arranged, it is a simple matter to weight each extraction enthalpy for the corresponding flow, if the latter can be estimated. A first approximation of the relative extraction flows may sometimes be estimated from the enthalpy rises across the heaters, with appropriate adjustment for the contribution of flashed drains. Having the value of H_s, substitution in Equations (8) and (7) yields the gain in heat rate due to regeneration.

Note also that these relations provide a simple means of estimating the change in heat rate that results from change in the heater system. The effect of interposing a heater between two existing heaters, or of cutting out a heater, or any of many other changes, may readily be estimated without complete heat balance calculations, by simply estimating the effect on H_s. Obviously, the results are only as accurate as the estimate of the change in H_s. These simple arithmetic manipulations clearly reveal the mechanism of the heater system in a manner not heretofore recognized by the writer.

Additional means of translating directly the effect of a change in H_s into a change in heat rate are also available, as presented in Appendix (2).

The foregoing relationships, when viewed in perspective, provide an especially concise example of the interplay of the First and Second Laws of Thermodynamics. To achieve a given feedwater enthalpy we need only to satisfy the First Law relationship of Equation (1), i.e., wH_s must have a certain value. No specification whatsoever is placed upon the means by which the value is realized. H_s may be high and w low, or vice versa. The clue as to which alternative is to be preferred is given by Equation (8), which demands a low value of H_s to obtain the maximum value of fw. H_s must be low, hence w must be high. Thus the First Law dictates the value of wH_s, but the Second Law demands that H_s have the lowest possible value, for best efficiency.

Considering broadly, then, the mechanism of H_s, it is seen that the lower the value of H_s, the more nearly the system complies with the precepts of the Second Law; any irreversibility whatsoever that occurs within the heater system will increase H_s, thus making it a simple criterion of the degree of excellence of the heater system, for fixed boundary conditions.

Output of Extracted Steam

Because the output due to the extraction from any opening is a linear function of the enthalpy and extraction flow at the opening, the flow-weighted enthalpy H_s may be used with the total extraction quantity w to obtain the total-output of the extracted steam.[4] That is, we may write

$$\text{Output of ext. steam} = wH_1 - \sum_{i=1}^{i=n} w_i H_i = w(H_1 - H_s) \quad (9)$$

or, relating it to the output of the condenser flow

$$\frac{\text{Output of ext. steam}}{\text{Output of condenser flow}} = \frac{w(H_1 - H_s)}{H_1 - H_c} \quad (10)$$

It is not clear from Equation (10) that H_s should be the minimum for best heat rate (maximum ratio of extraction output to condenser flow output), because $w = f(H_s)$, by Equation (1). However, solving Equation (1) for w, we have

$$w = \frac{h_f - h_c}{H_s - h_f} \quad (11)$$

Also, for future reference it is seen that

$$(1 + w) = \frac{H_s - h_c}{H_s - h_f} \quad (12)$$

and

$$\left(\frac{w}{1+w}\right) = \frac{h_f - h_c}{H_s - h_c} \quad (13)$$

Substituting Equation (11) in Equation (9) we have

$$\text{Output of ext. steam} = \frac{h_f - h_c}{H_s - h_f}(H_1 - H_s) = (h_f - h_c)\left(\frac{H_1 - h_f}{H_s - h_f} - 1\right) \quad (14)$$

The form of Equation (14) makes it immediately clear again that the lowest value of H_s gives the highest value of the extraction output per unit output of the condenser flow, hence the best heat rate. Furthermore, it is clear from Equation (11) that for a given value of h_f, w is the maximum when H_s is the minimum, and vice versa. Thus we may conclude, in summary, that for specified final feedwater enthalpy and steam conditions

1 The value of wH_s is fixed.
2 The lowest value of H_s gives the best heat rate.
3 The highest value of w gives the best heat rate.
4 Accurate quantitative evaluation of the gain due to regeneration may be accomplished through knowledge of H_s alone.

PART 2
USES OF H_s IN MONITORING PERFORMANCE

H_s has numerous applications in performance monitoring. A few of these are covered herewith.

Finding Turbine Efficiency From Operating Data

Consider the method by which H_s may be used to determine the efficiency of a turbine operating on the regenerative cycle. Turbine efficiency, for our purposes, is defined as the *used energy of*

[3] See Appendix (1) for derivation.

[4] Note that throughout this entire discussion all output quantities are used as "internal output," the output of the machine before application of mechanical and electrical losses. Where only the net electrical output is known, these losses must be added to it to obtain the internal output. The effect of such losses on heat rate is always obvious, and does not involve the thermal phenomena with which we are chiefly concerned.

one pound of condenser flow divided by the available energy between inlet and exhaust. If H_e is known from measurements,[5] the following relationship obtains, for a condenser flow of 1 lb.

Total output per lb of cond. flow

$$= (H_1 - H_c) + w(H_1 - H_e) \quad (15)$$

Hence $$H_c = \left(H_1 - \frac{\text{output}}{1 + w}\right)(1 + w) - wH_e \quad (16)$$

Note that the second term of the first factor is the "output per lb of throttle flow," given by

$$\text{Output per lb of throttle flow} = \frac{3413}{\text{Throttle steam rate}} \quad (17)$$

Thus Equation (16) may be written alternatively as

$$H_c = \left(H_1 - \frac{3413}{\text{T.S.R.}}\right)(1 + w) - wH_e \quad (18)$$

in which the first factor is analogous to the form normally used in a nonextraction cycle for finding exhaust enthalpy.

Having the exhaust enthalpy H_c the efficiency of the turbine may be found by the usual method. Note that for the simplified cycle of Fig. 1, in addition to the four fundamental measurements ideally required to determine H_e, only two additional measurements are required to find H_c, namely, H_1 and the throttle steam rate. It is to be emphasized that the method is applicable even in the most complex cycles, provided only that the true H_c, flow-weighted enthalpy of the extracted steam, is used. These simplifications over the usual method establish the utility of H_e for monitoring turbine efficiency.

Effect of Turbine Efficiency Change on Heat Rate, Δ_η. Having found the stateline end point H_c it may be compared with the standard value for existing conditions, and the difference interpreted as an effect on heat rate. The fractional change in heat rate, Δ_η, due to change in turbine efficiency may be found by comparing the actual with the expected power of the condenser flow, as shown, and relating the difference to the total power.

By subtracting the output of the extraction steam, $w(H_1 - H_e)$, from the total output, the output of the condenser flow is found. The output of the condenser flow, P_c, is directly related to the turbine efficiency. When it is compared with the expected output at the guaranteed turbine efficiency, a small difference ΔP_c will be found, in general. This difference is attributable to variation of the operating turbine efficiency from the expected value. It modifies the useful output against which the heat supplied is charged. Since the heat rate is inversely proportional to the output, Δ_η may be expressed in terms of the change in power of the condenser flow, ΔP_c, from the expected value, P_c, divided by the total power. Note that such an approach makes no assumption whatsoever as to the location of the stateline, because the *true* operating H_c, obtained from test data, is used in obtaining the extraction output P_e. This method will therefore be more accurate than methods which make use of a *predicted* stateline, the exact location of which usually is in considerable question.

To arrive at a relationship for Δ_η we may write the heat rate in terms of the heat supplied and the total power output

$$r = \frac{Q}{P_c + P_e} \quad (19)$$

for design turbine efficiency. When the turbine efficiency is not equal to the design value

$$r' = \frac{Q}{P_c + \Delta P_c + P_e} \quad (20)$$

Then, since Q is constant,

$$\Delta_\eta = \frac{r'}{r} - 1 = \left(\frac{\Delta r}{r}\right)_\eta = \frac{-\Delta P_c}{P_c + \Delta P_c + P_e} \approx \frac{-\Delta P_c}{P_t} \quad (21)$$

The problems involved in measuring output are not minimized here. Obviously this is the most difficult part of the entire procedure. It is clear that existing methods of measuring power may be used for a simple regenerative cycle and also for reheat cycles, where the low-pressure portion of the reheat cycle has its own alternator. In monitoring the low-pressure portion of a reheat cycle, however, it is necessary to deduct calculated output values (based on exhaust enthalpy measurement) of portions of the system above the reheat point, when these contribute to the power of the low-pressure alternator.

Monitoring the Heater System

Since the net result of the installation of feedwater heaters, with fixed turbine efficiency, is an increase in feedwater temperature and the extraction of w lb of steam per lb of condenser flow, the gain that results from feedwater heating must be exclusively a function of w and h_f. Since w is a function only of H_e, h_f, and h_c, it is obvious that for constant h_f and h_c the gain in heat rate due to feedwater heating is a function of H_e *only*. This reasoning confirms the previous analysis, and makes it apparent that *all* changes in the heater system that affect its thermodynamic performance also affect the value of H_e. The design heat balance infers a specific value of H_e. This value varies with load and is amenable to calculation from the heat balances themselves. For monitoring purposes it will be found that it is most useful to employ as a reference a plot of the design values of H_e against stage pressure of the highest extraction stage, or h_f; obviously, if the latter is used, the plot infers that the top heater is in service. When the top heater is not in service, a lower value of H_e will be obtained at a given throttle flow, but a higher value will result at any given h_f, reflecting the loss due to removing a heater.

To monitor the performance of the heater system it is necessary only to find the actual operating value of H_e by measurement and to compare it with the design value under the same conditions. When the difference between operating and design values has been found, the percentage increase in heat rate, Δ_{hs}, may be determined from any of various relationships, depending on the degree of accuracy required. One method is to use Equations (5), (7), and (8) to find the change in the gain, PG, hence the loss in heat rate. Explicit relations usually are more convenient, however. These relationships [derived in Appendix (3)] are, in order of increasing accuracy:

$$\Delta_{hs} = \left(\frac{\Delta r}{r}\right)_{hs} \approx (r - 1)w\,\frac{\Delta H_e}{H_e - h_c}\ [\equiv A, \text{ by definition}] \quad (22)$$

More accurately:

$$\Delta_{hs} \approx A\left[1 + \left(\frac{r}{r - 1}\right)A - \frac{\Delta H_e}{H_e - h_f} + \cdots\right] \quad (23)$$

And finally, the exact relationship is:

$$\Delta_{hs} = \frac{A\Big/\left(1 + \dfrac{\Delta H_e}{H_e - h_f}\right)}{1 - \left[\left(\dfrac{r}{r - 1}A\right)\Big/\left(1 + \dfrac{\Delta H_e}{H_e - h_f}\right)\right]} \quad (24)$$

[5] A method is described in Appendix (4) by which H_e may be found for an actual cycle by means of a few accurate measurements supplemented by corrections for miscellaneous minor effects that usually are present in actual cycles. The corrections may be "prescheduled" from results of previous tests, or they may be found from operating instruments, because they are small.

It may be shown that in normal cycles the percentage change in heat rate is roughly equal to the percentage change in H_e. Any of these relations may be used to find Δ_{hr} in a given situation, provided only that ΔH_e in Equations (22), (23), or (24) is the *true* value, attributable to heater faults only. It must not include extraneous variations in H_e that arise due to deviations of the exhaust pressure from design conditions, or other factors, as later discussed.

It has been found that for performance monitoring the relationship of Equation (22) is satisfactory for general use. When ΔH_e becomes large enough for the error in this relationship to be significant, it is also large enough for rather drastic measures to be taken in the power plant, and small errors in the estimation of the loss are relatively insignificant, compared to the loss itself.

Examples of High H_e. It is recognized at once that a given feedwater temperature may be attained by an infinite number of combinations of extraction quantities removed from the respective openings. In the poorest possible arrangement, all extraction might be taken from the turbine inlet at an enthalpy H_1, with sufficient throttling in the extraction line to hold the final feedwater enthalpy at h_f. In this instance the value of fw in Equations (8) would be zero, and no gain would result.

As another example, all of the extraction might be taken from the top extraction opening. In this case, $H_e = H_{top}$. In such a system the value of H_e is much higher than it would be if additional heaters were used below the top heater, to provide stepwise heating. Therefore the gain due to feedwater heating is considerably smaller. With multiple heaters, if all of the extraction quantities are equal, H_e is the numerical average of the enthalpies of all of the extractions. This average value is considerably lower than H_e ($= H_{top}$) of the hypothetical one-heater system, hence the heat rate is appreciably better. The problem of obtaining the *minimum* value of H_e (hence maximum w), obviously, is one of number and distribution of the extraction openings. It has been discussed at length in Ref. [1]. It is there shown that, for only slightly idealized conditions, minimum heat rate occurs when equal rises in enthalpy exist across the feedwater heaters.

Qualitative Monitoring of the Heater System. Occasionally it may be desirable to use only qualitative monitoring of a heater system. In these circumstances an alternative method is available. As discussed, the feedwater might be heated to the final temperature by using the top extraction opening only, if one were to ignore secondary effects in such a hypothetical system, such as increase in the pressure drop in the extraction line and increase in the heater terminal difference. The difference between the extraction enthalpy for the top heater, H_t, and the actual H_e is a measure of the additional thermodynamic gain achieved by using heaters below the top heater. It is therefore obvious that if the measured value of H_e is subtracted from the measured value of H_t we obtain $(H_t - H_e)$, a "figure of merit" that is applicable to the remaining heaters, since this difference represents the reduction in H_e achieved by using multiple heaters. Any fault in the heater system will be revealed by a decrease in the figure of merit, $(H_t - H_e)$. One of the chief virtues of such a system is that use of H_t as a reference enthalpy for H_e eliminates the need for correcting for turbine inlet conditions, because it establishes the location of the stateline. Furthermore, the top extraction usually is in the superheat region, simplifying enthalpy measurements.

Summary of Heater System Monitoring. It is clear, then, that shift of H_e to a higher value through such irreversibilities as terminal difference, pressure drop in the extraction lines, flashing of heaters, or the removal of a heater from service, causes increase in heat rate. In each instance the heating performed by the heater in question is reduced in amount. The reduction in duty is assumed by the next higher heater, requiring an increase in the extraction stream from its opening to accomplish the result. This extraction of a large quantity of steam from a higher point in the machine causes the rise in the value of H_e, reflecting the loss that has occurred.

Thus we may categorically state that *any* fault that may occur in the heater string will lead to values of H_e higher than design values. For this reason H_e, a primary determinant of heater performance, may be used in monitoring the effectiveness of the entire heater string, taken as a unit. Comparison of the actual value (obtained from four measurements, ideally)[6] with the design value (obtained from design heat balances) will reveal any faults that may have developed in the heater system. Furthermore, the change in plant heat rate caused by such deviations from the design value of H_e can be quantitatively evaluated by Equations (22), (23), or (24). It is apparent, then, that the H_e concept has an important application in heater-system monitoring, in addition to its other uses in design and analysis of regenerative plants.

Evaluation of Effect of Exhaust Pressure on Heat Rate, Δ_{bp}

It is convenient to use H_e in many types of analysis of turbine regenerative cycles, because it is a specific criterion of the effect of the heaters on heat rate. In analysis of exhaust pressure effects on heat rate, for example, one must consider carefully the changes in the heater system caused by the change in condensate enthalpy leaving the hot well. To illustrate this application we will outline the method of analysis. Detailed derivation of the results is given in Appendix (3).

Change in the exhaust pressure of the low-pressure turbine has two effects which contribute through the *turbine* to the change in heat rate: (*a*) The change in nonextraction cycle heat rate due to change in the back pressure itself (at constant turbine efficiency); and (*b*) the change in turbine efficiency that results from the change in back pressure. Our analysis of turbine effects caused by the change in exhaust pressure will be based on the assumption that the change in turbine efficiency with exhaust pressure is exactly equal to that implicit in the guarantees; this may not actually be the case, but the effect on heat rate of any variation from the design efficiency at various back pressures can be analyzed separately, and superimposed as a direct effect on heat rate, as has been discussed. In other words, Δ_{bp} is defined as the total change in cycle heat rate that results from change in exhaust pressure when the variation in turbine efficiency with exhaust pressure is in strict accordance with the designer's predictions.

A change in exhaust pressure results in a change in turbine output, which affects the heat rate. However, for a given value of heat supplied to the cycle, such a change is effective in changing the heat rate only because it affects the *heat rejected* from the system. Therefore, since the change in output with exhaust pressure is *caused* by the change in heat rejection, we may elect to ignore the change in turbine output, as such, focusing our attention only on the change in heat rejected, as a method of analysis.

Change in exhaust pressure also affects the heat rate through the *heater system*, because the condensate temperature leaving the hot-well changes, thereby imposing a different enthalpy rise on the heater system, for any given final feedwater temperature. This change in hot-well temperature changes the total extraction quantity w for two reasons. Assuming the hot-well temperature to be higher, for the moment, the resulting lower total rise across the heater system obviously will reduce the total extraction quantity required to perform the heating task, because the heat input to the condensate is reduced. If the change in extraction quantity were *proportional* to the change in rise across the heater sys-

[6] But considerably more for a cycle in which there are numerous secondary heat and mass flows.

tem, the problem would be greatly simplified. However, this is not the case. Because the higher condensate temperature results in a considerably lower enthalpy rise across the low-pressure heater, an *appreciable* percentage reduction in the extraction for this heater occurs. The higher heaters are not affected in nearly the same degree, because their rises tend to remain constant, as known by all heat-balance designers. As a consequence, the "center of gravity" of extraction enthalpy H_e increases. That is, H_e increases because a larger proportion of the total extraction quantity is taken from the turbine at the higher levels. This increase in H_e causes a reduction in the total extraction quantity [see Equation (11)] that adds to the basic reduction caused by reduction in over-all condensate enthalpy rise. In other words, the extraction quantity is reduced both because of the lower duty of the heater system, and because of the higher effective extraction enthalpy H_e. Change in the extraction quantity per pound of condenser flow constitutes a change in heat supplied, yielding a second effect of back pressure on heat rate.

Summarizing, the total effect on heat rate of an increase in exhaust pressure results from two factors. The first is the change in *heat rejected* that results from change in turbine exhaust enthalpy H_e and hot-well enthalpy h_c. The second is a change in *heat supplied* that results from a change in the extraction quantity per pound of condenser flow. These facts may be summarized by listing the factors which affect heat rate as the exhaust pressure changes:

1 Change in heat rejected per pound of condenser flow, $\Delta(H_e - h_c)$

2 Change in heat supplied, $\Delta w/(1 + w)$

(a) due to lower condensate enthalpy rise, $\Delta(h_f - h_c)$

(b) due to increase in H_e, $\Delta(H_e - h_f)$

If we quantitatively evaluate the elements listed, we may add their effects on heat rate to determine the total value of Δ_{bp}. The change in heat rejected, item (1), may readily be found under our assumption that the turbine efficiency conforms with the design value at all exhaust pressures. It is necessary only to evaluate $(H_e - h_c)$ for the design exhaust pressure and for the new exhaust pressure, using design values of turbine efficiency in both instances. The analysis of item (2), the change in heat supplied, is somewhat more complex. The fractional change in heat supplied, for constant final feedwater temperature, is equal to the fractional change in extraction per pound of throttle flow, $\Delta w/(1 + w)$.

Using H_e, the change in heat supplied may be evaluated, through consideration of the change in H_e caused by low-pressure heater changes, and the effect of exhaust pressure on heat rate thus evaluated. It is demonstrated in Appendix (3) that to a close approximation

$$\Delta_{bp} = \left(\frac{\Delta r}{r}\right)_{bp} \approx (r - 1)\left[\frac{\Delta(H_e - h_c)}{H_e - h_c} + \left(\frac{\Delta h_c}{H_e - h_c}\right)\left(1 + nw_1\frac{H_e - H_1}{R_1}\right)\right] \quad (25)$$

Equation (25) is a simplified version of the accurate relationship between heat rate and exhaust pressure, details of which are given in Appendix (3). The refinements there given are necessary only in the event of large deviations in exhaust pressure. It is considered that the simplicity of Equation (25) justifies its use in all but the most extreme situations. When heat is rejected by drains flashed from the lowest heater to the hot well an additional term must be included to account for changes in its value. Frequently the effect is small, however, and the form of Equation (25) is adequate.

Corrections of H_e to Standard Operating Conditions

To compare measured H_e values with design values for purposes of heater monitoring, it is necessary that all extraneous changes in H_e caused by deviations from standard operating conditions be removed from the test value of H_e. Some of the effects are discussed hereafter.

The exact location of a turbine stateline at points intermediate between the inlet and exhaust is not normally known by turbine designers, because it is essentially impossible to obtain representative test values of enthalpy at intermediate points, regardless of the care exercised in providing instrumentation to obtain it. Unfortunately, the uncertainty as to location of the stateline causes similar uncertainty in determination by the manufacturer of the exact value of the design H_e. The effect of variation from the predicted value of H_e due to poor estimation of the location of the stateline is indistinguishable from variations in heat rate caused by faults in the heater system. For this reason it is recommended that test values of H_e be established during initial operation of the plant, so that these values later may be compared with test values, for detecting faults. That is, since it is difficult to separate the effect of error in estimating the stateline and faults in the heater system, any errors in the estimated stateline location may best be found by test when the feedwater heating equipment is new, and presumably in perfect condition.

Variations from design steam conditions cause variations from design values of H_e, making it necessary to obtain corrections by analytical means. H_e varies as the distribution of extraction quantities varies. For example, as previously discussed, when turbine exhaust pressure is changed, an appreciable change occurs in the fraction of the total extraction that goes to the low-pressure heater. This change in distribution of the extraction will, in itself, cause changes in H_e. Furthermore, changes in location of the stateline resulting from changes in initial steam conditions change the value of H_e.

Nevertheless, *for any operating condition whatsoever*, a "design" value of H_e may be found, predicated on both heaters and turbine performing equal to guarantee. These values, found by heat balance calculation for the applicable operating conditions, may be plotted as a function of h_f. Obviously they may also be found by test. Absolute values found by calculation may vary somewhat from the true values for the machine, but calculated *changes* in H_e with operating conditions will be quite accurate. Thus it is possible to determine "correction factors" applicable to H_e in much the same manner that heat rate correction factors or steam rate correction factors normally are obtained. These correction factors may then be applied to test values of H_e, and the corrected results compared with design values for the evaluation of performance of the heater system.

Estimation of Corrections to H_e. Alternatively, change in H_e with initial conditions may be estimated. Consider, for a moment, the estimation of changes in H_e with changes in initial temperature. When H_e is plotted against h_f it is plotted, in effect, against heater pressures. If h_f and the exhaust pressure are fixed, all of the heater pressures are also fixed, regardless of initial temperature. Thus the relative distribution of extraction among the various extraction openings is identical with that under design conditions. For this reason, changes in H_e will be equal to changes in H read on the Mollier chart along an imaginary constant pressure line passing through the design value of H_e on the design stateline. In this manner, if the location of the stateline at any off-design temperature is known, the change in H_e at a given h_f may be estimated with excellent accuracy.

The estimation of ΔH_e with changes in initial pressure is somewhat more difficult, particularly where the inlet of the turbine is equipped with multiple control valves, overload valves, and stage bypass valves. However, for a normal reheat machine no control

valves are used at the inlet to the reheat turbine. Thus the pressure at the inlet determines h_f and vice versa. Once the relationship between H_e and h_f is found for the machine (from either design or test data) it will not change with variation in inlet pressure, at a given exhaust pressure, provided the stage areas of the turbine remain constant.

Variations in H_e with exhaust pressure occur because of the resulting large changes in low-pressure extraction. The method of handling changes in exhaust pressure presented in Appendix (3) makes it possible to estimate the magnitude of the change in H_e that results from changes in exhaust pressure. It is there shown that

$$\Delta H_e \approx n \frac{w_1}{w} \left(\frac{H_e - H_1}{R_1} \right) \Delta h_e \qquad (26)$$

where all terms are known from the design heat balance, except Δh_c, which results from the change in exhaust pressure. From this relationship and the design heat balances, changes in H_e with exhaust pressure may be found for any specified value of h_f.

In practice, it probably will be unnecessary to evaluate changes in H_e with changes in initial pressure and temperature, for purposes of monitoring a heater system. Values of H_e will be determined by test when the entire plant is in new condition, and used as reference values for future comparisons. However, such an approach is not reasonable with respect to variations caused by exhaust pressure, because exhaust pressure changes occur daily and seasonally. It therefore will probably be desirable to use corrections to H_e of the form shown in Fig. 2, for the purpose of correcting measured values to design exhaust pressure, for comparison with design H_e.

Changes in turbine efficiency affect H_e in an indeterminate way, depending on where in the turbine the fault lies. Obviously a fault below the low-pressure extraction point will not cause a change in the enthalpy at the higher levels unless the stage pressures are changed through plugging from deposit or damage. Similarly, a fault in stages above the top extraction point will affect the enthalpy of all succeeding stages in about the same degree. Distributed inefficiency will raise the lower enthalpies more than the higher. Thus the effect of a turbine fault in H_e depends on where the fault lies, normally difficult to determine. That a fault exists, on the other hand, may be discovered by check of the line-to-exhaust efficiency through means already described. It is proposed as a convention that in the absence of better information the fault be considered to be distributed uniformly throughout the machine, and the change in H_e be prorated from the change in stateline endpoint in accordance with the fraction of the total used energy that lies between the inlet and H_n, previously designated as f in Equation (6). That is

$$\Delta H_e = \Delta H_c(f) \qquad (27)$$

Obviously any known facts on the effect on H_e of turbine efficiency change should be used in lieu of this relationship, when they are available.

In brief, then, for monitoring a heater system it is noted that measured values of ΔH_e (with respect to design values) will include the effect of the following items:

(1) Change in condition of the heater system due to faults of any kind.

(2) Changes in exhaust pressure from design value at the given h_f, [Equation (26)].

(3) Change in turbine inlet temperature (see above).

(4) Change in turbine inlet pressure (see above).

(5) Change in turbine efficiency [Equations (18) and (27)].

The last four of these items have an effect on H_e which must first be removed from the measured deviation to obtain the deviation in H_e resulting from heater faults. That is, for a given measured deviation ΔH_e a portion may be attributable to the last four items listed. Corrections to the measured (operating) H_e must be made to arrive at the "corrected H_e," corresponding to design cycle conditions, in order to monitor the heater system. In most applications all of these corrections will be small indeed, with the exception of item (2), the correction for exhaust pressure.

To find the effect of turbine efficiency on H_e requires a determination of the deviation from standard efficiency (or standard H_e) that may have occurred, through calculation using Equations (18) and (27), and application of a correction to the measured H_e. The fourth effect listed is of no particular significance in a reheat cycle in which the reheat turbine has no control valves. The third item may be estimated from the turbine stateline, as discussed. The second item sometimes may be of appreciable magnitude, but its effect may be evaluated by the use of Equation (26) and subtracted from the total. When the basic ΔH_e resulting from heater faults is found, it may be interpreted as a change in heat rate through the use of Equations (22), (23), and (24), thus yielding Δ_{hs}, the fractional change in heat rate due to heater faults.

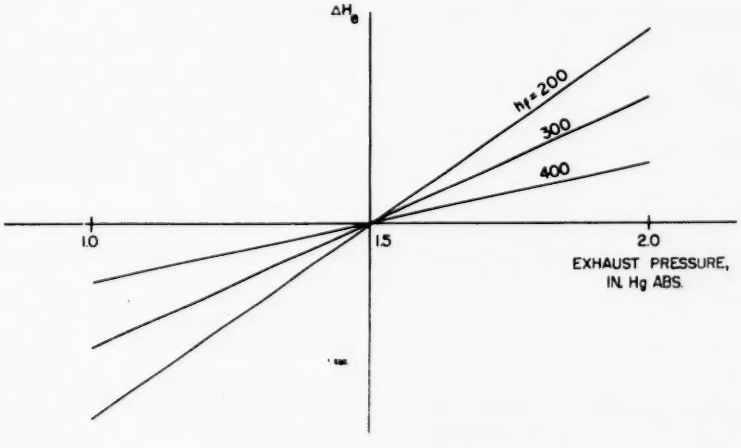

Fig. 2 ΔH_e correction for exhaust pressure

APPENDIX

(1) Gain in Heat Rate as a Function of H_e

If we let

$$f = \frac{H_1 - H_e}{H_1 - H_c} \tag{6}$$

we may find the gain in heat rate due to regeneration in terms of H_e and cycle constants. With regeneration the extra power produced by extraction steam is produced at 100 per cent thermal efficiency, i.e., a heat rate of 1.0 Btu/Btu. The total power produced then may be shown as follows:

P_c at a heat rate of r_c

P_e at a heat rate of 1.0

yielding $(P_e + P_c)$ at a heat rate of $\left[r_c - \frac{P_e}{P_e + P_c}(r_c - 1)\right]$

$$\text{Gain in heat rate} = \left(\frac{P_e}{P_e + P_c}\right)(r_c - 1) \tag{28}$$

PG, the fractional gain in heat rate

$$= \left(\frac{P_e}{P_e + P_c}\right)\left(1 - \frac{1}{r_c}\right) \tag{29}$$

However, under the definition of Equation (6),

$$\frac{P_e}{P_e + P_c} = \frac{w(H_1 - H_e)}{w(H_1 - H_e) + (H_1 - H_c)} = \frac{fw}{1 + fw} \tag{30}$$

Hence the gain in heat rate due to regeneration, by Equation (29), is

$$\text{PG} = \left(\frac{fw}{1 + fw}\right)\left(1 - \frac{1}{r_c}\right) \tag{7}$$

(2) Derivation of the Quantitative Effect of Change in H_e on Heat Rate

Because H_e is directly related to the effectiveness of the heater system in reducing heat rate, there obviously is a relationship between the fractional change in H_e and the fractional change in heat rate. To find the relationship let us assume fixed final feedwater enthalpy and condensate enthalpy entering the heater system, and a constant condenser flow of unity. It has previously been shown[7] that

$$L = (r - 1)\frac{\Delta q/q - \Delta Q/Q}{1 + \Delta Q/Q};$$

$$\text{when } \Delta q/q = 0, \quad L = (r - 1)\frac{-\Delta Q/Q}{1 + \Delta Q/Q} \tag{31}$$

A change in H_e causes a change in Q only by virtue of the change in extraction quantity (per pound of condenser flow) required to heat the condensate to the specified final feedwater temperature. Recognizing this fact and taking $\Delta q/q = 0$, because the condenser flow is constant at unity,

$$\frac{\Delta r}{r} \approx L \approx -(r - 1)\frac{\Delta w}{1 + w} \tag{32}$$

To find the effect of ΔH_e on heat rate we need only to find its effect on the extraction quantity w since this measures the change in heat supplied.

[7] Ref. [1], p. 375, Equation (10).

It has been shown that

$$w = \frac{h_f - h_c}{H_e - h_f}; \quad (1 + w) = \frac{H_e - h_c}{H_e - h_f}; \tag{11) (12}$$

$$\left(\frac{w}{1 + w}\right) = \frac{h_f - h_c}{H_e - h_c} \tag{13}$$

Differentiating Equation (11) and dividing by Equation (12), we have

$$\frac{dw}{1 + w} = -w\frac{dH_e}{H_e - h_c} \tag{33}$$

For values of ΔH_e that are small then,

$$\frac{\Delta w}{1 + w} \approx -w\left(\frac{\Delta H_e}{H_e - h_c}\right) \quad \text{(approximately)} \tag{34}$$

so that by Equation (32)

$$\frac{\Delta r}{r} \approx (r - 1)w\frac{\Delta H_e}{H_e - h_c} \quad [\equiv A, \text{ by definition}] \tag{22}$$

This relationship proves to be sufficiently accurate for most purposes. It is of great usefulness in monitoring the heater system. Because of its simplicity, minor inaccuracies may be excused in any but the most precise work.

While Equation (22) is the most useful form of all such relationships, it nevertheless is desirable to examine the error incurred by its use in any given case. Designating the value of the fractional change in heat rate given by Equation (22) as A, it may be shown that the exact value is given by

$$\frac{\Delta r}{r} = \frac{A \Big/ \left(1 + \frac{\Delta H_e}{H_e - h_f}\right)}{1 - \left[\left(\frac{r}{r - 1}A\right) \Big/ \left(1 + \frac{\Delta H_e}{H_e - h_f}\right)\right]} \tag{24}$$

and that, if A and ΔH_e are small, Equation (24) may be written as

$$\frac{\Delta r}{r} = A\left[1 + \left(\frac{r}{r - 1}\right)A - \frac{\Delta H_e}{H_e - h_f} + \ldots\right] \tag{23}$$

(3) Derivation of the Effect of Exhaust Pressure on H_e and Heat Rate

The loss in heat rate due to changes in heat rejected and heat supplied is given to a first approximation[8] by

$$L = (r - 1)\frac{(\Delta q/q) - (\Delta Q/Q)}{1 + \Delta Q/Q} \tag{31}$$

For small changes in heat supplied,

$$L \approx (r - 1)(\Delta q/q - \Delta Q/Q) \tag{35}$$

For large changes in $\Delta Q/Q$ the denominator in Equation (31) must be used.

To find the change in heat rate that results from change in exhaust pressure, according to the discussion in the text, we may then write, by Equation (35)

$$\Delta_{bp} = \left(\frac{\Delta r}{r}\right)_{bp} \approx \left[\frac{\Delta(H_c - h_c)}{H_e - h_c} - \frac{\Delta w}{1 + w}\right] \tag{36}$$

[8] The *exact* loss is found from $\frac{\Delta r}{r} = \frac{L}{1 - L}$, but L is normally so small that Equation (31) is usable.

The first term within the bracket corresponds to item (1) listed in the text. It may be found by using the Mollier chart, the steam tables, and the guarantee turbine efficiency. The second term within brackets represents the sum of the two effects given under item (2) in the text. Because determination of the first term is reasonably obvious, we will devote primary attention to evaluation of the second term within brackets.

Under the definiton of H_e we have seen that

$$w = \frac{h_f - h_e}{H_e - h_f} \tag{11}$$

When the exhaust pressure rises, h_c increases, so that the value of the numerator decreases, reducing w. This is by far the larger effect. Shifting of the center of gravity of the extractions to a higher level results in an increase of the H_e in the denominator. This causes a further decrease in w, although the effect is secondary. To evaluate $\Delta w/(1 + w)$ we may write from Equation (11)

$$\frac{dw}{w} = \frac{-dh_c}{h_f - h_c} - \frac{dH_e}{H_e - h_f} = \frac{-dh_c}{H_e - h_f}\left(\frac{1}{w} + \frac{dH_e}{dh_c}\right) \tag{37}$$

In finding the value of (dH_e/dh_c) it has been found that consideration of the effect of change in extractions on the higher heaters yields an expression that is too complex for practical use. However, the change in extraction on the higher heaters is small, while the change in extraction on the low-pressure heater is large. This suggests the possibility of considering only the latter to affect the value of H_e, for simplification purposes, since the whole effect of the second term in Equation (37) is secondary anyway. This approach will be used to obtain a usable expression, and the error that results will be shown to be small.

If the low-pressure heater is a contact heater, the extraction flow required is directly proportional to the enthalpy rise across it. However, when the next higher heater releases drains which enter the low-pressure heater, thereby providing for a part of the heater duty, the extraction required will be proportional to some power of the rise, larger than unity, which we shall designate as n. The value of n depends on the fractional contribution of heat by flashed drains to the duty of the low-pressure heater.[9] The fractional change in low-pressure heater extraction may then be expressed as a function of the fractional change in low-pressure heater rise, (dR_1/R_1),

$$\frac{dw_1}{w_1} = n\frac{dR_1}{R_1} = n\frac{-dh_c}{R_1} \tag{38}$$

Let us now evaluate dH_e/dh_c of Equation (37) by setting down the definition of H_e

$$H_e = \frac{w_n H_n + w_1 H_1}{w_n + w_1} = \frac{w_n H_n + w_1 H_1}{w} \tag{39}$$

in which w_n and H_n refer to the total of all extractions above the low-pressure heater and the average weighted enthalpy of these extractions, respectively. Differentiating Equation (39), and neglecting changes in $w_n H_n$, since they are small,

$$\frac{dH_e}{H_e} = \left(\frac{H_1}{H_e} - 1\right)\frac{dw_1}{w} = \left(\frac{H_1}{H_e} - 1\right) n\frac{w_1}{w}\frac{dR_1}{R_1} \tag{40}$$

from which

$$\frac{dH_e}{dh_c} = -\frac{dH_e}{dR_1} = \frac{dH_e}{H_e}\left(\frac{-H_e}{dR_1}\right) \approx n\frac{w_1}{w}\left(\frac{H_e - H_1}{R_1}\right) \tag{41}$$

By Equations (37) and (41)

$$\frac{dw}{w} = -\frac{1}{w}\frac{dh_e}{H_e - h_f}\left(1 + nw_1\frac{H_e - H_1}{R_1}\right) \tag{42}$$

or, by Equations (11) and (12)

$$\frac{dw}{1 + w} = \frac{dw}{w}\left(\frac{h_f - h_c}{H_e - h_c}\right) = \frac{-dh_c}{H_e - h_c}\left(1 + nw_1\frac{H_e - H_1}{R_1}\right) \tag{43}$$

Equation (43) (converted to finite increments) may be used in Equation (36) to find the part of the change in heat rate that results from changes in the heater system when the hot-well enthalpy rises an amount Δh_c. In other words, we may write

$$\Delta_{bp} = \left(\frac{\Delta r}{r}\right)_{bp} \approx (r - 1)\left[\frac{\Delta(H_e - h_c)}{H_e - h_c} + \left(\frac{\Delta h_c}{H_e - h_c}\right)\left(1 + nw_1\frac{H_e - H_1}{R_1}\right)\right] \tag{25}$$

As noted, changes in $w_n H_n$ have been neglected in differentiating Equation (31). If changes in the higher extractions are included in the effect on H_e, the second term within the parentheses of Equation (43) is reduced by a small amount, the magnitude of which is apparent from the accurate form of Equation (41), given herewith, but not derived.

$$\frac{dH_e}{dh_c} = n\frac{w_1}{w}\left(\frac{H_e - H_1}{R_1}\right)\left[1 - \frac{\dfrac{R_1}{h_f - h_c} - \dfrac{w_1}{w}\left(\dfrac{H_1 - h_f}{H_e - h_f}\right)}{1 - \dfrac{w_1}{w}\left(\dfrac{H_1 - h_f}{H_e - h_f}\right)}\right] \tag{44}$$

Values of the bracket of Equation (44) for an eight-heater cycle normally will be in the range of 0.95–0.98. It is therefore recommended that it be taken as unity, that is, that Equation (43) be considered to be correct, with only rare exceptions.

In summary, then, to find Δ_{bp}, including the effect of changes in the heater cycle (heat supplied), as well as changes in heat rejected, Equation (25) may be used where changes are small. Where the change in heat supplied is large, and it is desired to obtain the change in heat rate with greater precision, it is to be noted that appropriate adjustment of Equation (25) may be made, including $\Delta Q/Q$ in the denominator, as shown by Equation (31), to find L.

$$L_{bp} = (r - 1)\frac{\dfrac{\Delta(H_e - h_c)}{H_e - h_c} + \left(\dfrac{\Delta h_c}{H_e - h_c}\right)\left(1 + nw_1\dfrac{H_e - H_1}{R_1}\right)}{1 - \left(\dfrac{\Delta h_c}{H_e - h_c}\right)\left(1 + nw_1\dfrac{H_e - H_1}{R_1}\right)} \tag{45}$$

$$\Delta_{bp} = \left(\frac{\Delta r}{r}\right)_{bp} = \frac{L_{bp}}{1 - L_{bp}} \tag{46}$$

To find the effect of changes in exhaust pressure on H_e only, for purposes of heater cycle monitoring, it is seen that Equation (41) may be used as an excellent approximation, or Equation (44) for greater precision.

[9] It is readily seen that n is the ratio of total heater duty to the heat supplied by the low-pressure extraction steam. In the nomenclature of Ref. [1], p. 364

$$n = \frac{1}{1 - b(1 - k)}$$

where b is the flashed drain percentage and k is drain cooler effectiveness.

(4) Evaluation of H_e in an Actual Cycle

The evaluation of H_e in a simple regenerative cycle, uncomplicated by such items as make-up, drains flashed to the condenser, gland steam, steam-jet air ejectors, and boiler-feed pump, is a relatively simple matter. Under these circumstances, the value of H_e is given by

$$H_e = \frac{h_f - \left(\frac{1}{1+w}\right) h_c}{1 - \frac{1}{1+w}} \qquad (2a)$$

In any practical heat balance such simplicity is never achieved. That is, the presence of make-up water introduced into the condenser hot-well, flashed drains from the lowest heater, gland steam to feedwater heaters, or other idiosyncrasies, destroy the simplicity of the original relationships. However, by the use of correction factors θ the true value of H_e may be determined for an actual heat balance, with the minimum number of accurate measurements.

Correction factors may be found by writing a heat balance around the thermodynamic system, including all extraneous quantities, such as boiler-feed pump energy input, heater drains, and others, and solving it for H_e in a particular form. A "pseudo" H_e, that is, based only on flow and enthalpy measurements of condensate into and out of the heater system, is extracted as a factor, designated by H_e' in Equation (47). From the residual the correction factors may be found in terms of the extraneous quantities involved. Thus the basic heat balance is used as a foundation, and secondary items are treated as perturbations, primarily to economize on accurate instrumentation, but also because this method exposes to view the effects of each of the minor losses.

That is, it appears most economical of instrumentation to determine the pseudo H_e, using accurate transducers and the form of Equation (2a) as a first approximation, and then to modify this basic value by means of the θ corrections. Since the θ effects are of small magnitude, they are amenable to measurement with less accurate instrumentation, or in some cases, to "prescheduling" from the results of previous tests. The actual value of H_e will be equal to the pseudo H_e (designated as H_e') corrected for the extraneous items, the effect of each of which is small.

That is, we may write

$$H_e = H_e' \left[1 + \sum_1^n \theta_i\right] \qquad (47)$$

in which H_e is the true value of H_e, corrected for extraneous heat quantities. The method by which corrections are found is outlined hereafter.

Referring to Fig. 3, a cycle that includes typical extraneous items, the correction factors θ will be determine . Note that the symbols B and C are used to designate, respectively, the boiler and exhaust (condenser) flow, so that an analogy with Equation (47) may be written, in which the correction terms are shown as follows:

$$H_e = \left(\frac{h_f - \frac{C}{B} h_c}{1 - \frac{C}{B}}\right) [1 + \theta_m + \theta_d + \theta_e + \theta_p + \theta_g + \ldots .] \qquad (48)$$

To evaluate H_e we write the heat balance equation for the thermodynamic system included within the dashed boundary

$$H_e(B - C + m - g) + (C + w_d)h_c + E_e + E_p + gH_g = Bh_f + w_d h_d + mH_L \qquad (49)$$

Equation (49) may be solved for H_e, and by algebraic manipulation thrown into a form similar to Equation (48). We then have

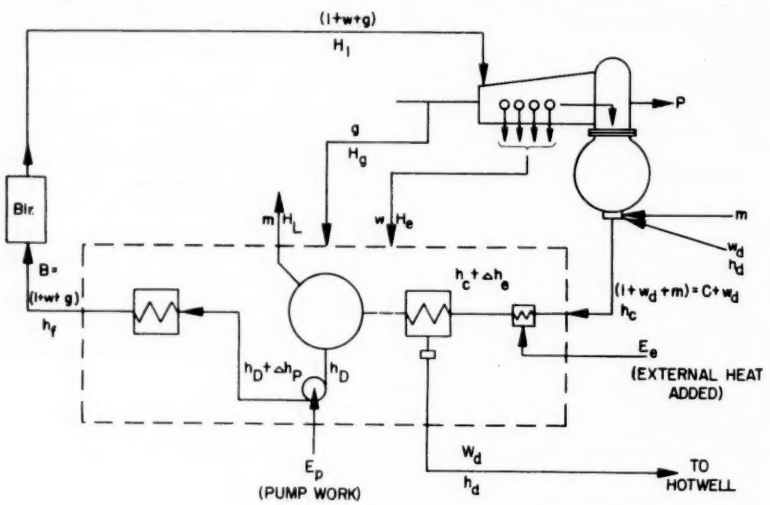

Fig. 3 Typical cycle with extraneous heat inputs and rejections

$$H_e = \left(\frac{h_f - \frac{C}{B}h_c}{1 - \frac{C}{B}}\right)\left[\frac{1 + \dfrac{(w_d/B)(h_d - h_c) + \dfrac{m}{B}H_L - \left(\dfrac{C + w_d}{B}\right)\Delta h_e - \Delta h_p - \dfrac{g}{B}H_g}{h_f - \dfrac{C}{B}h_c}}{1 + \dfrac{m - g}{B - C}}\right] \tag{50}$$

in which the first factor is H_e'.

Equation (50) yields a strictly accurate evaluation of H_e for Fig. 3. However, most of the terms in the bracket are of small magnitude, so that we may simplify it by neglecting terms of order higher than the first, to obtain an expression of the form of Equation (48). It is found that the correction terms have the following values:

$$\theta_m = K\frac{m}{B}(H_L - H_e') \tag{51}$$

$$\theta_d = K\frac{w_d}{B}(h_d - h_c) \tag{52}$$

$$\theta_e = K\left(\frac{C + w_d}{B}\right)(-\Delta h_e) \tag{53}$$

$$\theta_p = K(-\Delta h_p) \tag{54}$$

$$\theta_g = K\frac{g}{B}(H_e' - H_g) \tag{55}[10]$$

where K is defined by

$$K = \frac{(B/C)/(B/C - 1)}{H_e'} \tag{56}$$

Every variation of the heat-balance diagram will result in corresponding variations of the correction terms, hence the diagram of Fig. 3 and the analysis given here are intended only to illustrate the method by which such correction terms may be found, rather than to offer a generalized solution. The correction values given, nevertheless, cover several types of extraneous effects, and are applicable to numerous heat balances; they may therefore be used directly whenever the perturbation of the basic heat balance is of the form of those shown in Fig. 3.

Acknowledgment

The author wishes to thank the Bailey Meter Company, which sponsored this work, for its permission to publish this second step in the performance monitoring problem. Gratitude is also due Mr. H. H. Gorrie and Mr. H. T. Hoffman of this company, and Mr. C. P. Welch of The Babcock & Wilcox Co. for their helpful suggestions on the manuscript.

References

1 J. Kenneth Salisbury, "Steam Turbines and Their Cycles," John Wiley & Sons, New York, N. Y., 1950.

2 J. Kenneth Salisbury, "The Steam-Turbine Regenerative Cycle—An Analytical Approach," TRANS. ASME, vol. 64, 1942, pp. 231–245.

3 J. Kenneth Salisbury, "Power-Plant Cycle Evaluation," TRANS. ASME, vol. 71, 1949, pp. 593–604.

4 J. Kenneth Salisbury, "Analysis of the Steam-Turbine Reheat Cycle," TRANS. ASME, vol. 80, 1958, p. 1629.

[10] H_e is reserved to mean the effective extraction enthalpy of steam taken from the extraction openings, hence a correction shown to account for the effect on H_e' of gland steam. However, if true turbine exhaust enthalpy is to be found, exclusive of gland loss effect, the correction should be omitted and gland flow treated like extraction steam; that is, g must be added to w.

DISCUSSION

V. F. Estcourt[11]

The author is to be congratulated for his second major contribution on a very important subject. The difficulties and complications involved in arriving at the desired objective are evidenced by the magnitude of the two presentations which he has made during the past year. His present effort has been confined largely to the application of the Effective Extraction Enthalpy concept which he designates as H_e.

Because of the interposition of the reheater between turbine sections, the H_e concept has been applied only to the string of heaters associated with the turbine sections downstream of the reheater, i.e., the low pressure cycle. This is not considered to be a major objection since there is usually only one extraction upstream of the reheat point. Instrumentation for H_e merely replaces conventional instrumentation in the low pressure cycle. The instrumentation requirement for the high pressure cycle does not change as a result of using the H_e concept. In order to present this concept in its most favorable light, boiler feed flow must be measured between the top heater and the steam generator. The usual practice is to measure condensate flow in the low pressure portion of the feed heating cycle and compute boiler feed flow by a series of heat balances. If the boiler feed flow is measured between the top heater and the steam generator, only high pressure cycle instrumentation is required to determine test heat rate.

It follows that low pressure cycle instrumentation is required only for:

1 Determination of turbine end point for calculating turbine performance.

2 Determination of heater performance in the low pressure cycle.

It is clear that the primary reason for low pressure cycle instrumentation is to make it possible to analyze the performance of the turbine section and heaters in the low pressure cycle as separate component groups. In analyzing the H_e concept as presented by the author, it is important to consider its value when used for these two objectives.

The author's concept was applied to a turbine-generator unit for which an abundance of high accuracy test information was on hand. This unit is a nominally rated 100-mw tandem-compound machine with steam conditions of 1450 psi 1000/1000 F reheat and six stages of feedwater heating. A number of studies were made to determine the relative merits of the H_e concept as applied to this particular reheat cycle.

Of particular interest is the comparison of various alternate methods of performance determination with respect to instrumentation, man-power requirements, and the accuracy of results obtained. This comparison is summarized in Table 1. It includes in column 5 the so-called "Indirect Method" which involves computation of turbine cycle heat rate indirectly from the knowledge of plant input-output and boiler efficiency. While this method does not permit an analysis of turbine and heater

[11] Pacific Gas and Electric Company, San Francisco, Calif. Fellow ASME.

Table 1 Comparison of various methods of turbine cycle performance monitoring

	(1)	(2) Full scale ASME test procedure	(3) Medium accuracy test procedure	(4) Medium accuracy test procedure with H_e concept	(5) Indirect method
1.	**No. of measurements required**				
	a. Turbine cycle:				
	High pressure portion	28	16	16	5
	Low pressure portion	35	29	8	2
	Sub-total	63	45	24	7
	b. Generator	3	3	3	3
	c. Btu input to boiler	0	0	0	6
	d. Boiler losses	0	0	0	3
	e. Sub-total	66	48	27	19
2.	**Number of pre-programmed items**	10	10	10	2
3.	**Total (Item 1e, plus Item 2)**	76	58	37	21
4.	**Expected maximum error (turbine cycle heat rate)***				
	a. Instrumentation	0.49%	0.52%	0.52%	0.70%
	b. Pre-programmed items	Neg.	Neg.	Neg.	Neg.
	c. Computation method	Neg.	Neg.	Neg.	Neg.
	d. Total error for test heat rate	0.49	0.52	0.52	0.70
	e. Cycle correction	0.05	0.05	0.79	...
	f. Steam correction	0.03	0.03	0.03	...
	g. Total error for final test heat rate	0.57	0.60	1.34	...
5.	**No. of observers (incl. supervision)**	16	14	9	4

* Based on two standard deviations.

performance, it is included in the comparison because of the considerable information that can be obtained with a good degree of accuracy and relatively small instrumentation and manpower requirements. It is particularly suited to gas or oil-fired units.

The full scale ASME test procedure (Column 2) serves to indicate the manpower and instrumentation required to obtain the most accurate measure of turbine and heater performance. In an effort to reduce instrumentation to a minimum, the medium accuracy test procedure (Column 3) was analyzed to compare with the author's concept of conventional low pressure cycle instrumentation. It is seen from Table 1 that the use of the H_e concept results in appreciable reductions of manpower and instrumentation requirements. However, this is accomplished at the expense of accuracy in the determination of heater string performance as can be seen from a comparison of Items 4e for cycle correction. The term "cycle correction" is used here to indicate the deviation in heat rate resulting from heater string performance deviation from standard. Since all the heaters but one are usually in the low pressure cycle, the "cycle correction" is determined largely by low pressure cycle heater string performance. The poorer accuracy which results from the determination of this heater string deviation when using H_e is accounted for principally by the relatively large errors involved in measuring the flow rates required by this method, namely boiler feed flow, condensate, and drain flows. This compares with simply measuring boiler feed flow at a single point when using the methods in Columns 2 and 3.

An error analysis (not shown in Table 1) was made of the application of the H_e concept to compute low pressure turbine end point. This showed that the end point can be determined with an accuracy comparable to that of conventional methods, notwithstanding the effects of flow measurement errors, which do not adversely affect the accuracy of this particular computation. In addition, the end point may be determined directly. This results in a definite advantage over conventional iterative computation processes which are used where low pressure heaters operate on wet steam.

It therefore may be concluded that the H_e concept provides a very promising method of instrumenting the low pressure portion of the reheat cycle for the purpose of determining turbine end point, thereby providing a quick and accurate means of calculating IP-LP turbine performance. The advantages and disadvantages of the author's method may be summarized as follows:

(*a*) Reduction in the number of instruments required in the low pressure cycle as compared with conventional heater by heater type instrumentation, as follows:

Test procedure	No. of measurements required
Full scale ASME	35
Medium accuracy	29
H_e method	8

(*b*) Reduction in manpower requirements resulting from reduction in instrumentation, as follows:

Test procedure	No. of men required
Full scale ASME	16
Medium accuracy	14
H_e method	9

(*c*) Elimination of trial and error solution for turbine end point.

(*d*) Accuracy of end point determination comparable with accuracy of conventional iterative methods.

(*e*) The accuracy of computing low pressure heater string deviation is limited to about ±0.8 per cent of turbine cycle heat rate due to present limitation on the accuracy of flow measuring devices. Consequently, the method leaves something to be desired with respect to accuracy, pending the development of more accurate flow metering devices.

The author has made an outstanding contribution to the ther-

modynamics of the cycle and also has paved the way for a practical approach to accurate and inexpensive monitoring of the performance of cycle components.

H. T. Hoffman[12]

Throughout this paper and one presented last year (reference [4] of the paper) Mr. Salisbury makes reference to performance monitoring and the application of the paper's subject matter in this field. Perhaps the reader might wonder what is meant by this term and more particularly why the Bailey Meter Company should be sponsoring an activity of this type.

Two developments in recent years have made more or less continuous monitoring of power-plant performance feasible and considerable interest in the possibilities has been evidenced. These developments are the single-turbine single-boiler units and the growth of the technology in automatic data collection and processing.

A few years ago the Bailey Meter Company, at the instigation of several power companies, began to investigate the possibilities of continuously monitoring the performance of the turbine cycle and the boiler. This led to the discovery that there existed very little, if any, analytic description of the turbine cycle which could be used as the foundation for the projected performance monitoring—particularly since it was desired to provide some degree of fault isolation and improve the ability to detect very small changes in cycle heat rate. Very early in our effort the author enthusiastically accepted our invitation to work with us in this program.

It has been the writer's privilege to work directly with the author in the development of this new analytical approach to describing the turbine cycle. As each new concept evolved it was tested in one way or another to determine its validity and general applicability. The data used to test these concepts were derived from four sources; design heat balances for a variety of units, acceptance tests, special tests run for this purpose, and finally a digital computer program was written which produces "perfect" heat balances for any possible circumstance which might exist on the cycle used as the model. We are particularly indebted to Mr. C. E. Miller of American Electric Power for his large contribution in preparing the computer program. To date we have prepared approximately 40 heat balances with the computer program representing a variety of cycle conditions and faults.

Our goal in sponsoring this work is to provide the power industry with an analytic description of the turbine cycle which will facilitate the evaluation of any change in equipment condition or operating environment in terms of changes in heat rate. Further, this analytic technique is to be amenable to use with automatic data collecting and processing equipment. We are well aware that the material published to date is just scratching the surface, leaving much work to be done and that to provide a theoretical analytical description of the cycle is only part of the over-all problem. We are continuing to pursue the analytical development and hope to be able to periodically report our progress to the power industry.

In addition to this analytical development other facets of the problem are also being pursued. The question of analog versus digital techniques is being studied. This resolves itself to the question of the need, or the meaning, of continuous results, sampled results, or integrated results. Accuracy requirements are being studied and available transducers and techniques evaluated in the light of the results.

The present paper describing a new criterion for evaluating the performance of the regenerative cycle is the second of a series intended to place before the power industry the results of our efforts.

[12] Bailey Meter Company, Wickliff, Ohio.

M. J. Steinberg[13]

This paper presents a new method for analyzing the thermodynamic effectiveness of any regenerative feedwater-heating system under any fixed boundary conditions in terms of a single parameter or variable, designated by the symbol H_e, and defined as the flow-weighted average enthalpy of the steam extracted for feedwater heating. It is also referred to as the "effective extraction enthalpy."

Although the objective is primarily the monitoring of the heater system it can be applied to monitor the over-all performance of the cycle. The ability to do so by the measurement of a single parameter is very attactive to operating personnel whose interest is in obtaining the highest efficiency commensurate with operating conditions.

We have made practical use of the author's contributions starting with his first paper[14] presented in 1942. Since that time we have refined and simplified the author's analytical approach as originally propounded. Our discussion of the author's 1957 paper[15] illustrates our latest endeavor in this respect, and it is of interest to note that our treatment of extraneous flows into and out of the heater system, shown in Table 2 of our discussion, parallels the treatment described by the author in this paper as expressed by Equations (48), (49), and (50).

It is understandable, therefore, why we are again pleased to congratulate the author for this valuable and constructive contribution to the advancement of the art.

Since the material of the paper was prepared, presumably, for the purpose of monitoring a specific installation, we express the hope that the author will describe such application in a future paper.

Author's Closure

The author is indeed grateful for Mr. Estcourt's continued interest in the major problem of performance monitoring. It should be pointed out that Mr. Estcourt and his company were major influences in stimulating activity in this field, as mentioned in Mr. Hoffman's discussion. Mr. Estcourt's support and interest have been constant and undeviating; the value of such an environment in stimulating additional effort is inestimable.

In characteristic fashion Mr. Estcourt has gone directly to the point of the paper, that is the possibilities in improving test procedures and accomplishing a saving in the cost of testing. He has made a considerable contribution to the paper itself through his illustrations of the savings that may be accomplished by use of the method. In addition, Mr. Estcourt has correctly identified the crux of the problem, recognized by the author from the beginning, that is, the necessity for accurate flow measurement. Although Mr. Estcourt's illustration indicates a "cycle error" of about 0.8 per cent in using this method because of errors involved in measuring flow rates, the author has reason to believe that this can be greatly reduced, particularly where flow meters can be calibrated in series, and reproducibility is at least as large an objective as absolute accuracy of flow measurement.

Presumably it is obvious that the use of the effective extraction enthalpy H_e permits an explicit solution for the state-line end point, provided only that the condensate and boiler flows are known, and that extraneous flows can be measured with reasonable accuracy. In fact, if these flows are known, together with the accompanying enthalpy values, one need not know the enthalpy of the respective extractions to find the turbine-exhaust enthalpy. Since measurement of extraction enthalpy has always

[13] Division Engineer, Consolidated Edison Company of New York, Inc., New York, N. Y. Mem. ASME.

[14] Reference [2] of the paper.

[15] Ibid., [4] Ibid.

represented a considerable task, and an appreciable source of error, the obviation of such measurements, or alternatively the elimination of the need for reading the turbine state line (not usually well known) should add appreciably to the accuracy of turbine-efficiency determination. Specifically, it is possible to determine turbine efficiency entirely from test measurements, without the need for relying on the manufacturer's estimate of the location of the state line on the Mollier chart.

As inferred in Mr. Hoffman's discussion, the present paper and that presented last year on the subject of gain due to reheat are intended to provide two of the important tools for performance monitoring. It is the author's present plan to present later a summary paper on the application of analytical techniques, where their practicability has been clearly established by test, and probably still later to present jointly with a Bailey Meter author the results of test work in applying the theory.

Mr. Steinberg's interest in the regenerative cycle and all of its aspects has been continuous and enthusiastic. It is earnestly hoped that his efforts will remain undiminished throughout the development of instrumentation for an application of these methods to performance monitoring in actual power plants.

The author wishes to express his deepest gratitude to the Society for having awarded this paper the 1959 Prime Movers Committee Award.

J. W. MURDOCK[2]

Head, Applied Physics Division, U. S. Naval Boiler and Turbine Laboratory, U. S. Naval Base, Philadelphia, Pa. Mem. ASME

Power Test Code Thermometer Wells[1]

Design of thermometer wells involves strength and thermal considerations. Criteria for thermal evaluation have been well established, those for strength have not. This paper presents thermometer-well designs proposed for Power Test Code work. Forces imposed by static pressure, steady-state fluid impingement, vibration induced by Karman trail vortexes, and structure-borne vibration are discussed. Methods and equations are given to enable the selection of wells for given service conditions. Although these methods are confined to wells of Power Test Code design, the Appendix contains derivations of general equations that may be adapted for any cantilever-type thermometer well.

THE PURPOSE of this paper is (*a*) to propose thermometer-well dimensions for Power Test Code work at velocities below 300 fps and (*b*) to enable the designer to determine if a well of dimensions selected for thermal consideration is strong enough to withstand specific application conditions of temperature, pressure, velocity, and vibration.

Background. PTC Committee 19/B was formed in 1956 to revise the Power Test Code Supplement on Instruments and Apparatus—Part 3—Temperature Measurement. This committee has nearly completed the rewriting of this almost 30-year-old Supplement. Publication is expected in 1959. Early in the research incident to the rewrite, it became evident that designs of thermometer wells to meet service conditions were not covered in the technical literature or in the American Standards. The material concerning service ratings in the present Test Code Supplement [1][3] is obsolete and covers only forces imposed by static pressure.

Since it is impossible to measure temperature with wells that are not of sufficient strength to withstand service conditions, this subcommittee undertook the task of preparing criteria for well design. This paper is the result of this work. It is presented to generate discussion on this subject. The methods and designs presented herein are not final. Changes will be made if discussion reveals flaws in the analysis or methods.

It is not the intent of this subcommittee to duplicate material already covered by American Standards. Therefore, items such as materials, methods of attachment, and so on, have not been included in this discussion. *Where materials are specified for the purposes of illustration, no inference should be made that these materials are preferred.* Any material approved by the ASME may be used.

Strength Versus Measurement. Factors that enhance good measurement are those that tend to reduce strength as given in Table 1.

Table 1 Desirable factors

Factor	Ideal for measurement	Ideal for strength
Length	Long Conductivity errors reduced. Active portion of thermometer must be in flow stream.	Short Impingement force reduced. Higher natural frequency.
Thickness	Thin Reduced conductivity loss. Increased response.	Thick Greater moment of inertialess stress. Higher natural frequency.
Mass velocity	High Increased heat transfer. Increased response.	Low Reduces impingement forces lower von-Karman trail vortex frequency.

The table is not all inclusive but indicates that well-design methods must carefully balance these factors so that neither accuracy nor strength is compromised.

Requirements. The requirements for wells to be used in Power Test Code work are as follows:

1 They shall enable the measurement of temperatures to

[1] The opinions and assertions in this paper are the private ones of the author, and are not to be construed as official or reflecting the views of the Navy Department or the Naval Establishment at large.

[2] Adjunct Assistant Professor, Drexel Institute of Technology, Philadelphia, Pa.

[3] Numbers in brackets designate References at end of paper.

Contributed by the Power Test Codes Committee and presented at the Annual Meeting, New York, N. Y., November 30–December 5, 1958, of THE AMERICAN SOCIETY OF MECHANICAL ENGINEERS.

NOTE: Statements and opinions advanced in papers are to be understood as individual expressions of their authors and not those of the Society. Manuscript received at ASME Headquarters, August 29, 1958. Paper No. 58—A-176.

Nomenclature

a = length as shown in Fig. 5, in.
A = outside diameter at support point, in.
b = length as shown in Fig. 5, in.
B = outside diameter at tip of well, in.
d = inside diameter or bore, in.
D = outside diameter at a cross section, in.
E = modulus of elasticity, psi
f = frequency, cycles per sec
F = factor, dimensionless
g = acceleration of gravity, 32.16 fps/s
I = moment of inertia, in.[4]
K = constant, dimensions as required
L = length as shown in Figs. 2 and 5, in.
M = moment, in-lb
N = ratio, dimensionless
P = gage pressure, psig
r = frequency ratio
S = stress, psi
t = thickness as shown in Fig. 5, in.
v = specific volume of fluid, cu ft per lb
V = velocity, fps
W = weight, lb
x = distance as indicated in Fig. 5, in.
y = static displacement, in.
γ = specific weight, lb per cu in.
θ = angle as shown in Fig. 5, radians
π = 3.14159

Subscripts

a = axial stress
b = bending stress
e = equivalent vibratory pressure
M = magnification factor
f = frequency constant
n = natural frequency
o = operating pressure
r = radial stress, inner wall
R = radial stress, outer wall
s = shear stress
t = tangential stress, inner wall
T = tangential stress, outer wall
v = velocity stress, inner wall
V = velocity stress, outer wall
w = wake frequency
x = moment of inertia at a cross section 1, 2, 3 as designated

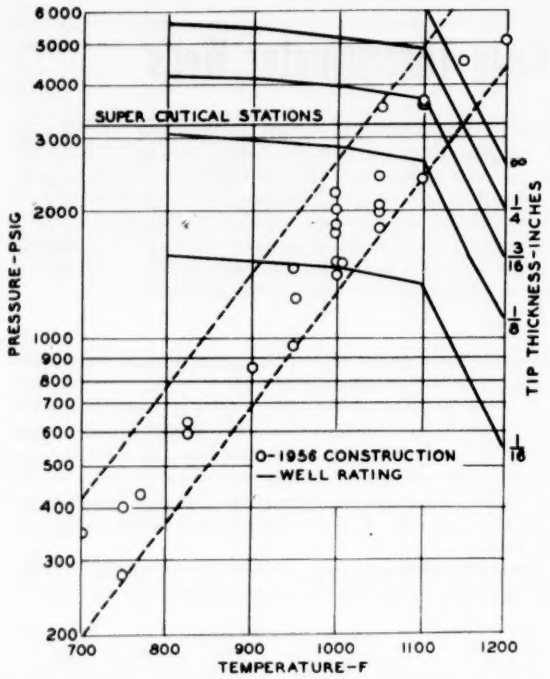

Fig. 1 Maximum pressure-temperature ratings of thermometer wells having a bore (*d*) of 7/16 in. for various tip thicknesses

tolerances specified by the individual Code under which the test is being conducted.

2 They shall be of sufficient strength and ruggedness to withstand all test and service conditions during the period of their installation.

3 They shall be of simple shape so that wells of reproducible thermal and strength characteristics may be fabricated without special equipment.

Proposed Power Test Code Wells

Design Considerations. *Shape.* A cylindrical well meets the requirement of simplicity. However, because of fluid impingement, the stress at the supported end will be greater than that at the tip. An ideal shape would have equal stress concentration at all sections, but would be impractical to fabricate. A tapered well was selected because it is in keeping with the concept of simplicity but at the same time allows for reducing the stress at the supported end.

Bore. The individual Power Test Code specifies either the tolerance of the measurement or the type of thermometer to be used. If the type of thermometer is not specified then a convenient one is selected on the basis of tolerance from the Supplement. The size of the bore must be such as to permit the insertion of all thermometers permitted by the Supplement; such as, liquid in glass, thermocouple, resistance, filled system, and bimetallic thermometers. For this reason a series of five sizes of bores, ranging from 1/4 to 1/2 in. in increments of 1/16 in. were selected for use. The bores are maximum rather than actual so that a primary element requiring a bore of 0.305 in. would use data given for the 5/16-in. bore (Size II) for stress and natural-frequency calculations.

Thickness. The thickness and material determine the maximum pressure rating of a well for a given temperature. These must be related to trends in central station design. Fig. 1 shows the trend of central station construction in 1956 [2]. It should be noted that all proposed construction falls between the dotted lines. Superimposed over the central station trends is a typical example of the effect of thickness. For purposes of illustration a 7/16-in. bore, made of Type 321 or 347 stainless steel, was chosen. With the bore held constant, thickness was varied and the maximum allowable static pressure for the tip was calculated and plotted for various temperatures. The increased pressure rating resulting from increased wall thickness must be balanced against increased size, which may be so large as to impede the flow seriously.

A 1/16-in. wall thickness is not very practical from a manufacturing standpoint and a 1/8-in. wall thickness will not meet present requirements. The 3/16-in. wall thickness was selected because it provides sufficient strength for all but two supercritical stations. Design of thermometer wells for these two stations will require metals of greater allowable stress than those presently provided by the Boiler and Pressure Vessel Code.

It should be noted that Power Test Code wells are used for many other services than central station work and in many applications a 1/8-in. thickness could be used. The main advantage to be gained from using a thinner wall is of course in response time. Most tests required under Power Test Codes are at steady-state conditions where time response is not an important consideration. It was decided to adhere to the 3/16-in. thickness for the Supplement to reduce the number of standard wells required.

Taper. With the wall fixed at the tip by the foregoing 3/16-in. selection, the diameter at the attachment or fixed end was set as being 3/16 in. greater than the tip diameter. This was chosen on the basis of impingement forces, natural-frequency considerations, and the necessity of keeping the taper to a minimum so that flow passage would not be blocked unduly.

Length. The length of the well is not specified. Length should be selected on the basis of thermal considerations only, in order that measurement tolerances will be met. The supplement will contain information for determining length on the basis of thermal considerations. Until the revised supplement is published it is suggested that the excellent summary and bibliography of Benedict [3] be used.

Proposed Designs. Wells of the form indicated in Fig. 2 and of the size given in Table 2 are proposed.

Table 2 Well dimensions, in.

Symbol	Size	I	II	III	IV	V
A	Minimum	13/16	7/8	15/16	1	$1^1/_{16}$
B	Minimum	5/8	11/16	3/4	13/16	7/8
d	Maximum	1/4	5/16	3/8	7/16	1/2

Attachment to pipe may be made in any manner approved by the Boiler and Pressure Vessel and Piping Codes. Any material approved by these codes for the intended service may be used. Tip designs for increased thermal response may be used provided that dimension *d* is not exceeded.

Strength Criteria. Well failures are caused by forces imposed by static pressure, steady-state flow, and vibration. Theoretical development of equations necessary for evaluation of these forces are given in the Appendix.

The principles involved in steady-state forces are well established. Application of vibration theory to well design merits further discussion to amplify data given in the Appendix.

Vibration

Natural Frequency. *Theoretical.* The theoretical natural frequency of any cantilever-type tapered well may be computed from Equations (6) and (16) of the Appendix. The complexity

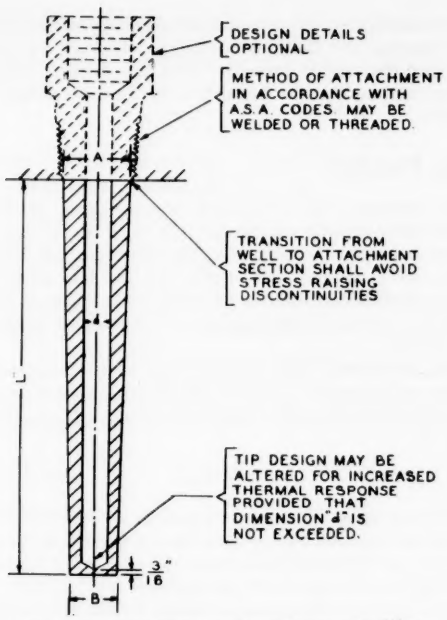
DESIGN DETAILS OPTIONAL
METHOD OF ATTACHMENT IN ACCORDANCE WITH A.S.A. CODES MAY BE WELDED OR THREADED.
TRANSITION FROM WELL TO ATTACHMENT SECTION SHALL AVOID STRESS RAISING DISCONTINUITIES
TIP DESIGN MAY BE ALTERED FOR INCREASED THERMAL RESPONSE PROVIDED THAT DIMENSION "d" IS NOT EXCEEDED.
A
L
d
B
3/16"

Fig. 2 Proposed Power Test Code thermometer wells

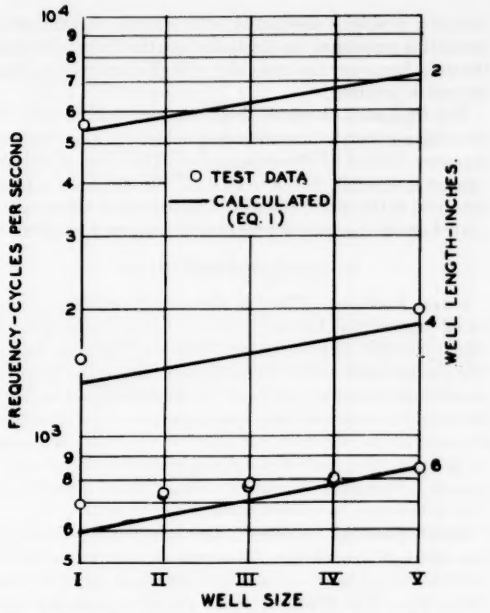

Fig. 3 Comparison of calculated versus experimental natural frequencies

of Equation (16) precludes its use for routine calculations. This equation was checked against graphical integration and found to be correct. Constants computed by Equations (6) and (16) are presented in Table 3 for use in the following:

$$f_n = \left(\frac{K_f}{L^2}\right)\left(\frac{E}{\gamma}\right)^{1/2} \qquad (1)$$

Table 3 Values of K_f

Well length,	Well size				
L, in.	I	II	III	IV	V
2	2.054	2.228	2.403	2.597	2.754
3	2.066	2.246	2.428	2.611	2.795
4	2.072	2.256	2.442	2.629	2.816
5	2.076	2.261	2.449	2.640	2.830
6	2.079	2.265	2.455	2.646	2.839
10	2.085	2.274	2.466	2.661	2.858
12	2.087	2.275	2.470	2.665	2.863

Experimental. To check the natural-frequency equation, two manufacturers submitted wells to be tested along with those supplied by the author's laboratory. All wells were made of mild steel. The modulus of elasticity was determined from a sample of the bar stock from which the wells were fabricated, and the specific weight was measured. To test the natural frequency of the wells they were mounted in a vise and struck. For wells of 6-in. length, an accurate determination of frequency was made by feeding the output of a strain gage into an oscilloscope and feeding another frequency into the scope until a Lissajous figure was obtained. For wells of less than 6-in. length the well vibration damped out too rapidly to obtain a Lissajous figure. An approximate frequency was determined by photographing the decay signal on the scope with a camera. A time signal permitted the counting of the number of vibrations against a time base. Fig. 3 shows the results of all tests compared with values calculated from Equation (1). Variation for wells of the same size but different source was less than 3 per cent. The difference between the calculated and test frequencies of the 6-in. wells varied from 2.7 per cent for Size V to 15.3 per cent for Size I.

Design. For design purposes Equation (1) should be used. The difference between theoretical and test values may be due either to assumptions made for theoretical development of equations or to method of test, or both. The theoretical values being lower than test are more conservative.

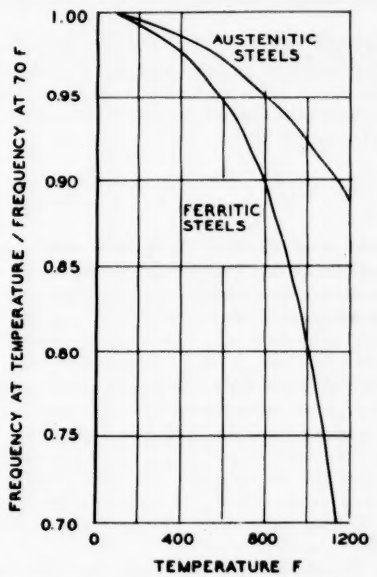

Fig. 4 Ratio of natural frequency at temperature to frequency at 70 F

Temperature Effect. When the temperature of a metal is increased, its modulus of elasticity decreases proportionately more than does its specific weight, thus reducing the natural frequency. Fig. 4 shows examples of this effect and is based on data given in the ASA Piping Code [4].

Karman Vortexes. The vortexes formed in the wake of a cylindrical object are of a periodic nature and give rise to an oscillating force [5]. This phenomenon has been responsible for many en-

gineering problems associated with electric transmission lines, submarine periscopes, smokestacks, and the Tacoma bridge, when the wake frequency has coincided with the natural frequency and resonance occurred.

The frequency at which these vortexes shed is given by the Strouhal number, a dimensionless product of wake frequency and diameter divided by stream velocity. The value of the Strouhal number is generally taken to be 0.22. In terms of the nomenclature used in this paper the wake frequency of a thermometer well (based on tip diameter for maximum frequency) is given by

$$f_w = 2.64(V/B) \tag{2}$$

System Excitation. There is always a possibility of vibration being transmitted by the structure (pipe) at frequencies that would coincide with the natural frequency or some harmonic of the thermometer well. Transmission within the fluid itself of oscillations caused by unbalances of machinery, valves, and so on, also could be responsible for well resonance. It is considered that to cause failure, the energy required would be of such magnitude as to cause other parts of the piping system to fail or to be so apparent as to require corrective action. These possible causes of well failure may be ignored in the design of wells.

Forced Vibration. *Damping.* The damping of metals is of a low order of magnitude. Damping of a metal is affected by prior history of heat-treatment, temperature, imposed stress, and frequency. The effects of these variables have not been well established for most metals so that accurate prediction of thermometer well damping under actual service conditions cannot be made.

Undamped Forced Vibration. The force exerted by the Karman vortexes is proportional to the square of the fluid velocity and hence to the square of the vortex frequency. The magnification factor, relationship of dynamic to static amplitude, under these conditions is given by [5]

$$F_M = \frac{(f_w/f_n)^2}{1 - (f_w/f_n)^2} = \frac{r^2}{1 - r^2} \tag{3}$$

Experimental Forced Vibration. Tests were conducted at the U. S. Naval Boiler and Turbine Laboratory to determine the magnitude of the force exerted by the Karman vortexes [6]. These tests were conducted on small cylinders excited by the impingement of an air jet issuing from a nozzle. Four strain gages were located at the base of these cylinders to measure the strain both in the direction of the air stream and perpendicular to the stream. Frequency ratios r from 0.7 to 8.6 were obtained with velocities ranging from 670 to 1100 fps. The lift and drag components of force were computed from strain-gage readings. Results indicated that the dynamic coefficient of drag and lift were approximately equal. Coefficient values varied from 0.001 to 0.029, the average being 0.005. All attempts to achieve resonance during these tests failed.

Scruton [7] demonstrated, in experiments with tall smokestacks of very small damping capacity, that a chimney could be excited at frequencies up to twice the Strouhal number. On this basis, a thermometer well brought into resonance could be in trouble at frequency ratios r from unity to 2.

Design Assumptions. For design purposes the following assumptions were made:

(*a*) The damping capacity of thermometer wells is zero and magnification is that predicted by Equation (3).

(*b*) Wells shall be designed for frequency ratios below unity. The author sought the advice of Prof. J. P. Den Hartog of Massachusetts Institute of Technology who recommended that a limit of 0.8 be placed on frequency ratio.

(*c*) The force exerted by the Karman vortexes is equal to the velocity pressure P_1.

These assumptions are ultraconservative since all metals have some damping, and the force exerted by the vortexes is much lower than the velocity pressure. They are, however, the only safe assumptions that can be made from the experimental data available.

Design Procedure

Stress Analysis. The condensed stress-analysis derivations given in the Appendix are based on the U. S. Naval Boiler and Turbine Laboratory practice [8]. This stress analysis, based on steady-state conditions, was modified to take into account the stress magnification caused by vibration. *The equations given in the design procedure apply only to wells of proposed Power Test Code Design.*

Maximum Pressure. The maximum pressure that a thermometer well can withstand for a given material and at a given temperature is computed from Equation (4); values of K_1 are given in Table 4.

$$P = K_1 S \tag{4}$$

Maximum Length. The maximum length for which a thermometer well can be made for a given service is dependent upon both vibratory and steady-state stresses. The necessity for keeping the frequency ratio at 0.8 or less imposes one limitation. The other limitation is stress considerations. Equation (5) is derived in the Appendix. Values of K_2 and K_3 are given in Table 4.

$$L_{max} = \frac{K_2}{V}\left(\frac{v(S - K_3 P_0)}{1 + F_M}\right)^{1/2} \tag{5}$$

Table 4 Values of stress constants

	Well size				
Constant	I	II	III	IV	V
K_1	0.420	0.397	0.375	0.296	0.265
K_2	37.4	39.9	42.3	44.7	47.0
K_3	0.105	0.146	0.190	0.237	0.284

Example. *Problem.* It is determined on the basis of thermal considerations that a 4-in. Size IV thermometer well is required to measure superheated steam at 2400 psig, 1050 F, flowing at a velocity of 300 fps. If the well material is to be Type 321 stainless steel, will the well be satisfactory for safety?

Solution. Step 1—Obtain the necessary data as follows:

Symbol		Item	Value	Reference
v	=	specific volume of superheated steam	0.3353 cu ft per lb	[9]
E_{70F}	=	modulus of elasticity at 70 F	28.0×10^6 psi	[10]
γ_{70F}	=	specific weight of metal at 70 F	0.290 lb per cu in.	[10]
S	=	allowable stress at 1050 F	13,100 psi	[11]
—	=	ratio of frequency at 1050 F to 70 F	0.918	Fig. 4

Step 2—Frequency Calculations

(*a*) Natural frequency, Equation (1)

$$f_{n(70F)} = \frac{2.629}{4^2}\left(\frac{28 \times 10^6}{0.290}\right)^{1/2} = 1612 \text{ cps}$$

$$f_n = 0.918 \times 1612 = 1482 \text{ cps}$$

(*b*) Strouhal frequency, Equation (2)

$$f_w = \frac{2.64 \times 300}{13/16} = 975 \text{ cps}$$

(*c*) Magnification factor, Equation (3)

$$r = f_w/f_n = 975/1482 = 0.656 < 0.8 \text{ (satisfactory)}$$

$$F_M = \frac{(0.656)^2}{1 - (0.656)^2} = 0.755$$

Step 3—Stress Calculation

(*a*) Maximum pressure, Equation (4)

$$P = 0.296 \times 13{,}100 = 3878 > 2400 \text{ (satisfactory)}$$

(*b*) Maximum stress length, Equation (5)

$$L_{\max} = \frac{44.7}{300}\left(\frac{0.3353\,(13{,}100 - 0.237 \times 2400)}{1 + 0.755}\right)^{1/2} = 7.3 \text{ in.}$$

$$7.3 \text{ in.} > 4 \text{ in. (satisfactory)}$$

Result. All the requirements for frequency and stress have been met, therefore this well is satisfactory for the intended service.

Conclusions

The methods of evaluation given in this paper represent a systematic approach to the problem of thermometer well design. It is hoped that the expected discussion of this paper will develop information which will amplify and improve these methods. A valuable contribution to the art would be the application of these methods to wells that have failed in service to determine if the failure could have been predicted. Such data are not available to the author.

The proposed Power Test Code thermometer wells are expected to satisfy 95 per cent of the present well problems. Increased temperature-pressure ratings of central stations now await advances in metallurgy. Such materials when available also will increase the ratings of the thermometer wells. For services where the proposed Power Test Code thermometer wells are not now suitable, the use of a fixed-beam type of well is recommended. Interest now centers on velocities below 300 fps. Higher velocities give rise to considerable differences between stagnation and static temperatures. For velocities in excess of 300 fps the fixed-beam type of well described in reference [12] is recommended.

An ASME Standard on thermometer well design is necessary. These devices are as widely used as other fittings now covered by appropriate standards.

Acknowledgments

The author is privileged to present the results of the efforts of many persons. The support and assistance rendered by the members of the Power Test Code Committee 19/B have made this paper possible. The author is indebted to the members of the professional staff of the U. S. Naval Boiler and Turbine Laboratory who assisted him in the preparation of this paper and conducted the experimental work. Last, but not least, the author would like to express his thanks to Prof. J. P. Den Hartog for his advice.

APPENDIX

Natural Frequency

Basic Equation. From the principles of mechanics the basic equation for the undamped free (natural) vibration of an elastic system with one degree of freedom is given as [13]

$$f_n = \frac{1}{2\pi}\left(\frac{12g}{y}\right)^{1/2} = \frac{3.127}{\sqrt{y}} \tag{6}$$

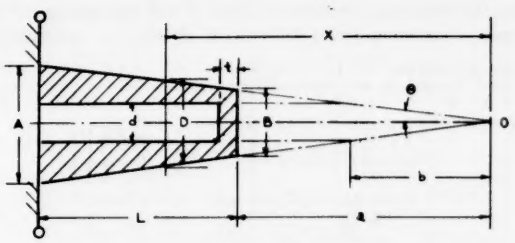

Fig. 5 Notation for integration

Elastic Curve. Since the Power Test Code thermometer wells are a form of a cantilever beam, their static displacement may be computed from the beam equations derived from the principles of strength of materials [14]; thus

$$E\frac{d^2y}{dx^2} = \frac{M}{I_x} \tag{7}$$

To integrate Equation (7), Fig. 5 was used for notation and method of attack.

Moment of Well. The weight of the well is the volume of the solid frustum of the cone minus the volume of the bore times the specific weight of the well material or

$$W = \frac{\gamma(x-a)}{12}\pi(D^2 + BD + B^2) - \frac{\pi(x-a-t)d^2\gamma}{4} \tag{8}$$

The moment of the well from x to a is the weight times the distance to the center of gravity. This was obtained by subtracting the moment of the solid frustum from that of the bore to obtain Equation (9); thus

$$M = \frac{\pi\gamma}{48}[(x-a)^2(D^2 + 2BD + 3B^2) - 6(x-a-t)^2d^2] \tag{9}$$

Moment of Inertia

$$I_x = \frac{\pi}{64}(D^4 - d^4) \tag{10}$$

Integration. Substituting the moment and moment of inertia of Equations (9) and (10) into Equation (7), Equation (11) was obtained:

$$\frac{-3E(d^2y)}{4\gamma(dx^2)} = \frac{(x-a)^2(D^2 + 2BD + 3B^2) - 6(x-a-t)^2d^2}{D^4 - d^4} \tag{11}$$

From the principles of trigonometry and using the relationship of Fig. 5

$$\tan\theta = \frac{A-B}{2L}, \quad \text{let } N = \frac{A-B}{L} = 2\tan\theta,$$

then

$$B = 2a\tan\theta = aN \tag{12}$$

$$D = 2x\tan\theta = xN \tag{13}$$

$$d = 2b\tan\theta = bN \tag{14}$$

Substituting Equations (12) to (14) into Equation (11), Equation (15) is obtained:

$$\frac{-3EN^2(d^2y)}{4\gamma\ (dx^2)} = \frac{(x-a)^2(x^2 - 2ax + 3a^2) - 6(x-a-t)^2b^2}{x^4 - b^4} \tag{15}$$

Equation (15) was integrated, noting the boundary conditions of dy/dx and y being equal to 0 when $x = L + a$. After integra-

tion the result was rewritten in terms of well dimensions and in terms of maximum static deflection to obtain

$$\frac{3E}{4\gamma}\left(\frac{A-B}{L}\right)^4 y = \frac{1}{2}(A-B)^2 + \frac{1}{4}\left\{\frac{3B^4}{d^2} - 5d^2 - 6\left[B + t\left(\frac{A-B}{L}\right)\right]^2\right\}\left[\frac{B}{d}\log_e\frac{(B-d)(A+d)}{(B+d)(A-d)} + \log_e\frac{A^2-d^2}{B^2-d^2}\right] + \frac{1}{2}\left\{6\left[B + t\frac{(A-B)}{L}\right]^2 - 7d^2 - \frac{3B^4}{d^2}\right\}\left\{\left[\frac{B}{d}\tan^{-1}\frac{d(B-A)}{d^2+AB}\right] + \frac{1}{2}\log_e\frac{A^2+d^2}{B^2+d^2}\right\} + 2\left\{\frac{B^3}{d^2} - 3\left[B + t\left(\frac{A-B}{L}\right)\right]\right\}\left[\frac{B}{2}\log_e\frac{(B^2+d^2)(A^2-d^2)}{(B^2-d^2)(A^2+d^2)} + d\tan^{-1}\frac{d(B-A)}{d^2+AB} + \frac{d}{2}\log_e\frac{(B-d)(A+d)}{(B+d)(A-d)}\right] \quad (16)$$

Equation (16) should be used with caution. The nature of its derivation—dependence on $(A - B)/L$—makes its numerical solution a series of subtractions of large numbers having small differences. It cannot be used for straight wells as its solution becomes indeterminate for this special case. To arrive at a numerical solution of reasonable accuracy it was found necessary to use seven-place log and trig tables. Four and five-place tables gave numerical errors in the amount of 20 per cent in some cases. Equation (16) was verified numerically by machine and graphical integration of Equation (11).

Stress Analysis

Stress Definitions

Axial stress (S_a) is that stress produced by the thrust of the fluid pressure on the well.

Radial stress (S_r, S_R) is the collapsing stress produced by the fluid pressure as calculated by the Lamé equation for thick-walled cylinders.

Shear stress (S_s) is the stress produced as pure shear due to the loading created by the impingement of the fluid on the well.

Tangential stress (S_t, S_T) is the hoop stress produced by the fluid pressure as calculated by the Lamé equation for thick-walled cylinders.

Velocity stress (S_v, S_V) is the bending stress created by the impingement of the fluid on the well.

Pressure Definitions

Static (P_0)—the static pressure is the gage pressure of the fluid in which the well is immersed.

Velocity (P_v)—the velocity pressure is obtained by dividing the impingement force by the projected well area. The impingement force is computed from the standard drag equation. The value of the coefficient of drag is dependent upon shape, size, and roughness of the immersed body; the Reynolds and Mach numbers of the flow impinging upon it. In the turbulent-flow regions, where most thermometer wells are used, the drag coefficient is somewhat less than unity. The value of drag coefficient was assumed to be unity for the purpose of this analysis to provide an extra margin of safety. The value of velocity pressure is given by

$$P_v = \frac{V^2}{9262v} \quad (17)$$

Stress Constants. Each of the individual stresses as defined were analyzed and equations for expressing their value were derived in terms of the following general equation:

$$S = KP_0 \text{ or } S = KP_v \quad (18)$$

where K is a stress constant. Table 5 summarizes the stress constants so obtained.

Table 5 Summary of stress constants

Type of stress	Symbol	Location	Equation for K
Velocity	K_v	Inner wall	$\frac{1.698(A+2B)dL^2}{A^4-d^4}$
$S = KP_v$	K_V	Outer wall	$\frac{1.698(A+2B)AL^2}{A^4-d^4}$
Axial $S = KP_0$	K_a	At support point	$\frac{A^2}{A^2-d^2}$
Radial	K_r	Inner wall	0
$S = KP_0$	K_R	Outer wall	1
Tangential	K_t	Inner wall	$2K_a$
$S = KP_0$	K_T	Outer wall	$\frac{A^2+d^2}{A^2-d^2}$
Shear $S = KP_v$	K_s	At support point	$\frac{0.6366(A+B)L}{A^2-d^2}$

Combined Stresses. The maximum-shear theory of failure was used to combine stresses. Stress combinations at the following locations at the support point were analyzed: Outer wall—upstream, outer wall—downstream, inner wall—upstream, inner wall—downstream.

An equation for combined stress was obtained for each of the three planes at each of the four locations or a total of 12 equations. It was possible to demonstrate that maximum stress could occur only at one of the three locations shown in Table 6.

Examination of the equations in Table 6 indicates that for static conditions (S_V, S_v, and $S_s = 0$), the maximum static stress will be S_1 or the inner-wall tangential stress. For static conditions the design must conform with the requirements of the ASME Code for Unfired Pressure Vessels. The applicable portion is given as a curve, Figure UG-31. The factor F, given in Table 7, was calculated by comparing results obtained from the equation for S_1 and Figure UG-31.

Application. For the proposed Power Test Code thermometer wells it can be demonstrated further that:

(a) Maximum stress at the support point is given by S_2.

(b) Shear stress may be neglected.

(c) The maximum static pressure that the well can withstand is determined by the tip conditions S_1.

(d) The minimum end thickness at the tip is $(B - d)/2$.

Table 6 Equations for maximum stress

Stress no.	Location: Wall	Location: Side	Equation	No.
S_1	Inner	Either	$2S_a$	(19)
S_2	Outer	Downstream	$[(S_a + S_V - S_R)^2 + 4S_s^2]^{1/2}$	(20)
S_3	Inner	Downstream	$[(S_a + S_v)^2 + 4S_s^2]^{1/2}$	(21)

Table 7 Values of factor F_A or F_B

$\frac{t}{D} = \frac{A-d}{2A}$ or $\frac{B-d}{2B}$ depending on reference plane

t/D From	t/D To	F
0.084	0.091	2.0
0.092	0.099	1.9
0.100	0.114	1.8
0.115	0.129	1.7
0.130	0.149	1.6
0.150	0.169	1.5
0.170	0.199	1.4
0.200	0.219	1.3
0.220	0.239	1.2
0.240	0.249	1.1
0.250	up	1.0

With the foregoing considerations the following practical equations may be derived:

For maximum static pressure from Equation (19)

$$S = F_B S_1 = F_B K_{t(B)} P \tag{22}$$

or

$$P = K_1 S \tag{4}$$

where

$$K_1 = 1/F_B K_{t(B)}$$

For maximum velocity from Equation (20) neglecting shear stress

$$S = F_A S_2 = F_A(S_a + S_U - S_R) \tag{23}$$

Substituting stress constants

$$S = F_A[(K_a - 1)P_0 + K_V P_V] \tag{24}$$

Solving for P_v

$$P_v = \frac{S - F_A P_0(K_a - 1)}{F_A K_V} \tag{25}$$

To the steady-state velocity pressure must be added the vibratory equivalent to obtain the total forces imposed:

$$P_v + P_s = P_v + F_M P_v = P_v(1 + F_M) \tag{26}$$

For the total forces Equation (25) becomes

$$P_v(1 + F_M) = \frac{S - F_A P_0(K_a - 1)}{F_A K_V} \tag{27}$$

Substituting Equation (17) for P_v in Equation (27)

$$\frac{V^2}{9262v}(1 + F_M) = \frac{S - F_A P_0(K_a - 1)}{F_A K_V} \tag{28}$$

Solving Equation (28) for V

$$V = \left\{\left[\frac{9262v}{(1 + F_M)}\right]\left[\frac{S - F_A P_0(K_a - 1)}{F_A K_V}\right]\right\}^{1/2} \tag{29}$$

Let $K_x = K_V/L^2$, then

$$V = \frac{1}{L}\left\{\left[\frac{9262v}{1 + F_M}\right]\left[\frac{S - F_A P_0(K_a - 1)}{F_A K_x}\right]\right\}^{1/2} \tag{30}$$

Let $K_2 = \left(\frac{9262}{F_A K_x}\right)^{1/2}$ and $K_3 = F_A(K_a - 1)$

Then Equation (30) may be written

$$V = \frac{K_2}{L}\left[\frac{v(S - K_3 P_0)}{1 + F_M}\right]^{1/2} \tag{5}$$

References

1 ASME Power Test Code Supplement on Instruments and Apparatus—Part 3—Temperature Measurement, Chapter 6, series 1929, pp. 17–21.

2 B. O. A. Skrotzki, "1956 Modern Plant Survey," *Power*, vol. 100, 1956, pp. 36–42.

3 R. P. Benedict, "Review of Practical Thermometry," ASME Paper 57—A-203, 1957.

4 "American Standard Code for Pressure Piping," ASA B31.1, 1955, pp. 93–94.

5 J. P. Den Hartog, "Mechanical Vibrations," McGraw-Hill Book Company, Inc., New York, N. Y., fourth edition, 1956, pp. 45–47, 305–308.

6 A. Egli and W. H. Day, "Analysis of Tests on Wake-Excited Vibration of Protection Tubes," U. S. Naval Boiler and Turbine Laboratory Report No. 2 of NBTL Test I-44, 1953.

7 C. Scruton, "Wind-Excited Oscillations of Tall Stacks," *The Engineer*, vol. 199, 1955, pp. 806–808.

8 "Thermowells, Cantilever Type, Stress Calculation Methods," Instrument Standard IS-104, U. S. Naval Boiler and Turbine Laboratory, Naval Base, Philadephia, Pa., 1957, pp. 1–18.

9 J. H. Keenan and F. G. Keyes, "Thermodynamic Properties of Steam," John Wiley & Sons, Inc. New York, N. Y., first edition, 28th printing, 1955.

10 Edited by S. L. Hoyt, "Metal Properties," ASME Handbook, McGraw-Hill Book Company, Inc., New York, N. Y., first edition, 1954, p. 62.

11 "Unfired Pressure Vessel Code," Section VIII, ASME Boiler and Pressure Vessel Code, 1956, pp. 96–97.

12 J. W. Murdock and E. F. Fiock, "Measurement of Temperature in High-Velocity Steam," TRANS. ASME, vol. 72, 1950, p. 1155.

13 W. G. McLean and E. W. Nelson, "Theory and Problems of Mechanics," Schaum Publishing Company, New York, N. Y., 1952, pp. 266–268.

14 W. A. Nash, "Theory and Problems of Strength of Materials," Schaum Publishing Company, New York, N. Y., 1957, pp. 112–114, 141–142.

DISCUSSION

Lowell A. Holcomb[4]

As the author stated in the conclusion of his comprehensive paper, "An ASME Standard on thermometer well design is necessary." Now this concerns cantilever type wells installed through a pipe wall. In other words, the pipe diameter is greater than the effective thermometer well length.

The discusser's company and many other aircraft and missile companies and government facilities perform fluid testing in small diameter pipe and tube systems. Normally, bare thermocouples mounted in a pipe or tube fitting are used except in the cases of temperature extremes or use of corrosive fluids. When thermometer wells are used, all conceivable types are installed in all conceivable ways, some good thermally and some not so good due to other practical considerations.

The discusser would like to see Power Test Code thermometer well design and installation criteria extended to include fluid power testing in the aircraft and missile applications. This would involve many more specific applications, conditions of temperature, pressure, velocity, and vibration.

Rawleigh M. Johnson[5]

I wish to emphasize the practical contribution of this paper from the viewpoint of safety. Experience indicates that the predominant cause of thermometer well breakage is of the nature of

[4] Test Engineer, Engineering Department, Convair/Pomona, Convair Division of General Dynamics Corporation, Pomona, Calif. Assoc. Mem. ASME.

[5] Engineer-in-Charge, Engineering Test Department, Ingersoll-Rand Company, Phillipsburg, N. J. Mem. ASME.

vibrations induced by either impact or the high velocity of the flowing fluids. Heretofore engineers have been prone to select thermometer well designs on a hit or miss basis, giving little thought to the potential hazards involved.

It is significant to note that, in this paper, the author has analyzed the problem in great detail and correctly concludes that a safe design must take into account the phenomena of vibration. To do this he has provided formula and methods permitting the design of wells for a wide range of pressures and temperatures. It should be noted that the stress calculation assumes that the vibration is not dampened. The method is original, easy to use, and gives a large measure of safety.

This paper is a useful and timely contribution to the literature. The methods will no doubt find wide application in the Power Test Codes and in the design of power plant equipment. The author deserves credit for the painstaking thoroughness and attention to detail which he has given the problem.

Frank M. Kamarck[6]

The author and the PTC Committee are to be congratulated on their fine work in bringing order and logic to the complex of problems that make up thermo-well design.

The following discussion is presented in response to the invitation extended in the paper and it is hoped that these comments may aid the committee in their task of preparing the final Power Test Code Supplement.

The paper states that: "It is not the intent of this subcommittee to duplicate material already covered by American Standards. Therefore, items such as materials, methods of attachment, and so on, have not been included in this discussion." It is my intention to show that these items have not been satisfactorily covered in the present Codes, and that these items cannot be separated from the design of thermo-wells.

I believe that the subcommittee should arrive at some conclusions on these omitted items and make recommendations to be considered and incorporated in the applicable Codes.

The paper states : "Attachment to pipe may be made in any manner approved by the Boiler and Pressure Vessel and Piping Codes." The present Codes do not present any reasonable suggestion concerning how a thermometer well (or steam sampling well) can be fastened into a pipe wall by welding.

For example, the Code for Pressure Piping ASA B31.1–1955 states:

"Para. 638(i) Minimum Requirements for Attachment Welds

Branch connections without additional reinforcement (including special made, integrally reinforced connection fittings) which abut the outside surface of the run wall, or which are inserted through a hole cut in the run wall, shall be attached by means of fully penetrated groove welds. The fully penetrated groove welds shall be finished with cover fillet welds having a minimum throat dimension not less than *tc*. [See Figs. 21(*a*) and 21(*b*).]"

The fully penetrated groove weld as shown in Fig. 21(*b*) is not feasible for attaching a thin walled thermometer well in the high pressure, high temperature piping of a modern power plant. For example, the Thomas H. Allen power plant for the city of Memphis has main steam piping with walls of 3 in. minimum thickness. To fully penetrate the pipe wall with weld material presents a problem of excessive machining, excessive mass of weld material with relation to the thin wall of the thermo-well, accompanied by high stresses due to the shrinkage of the weld material from molten to the cold state.

Fig. 21(*a*) presents a possible partial solution. A boss or sleeve can be welded to the pipe with a fully penetrated weld

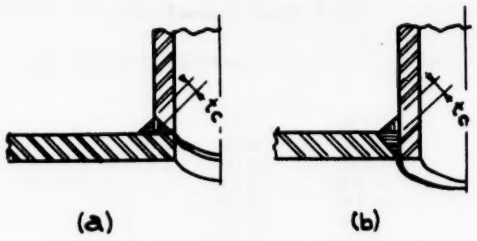

Fig. 21

through the wall of the boss or sleeve. But the problem reappears in attempting to fasten the thermo-well to the boss or sleeve. If the fastening of the thermo-well to the boss or sleeve is done with a simple fillet weld, then this would be a violation of this paragraph of the Code. (However, the Code, in paragraph 638 (a) and (f), permits the use of socket welding which is in the final analysis, a fillet weld.) The situation is not helped by the notation in the Code accompanying Fig. 21 that describes the illustrations as: "Some acceptable types of welded branch attachment details showing minimum acceptable welds."

The main object of a fully penetrated weld is to produce a sound weld throughout and especially at the root. It is extremely difficult to guarantee the weld for this size connection through any present known method of inspection.

In Fig. 6, showing thermo-wells for pressures above 2000 psig or temperature above 1055 F, a fully penetrated weld was used in attaching the boss to the pipe. In order to guarantee a sound root weld, the original root weld is cut out through the use of a larger drill. The thermo-well is attached to the boss by means of a J-weld topped with a fillet. By cupping the weld into the boss, more weld material is used to compensate against possible defect at the root of the weld.

In Fig. 7 for pressures not exceeding 2000 psig or temperature 1055 F, the thermo-well is attached directly to the pipe wall by means of the J-weld, cupped into the pipe wall, and topped with a fillet weld.

In Fig. 8 for pressure not exceeding 900 psig and temperature 750 F, the thermo-well is screwed into a threaded forging, which is in turn attached to the pipe by means of a fully penetrated weld.

The Code for Pressure Piping in paragraph 125, allows the use of $1^1/_2$ in. nominal size of screwed connection for pressures above 600 psi but not above 2500 psi. Threaded thermo-wells were limited to 900 psig and 750 F, because of the problem of maintaining a leakproof joint with threads under temperature. Any unevenness of heating of the two members joined may vary the expansion. The effect of temperature on the thread sealant, combined with the unevenness in the thread surfaces, and distortion due to stress, may open up a leakage path after a number of thermal cycles.

The other applicable code that would involve power piping is the Boiler Code. Para. P-268 (h) (2) (a) has less stringent requirement: "Sufficient welding shall be provided on either side of the plane through the center of the opening parallel to the longitudinal axis of the shell to develop the strength of the reinforcing parts through shear or tension in the weld, whichever is applicable." Para. P-268 (h) (2) (d) states: "The location and minimum size of attachment welds shall conform to the requirements shown for typical examples in figure P-36." Figure P-36 indicates a diverse number of welds of which only the fully penetrated welds and the cup welds topped with fillets could be adapted to fastening the thermo-wells.

The paper states that: "Any material approved by these Codes for the intended service may be used."

[6] Staff Engineer, Burns and Roe, Inc., New York, N. Y. Mem. ASME.

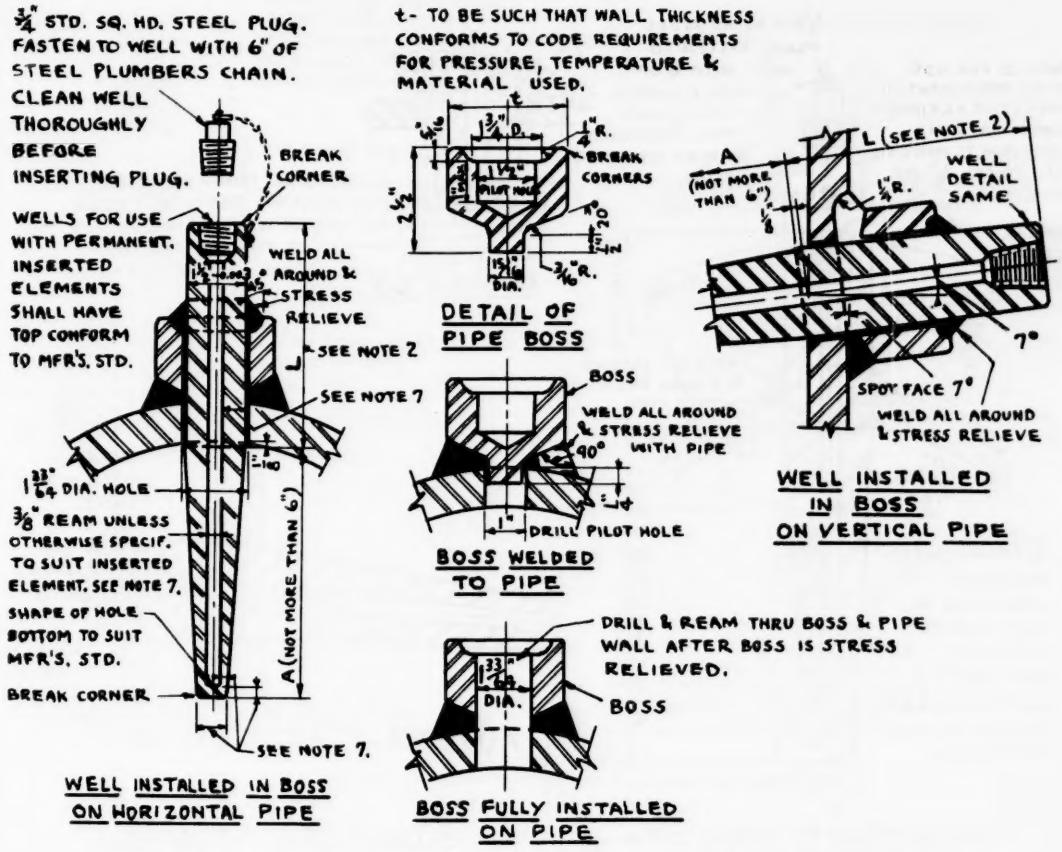
3/4" STD. SQ. HD. STEEL PLUG. FASTEN TO WELL WITH 6" OF STEEL PLUMBERS CHAIN.
CLEAN WELL THOROUGHLY BEFORE INSERTING PLUG.
BREAK CORNER
WELLS FOR USE WITH PERMANENT INSERTED ELEMENTS SHALL HAVE TOP CONFORM TO MFR'S. STD.
WELD ALL AROUND & STRESS RELIEVE
SEE NOTE 2
SEE NOTE 7
1 33/64 DIA. HOLE
3/8" REAM UNLESS OTHERWISE SPECIF. TO SUIT INSERTED ELEMENT. SEE NOTE 7.
SHAPE OF HOLE BOTTOM TO SUIT MFR'S. STD.
BREAK CORNER
A (NOT MORE THAN 6")
SEE NOTE 7.
WELL INSTALLED IN BOSS ON HORIZONTAL PIPE
t- TO BE SUCH THAT WALL THICKNESS CONFORMS TO CODE REQUIREMENTS FOR PRESSURE, TEMPERATURE & MATERIAL USED.
t
3/4" D.
1/4" R.
BREAK CORNERS
1 1/2" PILOT HOLE
2 1/2"
20°
1/16" IN
15/16" DIA.
3/16" R.
DETAIL OF PIPE BOSS
BOSS
WELD ALL AROUND & STRESS RELIEVE WITH PIPE
90°
1" DRILL PILOT HOLE
BOSS WELDED TO PIPE
DRILL & REAM THRU BOSS & PIPE WALL AFTER BOSS IS STRESS RELIEVED.
1 33/64" DIA.
BOSS
BOSS FULLY INSTALLED ON PIPE
A (NOT MORE THAN 6")
1/8
L (SEE NOTE 2)
WELL DETAIL SAME
1/4" R.
7°
SPOT FACE 7°
WELD ALL AROUND & STRESS RELIEVE
WELL INSTALLED IN BOSS ON VERTICAL PIPE

Fig. 6 Thermometer or thermocouple test wells for high pressure or temperature service, above 2000 psig or 1055 F

NOTES:

1 For pipe less than 12-in. diam specify dimension "A" in increments of 1 in. so tip of well will reach center line of pipe $\pm 1/2$ in. For pipe more than 12-in. diam, "A" shall be not more than 6 in.

2 Specify dimension "L" in increments of $1/2$ in. so end of well will extend through insulation, a min of $1/2$ in.

3 Material of well and boss shall be the same as the pipe into which it is welded.

4 Manufacturer shall stamp projection of well to indicate material used with ASTM No., and tag No.

5 All wells shall be tested in accordance with applicable codes by manufacturer.

6 Approval by Chief Mechanical Engineer must be secured for applications of wells into piping where steam velocities exceed 18000 fpm or liquid velocities exceed 15 fps.

7 Check wall thickness required for pressure, temperature, and material used. See current ASME code sect. VIII "Unfired Pressure Vessels" ("Chart for determining wall thickness of tubes under external pressure").

8 In any case immersion into the flowing stream shall be not less than 3 in. In a pipeline 4 in. or smaller in size the well must be arranged axially in the pipe facing the oncoming flowing media where possible and inserted in an elbow or tee. In pipelines smaller than 4 in. the tee or elbow should be one size larger than the line; and in the pipelines 2 in. or smaller, an enlarged section of pipe shall be provided immediately upstream of the elbow or tee so as to avoid serious impedance of flow by the well.

Table 8 Thermal conductivity and thermal expansion

Materials ASTM Nos	Thermal conductivity, Btu/ft²/hr/deg F/ft				Thermal expansion, inches per inch from 70 F					
Temp deg F →	212	750	930	1100	200	400	600	750	850	1050
Carbon Steel A105-I or II	27.	24.			0.0008	0.0023	0.0038	0.0051	0.006	0.0079
1¼% Cr-½% Mo A 182-F11	24.	22.	20.		0.0008	0.0023	0.0038	0.0051	0.006	0.0079
2¼% Cr-1% Mo A 182-F22	24.	22.	20.	18.	0.0008	0.0023	0.0038	0.0051	0.006	0.0079
13% Cr Stainless A 182-F6	14.4	16.	16.7		0.0007	0.0019	0.0024	0.0043	0.005	0.0057
18% Cr-8% Ni Austenitic Stainless A 182-F321	9.3	11.6	12.8	13.	0.0012	0.0032	0.0052	0.0068	0.0079	0.010

Converted thermal conductivity data from ASM "Metals Handbook," 1948 edition
Converted thermal expansion data from "Code for Pressure Piping," 1955.

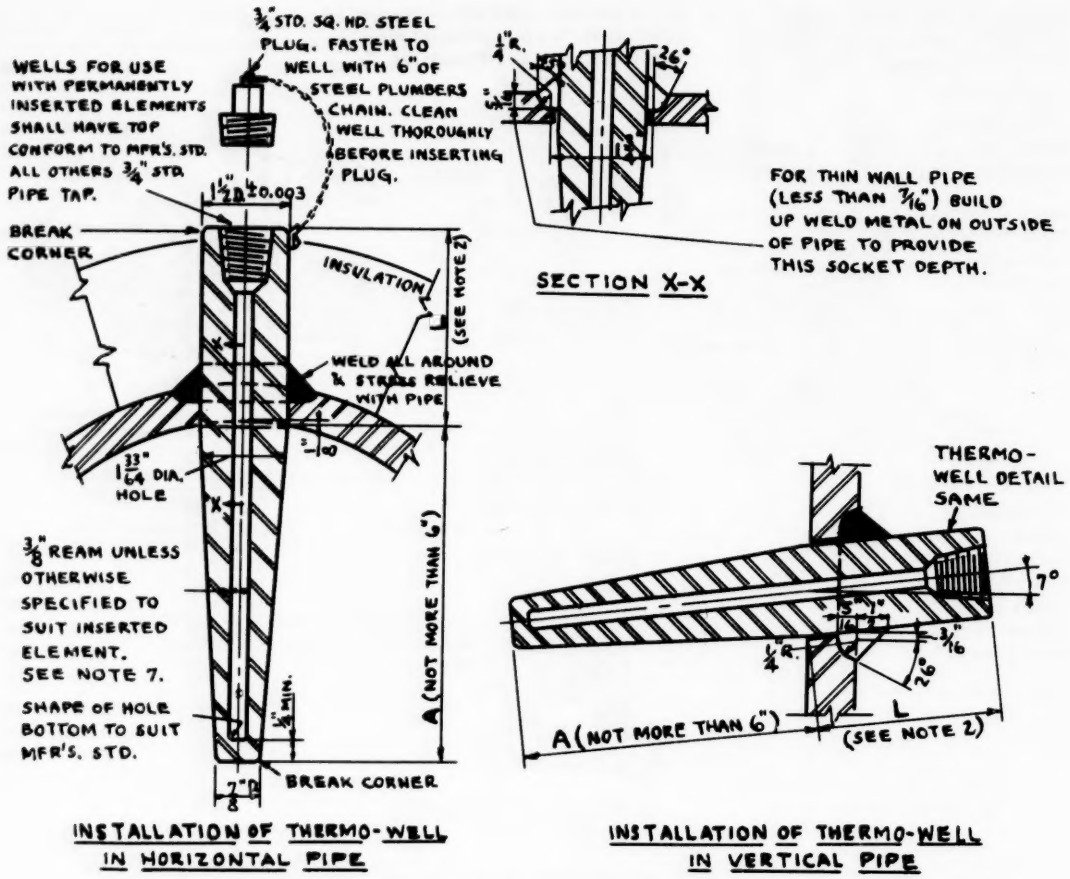
3/4" STD. SQ. HD. STEEL PLUG. FASTEN TO WELL WITH 6" OF STEEL PLUMBERS CHAIN. CLEAN WELL THOROUGHLY BEFORE INSERTING PLUG.
WELLS FOR USE WITH PERMANENTLY INSERTED ELEMENTS SHALL HAVE TOP CONFORM TO MFR'S. STD. ALL OTHERS 3/4" STD. PIPE TAP.
1 1/2 R ± 0.003
BREAK CORNER
INSULATION
L (SEE NOTE 2)
WELD ALL AROUND & STRESS RELIEVE WITH PIPE
1 33/64 DIA. HOLE
3/8" REAM UNLESS OTHERWISE SPECIFIED TO SUIT INSERTED ELEMENT. SEE NOTE 7.
SHAPE OF HOLE BOTTOM TO SUIT MFR'S. STD.
A (NOT MORE THAN 6")
BREAK CORNER
INSTALLATION OF THERMO-WELL IN HORIZONTAL PIPE
1/4" R.
26°
SECTION X-X
FOR THIN WALL PIPE (LESS THAN 3/16") BUILD UP WELD METAL ON OUTSIDE OF PIPE TO PROVIDE THIS SOCKET DEPTH.
THERMO-WELL DETAIL SAME
7°
3/16
A (NOT MORE THAN 6")
L (SEE NOTE 2)
INSTALLATION OF THERMO-WELL IN VERTICAL PIPE

Fig. 7 Thermometer or thermocouple test wells for high pressure or temperature service, not exceeding 2000 psig or 1055 F

NOTES:

1 For pipe of 12-in. diam or less specify dimension "A" in increments of 1 in. so tip of well will reach center line of pipe $\pm 1/2$ in. For pipe more than 12-in. diam, "A" shall be not more than 6 in.

2 Specify dimension "L" in increments of $1/2$ in. so end of well will extend through insulation approx. $1/4$–$1/2$ in.

3 Material of well shall be the same as the pipe into which it is welded.

4 Manufacturer shall stamp projection of well to indicate material used with ASTM No. and tag No.

5 All welds shall be tested in accordance with applicable codes by manufacturer.

6 Approval by Chief Mechanical Engineer must be secured for applications of wells into piping where steam velocities exceed 18000 fpm or liquid velocities exceed 15 fps.

7 Check wall thickness required for pressure, temperature, and material used. See current ASME code sect. VIII "Unfired Pressure Vessels" ("Chart for Determining Wall Thickness of Tubes under External Pressure").

8 In any case, immersion into the flowing stream shall be not less than 3 in. In a pipeline 4 in. or smaller in size the well must be arranged axially in the pipe facing the oncoming flowing media where possible and inserted in an elbow or tee. In pipelines smaller than 4 in., the tee or elbow should be one size larger than the line; and in pipelines two inches or smaller, an enlarged section of pipe shall be provided immediately upstream of the elbow or tee so as to avoid serious impedance of flow by the well.

It is evident from the thermal conductivity data (Table 8) that carbon steel and chrome moly alloys will provide faster response on temperature for the same thickness of well wall. The effect of film due to fluid should be the same for similarly finished steels. The oxide layer on the surface of the stainless will be thinner than on the carbon steel and the alloy steel, depending on the exposure to air prior to going into service of the plant. But once the plant is in operation, the growth of the oxide layer on thermo-well exterior will stop since the steam and feed water in the modern power plant is practically oxygen free.

Accordingly, it was decided to use the same material for the thermo-well as was required for the piping for the high pressure and high temperature services.

However, in some applications such as circulating water there are conditions of corrosion. It was decided to use high chrome alloy ASTM A182-F6 (shown on Fig. 8) for all services up to 900 psig and 750 F. This high chrome alloy has good corrosion resistance and better conductivity than austenitic stainless, but has low weldability characteristics. It is better for a screwed connection application with carbon steel or alloy steel than austenitic stainless since the thermal expansion values are closer. Also, it is better economically.

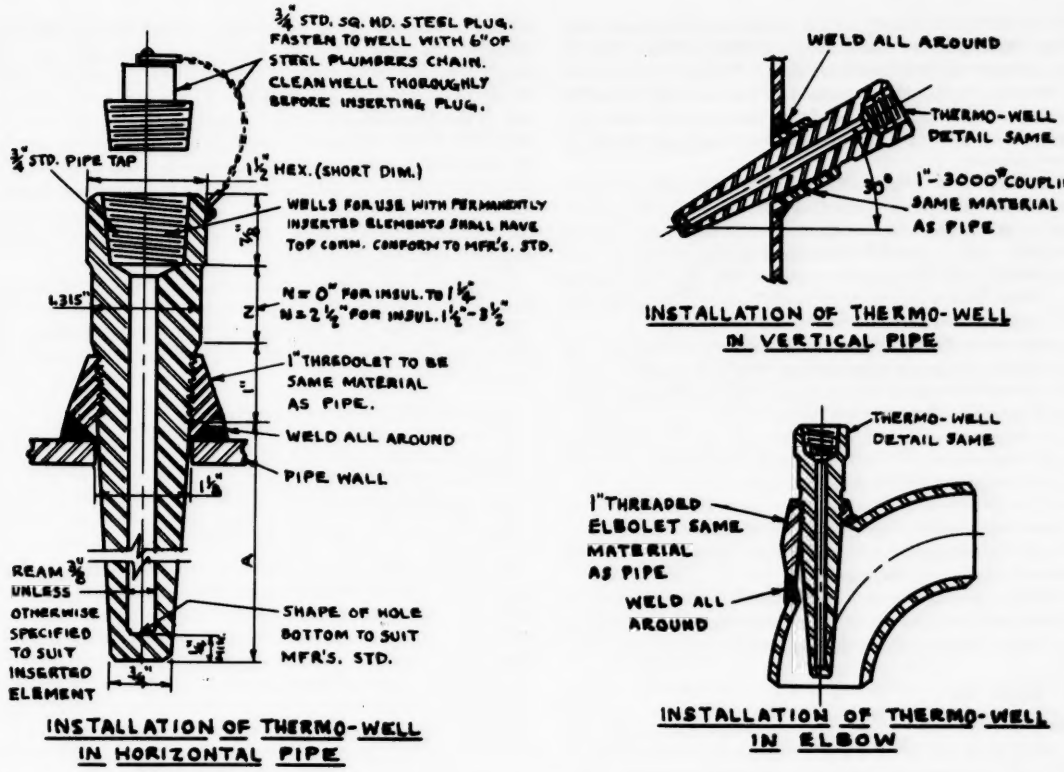
¾" STD. SQ. HD. STEEL PLUG. FASTEN TO WELL WITH 6" OF STEEL PLUMBERS CHAIN. CLEAN WELL THOROUGHLY BEFORE INSERTING PLUG.
¾" STD. PIPE TAP
1½" HEX. (SHORT DIM.)
WELLS FOR USE WITH PERMANENTLY INSERTED ELEMENTS SHALL HAVE TOP CONN. CONFORM TO MFR'S. STD.
4.315"
N = 0" FOR INSUL. TO 1¼"
N = 2½" FOR INSUL. 1¼"-3½"
1" THREDOLET TO BE SAME MATERIAL AS PIPE.
WELD ALL AROUND
PIPE WALL
REAM ⅜" UNLESS OTHERWISE SPECIFIED TO SUIT INSERTED ELEMENT
SHAPE OF HOLE BOTTOM TO SUIT MFR'S. STD.
INSTALLATION OF THERMO-WELL IN HORIZONTAL PIPE
WELD ALL AROUND
THERMO-WELL DETAIL SAME
30°
1"-3000# COUPLING SAME MATERIAL AS PIPE
INSTALLATION OF THERMO-WELL IN VERTICAL PIPE
THERMO-WELL DETAIL SAME
1" THREADED ELBOLET SAME MATERIAL AS PIPE
WELD ALL AROUND
INSTALLATION OF THERMO-WELL IN ELBOW

Fig. 8 Thermometer or thermocouple test wells for low pressure steam or water service

NOTES:

1 Material of well shall be high chrome alloy ASTM A182-F6.
2 Manufacturer shall stamp projection of well to indicate material used with ASTM No. and tag No.
3 For pipe of 12-in. diam or less, specify dimension "A" in increments of 1 in. so tip of well will reach center line of pipe $\pm 1/2$ in. For pipe more than 12-in. diam dimension "A" shall be not more than 6 in.
4 Approval by Chief Mechanical Engineer must be secured for application of wells into piping where steam velocities exceed 18000 fpm or liquid velocities exceed 15 fps.
5 Wells with dimension "A" over 6 in. may be used with low velocities (for example, circulating water) with approval of Chief Mechanical Engineer.
6 In any case, immersion into the flowing stream shall be not less than 3 in.
7 In a pipeline 4-in. diam or smaller in size, the well must be arranged axially in the pipe facing the oncoming flowing media where possible and inserted in an elbow or tee.
8 In pipelines smaller than 4 in., the tee or elbow should be one size larger than the line; and in pipelines 2 in. or smaller, an enlarged section of pipe shall be provided immediately upstream of the tee or elbow so as to avoid serious impedance of flow by the well.

For use with:
Water service not exceeding 900 psig—steam service not exceeding 750 F for 900 psig.

Another important reason for maintaining the high pressure and high temperature wells of the same material as the piping, is the problem of welding austenitic stainless steel to carbon steel or alloy steel.

To quote the comprehensive review of "Welding Stainless Steel to Carbon or Low-Alloy Steel," by J. B. Rutherford in the *Welding Journal*, January, 1959: "The application of stainless steel to low alloy welding to the field of high-pressure, high-temperature steam generation is fraught with difficulties, as is evidenced by the amount of research performed in this field."

J. E. Donahue of Westinghouse in his article "Butt Welding Austenitic Stainless Steel to Ferritic Steel in Cylindrical Shapes," (*Welding Journal*, November, 1957) favors the use of transition pieces containing the transition weld: "Use sufficient length in the transition piece on each side of the transition weld. This is necessary to provide the flexibility needed to absorb the differential growth in diameter at the transition weld. It also assures that the subsequent ferritic-to-ferritic weldment and the subsequent austenitic-to-austenitic weldment at the ends of each transition piece are unaffected by the discontinuity at the transition weld. Thus the weldments at the ends of the transition piece, which may be in locations less than ideal, are not subject to the additional loading from the transition weld.

"In essence, then, the design produces a transition weld free of mechanical stress concentration factors, in a piece sufficiently long to provide adequate flexibility for absorbing the differential diameter growth."

This method of welding austenitic steel to low alloy steel has been used successfully by Westinghouse, and has shown the reliability, to date, demanded in high-pressure, high-temperature service. But the cost is understandably higher than that of a simple joining weld.

The extensive bibliography on this subject contains papers with differing conclusions on many phases of this problem—for example, preheat and stress relief required. I believe that, at this time, the problem should be avoided and thermo-wells that are to be welded into the pipe should be of the same material as the pipe. Response time, reliability and over-all lower cost point to this as the best solution.

This leads us into the related question of wall thickness of the thermo-wells. The paper states that: "It was decided to adhere to the $^3/_{16}$-in. thickness for the supplement to reduce the number of standard wells required." The paper also states that: "For static conditions the design must conform with the requirements of the ASME Code for Unfired Pressure Vessels. The applicable portion is given as a curve, Figure UG-31."

If a thermo-well with a $^7/_8$-in. tip diameter were used for 2000 psig at 1055 F of chrome-moly material ASTM A 182-F22 having a code allowable stress of 5640 psi, the thickness required at the tip per Figure UG-31 would be 0.219 in.

If for the same conditions austenitic steel A 182-F321 with a code allowable stress of 12,800 psi is used, the thickness required at the tip per Figure UG-31 would be 0.131 in.

From the foregoing, it is not clear how the recommended $^3/_{16}$-in. thickness was arrived at so as to apply to all materials at all pressures and temperatures. A clearly defined limitation should be placed on the $^3/_{16}$-in. tip thickness.

It would be desirable to give for the present code materials the maximum pressure and temperature conditions for which the $^3/_{16}$-in. thickness standard thermo-well would be satisfactory.

A. F. Smith, 3rd[7]

The damage to rotating and other equipment which could possibly result from the failure of thermometer wells indicates that considerable care and effort should be exercised in design to prevent such failures without materially reducing the accuracy of the temperature measurements. As shown so clearly in Table 1, nearly all the factors which improve well strength tend to reduce accuracy and response rate. This paper is doubly welcome not only because it focuses attention on well design and provides the designer with a much needed procedure, but also because it holds forth the promise of the adoption of a standard ASME thermometer well.

About two years ago, our company began an investigation of thermometer well and sampling nozzle design methods which culminated in a design procedure quite similar to that developed in this paper. This procedure which has been in internal use in our company for over a year, was based in part on the author's earlier work. It is particularly gratifying to find that the method contained in this paper includes provisions for forced vibration induced by Karman vortexes. Undoubtedly, this has been neglected frequently in the past. Investigations of the few well failures known to us suggest that failure was due to Karman vibration.

It may be suggested that the Strouhal number is a function of Reynolds number or some other factor or, if a constant, its exact value may differ from the 0.22 used by the author. However, on the basis of the data available, it appears that no better assumption is possible. In addition, the assumption of a limiting frequency ratio of 0.8 provides for some deviations in this value.

The author has wisely avoided discussing material selection and methods of attachment. Both present problems of their own affecting the over-all design and size of the well. Here also, solutions facilitating these problems may reduce the response or accuracy of the well by increasing its over-all size or restricting its immersion.

Two common methods of attaching thermometer wells are by welding or threading them into a boss mounted on the outside of the pipe. In these cases, it is important to note that the well length L to be used for strength calculations is the distance from the tip to the point of rigid support. This is particularly important in the determination of the frequency ratio since the natural frequency of the well varies inversely as the square of this length. For thick walled piping such as steam lines in modern central stations, this length may significantly exceed the immersion length. Consequently, it is desirable that the well be supported as close to the inner pipe wall as possible. This will permit either longer immersion lengths or lighter wells.

The over-all size of the well may also be reduced by selecting a material with a higher allowable stress than that normally used for the piping. This may introduce differences in expansion coefficients and welding difficulties. Some of the factors desirable in the material selected are:

High strength at elevated temperatures.
High modulus of elasticity.
High fatigue strength of endurance limit.
Good damping characteristics.
Low notch sensitivity.
Expansion coefficient similar to pipe material.

In general, these are the same characteristics required for first stage turbine blading. One steel manufacturer who was consulted regarding this problem recommended the use of a ferritic-type stainless steel with an approximate composition of 12–14 per cent chromium, 1 per cent nickel, 1 per cent molybdenum, 1 per cent tungsten for temperatures below 1100 F. This type steel was recommended because it was believed superior to austenitic types in strength, damping ability, and notch sensitivity and because it has an expansion coefficient substantially the same as the normal pipe materials.

One disadvantage of this metal is that strength welding is not recommended. This is not a serious limitation since the wells may be threaded into bosses and seal-welded. One method of attachment developed by our company threads this type well into a pre-fit boss mounted in the pipe wall. This method of attachment also provides for positive support of the well at the inner pipe wall, thus minimizing the unsupported length of the well. It also permits omission of the wells from the pipe when the lines are blown out and facilitates later removal for inspection after the line has been in service. We feel that it is highly desirable to remove the wells from lines to be blown out in order to avoid the possibility of damage to the well and the formation of additional stress concentrations from nicks caused by particles blown out. Furthermore, the blowing out procedure subjects the well to fluid velocities not normally recognized in the design of the well.

In conclusion, this is a very worth-while paper on a neglected subject and it is hoped an ASME Standard on thermometer well design is evolved as a result. Two suggestions for improvement may be made. It would be helpful if the well length L were explicitly defined as the unsupported length of the well. While this is implicit in the present form of the paper, possible misapplications might be avoided by making it definite. Secondly, it would be helpful if the standard well sizes developed by the author were expanded to include one with a $^5/_8$-in. bore, a bore size required by some resistance type thermometers.

J. O. Smith[8]

As the author has pointed out, the nature of flow-excited vibration as related to thermometer wells in pipelines, and the nature and magnitude of the forces causing such disturbances, are topics

[7] Mechanical Engineer, Gilbert Associates, Inc., Reading, Pa.

[8] Senior Engineer, Engineering Research Department, The Detroit Edison Company, Detroit, Mich.

about which little information has been available to the engineer. In large diameter piping carrying steam of high density and velocity, the problem of lateral vibration of thermometer wells can be serious.

Shortly after the first unit of one of our new power plants became operational, it was observed that certain of the thermostat wells in the main steam and reheat steam lines were undergoing continuous vibration of appreciable amplitude at relatively high frequencies. The outwardly visible manifestation of the well vibration was the lateral vibration of the control rods protruding from the bores of these wells. The disturbances caused repeated failures of control mechanisms attached to the rods. Concern as to the stresses that resulted from such vibration prompted an investigation aimed at shedding light on the mechanism of excitation by fluid flow and the magnitude of the alternating forces acting on the wells.

Tests were conducted on four model wells installed in 2-in. diameter piping, using compressed air as the flow medium. The model wells were $^1/_4$-in. in diameter and were designed to have lateral natural frequencies of 140, 205, 320, and 790 cps, respectively. Bonded strain gages were installed such that their output was proportional to the lateral deflection of the wells. The tests consisted of passing compressed air through the pipe in increments of velocity up to 240 ft per sec. At each velocity increment, an oscillograph recording was made of the oscillating strain in the cylinder assembly.

In view of the widespread acceptance of the concept of forced vibration in accordance with the Strouhal relationship [the authors' formula (2)], the test results were surprising. The Strouhal relationship implies that the frequency of vortex shedding and, correspondingly, the frequency of the alternating forces acting on a cylinder vary as a linear function of flow velocity. If this were the case, the frequency of the vibration induced by the forces would vary in a like manner. Maximum amplitudes would develop at some "critical" velocity at which the ratio f_w/f_n is unity, as in the case of any forced vibration. The vibration of the well models, however, took place at their respective natural frequencies at all flow velocities. The amplitudes did not peak at the calculated "critical" velocities, but instead increased continuously with flow velocity approximately in proportion to the stagnation pressure ($V^2\rho/2$).

The conclusion drawn from these results was that the phenomenon is one of self-excitation, rather than forced vibration. As such, there is no single "critical" velocity at which resonant vibration takes place. Rather, the system is in resonance at all flow velocities. The amplitude at any velocity is proportional to the lateral exciting force and inversely proportional to the damping present in the system.

Further observations on the aforementioned vibrating thermostat wells lent some credence to the conclusion of self-excitation. The frequencies at which these wells were vibrating, as measured with a sound frequency analyzer, coincided approximately with their calculated fundamental natural frequencies.

By the use of additional experimental data on the resilience and damping capacity of the model wells, the magnitude of the lateral exciting pressure was established as approximately 0.05 times the stagnation pressure. This value was based upon assumptions that (1) the pressure acted over the entire projected area of the well, and (2) the pressure alternated sinusoidally at precisely the natural frequency of the well.

It is of interest to note that recent literature has reported findings very much in line with the results of the tests herein discussed. An investigation by Ozker and Smith[9] into the nature of wind-induced vibration of tall smoke stacks led to the conclusion that such vibration is self-excited. The results of wind tunnel studies on cylinders of various sizes led Penzien[10] to similar conclusions.

[9] M. S. Ozker and J. O. Smith, "Factors Influencing the Dynamic Behavior of Tall Stacks Under the Action of Wind," TRANS. ASME, vol. 78, 1956, p. 1381.

Author's Closure

The discussions submitted materially enhance the value of this paper. The author wishes to thank each of the discussers for his individual contribution. The following comments are made to each discussion in the order of presentation:

Mr. Lowell A. Holcomb's desire to see thermometer well design and installation criteria extended to include fluid power testing in aircraft and missile application may in part be fulfilled when the new Power Test Code Supplement on Temperature Measurement is published. Although no specific design applications will be included, this Supplement will contain basic information for designing a thermally correct installation for any given application. A comprehensive ASME Standard on well design would include aircraft and missile applications.

Mr. Rawleigh M. Johnson's discussion confirms the basic tenets of this paper.

Mr. Frank M. Kamarck's discussion, although it contains much that is beyond the scope of this paper, is pertinent. The problems involved in well design are not those of strength alone, but also of thermal properties of materials and methods of attachment as Mr. Kamarck vividly illustrates. The following detailed comments of his discussion are made:

1 The method of attachment of the thermometer well to the pipe is under the cognizance of the ASME Boiler and Pressure Vessel Committee. Problems connected with attachments should be taken up directly with that group.

2 In regard to the material to be used for thermometer wells and the $^3/_{16}$-in. wall thickness for all wells, it is not stated nor intended that they, to quote Mr. Kamarck ". . . apply to all materials at all pressures and temperatures." Because of the infinite number of applications possible it was decided to standardize on *size*. The author's statement that "Any material approved by these (ASME) codes for the intended service may be used" and the design procedure precludes the use of materials beyond their allowable stress limitations. It would be impractical to list concisely the maximum pressure and temperature limitations for which the $^3/_{16}$-in. thickness thermometer well would be satisfactory since this would involve materials, velocities, and application as well as the temperature and pressure. The Design Procedure enables this information to be computed quickly for a given set of conditions.

Mr. A. F. Smith, III's discussion commends the author for omitting those items which Mr. Kamarck feels necessary. However, both discussions show the clear-cut need for a comprehensive standard and both are valuable in pointing out the areas in which further work should be done. The length of the well L is the unsupported length of well. The author thought that this was clear from his Fig. 2, but if any doubt exists it is hoped that this statement will prevent possible errors arising from misunderstandings. In regard to Mr. Smith's request for the inclusion of a $^5/_8$-in. bore, this size was considered by the PTC 19B but was not considered necessary for the purpose of a Power Test Code.

Mr. J. O. Smith's discussion cites excellent papers and unpublished test results to support the theory that there is no "critical" velocity at which resonance would occur. A recent paper,[11] not available to the author at the time of his preparation, gives evi-

[10] J. Penzien, "Wind Induced Vibration of Cylindrical Structures," *Journal ASCE*, vol. 83, No. EM-1, January, 1957.

[11] D. M. McGregor, "An Experimental Investigation of the Oscillating Pressures on a Circular Cylinder in a Fluid Stream," UTIA Technical Note No. 14, Institute of Aerophysics, University of Toronto, June, 1957.

dence of the Strouhal effect at velocities up to 240 ft/sec in air (same upper limit as Mr. Smith's experiments). A value of $S = 0.198$ was reported. It is evident from the published literature that further research is necessary to determine the true nature of well failures for vibration. The method proposed by the author is conservative. Until research confirms the validity of either concept, or suggests a different one, it would be better to forego the use of longer wells in return for assurance of safety.

In Summary. The discussions submitted confirm the original thesis of this paper that an ASME Standard for Thermometer Wells is necessary. It further indicates the need for research to determine the true nature of thermometer well vibration.

A. A. PUTNAM

Assistant Chief,
Battelle Memorial Institute,
Columbus, Ohio
Mem. ASME

Flow-Induced Noise in Heat Exchangers

ONLY rarely have noise generations, excessive pressure losses, tube failures, and wall buckling, all resulting from vortex shedding, constituted a severe problem in heat exchangers, in the past. However, with the increasing emphasis on more compact heat exchangers and higher velocities in heat exchangers, the kinetic energy available for producing strong vorticity and overcoming damping losses is increasing. At the same time, cleaner designs are leading to a decrease in the relative acoustic-damping losses within heat exchangers. Thus the problems associated with vortex shedding can be expected to become more common and more acute.

It is the purpose of this paper to outline the general mechanisms by which this noise is generated and to present some examples in which difficulties have been caused by the vortex-shedding phenomenon. A future course of action in handling these problems is suggested.

Types of Vibration Involved

Before discussing the over-all problems of vortex-induced noise, it is well to consider the three types of oscillations or vibrations that can be involved. The first is the vortex shedding itself. An example of this phenomenon is shown in Fig. 1. It is seen that vortexes periodically shed from alternate sides of the obstacle, causing a wavy flow pattern in the wake of the obstacle [1].[1] The frequency of the vortex shedding from a rod is proportional to the flow velocity and inversely proportional to the rod diameter, for Reynolds number in the range of about 200 to 500,000. The dimensionless group which results from this relation, $\nu D/V$, is termed the Strouhal number, after one of the early investigators in this field. It should be mentioned that occasionally the inverse group, $V/\nu D$, is given this name; this can lead to confusion.

The second type of oscillation to be considered is that associated with the acoustic characteristics of the heat exchanger; specifically it is the oscillation normal to both flow directions and tube length. In a rectangular duct, the transverse acoustic oscillation of the lowest frequency has a wave length equal to twice the duct width. In the fundamental mode the gases slosh across the tubes from one side of the duct to the other. Other possible frequencies in this simple system are equal to multiples of the fundamental frequency. It can be easily visualized how such oscillations can couple with vortex shedding from the tubes such as just described. Fig. 2 shows possible alternate phases of such a coupled oscillation as solid and dotted lines.

Fig. 1 Alternate vortexes in wake

The third type of vibration that can occur is mechanically related to the heat-exchanger element itself. The square of the frequency of vibration of such an element is proportional to the flexural rigidity of the element, and inversely proportional to the cross-sectional area, density, and fourth power of the length. The proportionality constant depends on the end conditions of the element and the particular mode of oscillation. Coupling of the vibration of an element of the heat exchanger with the vortex shedding from the heat-exchanger element occurs when the pressure forces associated with the vortex shedding push the element from side to side, and the resulting movement of the element sharpens or makes more precise the timing of the vortex shedding.

To summarize, the type of noise under discussion can be generated by three mechanisms. In the one, the natural frequency of vortex shedding at a particular flow rate is close to a natural acoustic frequency of the exchanger [2]. The two systems thus couple, and kinetic energy in the flow stream is converted into acoustic pressure waves. Not only can the noise be intense, but in severe cases, walls can buckle under the pressure effects [3]. This type of coupling will be the subject of the present discussion.

In the second mechanism, a natural frequency of the heat-exchanger tubes or plates may be near the natural vortex-shedding frequency of these heat-exchanger elements. In this instance the tube will start to vibrate and reinforce the vortex shedding. The consequences of this mechanism are severe noise, and fatigue or structural failures. This type of difficulty is to be expected more often in small heat exchangers with lightly built elements. Only recently, there has been reported a variation of this type of coupling, in which flow parallel instead of perpendicular to the tubes of the tube bank leads to a coupling of vortex shedding along the tubes with the natural frequency of the tubes [4]. This phenomenon appears to be much more complex than the usual type, if only from the fact that the amplitude of oscillation affects the frequency significantly.

A third possible condition is one in which vortex-shedding frequency, tube frequency, and acoustic frequency of the system all couple together.

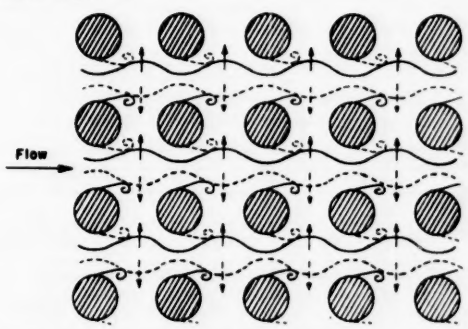

Fig. 2 Alternate phases of a possible coupled acoustic and aerodynamic oscillation

[1] Numbers in brackets designate References at end of paper.

Contributed by the Gas Turbine Power Division and presented at the Annual Meeting, New York, N. Y., November 30–December 5, 1958, of THE AMERICAN SOCIETY OF MECHANICAL ENGINEERS.

NOTE: Statements and opinions advanced in papers are to be understood as individual expressions of their authors and not those of the Society. Manuscript received at ASME Headquarters, August 18, 1958. Paper No. 58—A-103.

Several cases of vortex shedding in which acoustic coupling with the system occurred will now be discussed. However, it is well first to consider a simple system of two parallel rods [5]. When the rods are more than a diameter apart, the frequency of vortex shedding for each is that for a single isolated rod. As the rods are moved closer together, the outer vortexes begin to act as a pair, with a decreasing frequency, and the inner vortexes also act as pairs with increasing frequency. When the rods are very close, the lower frequency moves upward again, ending at contact of the rods at a frequency of about the same value as would be obtained for a single rod of twice the original diameter. The higher frequency stops at a gap distance of about one half the rod diameter, and another much lower frequency takes its place. It might be deduced from these tests that in a multiple bank of rods, widely spaced, the single-rod frequency can be expected. However, when the rods are close together, the frequency will depend on gap width as well as rod diameter.

Noise in In-Line Tube Banks

Banks of heat-exchanger elements can be considered in two general classes, in-line and staggered. Most of the reported cases of oscillation have concerned in-line tube arrangements, such as shown in Fig. 3. For instance, Baird reported a severe case of pulsations in the superheater-economizer duct of the Etiwanda Steam Station [3]. This pulsation was so severe that the duct walls were permanently distorted outwardly. This is not surprising since amplitudes of ±3 psi were reported at the walls. It was found that the second mode of oscillation was generated along the 38-ft distance perpendicular to both tube lengths and flow direction. The use of properly spaced baffles between the tube rows at velocity antinodes (pressure nodes) effected a cure.

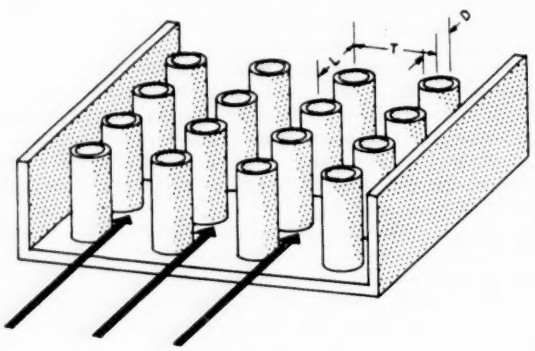

Fig. 3 In-line tube bank

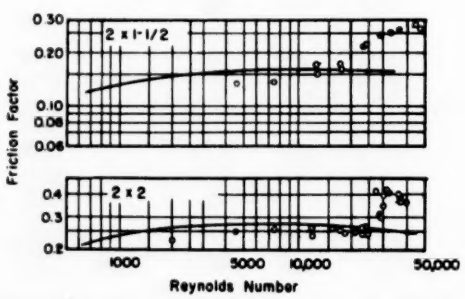

Fig. 4 Pressure-drop increase at onset of noise

Halliday reported a case of vibration in the boiler uptake immediately above the economizer; this problem developed in the dockside trials of a rather large ship [2]. The acoustic mode of vibration was the first transverse mode in the duct, in which the tubes were in an in-line pattern. The interesting feature of this report is that a $^1/_8$-scale model of the system was fabricated, and various splitter-plate sizes and locations tested to find a suitable means to suppress the oscillation. It was found that a splitter plate $^1/_8$ of a wavelength in length, located $^1/_2$ wavelength above the economizer, satisfactorily eliminated the oscillation in both model and prototype.

Jones and Monroe, in studying the pressure-drop and heat-transfer characteristics of a variety of experimental heat exchangers, found another difficulty beyond that of the noise [6]. As shown in Fig. 4, when the noise occurred, and over the range of Reynolds numbers in which it occurred, the pressure drop increased to almost double the expected value. Later tests in which the natural frequency of the tubes was varied showed no change in results; this indicated that the phenomenon was the acoustic-aerodynamic type [7].

An extensive study of noise in in-line heat exchangers has been reported by Grotz and Arnold [8]. Fig. 5 shows a possible correlation of these data on the basis of a Strouhal number, based on transverse distance between elements, and a function of the spacing ratios. Sufficient data are presented to indicate that there is some degree of correctness in such a relation, but it is also easy to show that the suggested relation cannot be generally true. For instance, for widely spaced tubes, the Strouhal number based on individual tubes should be constant. For in-line tubes with the lines of tubes far apart, the terms containing the spacing T should drop out of the fundamental equation for frequency. Likewise, for tube banks with a small value of T/D and a large value of L/D, the frequency should be some function of D and T, and principally depend on the difference, $T - D$.

Grotz and Arnold also present a discussion of the range of flow rates about the mean value over which coupling and thus oscillations occur, and the proper use of splitters to elimi-

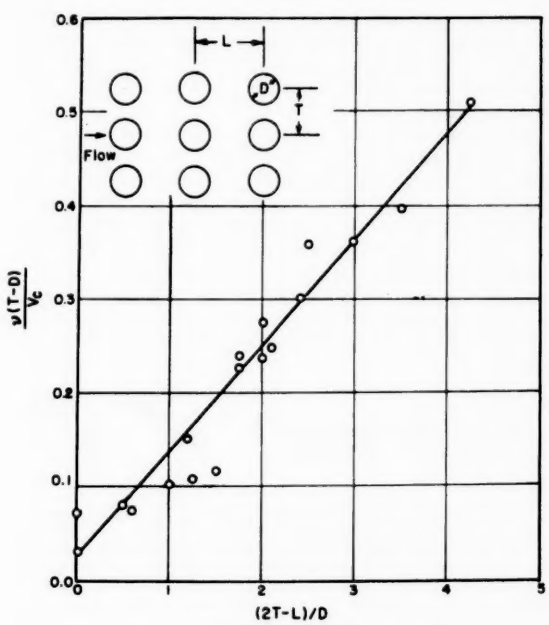

Fig. 5 Correlation of noise data from in-line heat exchangers

nate oscillations. It is pointed out that a diagonal splitter should cut out all the transverse oscillations. However, the use of such a baffle was found to induce a new type of oscillation at higher flow rates.

Noise in Staggered Tube Banks

Fig. 6 shows a staggered arrangement of tubes; this may be compared with the in-line arrangement of Fig. 3. Not as many instances of difficulties with staggered arrangements of tubes have been reported as with in-line tubes. One example which might be mentioned, however, is a case of a severe oscillation produced by a bank of diamond-shaped tubes in an experimental locomotive air heater [9]. As near as can be determined from available data, the Strouhal number was in the proper range to indicate the occurrence of vortex shedding coupled with transverse acoustic oscillation. Because of the staggered arrangement, and the restricted areas at the inlet and outlet, splitters or other baffling could not be used to eliminate the oscillation. However, a change in tube shape to cylindrical corrected the difficulty over the needed range of operation.

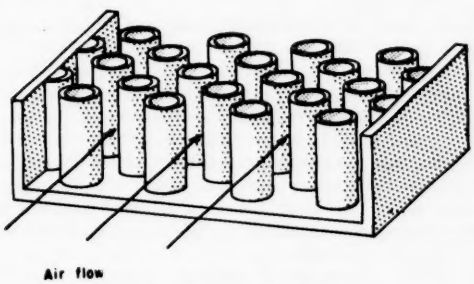

Fig. 6 Staggered-tube bank

In a study at Battelle of deposition on heat-exchanger elements, the experimental heat-exchanger section shown in Fig. 6 produced three successively higher oscillation frequencies at three successively higher flow rates [10]. The Strouhal number, based on the free-area velocity and tube diameter, averaged about 0.46 for these three noise conditions. The acoustic mode of oscillation was transverse across the width of the duct, and the first, second, and third modes successively appeared as the velocity was increased. The noise output in the vicinity of the unit was about 124 db for all three modes.

Concluding Remarks

To summarize this discussion, noise or vibration problems in heat exchangers may be encountered in those instances when a natural acoustic frequency of the exchanger in the direction normal to the flow direction and tube length is close to the frequency determined from the Strouhal number. In this case, coupling can occur giving oscillation of a large amplitude. Even if the noise can be tolerated, and the strength of a system is such that failures do not occur, an excessive pressure drop occurs in the system when such oscillations occur [6].

When the banks of tubes are closely spaced, interaction takes place between the vortexes shedding from the various banks of tubes. Experiments on pairs of tubes [5], in-line tubes [8], and staggered tubes [10] have shown that the Strouhal number no longer has a value of about $^1/_5$, as for a single isolated tube, and the critical dimension may be tube spacing rather than tube diameter. Furthermore, there are some indications in the literature that not only must higher modes of the acoustic frequency of the ducting and higher modes of the vibrating frequency of the tubes be considered, but in certain cases even multiples and submultiples of the vortex-shedding frequency may have to be considered [5, 11, 12].

Several types of equipment alterations have been found useful in suppressing the high amplitude noise. In one instance the heat exchanger was divided into sections by flat plates or flow splitters, thus increasing the lowest possible acoustic frequency [3]. In another instance the installation of splitter plate in the section upstream of the heat exchangers was found sufficient [2]. However, in these instances, an increase to higher flow velocities would probably have caused the problem to arise again. In a third case, dividing the heat exchanger diagonally successfully eliminated vortex shedding [8]. In this instance another type of oscillating phenomenon appeared at high velocities and warrants further study. Finally, an instance is reported in which a change in tube shape effected a cure.

It may be concluded that individual instances of vortex-shedding problems may be cured by trial and error, based on some experience and judgment. On the other hand, insufficient information is available to predict for tube banks, the flow rates at which frequencies will be most prominent, the range over which coupling will occur, or the noise amplitude. As flow rates become higher, sizes are reduced, and systems are "cleaned up," more difficulties resulting from the vortex-shedding phenomenon are to be expected. However, the fact that results can be scaled so well in this field gives considerable hope for an eventual method of routine design to obviate the problem. Toward this end, a four-stage program of research may be suggested.

The first phase of such a program would be a search of the literature and survey of manufacturers for pertinent information. Much of the general information on vortex shedding, pertinent to the problem, is already available [13] but specific items mentioned in reports on other subjects, information available from manufacturers, pertinent test results on vibrating heat exchangers or similar configurations, and pertinent acoustic-damping information would have to be located and classified.

The second phase of the program would be an evaluation of this information. It is believed that an analysis of the available data from the point of view of organizing it for this particular problem would be of great profit. On the other hand, there would be large areas in which information would be lacking, incomplete, or conflicting. These areas would be the subject of further study.

The third phase of the program would cover experimental work. The vortex-shedding frequency and noise amplitude would be studied in a variety of heat-exchanger sections, with a view to obtaining general relations and predictions. This program would be aided by visual studies in liquid-flow systems of the vortex-shedding phenomenon, and by acoustic studies of typical heat-exchanger configurations to determine natural frequencies, amplitude patterns, and damping losses.

In the fourth phase, a study would be made of various methods of reducing, eliminating, or controlling the deleterious effects of the vortex-shedding phenomenon.

Because of the simple scaling relations that occur in the field, the results of such a program would be of value in the design of all sizes of heat exchangers.

References

1 E. G. Richardson, "Dynamics of Real Fluids," Edward Arnold & Company, London, England, 1950.

2 John Halliday, "Boiler Vibration Caused by Combustion Gas Flow," ASME Paper No. 56—A-216.

3 R. C. Baird, "Pulsation-Induced Vibration in Utility Steam-Generating Units," *Combustion*, vol. 25, April, 1954, p. 38.
4 D. Burgreen, J. J. Byrnes, D. M. Benforado, "Vibration of Rods Induced by Water in Parallel Flow," TRANS. ASME, vol. 80, 1958, pp. 991–1003.
5 H. M. Spivack, "Vortex Frequency and Flow Pattern in the Wake of Two Parallel Cylinders at Varied Spacing Normal to an Air Stream," *Journal of Aeronautical Sciences*, vol. 13, June, 1946, p. 289.
6 C. E. Jones and E. S. Monroe, Jr., "Convective Heat Transfer and Pressure Drop of Air Flowing Across In-Line Tube Banks. Part I—Apparatus, Procedures, and Special Effects," TRANS. ASME, vol. 80, 1958, pp. 18–24.
7 A. J. Gram, C. O. Mackey, and E. S. Monroe, Jr., "Convective Heat Transfer and Pressure Drop in Air Flowing Across In-Line Tube Banks. Part II—Correlation of Data for Ten-Row-Deep Tube Bank," TRANS. ASME, vol. 80, 1958 (see comments by D. Dropkin), pp. 25–35.
8 B. J. Grotz and F. R. Arnold, "Flow-Induced Vibrations in Heat Exchangers," TN No. 31 to Office of Naval Research from Stanford, AD 104568, August, 1956.
9 R. M. Hardgrove, personal communication.
10 Carl Speich, personal communication.
11 A. B. C. Anderson, "Vortex Ring Structure-Transition in a Jet Emitting Discrete Acoustic Frequencies," *Journal of Acoustical Society of America*, vol. 28, 1956, p. 914.
12 W. E. Benton, "On Edge Tones," *Proceedings, Philosophical Society (London)*, series A, vol. 38, 1925–1926, p. 109.
13 A. A. Putnam, et al., "Injection and Combustion of Liquid Fuels," WADC TR 56-344, AD 118, 142, PB 131,008, chapter 13, March, 1957.

DISCUSSION

F. R. Arnold[2]

In his interesting survey of the status of research in flow-induced noise and vibrations in tube in-line heat exchangers, the author presents in Fig. 5 a possible correlation of noise data using as parameters a special Strouhal number $\nu(T - D)/V_c$, where $T - D$ is the least distance between tubes across the flow, and another he chooses as $(2T - L)/D$. He criticizes some aspects of his correlation by showing that it cannot be generally true since it is not suited for certain limiting cases. The writer would like to suggest a different set of parameters which he believes may be used to display the data consistently, including the limiting cases.

If we assume that we are experimenting under conditions such that the only significant variables are flow velocity V_c, tube diameter D, tube spacing in the direction of flow L, tube spacing transverse to flow T, and vortex shedding frequency ν, three dimensionless parameters are needed to organize the results. A set of independent parameters considered to be suitable consists of the usual Strouhal number based on tube diameter, namely $\nu D/V_c$, plus the ratios D/L and D/T. The latter two have values which lie between *zero* and *unity*, and at these limits are easily identified with recognizable physical situations. To use only two parameters, which nevertheless include the five variables, requires that more details of the functional relationship between them are known or else are guessed. While a graph of two such parameters might happen to fit a limited number of data, it would be very unusual to get a good fit for all data including extreme or limiting conditions as well.

By employing the three parameters suggested here, the Strouhal numbers may be plotted as a surface over the D/L, D/T-plane. The limiting edges of this surface correspond to especially significant limits of tube-bank configurations.

If one examines the intersection of the surface with the $\nu D/V_c$, D/L-plane at $D/T = 0$ one sees a curve representing all data corresponding to tests on all configurations of a single row of tubes in line with the flow. If one looks at the intersection of the surface with the $\nu D/V_c$, D/L-plane at $D/L = 0$, one should see a curve displaying the results of all tests on all single banks of tubes transverse to the flow. The curve corresponding to $D/L = 1$ would display results for banks of tubes that are touching each other in the flow direction, but with variable transverse spacing; while that for $D/T = 1$ would represent tubes in contact transverse to the flow, hence a series of corrugated plates broadside to the flow and blocking the test duct. The single corner of the surface located at $D/L = 0$ and $D/T = 0$, that is on the ν/DV_c-axis, is located at the Strouhal number for a single tube in a fluid flow.

An examination of the data taken in connection with the work forming the basis for the author's reference [8] indicates that the three parameters here suggested may be very good, and it is hoped that the results of future research in this increasingly important area will be available in greater quantities to produce a truly adequate correlation. This is needed to predict accurately the flow conditions likely to excite vibrations or produce flow impedance. Inability to control these conditions can lead not only to mechanical failure of components and to noise, but also to thermal failures in fuel elements of nuclear reactors if flow impedances in the coolant circulation should suddenly occur.

R. C. Baird[3]

In the matter of heat-exchanger noise and vibration, engineers appear to be caught in a sort of cross-fire. On the one hand, a manufacturer of a competitively priced product requires adherence to well-established shapes of uniform dimensions. On the other, the use of such shapes invites trouble from resonant-type dynamic forces and noise resulting from unstable fluid flow.

To illustrate the touchy relationship between the dimensional parameters important to boiler noise and vibration the exchanger sections of two "identical" boilers in the same plant can exhibit entirely different susceptibilities to gas pulsation. Sometimes the only apparent explanation lies in the slight differences in the precise design rectilinearity of exchanger tubes. In other words sloppiness in tube installation will render one boiler nonresponsive at design gas flow, while its accurately constructed mate pulsates with abandon.

Another example is the situation where pulsation of a new boiler gradually diminishes (or increases) with time as the tubes become increasingly fouled. A good cleaning can oftimes cause a reversion to the original condition. It has been observed that this can be caused by a deposition of $^1/_{16}$ in. or less on 2-in-diameter tubes just on their downstream sides.

In resonance-type pulsation and/or vibration, the level of the exciting energy is relatively unimportant. It is the acoustical-mechanical nature of the structure together with its low dissipative characteristics which allows the small oscillating energy increments to add cycle by cycle so that the oscillation can after a time represent a high level of dynamic energy.

It would seem that work in accordance with the third phase of the author's suggested program leading to prediction of the dynamic characteristics of fluid-flow systems is particularly desirable. Such could even lead directly toward new designs involving clever and economical use of dynamically inert geometrical shapes. It is agreed that successful prediction of the dynamic-flow characteristics of heat exchangers is in great need of fundamental information.

G. Theoclitus[4]

The author has raised some interesting points of which we have been aware for some time, although not to the extent brought out in the paper.

A few years ago we undertook a project to study the heat-trans-

[2] Associate Professor of Mechanical Engineering, Stanford University, Stanford, Calif. Assoc. Mem. ASME.

[3] Engineer and Consultant, Santa Monica, Calif. Mem. ASME.

[4] The Air Preheater Corporation, Wellsville, N. Y. Mem. ASME.

Table 1 In-line pins—square spacing
Diameter of pins, tests 1–9, $D = 0.128$ in.; tests 10–12, $D = 0.109$ in.

Test No.	Pin Spacing in Flow Direction L	Pin Spacing Transverse to Flow T	Pin Length	Acoustic Freq. of Duct Normal to Flow and Pin Length (Fundamental) C.P.S.	Acoustic Freq. of Duct Normal to Flow and Parallel to Pin Length C.P.S.	Natural Freq of Pins (Fund) C.P.S	Vortex Freq. at Peaks $f = \frac{0.2V}{D}$ First Peak C.P.S.	Vortex Freq. at Peaks $f = \frac{0.2V}{D}$ Second Peak C.P.S.	Relative Increase in Friction Factor -Percent- First Peak	Relative Increase in Friction Factor -Percent- Second Peak	Shape of Friction Factor vs. Reynolds No. Curve
1	2D	2D	12 D	1560	4220	6630	1700	2550	194	165	
2	2D	2D	8 D	1560	8100	12400	1730	3010	186	165	
3	2D	2D	4 D	1560	16200	59600	1930	2665	138	147	
4	3D	3D	12 D	1680	4220	6630	2170		161		
5	3D	3D	8 D	1680	8100	12400	2245		155		
6	3D	3D	4 D	1680	16200	59500	2160		148		
7	4D	4D	12 D	1560	4220	6630	2430		128		
8	4D	4D	8 D	1560	8100	12400	2460		136		
9	4D	4D	4 D	1560	16200	59500	2090		138		
10	2.29 D	2.29 D	41.3 D	1260	1440	657	1390		193		
11	2.66 D	2.66 D	41.3 D	1260	1440	657	1590		191		
12	3.03 D	3.03 D	41.3 D	1260	1440	657	1560		203		

Table 2

Pin Spacing	Strouhal No.
2D × 2D	0.175
3D × 3D	0.158
4D × 4D	0.136
2.29D × 2.29 D	0.181
2.66D × 2.66 D	0.158
3.03D × 3.03 D	0.162

Table 3

Pin Spacing	$\frac{2T-L}{D}$	$\frac{f(T-D)}{V}$
2D × 2D	2	0.184
2D × 2D	2	0.180
2D × 2D	2	0.162
3D × 3D	3	0.310
3D × 3D	3	0.300
3D × 3D	3	0.310
4D × 4D	4	0.387
4D × 4D	4	0.381
4D × 4D	4	0.453
2.29D × 2.29D	2.29	0.234
2.66D × 2.66 D	2.66	0.262
3.03D × 3.03 D	3.03	0.329

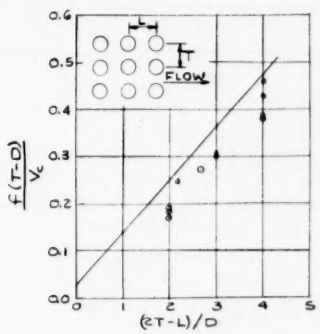

fer and flow-friction characteristics of some compact pin-fin heat exchangers. At that time we first observed the noise and vibration at the higher flow velocities which we attributed to a resonance condition produced by the vortex-shedding phenomenon. In the range where the noise and vibration occurred there was a marked increase in the pressure drop but no noticeable change in heat transfer.

The various geometries tested together with other pertinent data are included in Table 1. The information indicates that the resonance condition is generally due to the fundamental vortex-shedding frequency and the natural acoustic frequency of the duct normal to flow and pin length. Probably there is also some resonance due to the fundamental or higher modes of the vortex-shedding frequency with the acoustic frequency of the duct normal to flow and parallel to pin length.

There is no evidence to indicate that there was any pin vibration in any of these tests. In most of the tests, the natural frequency of the pins was too high to be reached by the flow velocity but in tests 10, 11, and 12 the velocity was in the region necessary to create the proper vortex-shedding frequency but no sign of such resonance was observed.

The reason for the double peaks in tests 1, 2, and 3 may possibly be caused by the higher modes of the vortex-shedding frequency.

Unfortunately frequency measurements were not taken during the tests and therefore the vortex-shedding frequency must be computed through the Strouhal number with no other check. Using a constant of 0.2 the vortex-shedding frequency for the $2D \times 2D$ and $2.29D \times 2.29D$ compare closely with the acoustic frequency of the duct normal to flow and pin length. The correlation becomes progressively worse with increased spacing. If we assume that the two frequencies are identical we can find what the Strouhal number should be, Table 2.

Although it is not entirely consistent there appears to be a trend for the Strouhal number to deviate more from the value of 0.2 at the greater pin spacing. This introduces an interesting paradox since it states that as the pin spacing increases the pin behaves less and less like an isolated pin. This is in line with what the author was referring to when he found it difficult to reconcile the correlation, Fig. 5, with the theory. The foregoing figures can be converted to additional points for Fig. 5. These fall below the line but the correlation is good, Table 3.

The author states that if the pins or tubes are spaced more than a diameter apart they will behave like isolated pins. This fact is more valid for the spacing normal to flow than the spacing parallel to flow.

Steinman[5] points out that for vortex stability the width between rows of eddies h and distance between successive eddies l must have the following relationship:

$$h/D = 1.3 \qquad l/D = 4.3$$

[5] D. B. Steinman, "Problems in Aerodynamic and Hydrodynamic Stability," Proceedings of the Third Hydraulics Conference, 1947.

This fact indicates that if the pins are not spaced more than one diameter apart normal to flow and four diameters apart parallel to flow some interference will occur and the aerodynamics become very complex.

The author has done an excellent job in preparing this report and should be congratulated. The four-stage research program he has outlined should contribute a great deal to the subject particularly as he points out: "As velocities become higher, sizes are reduced and systems are cleaned up."

Author's Closure

The author wishes to thank Messrs. Arnold, Baird, and Theoclitus for their thoughtful comments. Mr. Baird adds to the discussion some practical examples of the difficulties that may be encountered, based on his experience. In a sense, it is discouraging, however, to find that occasionally one way to get out of trouble is to build a "sloppy" unit, or to allow a unit to "crud up."

Professor Arnold points out that there are two independent variables and one dependent variable involved in our problem of predicting vortex-shedding frequency; therefore, plots such as in Fig. 5 would be expected to be acceptable only for a limited range of variables. An alternative three-dimensional plot to what Professor Arnold suggests uses L/D and T/D as the independent group. This has the advantage that these relations bear a greater resemblance to the physical spacing in a heat-exchanger unit. The disadvantage is that the range of these variables is from 1 to infinity. Since more confidence is had in interpolation and extrapolation of results in a finite region, the use of D/L and D/T in the manner suggested by Professor Arnold is to be recommended for analysis.

Mr. Theoclitus presents some extremely interesting additional data, which tend to confirm the simple relation suggested in Fig. 5. Since the data used in Fig. 5 were based on observations at the onset of noise, while those reported in Table 1 are for peak amplitude, the displacement of the entire set is to be expected. It would appear that the extrapolation of the curve through the new data would go through the origin.

Mr. Theoclitus points out a possible misinterpretation of the discussion of the work of Reference [5]. The intention was to indicate the complication that might occur as side-by-side tubes were moved close. If the tubes are in line, then the wake of the first will propagate downstream and affect the flow around the second tube, and so on. Thus, as Mr. Theoclitus indicates, spacing in the direction of flow cannot be expected to have the same influence as spacing transverse to the flow.

An interesting extrapolation of Mr. Theoclitus' remarks about Steinman's work can be made. If the spacings indicated are used to fill an entire region with vortexes, the natural frequency of the region might be expected to correspond with the single tube frequency. If a set of in-line tubes is superimposed on this region in a reasonable manner, one possible value of T/D for this tube array is 2.6, and one value for L/D is 2.15. For the two sets of data of Reference [8] for tube spacings near these values, the value of Strouhal number is close to the single tube value of about 1/5.

The Effect of Fuel Types and Admission Method Upon Combustion Efficiency

H. N. McMANUS, JR.[1]
W. E. IBELE[2]
T. E. MURPHY[3]

A series of tests to determine the effect of combustion-chamber length for three different types of fuel admission (gaseous, spray, and vaporized) upon combustion efficiency was performed in identical combustor geometries and with similar air-flow patterns. The effects of fuel-air ratio and full-section velocity were examined for individual methods of admission. The effect of fuel volatility also was examined. It was found that the vaporized fuel type of admission was superior in efficiency to the spray-fuel admission in all comparable cases. Increased fuel volatility improved performance in the case of the vaporizer but did not affect the performance of the spray nozzle. The performance of vaporizing tubes was found to vary inversely with size. An optimum size was exhibited.

THE TWO BASIC schemes of fuel admission that have been used in aircraft gas turbines have employed the spray nozzle in its simple and more sophisticated forms and the so-called vaporizing tube. Spray admission of fuel has found the greatest favor among designers, although the vaporizing technique would seem to possess certain unique advantages.

A review of the unclassified literature discloses that a reasonably large amount of information is available about spray admission; however, very little information of a basic or applied nature has appeared about the fuel vaporizer although its use was suggested and investigated almost simultaneously with the advent of the gas turbine engine [1, 2].[4] It is well to note that use of a gaseous fuel such as butane offers a third possible method of fuel admission. However, this method has not been employed in practical aircraft engines. No direct comparison of the performance of the three methods in identical geometries has appeared.

In view of the desirability of having a direct comparison of these techniques, a series of studies was made which included tests to permit evaluation of the performance of the possible fuel-admission systems in the same burner configuration. The work proceeded in three distinct phases:

1 A burner yielding maximum flexibility of air-admission patterns was constructed and operated with gaseous fuels. The effect of full-section combustor velocity and length of combustion zone upon burner efficiency was investigated [3].

2 An atomizing fuel nozzle was fitted in the burner and the effect of fuel volatility and burner length upon efficiency determined [4].

3 A vaporizing tube was designed for use in the burner. The effect of cane size and volume of primary combustion zone, i.e., the burner volume upstream of the vaporizer outlets, was noted. Additionally, four fuels were tested in the optimum vaporizer tube, and again the effect of combuster length upon efficiency was noted. The effect of fuel-air ratio upon cane performance was also investigated [5, 6].

Apparatus

The apparatus which was used in this series of investigations is shown schematically in Fig. 1. The compressor used was of the centrifugal type and pumped air to a large drum. The air flowed from the calming drum to the upper and lower air manifolds of the combustion chamber, first passing through an orifice

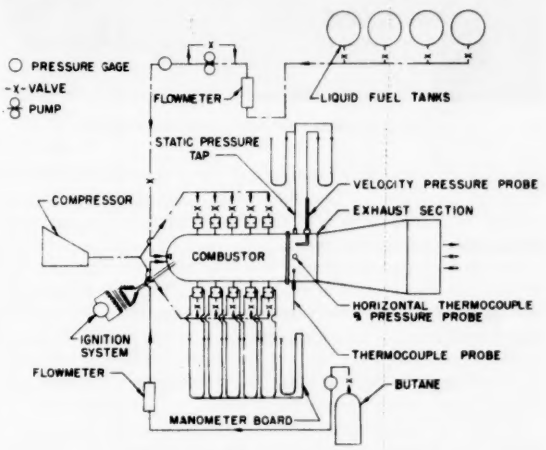

Fig. 1 Schematic diagram of test equipment

plate. The air flowed from the manifolds to the combustion chamber through a set of 48 rectangular ducts. Each of these ducts was fitted with a calibrated orifice for flow measurement and a butterfly-type valve for flow control. An over-all view of the burner with side plate in place and removed is shown in Fig. 2.

The burner was designed to approximate two-dimensional flow and was 2 in. wide, 5 in. deep, and 20 in. long and was constructed from stainless steel. The air was admitted from

[1] Assistant Professor of Mechanical Engineering, Cornell University, Ithaca, N. Y. Assoc. Mem ASME.
[2] Associate Professor of Mechanical Engineering, University of Minnesota, Minneapolis, Minn. Assoc. Mem. ASME.
[3] Associate Professor of Mechanical Engineering, University of Minnesota, Minneapolis, Minn.
[4] Numbers in brackets designate References at end of paper.

Contributed by the Gas Turbine Power Division and presented at the Annual Meeting, New York, N. Y., November 30-December 5, 1958, of THE AMERICAN SOCIETY OF MECHANICAL ENGINEERS.

NOTE: Statements and opinions advanced in papers are to be understood as individual expressions of their authors and not those of the Society. Manuscript received at ASME Headquarters, August 19, 1958. Paper No. 58—A-128.

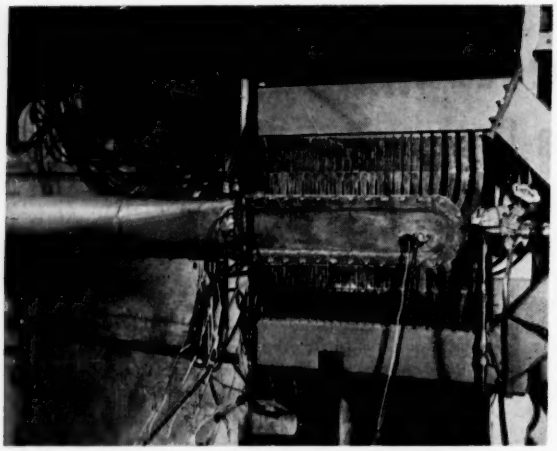

Fig. 2(a) Side view of burner

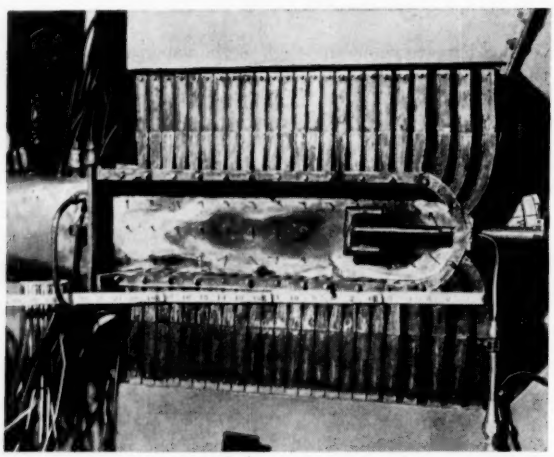

Fig. 2(b) Side view with side plate removed

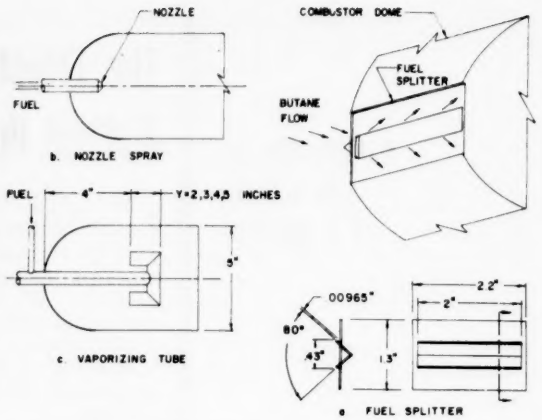

Fig. 3 Fuel-admission apparatus: (a) Fuel splitter (gaseous); (b) spray nozzle; (c) vaporizing tube

the 48 ducts through rectangular slots which extended the full width of the burner. The slots were designed in this way to inhibit the formation of a zone of recirculation in the upstream end if the operator so desired.

The gaseous fuel was stored in a tank in liquid form and was supplied to the system after first passing through a pressure-reducing valve, a throttle valve, and a rotameter. The gaseous fuel flowed into a duct which connected to the upstream end of the burner on its center line. A wedge-shaped flow splitter was used to direct the gaseous fuel toward the upper and lower part of the burner and is shown in Fig. 3(*a*).

Liquid fuel was supplied to the burner by means of fuel pumps fitted with manual bypass valves for delivery-pressure control. An atomizing-type nozzle was fitted into the upstream end of the burner on the center line. This nozzle delivered an essentially flat spray with an angle of 63 deg at 60 psig and had a capacity of 3 gph. The nozzle installation is shown in Fig. 3(*b*). Before installation its characteristics with different fuels and pressures were determined. A rotameter in the fuel-supply line was used to measure the fuel flow. The original gaseous fuel system was modified so that operation with gaseous fuel was still possible. This arrangement proved useful in effecting ignition.

The vaporizer tube employed was constructed in the form of a T and was fabricated from $^{5}/_{8}$-in-OD stainless-steel tubing with 0.028-in. wall. The installation and final dimensions of this unit are shown in Fig. 3(*c*). The tube was fitted with an air supply which could be adjusted independently of the main air to give the desired fuel-air ratio in the tube. The fuel flowing was measured by a calibrated rotameter.

Total-head probes in conjunction with side-wall static taps were used to determine the exit-velocity profile. Shielded thermocouples were employed for measurement of exhaust-gas temperatures, and the temperatures of the entering fuel and air were measured by bare thermocouples mounted in the supply lines. All pressure measurements were made with water-filled U-tube manometers. In addition to the foregoing instrumentation, the combustion chamber was fitted with 39 unshielded chromel-alumel thermocouples which were located $1^{1}/_{2}$ in. apart throughout the burner. These were installed for the purpose of obtaining the order of magnitude of the temperatures in the burner for various operating conditions.

Procedure

The operating procedure followed was basically the same for all tests. After establishing the air flow in the system, the desired combustion-chamber air pattern was set approximately by adjustment of the individual butterfly valves. Following this, combustion was established and the fuel flow brought up to the desired rate. The air pattern in the combustor was then readjusted to compensate for any change brought about by the hot gas flow. The primary combustion zone was defined as the distance from the upstream end of the burner to the point where the quench air was admitted. This distance was varied by adjustment of the air-inlet ports.

After stable conditions had been established, readings of fuel flow, air-mass flow, inlet and exit-gas temperatures, and exit dynamic pressures were made. In some cases, readings of the 39 combustion-chamber thermocouples were made. Following the recording of the foregoing data, the air patterns were readjusted to the next desired condition and the procedure repeated. In the majority of cases, the alteration consisted of moving the quench ports to vary the length of the combustion zone.

The basic air pattern used was one wherein sufficient air was admitted through the upstream-burner ports to provide a stoichiometric fuel-air mixture in the combustion zone of the burner. Downstream of these ports, a small quantity of air was permitted to bleed through a group of ports to prevent fuel entering the air manifolds. The combustion zone was terminated by

admitting large quantities of air at high velocity to effect quenching of the reaction.

The information obtained was used to calculate fuel-air ratio and combustion efficiency.[5]

Presentation of Results

The effect of the size of the combustion zone upon burner efficiency for a gaseous fuel (butane) is shown in Fig. 4. The full section velocity in the combustion chamber is plotted as a parameter. Fig. 5 shows the effect of fuel-air ratio upon the performance of various size vaporizing tubes. The cane size noted is the length of the upstream extensions of the vaporizing tube. In Figs. 6, 7, and 8 a comparison is presented between the performance of a nozzle burner and a vaporizing-tube burner for various fuel-air ratios and for fuels of different volatility. Fig. 9 shows the effect of combustion-chamber length upon efficiency for several sized canes employing naptha as the fuel.

Discussion of Results

In Fig. 4 it can be noted that, for the test burner used, the combustion efficiency increased quite rapidly as the length of the combustion zone increased. An interesting feature is that after a particular combustion-zone size was attained for a given full-section velocity, additional increments of length exerted little effect on combustion efficiency. It will be noted that the highest velocities used resulted in the greatest combustion efficiency. In one sense this result was contrary to expectations, but would tend to indicate that in this burner the more violent mixing with the higher velocities resulted in more complete combustion. At the higher velocity the greater efficiency due to improved mixing was attained, however, only with a substantial increase in burner length. The temperature probes in the burner

[5] An average exit temperature was calculated by assuming Cp constant and using equal flow areas, A_i. This gave the relation

$$T_{exit} = \sum_i (\rho V T)_i / \sum_i (\rho V)_i$$

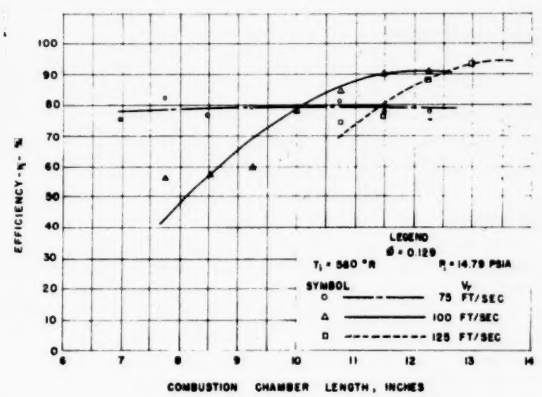

Fig. 4 Efficiency as a function of combustion-chamber length for butane

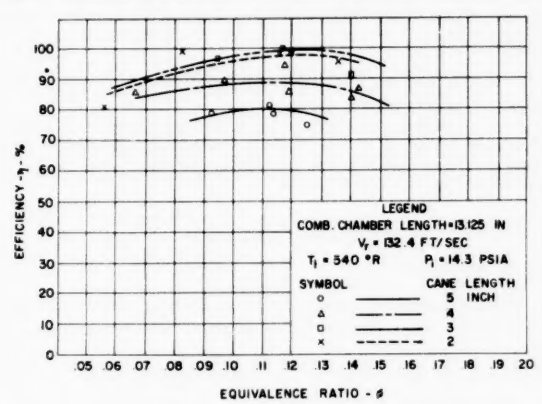

Fig. 5 Efficiency as a function of equivalence ratio for naptha

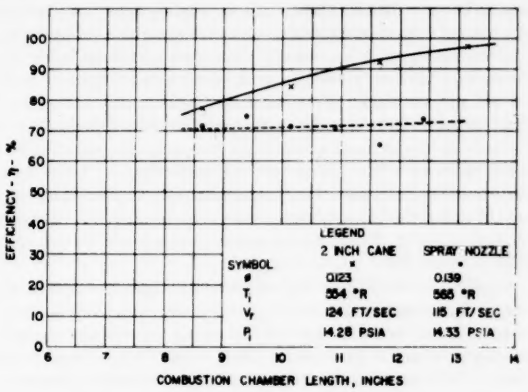

Fig. 6 Efficiency as a function of combustion-chamber length for aviation gasoline

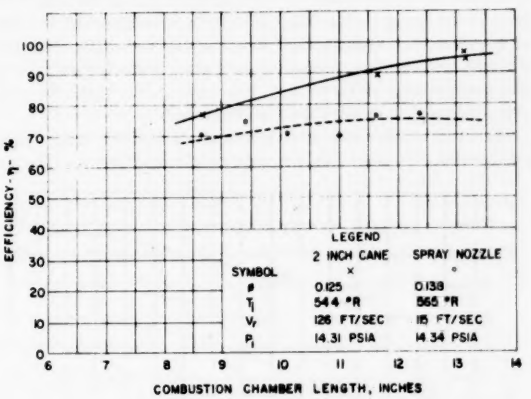

Fig. 7 Efficiency as a function of combustion-chamber length for naptha

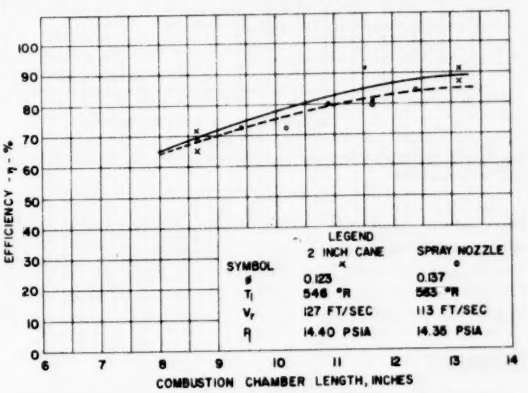

Fig. 8 Efficiency as a function of combustion-chamber length for kerosene

indicated that a very hot region existed at the center line of the combustion unit and extended into the tailpipe when gaseous fuels were used. The depth of this zone was somewhat reduced at higher velocities, thus supporting the contention that better mixing existed.

The test results in Fig. 5 show that a substantial decrease in combustion efficiency occurred with an oversize cane. When designing the cane it had been expected that advantages would exist if a large cane was used in that more complete vaporization would occur. Hence the results in Fig. 5 were not expected. Additional data showed that a cane with upstream projections of approximately $2^1/_2$ in. would yield the maximum efficiency. Decrease of fuel-air ratio caused the combustion efficiency to fall off for all cane sizes. This could be attributed to a decrease in heat transfer between the tube and the fuel flowing therein because of the reduced combustion temperatures resulting with lean mixtures. The effect of the reduction in heat transfer would be exaggerated since less completely vaporized mixtures would enter the burner, thus further depressing the efficiency. A similar set of circumstances would account for the fall off at higher equivalence ratios.

Figs. 6, 7, and 8 show the efficiency performance that existed for a spray nozzle and a 2-in. cane operating under similar conditions. It can be noted that the vaporizing type of fuel admission results in a sizable increase of combustion efficiency for all fuels used. Additionally, the gain in efficiency becomes greater as the length of the combustion zone is increased.

Comparison of these figures shows that with decreased fuel volatility the performance of the vaporizer tube falls off, while that of the spray nozzle holds relatively constant. In the case of kerosene, the spray-nozzle performance was higher than in the case of the other fuels and compared quite favorably with the performance of the cane. However, in all cases the cane performance was better than the fuel nozzle.

Fig. 9 shows the effects of combustion-chamber length upon combustion efficiency for a spray nozzle and several different

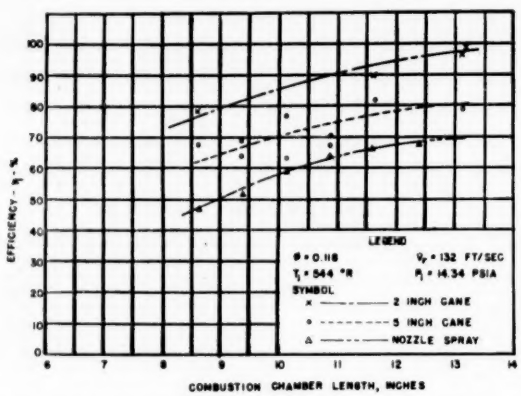

Fig. 9 Efficiency as a function of combustion-chamber length for naptha and various canes

sized canes. With the longer combustion-chamber length the efficiency of both canes and the spray nozzle is improved. The performance of the canes is superior in both cases to that of the nozzle. The effect of cane size is apparent and illustrates the trends already discussed.

Conclusion

For similar geometry and air-flow distribution the vaporizing-tube burner has been shown to be markedly superior, in so far as combustion efficiency is concerned, to the more conventional spray nozzle. The performance of the vaporizing tube was found to fall off with decreased fuel volatility while that of the spray nozzle remained essentially unchanged, and even improved when used with kerosene.

Contrary to expectations, the cane performance was found to vary inversely with length; i.e., heat-transfer area, rather than directly. An optimum cane size was found to exist.

An increase in combustion-chamber length has been shown to influence combustion efficiency favorably. In the case of the gaseous fuel for a fixed reference velocity a length was found to exist beyond which additional length increments produced no beneficial effect. In the case of the gaseous fuel, better performance was found to be possible with higher full-section velocities if the length of the combustion zone was increased.

Nomenclature

The following nomenclature is used in the illustrations:

p = pressure, psia
T = temperature, deg R
V = velocity, fps
$\eta_b = \Delta T_{\text{actual}}/\Delta T_{\text{ideal}}$ = combustion efficiency, per cent
ρ = density, pcf
ϕ = equivalence ratio

Subscripts

i = inlet
r = reference

Acknowledgments

The authors wish to acknowledge the advice and encouragement of Dr. Newman A. Hall of Yale University, who gave initial impetus to the work reported here, and the assistance of Messrs. Andre, Ryberg, Miller, and Barnes who, as graduate students at the University of Minnesota, performed the experimental work.

References

1 F. W. Godsey and L. A. Young, "Gas Turbines for Aircraft," McGraw-Hill Book Company, Inc., New York, N. Y., 1949, pp. 148–150.

2 W. D. Pouchot and J. R. Hamm, "Characteristics of a Vaporizing Combustor for Aviation Gas Turbines," TRANS. ASME, vol. 76, 1954, pp. 801–807.

3 P. L. Andre, Jr., "A Study of the Effect of Air Distribution on the Combustion Process in a Simulated Turbo-Jet Combustion Chamber," MS thesis, Department of Mechanical Engineering, University of Minnesota, 1953.

4 J. G. Ryberg, "The Effect of Various Liquid Fuels on the Optimum Length of an Open Cycle, Gas Turbine Burner," MS thesis, Department of Mechanical Engineering, University of Minnesota, 1953.

5 W. L. Miller, "Design and Performance of a Vaporizer Type Fuel Inlet System," MS thesis, Department of Mechanical Engineering, University of Minnesota, 1954.

6 R. J. Barnes, "A Study of the Effect of Various Fuels on the Optimum Length of a Gas Turbine Combustor Equipped With a Vaporizer Tube," MS thesis, Department of Mechanical Engineering, University of Minnesota, 1954.

DISCUSSION

P. G. Dooley[6]

The authors have presented an interesting report on their work with a very unique test apparatus. The conclusions are well substantiated by the data for the research conducted and must be evaluated as related to specific applications. The use

[6] Pratt & Whitney Aircraft, Division of United Aircraft Corporation, East Hartford, Conn.

of the same test configuration for gaseous fuel, vaporizing, and liquid injection is certainly a very direct approach for research testing; however, for a comparison of the relative merits for a specific application, each fuel should be evaluated in a chamber approaching its own optimum. Even a variation of the air-flow pattern within the equipment used might well change the magnitude of effects of the variables investigated.

It is especially interesting to note that with kerosene, which is similar to fuels used in aircraft gas turbines, the difference in efficiency between the spray and vaporizing injection systems is quite small. This should not be surprising since both systems are in day-to-day use in competitive engines and, if either were unquestionably superior, the other would long since have dropped from the scene.

The existence of a hot region on the center line of the burner which extended into the tailpipe when gaseous fuel was tested illustrates a fundamental problem of dispersion and mixing of the fuel with the entire air stream. Good mixing is required before a turbine can be subjected to such a gas stream. This dispersion is inherently easy to accomplish in a short length with liquid-spray injection and this very dispersion, which contributes to uniformity of temperature distribution, may result in an earlier quenching and cause the low efficiencies indicated with spray injection.

Presentation of the temperature data would add greatly to the value of this paper making it a more complete report of the tests conducted.

George Opdyke, Jr.[7]

This paper discusses a subject of considerable practical interest, and it is reasonable to question how applicable the conclusions are to combustors other than the model used in these tests. The marked superiority of the vaporizing combustor indicated by these tests is surprising. Fig. 9 indicates that the vaporizer is more than 25 efficiency points better than the atomizer, or, for equal efficiency, the vaporizer need be only one half the length of the atomizer. This is probably nontypical.

It has been the experience at Lycoming that the air admission pattern in the upstream end of the primary zone is critical and can easily affect efficiency by 10 points, so it seems reasonable to say that an air-flow pattern which is optimum for the 2-in. vaporizer is not necessarily optimum for the atomizer.

Performance tests with fuels of varying volatility in experimental versions of the Lycoming T 53 combustor, a vaporizing type, at inlet conditions similar to those used by the authors, give nearly the same results as reported here. There is no essential efficiency change when using Avgas or JP-4, but a medium diesel fuel lowers combustor efficiency 15 to 20 points, to 75 or 80 per cent. When atomizing fuel nozzles are substituted, efficiency is less affected.

The effect of vaporizer heat-transfer area determined at Lycoming is contrary to the unusual results reported here. Vaporizers of the same T shape in an experimental T 53 combustor had their upstream projections increased in length from $1^1/_2$ to $3^1/_4$ in. with the result that efficiency increased two points, up to 93 per cent, at an air/fuel ratio of 60/1. In an experimental T 55 combustor, an increase of upstream projection length from $1^1/_4$ to $1^3/_4$ in. increased efficiency 5 points to 93 per cent. The optimum vaporizer size we choose is a compromise between one large enough to give good vaporization and efficiency at altitude conditions and small enough not to be overheated and melted at sea level conditions.

A variation in the distance from the vaporizer exit to the upstream end of the combustor is an important parameter in the design of Lycoming vaporizing combustors. There is an optimum distance which is a function of the air-admission pattern used.

The air/fuel ratio inside the vaporizing tube and the efflux velocity of the vaporized mixture is also important. Would the authors give the proportion of total combustion air flow which was passed through the vaporizer, and tell whether this was varied?

The effect on efficiency of varying combustion chamber reference velocity is also a function of combustor design. At Lycoming, some experimental combustors have exhibited no variation in efficiency over a 3 to 1 range in velocity, while others have shown both a slightly rising or falling trend in efficiency while velocity increases. As the authors suggest, the improved mixing caused by the increased velocity of air jets into the combustion zone is probably responsible for the improved efficiency, while we find that a shift in air admission pattern can be responsible for efficiency loss. However, a comparison of the T 53 and T 55 combustors shows that the heat release per unit area of combustor cross section has been increased by $2^1/_2$ times, with combustor length, pressure drop, and efficiency held essentially constant.

To summarize, a comparison of the test results reported here with the experience gained at Lycoming in the development of two vaporizing-type combustors shows several points of agreement. We agree that decreasing fuel volatility sufficiently is harmful to the efficiency of vaporizing combustors but is less harmful to atomizing combustors; and that high efficiency can be maintained as throughput is somewhat increased. We do not find that efficiency varies inversely with vaporizing area. We support the major conclusion that vaporizing combustors can have excellent efficiency characteristics, but do not believe that these tests have shown the atomizing combustor to its best advantage.

Authors' Closure

The authors join in thanking Messrs. Dooley and Opdyke for their comments and discussion. The air-flow pattern selected for fuel comparison in this particular combustor was one giving near optimum performance for the fuels tested. It may well be that, with a different combustor geometry, different air-flow patterns might be required to realize optimum performance for each fuel.

With respect to Mr. Opdyke's questions, the air/fuel ratio by mass inside the vaporizing tube was about 42 to 1 for all fuels. The efflux velocity was of the order of 100 ft/sec and constant. The air flow through the vaporizer tube was approximately 3 per cent by mass of the total air flow for all fuels.

It is the authors' hope that the results presented will assist in some small measure the understanding of combustors through the isolation of principle design parameters.

[7] Supervisor, Combustion Section, Gas Turbine Department, Lycoming Division, AVCO Manufacturing Corporation, Stratford, Conn. Assoc. Mem. ASME.

Torsion of a Prismatical Bar Whose Section Is a Crescent[1]

F. SISTO

Propulsion Division Chief, Curtiss-Wright Research Division, Clifton, N. J.[2]

The Saint Venant torsion problem is solved for a region bounded by two circular arcs forming a crescent. The region is conformally transformed to an infinite strip and the stress function is obtained by Fourier integral. Subsequent quadratures for evaluation of the torsion constant are obtained explicitly with the exception of a single infinite integral which may easily be evaluated numerically. Some values of the torsion constant are given, and an approximate formula valid for small "camber" is presented.

THE NECESSITY FREQUENTLY ARISES for the evaluation of the torsion characteristics of compressor and turbine blades in axial-flow turbomachines. In some cases the airfoil section consists of a region bounded by two circular arcs defining a crescent; i.e., the section has a large "camber." In other cases the circular-arc assumption is only an engineering approximation.

The solution of the Saint Venant torsion problem for this cross section is obtained in the sequel. Exact solutions of the problem have been obtained in the past, but these have been either (*a*) chiefly heuristic [1],[3] or (*b*) limited by the restriction that the angle subtended by one of the defining arcs is precisely twice the angle subtended by the other arc [2].

Theoretical Development

Consider a region in the complex z-plane ($z = x + iy$) bounded by two circular arcs η_1 and η_2 as in Fig. 1. These arcs subtend the angles α_1 and α_2, respectively. The common termini of the arcs are situated at $(-1, 0)$ and $(1, 0)$. The stress function ϕ [3] to be obtained must satisfy Poisson's equation

$$\phi_{xx} + \phi_{yy} = F, \text{ a constant} \tag{1}$$

and vanish on the boundary η_1, η_2.

By employing the conformal transformation

$$z = \text{ctnh } \zeta/2, \quad \zeta = \log [(z + 1)/(z - 1)] \tag{2}$$

the region under consideration is mapped into an infinite strip in the ζ-plane ($\zeta = \xi + i\eta$), as shown in Fig. 2. In the ξ, η co-ordinates Equation (1) becomes

$$\phi_{\xi\xi} + \phi_{\eta\eta} = F (\cosh \xi - \cos \eta)^{-2} \tag{3}$$

It may be verified that $^1/_2 F \cos \eta (\cosh \xi - \cos \eta)^{-1}$ is a solution of Equation (3). Hence it will suffice to determine ϕ in the form

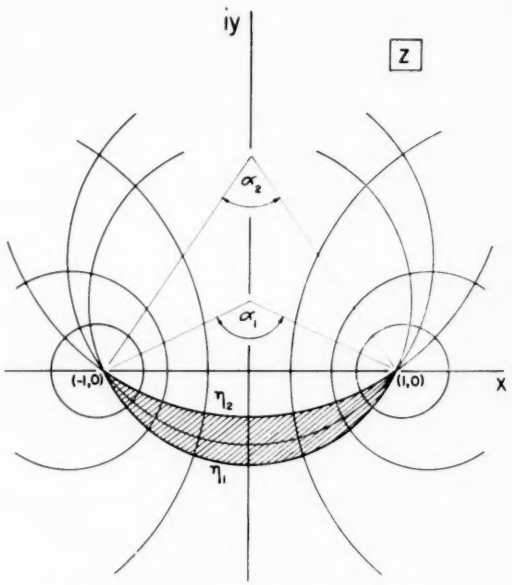

Fig. 1 Crescent-shaped region in the physical z-plane

$$\phi = F/4 [2 \cos \eta (\cosh \xi - \cos \eta)^{-1} + \phi_1] \tag{4}$$

where ϕ_1 is a solution of Laplace's equation chosen so that ϕ vanishes on the boundary.

In the ζ-plane, product solutions of $\phi_{1\xi\xi} + \phi_{1\eta\eta} = 0$ having the proper symmetry condition in ξ may be superimposed formally by integration

$$\phi_1 = \int_0^\infty [A(u) \exp (-u\eta) + B(u) \exp (u\eta)] \cos u\xi \, du \tag{5}$$

The arbitrary coefficients $A(u)$ and $B(u)$ are determined by the boundary conditions

$$2 \cos \eta_1 (\cosh \xi - \cos \eta_1)^{-1} + \phi_1 (\xi, \eta_1) = 0 \tag{6a}$$

$$2 \cos \eta_2 (\cosh \xi - \cos \eta_2)^{-1} + \phi_1 (\xi, \eta_2) = 0 \tag{6b}$$

which are obtained from Equation (4) by specializing η. Utilizing Equation (5) for ϕ_1, the boundary conditions appear as

$$\int_0^\infty [A(u) \exp (-u\eta_1) + B(u) \exp (u\eta_1)] \cos u\xi \, du = -2 \cos \eta_1 (\cosh \xi - \cos \eta_1)^{-1} \tag{7a}$$

---

[1] After this paper was written it was learned that a similar development had been presented previously in the Russian literature, viz., Uflyand, "The Torsion of a Prismatic Bar With a Profile Bounded by Arcs of Two Intersecting Circles," *Doklady Akad. Nauk SSSR* (n.s.) vol. 68, 1949, pp. 17–20. The present paper, however, presents new results of particular value in application to turbomachine blades.

[2] At present, Associate Professor of Mechanical Engineering, Stevens Institute of Technology, Hoboken, N. J.

[3] Numbers in brackets designate References at end of paper.

Contributed by the Gas Turbine Power Division and presented at the Gas Turbine Power Conference, Cincinnati Ohio, March 8–11, 1959, of THE AMERICAN SOCIETY OF MECHANICAL ENGINEERS.

NOTE: Statements and opinions expressed in papers are to be understood as individual expressions of their authors and not those of the Society. Manuscript received at ASME Headquarters, June 28, 1957. Paper No. 59—GTP-6.

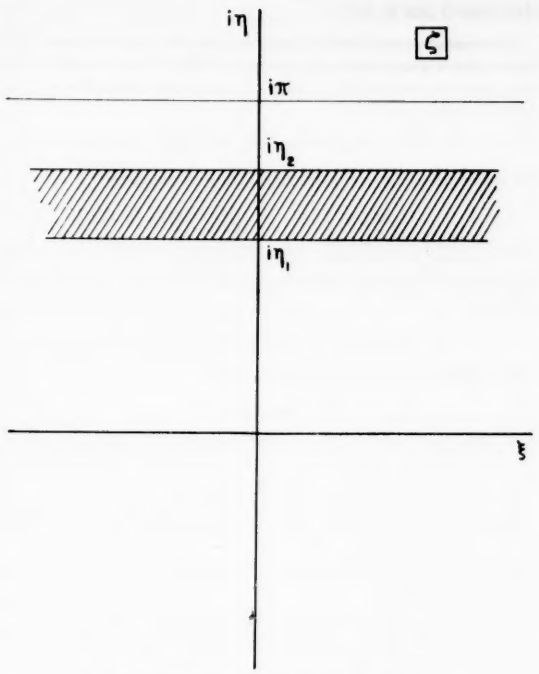

Fig. 2 Cross section transformed to the ζ-plane

$$\int_0^\infty [A(u)\exp(-u\eta_2) + B(u)\exp(u\eta_2)]\cos u\xi\, du = -2\cos\eta_2(\cosh\xi - \cos\eta_2)^{-1} \quad (7b)$$

These equations may be inverted by Fourier's integral theorem to yield

$$A(u)\exp(-u\eta_1) + B(u)\exp(u\eta_1) = \pi^{-1}\int_{-\infty}^{\infty}[-2\cos\eta_1(\cosh\tau - \cos\eta_1)^{-1}\cos u\tau]d\tau \quad (8a)$$

$$A(u)\exp(-u\eta_2) + B(u)\exp(u\eta_2) = \pi^{-1}\int_{-\infty}^{\infty}[-2\cos\eta_2(\cosh\tau - \cos\eta_2)^{-1}\cos u\tau]d\tau \quad (8b)$$

If use is made of the following evaluation [4]

$$2\cos\eta\int_{-\infty}^{\infty}\cos u\tau(\cosh\tau - \cos\eta)^{-1}d\tau = 4\pi\operatorname{ctn}\eta\sinh u(\pi-\eta)\operatorname{csch}u\pi$$

then Equations (8*a*, 8*b*) may be solved simultaneously to give $A(u)$ and $B(u)$. With $A(u)$ and $B(u)$ so determined and inserted in Equation (5), the final expression for ϕ_1 becomes

$$\phi_1 = -4\operatorname{ctn}\eta_1\int_0^\infty\frac{\sinh u(\pi-\eta_1)\sinh u(\eta_2-\eta)}{\sinh u\pi\sinh u(\eta_2-\eta_1)}\cos u\xi\, du + 4\operatorname{ctn}\eta_2\int_0^\infty\frac{\sinh u(\pi-\eta_2)\sinh u(\eta_1-\eta)}{\sinh u\pi\sinh u(\eta_2-\eta_1)}\cos u\xi\, du \quad (9)$$

The problem is now solved in principle. Equations (4) and (9) give the stress function which satisfies the governing differential equation and the associated boundary conditions.

Torsion Constant

Of practical interest is M_t, the torque transmitted through the crescent-shaped cross section. This quantity is given by the well-known expression [3]

$$M_t = 2\int\int\phi\, dx\, dy \quad (10)$$

where the integration is taken over the entire area of the cross section.

Transformed to ζ-plane co-ordinates, and with appropriate substitutions for ϕ, Equation (10) becomes

$$M_t = F(I + J + K) \quad (11)$$

where the integrals

$$I = 2\int_{\eta_1}^{\eta_2}\int_0^\infty\cos\eta(\cosh\xi - \cos\eta)^{-3}d\xi\, d\eta \quad (12a)$$

$$J = -4\operatorname{ctn}\eta_1\int_{\eta_1}^{\eta_2}\int_0^\infty\int_0^\infty\frac{\sinh u(\pi-\eta_1)\sinh u(\eta_2-\eta)\cos u\xi\, du\, d\xi\, d\eta}{\sinh u\pi\sinh u(\eta_2-\eta_1)(\cosh\xi - \cos\eta)^2} \quad (12b)$$

$$K = 4\operatorname{ctn}\eta_2\int_{\eta_2}^{\eta_1}\int_0^\infty\int_0^\infty\frac{\sinh u(\pi-\eta_2)\sinh u(\eta_1-\eta)\cos u\xi\, du\, d\xi\, d\eta}{\sinh u\pi\sinh u(\eta_1-\eta_2)(\cosh\xi - \cos\eta)^2} \quad (12c)$$

are evaluated in Appendix I.

When the integrated forms of I, J, and K are suitably combined, the final expression for M_t may be displayed as

$$M_t/F = \frac{1}{4}[2\operatorname{ctn}\eta + \operatorname{ctn}\eta\csc^2\eta + (\pi-\eta)\csc^4\eta]_{\eta_1}^{\eta_2} + 2\pi(\operatorname{ctn}\eta_2 - \operatorname{ctn}\eta_1)^2 L \quad (13)$$

where L is the infinite integral

$$L(\eta_1,\eta_2) = \int_0^\infty\frac{u\sinh u(\pi-\eta_1)\sinh u(\pi-\eta_2)}{\sinh u(\eta_2-\eta_1)\sinh^2 u\pi}du \quad (14a)$$

Equation (14*a*) may be integrated explicitly for particular values of η_1 and η_2, but this, in general, will not be of great advantage unless many evaluations are contemplated in conjunction with interpolation techniques.

For numerical integration Equation (14*a*) may be transformed to the following alternative representation under the substitution $x^n = \exp(-u\pi)$

$$L = n^2/(2\pi^2)\int_0^1 x^\alpha\ln(1/x)(1-x^\beta)(1-x^\gamma)(1-x^\delta)^{-2}(1-x^\epsilon)^{-1}dx \quad (14b)$$

where

$$\left.\begin{aligned}\alpha &= n\eta_2/\pi - 1 = n[1-\alpha_2/(2\pi)] - 1\\ \beta &= n(1-\eta_1/\pi) = n\alpha_1/(2\pi)\\ \gamma &= n(1-\eta_2/\pi) = n\alpha_2/(2\pi)\\ \delta &= n\\ \epsilon &= n(\eta_2-\eta_1)/\pi = n(\alpha_1-\alpha_2)/(2\pi)\end{aligned}\right\} \quad (14c)$$

and $n > \pi/\eta_2 = \pi(\pi - \alpha_2/2)^{-1}$, but is otherwise arbitrary. At the upper limit, the integrand assumes the value $\beta\gamma\delta^{-2}\epsilon^{-1}$, while at the lower limit it is zero. The alternate values just given for the exponents result from the identity

$$\alpha_{1,2} = 2(\pi - \eta_{1,2}) \quad (14d)$$

which may be verified from an analysis of Equation (2) and Fig. 1.

Approximate Expression

For conditions of small to moderate camber, say $\alpha_2 < \alpha_1 < \pi/2$, representative of current axial-compressor blading, it is possible to develop an approximation for the transmitted torque, M_t

Substituting Equation (14*d*) in Equations (13) and (14*a*), and expanding formally in powers of $\alpha_1/2$ and $\alpha_2/2$, the integral may be evaluated by termwise integration and the expressions combined to give the following series representation:

$$-M_t/F = 1/420\,(\alpha_1 - \alpha_2)^3[1 + 1/18\,(\alpha_1 + \alpha_2)^2 + 1/23{,}760\,(69\alpha_1^4 + 124\alpha_1^3\alpha_2 + 254\alpha_1^2\alpha_2^2 + 124c{:}\,\alpha_2^3 + 69\alpha_2^4) + \ldots] \quad (15)$$

The integrations which are performed in arriving at this result depend only on the identity

$$\int_0^\infty x^{2n} \operatorname{csch}^2 x\, dx = B_{2n-1}\,\pi^{2n}$$

where the B_{2n-1} are the Bernoulli numbers, $B_1 = 1/6$, $B_3 = 1/30$, $B_5 = 1/42$, and so on. This identity may be established easily by induction after evaluating the integral for a few values of n. In these latter evaluations, all that is necessary is the expansion

$$\operatorname{csch}^2 x = 4 \sum_1^\infty m \exp(-2mx)$$

after which termwise integration, followed by summation of the resulting series, yields the desired result.

The truncated series appearing in Equation (15) can be shown to yield results with an error of less than 1 per cent for the case $2\alpha_2 = \alpha_1 \leqslant \pi/2$.

Numerical Results

Equation (14*b*) has been evaluated numerically using 20 intervals in Gregory's integration formula [5] with seventh differences. This was done for two cases: $\alpha_1 = \pi$, $\alpha_2 = \pi/6$ and $\alpha_1 = \pi$, $\alpha_2 = \pi/3$.

In three other cases, Equation (14*a*) was integrated explicitly in closed form. This was done for specific values of α_2 as follows: $\alpha_2 = \alpha_1/2$, $\alpha_2 = 2\alpha_1/3$, and $\alpha_2 = 5\alpha_1/6$. The method is summarized in Appendix II.

With these values of L, the torsion constant $(-M_t/F)$ was calculated for five values of α_2 with $\alpha_1 = \pi$. The results appear in Table 1.

Table 1 Values of torsion constant; $\alpha_1 = \pi$

α_2	$-M_t/F$	$M_t/(G\theta c^4)$
0	(0.148)	(0.0185)[a]
$\pi/6$	0.1042	0.01302
$\pi/3$	0.06665	0.008331
$\pi/2$	0.03651	0.004563
$2\pi/3$	0.01465	0.001831
$5\pi/6$	0.002614	0.0003267

[a] See reference [6].

It will be recalled that the separation between the apexes of the crescent has been taken as two units. Hence, if this separation, or chord, is called c, and if the constant F appearing previously is related to the angle of twist per unit length θ by

$$F = -2G\theta$$

then the third column in Table 1 may be generated by dividing the second column by 8. G is the modulus of rigidity.

Maximum Shear Stress

The shear-stress distribution, and in particular the maximum shear stress which occurs at the mid-point of the concave boundary, may be obtained by taking appropriate derivatives of the stress function ϕ

$$\tau_{zx} = \phi_y, \quad \tau_{yz} = -\phi_x$$

In transformed co-ordinates there may be obtained

$$\tau_{zx} = \phi_\xi \xi_y + \phi_\eta \eta_y, \quad \tau_{yz} = -(\phi_\xi \xi_x + \phi_\eta \eta_x)$$

At the point of maximum stress, from the condition that the line of action of the stress must be tangential to the boundary, the condition

$$\tau_{yz} = 0$$

is obtained, while from symmetry in ξ

$$\phi_\xi = 0$$

Consequently, the expression for maximum shear stress becomes

$$\tau_{\max} = \phi_\eta \eta_y$$

Using Equations (2), (4), and (9) this relation may be written

$$\tau_{\max} = F/4 \left\{ \frac{\partial}{\partial \eta} \left[2 \cos\eta\,(\cosh\xi - \cos\eta)^{-1} - 4 \operatorname{ctn}\eta_1 \int_0^\infty \frac{\sinh u(\pi - \eta_1) \sinh u(\eta_2 - \eta)}{\sinh u\pi \sinh u(\eta_2 - \eta_1)} \cos u\xi\, du + 4 \operatorname{ctn}\eta_2 \int_0^\infty \frac{\sinh u(\pi - \eta_2) \sinh u(\eta_1 - \eta)}{\sinh u\pi \sinh u(\eta_2 - \eta_1)} \cos u\xi\, du \right] \cdot \frac{\partial}{\partial y} \left[\tan^{-1} \left(\frac{-2y}{x^2 + y^2 - 1} \right) \right] \right\}_{\substack{x=\xi=0 \\ \eta=\eta_2}} \quad (16)$$

When the indicated differentiations have been performed, and appropriate substitutions made, the relation may be written

$$\tau_{\max} = F/4 \left[-2 \sin\eta_2\,(1 - \cos\eta_2)^{-2} + 4 \operatorname{ctn}\eta_1 \int_0^\infty \frac{u \sinh u(\pi - \eta_1)}{\sinh u\pi \sinh u(\eta_2 - \eta_1)}\, du - 4 \operatorname{ctn}\eta_2 \int_0^\infty \frac{u \sinh u(\pi - \eta_2) \cosh u(\eta_2 - \eta_1)}{\sinh u\pi \sinh u(\eta_2 - \eta_1)}\, du \right] [1 - \cos\eta_2] \quad (17)$$

Numerical evaluation of the maximum shear stress has not been made, but it is apparent that the integrals appearing in Equation (17) are similar in form to Equation (14*a*) and will yield to a similar treatment.

Summary

The exact solution of the torsion problem for a bar with crescent-shaped cross section has been derived. This solution is contained in the stress function ϕ given by Equations (4) and (9). Derived quantities of interest, the torsion constant and the maximum shearing stress, are given in Equations (13), (14*a*), and (17). An approximation for the torsion constant is given in Equation (15).

APPENDIX I

In this Appendix, the manipulations of Equations (12*a*, *b*, *c*) leading to Equation (13) are indicated.

The innermost integral in Equation (12*a*) depends on the evaluation

$$\int_0^\infty (\cosh \xi - \cos \eta)^{-3}\, d\xi = 1/2[(\pi - \eta) \csc^5 \eta + 3 \cos \eta \csc^4 \eta + 3 (\pi - \eta) \cos^2 \eta \csc^5 \eta] \quad (18)$$

which may be obtained in reference [4] and need not be repeated here.

With Equation (18) substituted in Equation (12*a*), the expression for I becomes

$$I = \int_{\eta_1}^{\eta_2} [(\pi - \eta) \cos \eta \csc^3 \eta + 3 \cos^2 \eta \csc^4 \eta + 3 (\pi - \eta) \cos^3 \eta \csc^5 \eta]\, d\eta \quad (19)$$

In this form, the remaining integrations are of elementary nature and may be readily performed to yield

$$I = [1/2 \operatorname{ctn} \eta + (\pi - \eta) \csc^2 \eta - 3/4 \cos \eta \csc^3 \eta - 3/4 (\pi - \eta) \csc^4 \eta]_{\eta_1}^{\eta_2} \quad (20)$$

Turning to Equations (12*b*) and (12*c*), it is evident that, except for a sign change, the expressions for J and K are identical, but with subscripts 1 and 2 interchanged. Hence it will suffice to determine J only, whereupon K may be obtained by a cyclic rotation of η_1 and η_2.

By using the relation [4]

$$\int_0^\infty \cos u\xi (\cosh \xi - \cos \eta)^{-2}\, d\xi = \pi \frac{u \cosh u(\pi - \eta) \sin \eta + \sinh u(\pi - \eta) \cos \eta}{\sinh u\pi \sin^3 \eta}$$

the order of integration may be formally interchanged and the ξ-integration performed first in Equation (12*b*), yielding the following expression for J:

$$J = -4\pi \operatorname{ctn} \eta_1 \int_0^\infty \frac{\sinh u(\pi - \eta_1)}{\sinh^2 u\pi \sinh u(\eta_2 - \eta_1)} [J_1 + J_2]\, du \quad (21a)$$

where

$$J_1 = u \int_{\eta_1}^{\eta_2} \cosh u(\pi - \eta) \sinh u(\eta_2 - \eta) \csc^2 \eta\, d\eta \quad (21b)$$

$$J_2 = \int_{\eta_1}^{\eta_2} \sinh u(\pi - \eta) \sinh u(\eta_2 - \eta) \csc^3 \eta \cos \eta\, d\eta \quad (21c)$$

Expanding the hyperbolic sines and cosines of difference arguments in terms of single arguments, and performing the required multiplications, it may readily be shown that

$$J_1 = u[\cosh u\pi \sinh u\eta_2 J_{11} - \cosh u(\pi + \eta_2) J_{12} + \sinh u\pi \cosh u\eta_2 J_{13}] \quad (22a)$$

$$J_2 = \sinh u\pi \sinh u\eta_2 J_{21} - \sinh u(\pi + \eta_2) J_{22} + \cosh u\pi \cosh u\eta_2 J_{23} \quad (22b)$$

where

$$\left.\begin{aligned} J_{11} &= \int \cosh^2 u\eta \csc^2 \eta\, d\eta = -1/2[\operatorname{ctn} \eta] + 1/2K_1 \\ J_{12} &= \int \sinh u\eta \cosh u\eta \csc^2 \eta\, d\eta = 1/2\, K_2 \\ J_{13} &= \int \sinh^2 u\eta \csc^2 \eta\, d\eta = 1/2[\operatorname{ctn} \eta] + 1/2K_1 \\ K_1 &= \int \cosh 2u\eta \csc^2 \eta\, d\eta \\ K_2 &= \int \sinh 2u\eta \csc^2 \eta\, d\eta \\ J_{21} &= \int \cosh^2 u\eta \cos \eta \csc^3 \eta\, d\eta = -\frac{1}{2} [\cosh^2 u\eta \csc^2 \eta] + u/2K_2 \end{aligned}\right\} \quad (23)$$

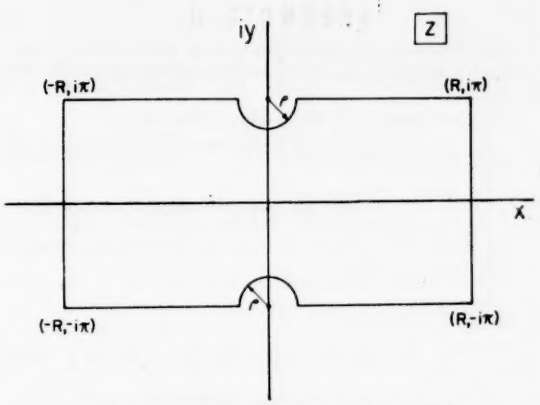

Fig. 3 Contour of integration for evaluating $N(\eta)$

$$\left.\begin{aligned} J_{22} &= \int \sinh u\eta \cosh u\eta \cos \eta \csc^3 \eta\, d\eta = -1/2[\sinh u\eta \cosh u\eta \csc^2 \eta] + u/2K_1 \\ J_{23} &= \int \sinh^2 u\eta \cos \eta \csc^3 \eta\, d\eta = -1/2\, [\sinh^2 u\eta \csc^2 \eta] + u/2\, K_2 \end{aligned}\right\} \quad (23)\ (cont).$$

where the limits on all integrals and square braces are from η_1 to η_2.

Upon summing J_1 and J_2 as given by Equations (22*a*, *b*), with the substitutions (23), it is found that K_1 and K_2 cancel. After some reduction, the final expression for $J_1 + J_2$ becomes

$$J_1 + J_2 = u/2(\operatorname{ctn} \eta_2 - \operatorname{ctn} \eta_1) \sinh u(\pi - \eta_2) + 1/2 \csc^2 \eta_1 \sinh u(\pi - \eta_1) \sinh u(\eta_2 - \eta_1) \quad (24)$$

Returning to Equation (21*a*), with $J_1 + J_2$ given by Equation (24), the final expression for J is given by

$$J = -2\pi \operatorname{ctn} \eta_1 (\operatorname{ctn} \eta_2 - \operatorname{ctn} \eta_1)\, L(\eta_1, \eta_2) - 2\pi \cos \eta_1 \csc^3 \eta_1 \int_0^\infty \sinh^2 u(\pi - \eta_1) \operatorname{csch}^2 u\pi\, du \quad (25a)$$

where $L(\eta_1, \eta_2)$ is given by Equation (14*a*). And hence, by cyclic interchange of subscripts and multiplication by -1, the expression for K becomes

$$K = 2\pi \operatorname{ctn} \eta_2 (\operatorname{ctn} \eta_1 - \operatorname{ctn} \eta_2)\, [-L(\eta_1, \eta_2)] + 2\pi \cos \eta_2 \csc^3 \eta_2 \int_0^\infty \sinh^2 u(\pi - \eta_2) \operatorname{csch}^2 u\pi\, du \quad (25b)$$

Equations (25*a*) and (25*b*) may now be summed to yield

$$J + K = 2\pi (\operatorname{ctn} \eta_1 - \operatorname{ctn} \eta_2)^2 L(\eta_1, \eta_2) + 2\pi[\cos \eta_2 \csc^3 \eta_2 N(\eta_2) - \cos \eta_1 \csc^3 \eta_1 N(\eta_1)] \quad (26)$$

where

$$N(\eta) = \int_0^\infty \sinh^2 u(\pi - \eta) \operatorname{csch}^2 u\pi\, du \quad (27a)$$

The evaluation of N is performed by a contour integration of the function

$$\exp [2z(1 - \eta/\pi)] \operatorname{csch}^2 z$$

around the limiting contour shown in Fig. 3, as $R \to \infty$ and $\rho \to 0$. The result is simply

$$N(\eta) = 1/(2\pi)[1 + (\pi - \eta) \operatorname{ctn} \eta] \quad (27b)$$

Introducing (27*b*) into Equation (26) and combining the result with Equation (20), according to Equation (11), reproduces Equation (13), the desired result.

APPENDIX II

In this Appendix, the evaluation of $L(\eta_1, \eta_2)$, Equation (14*a*), is indicated for three specific ratios of α_1 and α_2 [see Equation (14*d*)].

From Equations (27*a*, *b*) the validity of the identity

$$\int_0^\infty \sinh^2 ax \operatorname{csch}^3 x \, dx = 1/2(1 - a\pi \operatorname{ctn} a\pi), \quad 0 < a < 1 \quad (28)$$

may be established. This result may be differentiated formally with respect to a to yield

$$\int_0^\infty x \sinh ax \cosh ax \operatorname{csch}^2 x \, dx = \pi/4(a\pi \csc^2 a\pi - \operatorname{ctn} a\pi), \quad 0 < a < 1 \quad (29a)$$

Then, by manipulation of identities, the following results may be obtained:

$$\int_0^\infty x \sinh bx \operatorname{csch}^2 x \, dx = \pi/2[(b\pi/2) \csc^2 (b\pi/2) - \operatorname{ctn} (b\pi/2)], \quad 0 < b < 2 \quad (29b)$$

$$\int_0^\infty x \sinh [(c - d)x] \operatorname{csch}^2 x \, dx = \pi/2[(c - d)\pi/2 \csc^2 (c - d)\pi/2 - \operatorname{ctn} (c - d)\pi/2], \quad 0 < (c - d) < 2 \quad (29c)$$

$$\int_0^\infty x \sinh [(c + d)x] \operatorname{csch}^2 x \, dx = \pi/2[(c + d)\pi/2 \csc^2 (c + d)\pi/2 - \operatorname{ctn} (c + d)\pi/2], \quad 0 < (c + d) < 2 \quad (29d)$$

$$\int_0^\infty x \sinh cx \cosh dx \operatorname{csch}^2 x \, dx = \pi/4\{c\pi/2[\csc^2 (c - d)\pi/2 + \csc^2 (c + d)\pi/2] - d\pi/2[\csc^2 (c - d)\pi/2 - \csc^2 (c + d)\pi/2] - [\operatorname{ctn} (c - d)\pi/2 + \operatorname{ctn} (c + d)\pi/2]\} = -\pi/2 \sin c\pi (\cos d\pi - \cos c\pi)^{-1} + \pi^2/2\left[\frac{c(1 - \cos c\pi \cos d\pi) - d \sin c\pi \sin d\pi}{(\cos d\pi - \cos c\pi)^2}\right], \quad 0 < d < c < 1 \quad (29e)$$

Case I: ($2\alpha_2 = \alpha_1$). In this case, the expression for $L(\alpha_1, \alpha_2)$ may be set equal to

$$L = \int_0^\infty \frac{u \sinh u\alpha_1/2 \sinh u\alpha_1/4}{\sinh u\alpha_1/4 \sinh^2 u\pi} \, du = \frac{1}{\pi^2} \int_0^\infty \frac{v \sinh \alpha_1 v/(2\pi)}{\sinh^2 v} \, dv$$

This integral may be evaluated by using Equation (29*b*)

$$L = 1/(2\pi)[\alpha_1/4 \csc^2 (\alpha_1/4) - \operatorname{ctn} (\alpha_1/4)] \quad (30a)$$

Case II: ($3\alpha_2 = 2\alpha_1$). In this case, the expression for $L(\alpha_1, \alpha_2)$ must be put equal to

$$L = \int_0^\infty \frac{u \sinh u\alpha_1/2 \sinh u\alpha_1/3}{\sinh u\alpha_1/6 \sinh^2 u\pi} \, du = 2/\pi^2 \int_0^\infty \frac{v \sinh v\alpha_1/(2\pi) \cosh v\alpha_1/(6\pi)}{\sinh^2 v} \, dv$$

which may, in turn, be evaluated by using (29*e*)

$$L = \left[\frac{\alpha_1}{2\pi}\left(1 - \cos\frac{\alpha_1}{2}\cos\frac{\alpha_1}{6}\right) - \frac{\alpha_1}{6\pi}\sin\frac{\alpha_1}{2}\sin\frac{\alpha_1}{6}\right]\left[\cos\frac{\alpha_1}{6} - \cos\frac{\alpha_1}{2}\right]^{-2} - \frac{1}{\pi}\sin\frac{\alpha_1}{2}\left[\cos\frac{\alpha_1}{6} - \cos\frac{\alpha_1}{2}\right]^{-1} \quad (30b)$$

Case III: ($6\alpha_2 = 5\alpha_1$). In this case, the expression for $L(\alpha_1, \alpha_2)$ is equal to

$$L = \int_0^\infty \frac{u \sinh u\alpha_1/2 \sinh 5u\alpha_1/(12)}{\sinh u\alpha_1/(12) \sinh^2 u\pi} \, du = 1/\pi^2 \int_0^\infty \frac{v}{\sinh^2 v}\left[\sinh\frac{v\alpha_1}{2\pi} + 2\sinh\frac{v\alpha_1}{2\pi}\left(\cosh\frac{v\alpha_1}{6\pi} + \cosh\frac{v\alpha_1}{3\pi}\right)\right] dv$$

Making use of Equation (29*b*) and repeated use of Equation (29*e*) the expression for L may be expressed finally

$$L = 1/(2\pi)[\alpha_1/4 \csc^2 (\alpha_1/4) - \operatorname{ctn} (\alpha_1/4)] + \frac{\alpha_1/(2\pi)[1 - \cos (\alpha_1/2) \cos (\alpha_1/6)] - \alpha_1/(6\pi)[\sin (\alpha_1/2) \sin (\alpha_1/6)]}{[\cos (\alpha_1/6) - \cos (\alpha_1/2)]^2} - \frac{1}{\pi}\frac{\sin (\alpha_1/2)}{\cos (\alpha_1/6) - \cos (\alpha_1/2)} + \frac{\alpha_1/(2\pi)[1 - \cos (\alpha_1/2) \cos (\alpha_1/3)] - \alpha_1/(3\pi)[\sin (\alpha_1/2) \sin (\alpha_1/3)]}{[\cos (\alpha_1/3) - \cos (\alpha_1/2)]^2} - \frac{1}{\pi}\frac{\sin (\alpha_1/2)}{\cos (\alpha_1/3) - \cos (\alpha_1/2)} \quad (30c)$$

References

1 I. S. Sokolnikoff and E. S. Sokolnikoff, "Torsion of Regions Bounded by Circular Arcs," *American Mathematical Society Bulletin*, vol. 47, 1938, pp. 384–387.

2 S. Timoshenko, "Theory of Elasticity," McGraw-Hill Book Company, Inc., New York, N. Y., first edition, 1934, pp. 238–239.

3 Ibid., pp. 230–231.

4 C. B. Ling, "The Stresses in a Plate Containing an Overlapped Circular Hole," *Journal of Applied Physics*, vol. 19, 1948, pp. 405–411.

5 H. Jeffreys and B. S. Jeffreys, "Methods of Mathematical Physics," Cambridge University Press, Cambridge, England, third edition, 1956, pp. 283–284.

6 R. J. Roark, "Formúlas for Stress and Strain," McGraw-Hill Book Company, Inc., New York, N. Y., third edition, 1954, p. 179.

A. L. LONDON

Professor of Mechanical Engineering, Stanford University, Stanford Calif. Mem. ASME

F. R. BIANCARDI

Engineer, United Aircraft Corporation, Research Department, East Hartford, Conn.

J. W. MITCHELL

Graduate Student, Mechanical Engineering, Stanford University, Stanford, Calif.

The Transient Response of Gas-Turbine-Plant Heat Exchangers—Regenerators, Intercoolers, Precoolers, and Ducting

This is the second report of a program dealing with the transient response of heat exchangers [1a], [1b].[1] Analog solutions are used to supplement some analytical solutions so as to provide fairly complete coverage for the heat exchangers encountered in gas-turbine plants. Because a gas flow exists on at least one side of the heat-transfer surface, these exchangers are characterized by a large wall-capacitance effect. Where greater generality is possible, the extension to other heat exchangers is indicated.

A HIGH THERMAL EFFICIENCY gas-turbine plant, unlike the simple-cycle system, is characterized by one or more rather massive heat-exchanger components. These are the regenerator, providing preheat for the compressed gas prior to the heating that takes place either in a combustion chamber or, possibly, a nuclear reactor; one or more intercoolers between compressor stages; and, in the case of the closed-cycle plant, a precooler prior to the first compressor stage. The source of thermal energy for the regenerator is the turbine-exhaust gas and thus the regenerator functions as an economizer of fuel energy. The coolants for the precooler and intercoolers are usually water.

The transient response of the plant to load changes is not instantaneous because of the thermal capacity associated with the massiveness of these heat exchangers, together with the capacitance of the fluids. This lag is due to thermal capacitance-resistance effects and not "thermal inertia" as frequently implied in the literature. There is no natural analog to inertia in any heat-transfer circuit.

There are few solutions in the literature for the transient response of heat exchangers applicable to gas-turbine plants. It is the purpose of this report to summarize these in graphical form and supplement them with additional results obtained analytically and by an electromechanical analog. These results will be reported graphically, employing a suitable set of nondimensional parameters, in a form immediately useful to the designer for, at least, preliminary estimating purposes. The lag in the temperature response of a fluid as a result of duct-wall capacity is also of interest; consequently, this "single-fluid" heat exchanger will be treated along with the "two-fluid" regenerator, intercooler, and precooler problems.

While these results are also applicable to the heat exchangers found in steam power plants and the process industries, primary emphasis will be given in this report to gas-turbine-plant exchangers. Two gains are achieved by this limitation; namely, (*a*) by having a specific application in mind the physical significance of the nondimensional parameters will be more apparent, and (*b*) a convenient limitation on the number and range of the parameters is gained.

This presentation is an extension of the work reported in [1*a*]

[1] Numbers in brackets designate References at end of paper.

Contributed By the Gas Turbine Power Division and presented at the Gas Turbine Power Conference, Cincinnati, Ohio, March 8–11, 1959, of THE AMERICAN SOCIETY OF MECHANICAL ENGINEERS.

NOTE: Statements and opinions advanced in papers are to be understood as individual expressions of their authors and not those of the Society. Manuscript received at ASME Headquarters, December 31, 1958. Paper No. 59—GTP-5.

Nomenclature

A = heat-transfer area, ft²
C = fluid capacity rate, mass flow rate × specific heat, Btu/hr deg F
$\bar{C}$ = fixed capacity, Btu/deg F
L = total flow length, ft
N_{tu} = number of heat-exchanger transfer units, dimensionless = AU/C_{min} or Equation (4)
R = total heat-transfer resistance, hr deg F/Btu
t = temperature, deg F
U = over-all unit heat-transfer conductance, Btu/hr ft² deg F
V = flow velocity, ft/sec
x = flow-length variable, ft
X = a function of θ^*, N_{tu}, R^*, $\bar{C}_w^*$ defined under Equation (14)
Y = a function of $\bar{C}_w^*$ and R^* defined under Equation (14)
ϵ = heat-transfer effectiveness, dimensionless
δ_ϵ = defined under Equation (23)
θ = time, sec
θ_d = dwell time, sec = $(\bar{C}/C) = (L/V)$
ϕ = denotes a functional relation

Subscripts

c = cold fluid or cold-fluid side
d = dwell time of fluid
f = fluid, either hot or cold
h = hot fluid or hot-fluid side
in = inlet section
w = wall
max = maximum capacity rate or associated with C_{max}
min = minimum capacity rate or associated with C_{min}
out = outlet section
ss = steady state

Nondimensional Quantities Characterized by ( )*

θ^* = time relative to dwell time, Equation (4)
θ_d^* = dwell-time ratio, Equation (4)
$\bar{C}_w^*$ = wall capacity relative to fluid capacity, Equation (4)
R^* = relative resistance ratio, Equation (4)
t_h^*, t_c^*, ϵ_h^*, ϵ_c^*, ϵ_f^* = relative temperature differences, Equations (3) and (7)
z^* = defined Equation (17*b*)
τ^* = defined Equation (17*b*)

and [1*b*]. Where necessary for completeness, some repetition of this earlier work is included.

The General Problem

In Fig. 1 the analytical model of a counter of parallel-flow heat exchanger is described schematically. The following idealizations are basic to the analysis:

1 The temperature t of each of the fluids and the wall are functions of time θ and distance x only; $t = t(x, \theta)$. This idealization one-dimensionalizes the problem.

2 The mass-flow rates, w_c and w_h, are constant.

3 The system is over-all adiabatic; that is, perfect insulation surrounds the exchanger.

4 No internal source exists for thermal-energy generation, as by nuclear fission, chemical reaction, or electrical heating.

5 The heat-transfer resistance is lumped between the flowing fluids. The wall resistance is divided as shown in Fig. 1.

6 Zero thermal conduction in both the wall and the fluids is assumed parallel to the flow direction.

7 Properties of the fluids and the wall, such as specific heat, thermal conductivity, density, and also the heat-transfer coefficients, are independent of temperature, time, and position.

8 Fluids are assumed to be low-velocity liquids or gases at essentially constant pressure so that enthalpy can be treated as a function of temperature, using the specific heat property.

9 The thermal capacity of the shell of the exchanger is considered as negligible relative to that of the heat-transfer surface.

Virtually all of these idealizations are also required for the conventional analysis of the steady-state performance of a heat exchanger.

Based upon these nine idealization, the differential equations relating the system temperatures may be derived from energy-balance and heat-transfer-rate equation considerations applied to a differential element dx of the heat exchanger. The resulting three coupled, linear, partial differential equations expressing temperatures t_h, t_w, and t_c as functions of x and θ follow:

$$\left.\begin{aligned}
\left\{\frac{t_h - t_w}{R_h L}\right\} &= -\left\{\frac{\bar{C}_h}{L}\frac{\partial t_h}{\partial \theta}\right\} \pm \left\{C_h \frac{\partial t_h}{\partial x}\right\} \\
\left\{\frac{t_w - t_c}{R_c L}\right\} &= \left\{\frac{\bar{C}_c}{L}\frac{\partial t_c}{\partial \theta}\right\} + \left\{C_c \frac{\partial t_c}{\partial x}\right\} \\
\left\{\frac{t_h - t_w}{R_h}\right\} - \left\{\frac{t_w - t_c}{R_c}\right\} &= \left\{\bar{C}_w \frac{\partial t_w}{\partial \theta}\right\} \\
(-\text{ parallel flow};\ +\ &\text{counterflow})
\end{aligned}\right\} \quad (1)$$

Looking at the first equation of the set, it may be noted that the left-hand term comes from the rate-equation expression for the heat transfer from the hot fluid to the wall; the first term on the right is from the decrease of energy storage in the hot fluid; the second term on the right (for counterflow) comes from the excess of inflow over outflow thermal energy in the C_h stream. A parallel interpretation can be made for the second equation of the set for the wall-to-cold fluid heat transfer. For the third equation, the two terms on the left come from the difference between the two heat-transfer rates, to the wall from the hot fluid and from the wall to the cold fluid. The right-hand term comes from the rate of thermal-energy storage in the wall element.

Initial and boundary conditions to accompany the Equation (1) set may be expressed generally as

$$\left.\begin{aligned}
t_{h,\,\text{initial}} &= t_h(x, 0);\quad t_{h,\,\text{boundary}} = t_h(0 \text{ or } L, \theta) \\
t_{w,\,\text{initial}} &= t_w(x, 0);\quad t_{c,\,\text{boundary}} = t_c(0, \theta) \\
t_{c,\,\text{initial}} &= t_c(x, 0)
\end{aligned}\right\} \quad (2)$$

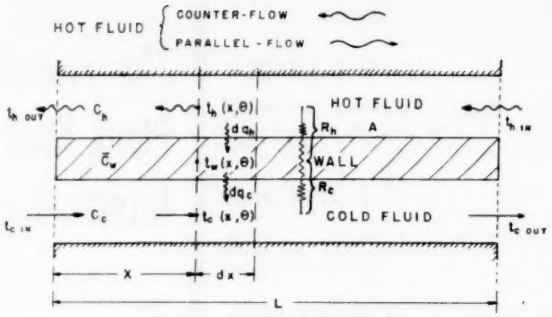

Fig. 1 Idealized heat exchanger

Because the differential equations and boundary conditions are available, Equations (1) and (2), it is possible to formulate an adequate set of nondimensional parameters by purely formal methods. In fact, many sets of parameters may be formulated, each being convertible to any other set. In the judgment of the particular analyst or experimentalist one set may have advantages over another in terms of (*a*) readily understandable and "nameable" nondimensional groupings; (*b*) groupings which experimentally are most readily varied, keeping the others constant; and (*c*) groupings which have been used previously in related problems and therefore are "old friends."

With these criteria in mind, the following set of nondimensional parameters was conceived, the left-hand terms denoting the dependent temperature parameters and the right-hand terms the independent operating and design parameters:

$$\underbrace{t_h^*, t_w^*, t_c^*, \epsilon_h^*, \epsilon_c^*}_{\text{steady state versus transient parameters}} = \phi\left(N_{tu}, \frac{C_{\min}}{C_{\max}}, x^*, \theta^*, \theta_d^*, R^*, \bar{C}_w^*\right) \quad (3)$$

where

$$\left.\begin{aligned}
N_{tu} &\triangleq \frac{AU}{C_{\min}} \triangleq \frac{1}{(R_c + R_h)C_{\min}} \triangleq \text{number of transfer units} \\
\frac{C_{\min}}{C_{\max}} &\triangleq \text{capacity-rate ratio of fluids} \\
x^* &\triangleq \frac{x}{L}, \text{ dimensionless flow length} \\
\theta^* &\triangleq \frac{\theta}{\theta_{d\min}}, \text{ dimensionless time} \\
\theta_d^* &\triangleq \frac{\theta_{d\min}}{\theta_{d\max}}, \text{ dwell-time ratio} \\
R^* &\triangleq \frac{R_{\min}}{R_{\max}}, \text{ heat-transfer resistance ratio} \\
\bar{C}_w^* &\triangleq \frac{\bar{C}_w}{\bar{C}_{\min}}, \text{ wall-to-fluid capacity ratio}
\end{aligned}\right\} \quad (4)$$

Note that θ_d^* and R^* may be equal to, greater than, or less than unity in that the subscript "min" means being associated with the minimum of C_c and C_h, and not that $\theta_{d\min}$ is necessarily less than $\theta_{d\max}$.

With respect to the dependent nondimensional parameters of Equation (3), it will suffice at this time not to define t_h^*, t_w^*, and t_c^* completely, other than to note that the temperatures would be referred to a convenient reference temperature as the datum, a reference temperature which remains constant with

time, as specified by the boundary and initial conditions. For instance, $t_{c\,\text{in}}$ would be chosen if the $t_{c\text{out}}$ response to a $t_{h\,\text{in}}$ change is to be investigated. $\epsilon_h{}^*$ and $\epsilon_c{}^*$ are the temperature parameters of major interest for the control problem. These are defined in the following text so as to have a magnitude of zero at $\theta = 0+$ and unity for $\theta = \infty$ for the response to step changes.

For steady-state heat-exchanger analysis, the nondimensional "temperature" parameter is the effectiveness ϵ_{ss} defined as the actual heat-transfer rate divided by the maximum possible heat-transfer rate as limited by thermodynamic considerations [2],

$$\epsilon_{ss} = \frac{C_h(t_{h\,\text{in}} - t_{h\text{out}})}{C_{\min}(t_{h\,\text{in}} - t_{c\,\text{in}})} = \frac{C_c(t_{c\text{out}} - t_{c\,\text{in}})}{C_{\min}(t_{h\,\text{in}} - t_{c\,\text{in}})} \tag{5}$$

For the transient problem, a time-dependent effectiveness for each fluid may be specified in analogy to Equation (5) as follows:

$$\left.\begin{aligned} \epsilon_h(\theta) &= \frac{C_h[t_{h\,\text{in}}(\theta) - t_{h\text{out}}(\theta)]}{C_{\min}[t_{h\,\text{in}}(\theta) - t_{c\,\text{in}}(\theta)]} \\ \epsilon_c(\theta) &= \frac{C_c[t_{c\text{out}}(\theta) - t_{c\,\text{in}}(\theta)]}{C_{\min}[t_{h\,\text{in}}(\theta) - t_{c\,\text{in}}(\theta)]} \end{aligned}\right\} \tag{6}$$

A dimensionless parameter which normalizes changes in the time-dependent effectiveness for each fluid and represents the transient response is defined as the generalized effectiveness $\epsilon_f{}^*(\theta)$ for either fluid as follows:

$$\epsilon_f{}^*(\theta) = \frac{\epsilon(\theta) - \epsilon(\theta = 0+)}{\epsilon(\theta = \infty) - \epsilon(\theta = 0+)} \tag{7}$$

where $\epsilon(\theta = \infty) \equiv \epsilon_{ss}$ of Equation (5) for conditions such that a steady-state solution exists. It is clear that $\epsilon_f{}^*$ is zero at $\theta = 0+$ and unity for $\theta = \infty$ for a step-function change. Thus the approach of $\epsilon_f{}^*(\theta)$ to unity is a measure of the degree of approach to the new equilibrium.

The differential-equation set (1), expressed in terms of the nondimensional parameters set (4), becomes (C_c is arbitrarily taken as $C_{\min}$, but this specification ultimately is not restrictive)

$$\left.\begin{aligned} (t_h{}^* - t_w{}^*) &= \frac{1}{(R^* + 1)N_{tu}(C_{\min}/C_{\max})} \left[-\frac{1}{\theta_d{}^*}\frac{\partial t_h{}^*}{\partial \theta^*} + \frac{\partial t_h{}^*}{\partial x^*} \right] \\ (t_w{}^* - t_c{}^*) &= \left[\frac{R^*}{R^* + 1}\right]\left[\frac{1}{N_{tu}}\right]\left[\frac{\partial t_c{}^*}{\partial \theta^*} + \frac{\partial t_c{}^*}{\partial x^*}\right] \\ R^*(t_h{}^* - t_w{}^*) - (t_w{}^* - t_c{}^*) &= \left[\frac{R^*}{R^* + 1}\right]\left[\frac{\bar{C}_w{}^*}{N_{tu}}\right]\left[\frac{\partial t_w{}^*}{\partial \theta^*}\right] \end{aligned}\right\} \tag{8}$$

The guiding viewpoint in specifying the nondimensional parameters was that the set should include the normal steady-state parameters, as described in [2]

$$t_{ss}{}^* \text{ (or } \epsilon_{ss}{}^* \text{ at } x^* = 1) = \phi(N_{tu}, C_{\min}/C_{\max}, x^*),$$

plus those needed for the transient problem as noted in Equation (3). This is then a justification for the use of the more complex nondimensional coefficients of the foregoing equations, as for example

$$\left[\frac{R^*}{R^* + 1}\right]\left[\frac{1}{N_{tu}}\right]$$

for its equivalent R_eC_e. Obviously the particular form of the functional relation for Equation (3) depends on flow arrangement—counterflow or parallel-flow—and also on the specified initial and boundary conditions, Equation (2). But even after these specifications, the seven independent nondimensional parameters on the right side are too numerous to permit the graphical presentation of a solution of the Equation (8) set even if it were available. However, no such reasonably general analytical solutions are available because of mathematical difficulties. Paynter and Takahashi [3] come the closest to a general solution, but it is only in Laplace-transform form. The inverse transformations are established only approximately for special cases by synthesizing a solution out of lag-delay, root-lag-delay, and multilag models.

To simplify the general problem to the point where the results can be presented in reasonably simple graphical form, the following restrictions will be imposed:

1 The initial conditions, Equation (2), existing at time $\theta = 0-$ will always correspond to a steady-state condition.

2 The boundary conditions, Equation (2), generally will be either a step change of $t_{h\,\text{in}}$ or $t_{c\,\text{in}}$. Only brief consideration will be given to the problem involving a step change in flow rate.

3 When flow arrangement is important, only the counter-flow situation will be considered.

4 Generally, only the fluid-temperature response at the outlet-flow section will be considered; that is, $x = 0$ or L (or $x^* = 0$ or 1). The wall temperature also will be considered for the insulated duct problem.

5 The flow-capacity-rate-ratio parameter $C_{\min}/C_{\max}$ will be taken either as unity, which corresponds closely to the gas-turbine regenerator problem ($C_{\min}/C_{\max} \approx 0.95$ to 0.97) or as zero, which corresponds approximately to the intercooler or precooler problem ($C_{\min}/C_{\max} \approx 0.1$ to 0.2). This parameter, of course, has no meaning for the insulated-duct problem which also will be considered.

These restrictions are implied schematically in Figs. 2(*a*) to 2(*e*) for the regenerator, intercooler or precooler, and insulated-duct problems.

Under these circumstances Equation (3) in reduced form becomes

$$\epsilon_f{}^* = \phi(N_{tu}, \theta^*, \theta_d{}^*, R^*, \bar{C}_w{}^*) \tag{9}$$

with $C_{\min}/C_{\max}$ either 1 or 0. Even with five instead of seven independent parameters, further reductions are necessary and these will be considered separately for each of the special solutions which follow in the next section.

Solutions

The Gas-Turbine Regenerator (Fig. 2*a*). Two characteristics of the regenerator are $C_{\min}/C_{\max} \approx 1$ and $\bar{C}_w \gg \bar{C}_c$ or $\bar{C}_h$ on the order of 1000 fold. To exploit these characteristics the Equation (8) set will be combined by forming $R^*(t_h{}^* - t_w{}^*)$ from the first equation and substituting together with $(t_w{}^* - t_c{}^*)$ from the second into the third, with the result,

$$-\frac{1}{\theta_d{}^*}\frac{\partial t_h{}^*}{\partial \theta^*} + \frac{\partial t_h{}^*}{\partial x^*} + \frac{\partial t_c{}^*}{\partial \theta^*} + \frac{\partial t_c{}^*}{\partial x^*} = \bar{C}_w{}^*\frac{\partial t_w{}^*}{\partial \theta^*}$$

All the time derivatives are of the same order of magnitude. A reasonable range for $\theta_d{}^*$ is 1/4 to 4. Consequently, since $\bar{C}_w{}^*$ is of the order of 1000 it follows that the time-derivative terms

$$\frac{1}{\theta_d{}^*}\frac{\partial t_h{}^*}{\partial \theta^*}, \frac{\partial t_c{}^*}{\partial \theta^*} \ll \bar{C}_w{}^*\frac{\partial t_w{}^*}{\partial \theta^*}$$

and thus these small terms must also be negligible relative to $(\partial t_h{}^*/\partial x)$ and $(\partial t_c{}^*/\partial x^*)$. Under these circumstances the Equation (8) set reduces to

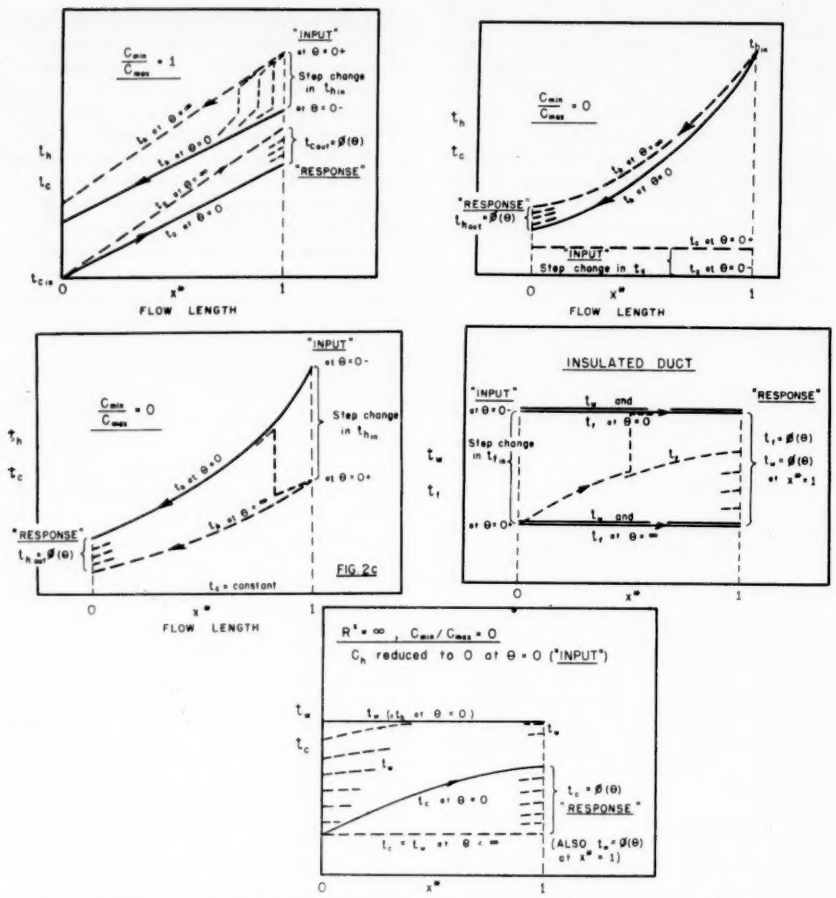

Fig. 2 Descriptions of the problems under consideration in terms of input and response. (a) Regenerator, (b) intercooler and precooler, (c) intercooler and precooler, (d) insulated duct, (e) response to flow cutoff (of C_{max} fluid) for a $C_{min}/C_{max} = 0$ exchanger.

$$\left.\begin{aligned}(t_h^* - t_w^*) &= \frac{1}{(R^*+1)}\frac{1}{N_{tu}}\frac{\partial t_h^*}{\partial x^*}\\ (t_w^* - t_c^*) &= \frac{R^*}{(R^*+1)}\frac{1}{N_{tu}}\frac{\partial t_c^*}{\partial x^*}\\ R^*(t_h^* - t_w^*) - (t_w^* - t_c^*) &= \frac{R^*}{(R^*+1)}\frac{\bar{C}_w^*}{N_{tu}}\frac{\partial t_w^*}{\partial \theta^*}\end{aligned}\right\} \quad (10)$$

The solution of these equations should then be expressible as

$$t_h^*, t_c^*, t_w^* = \phi\left(N_{tu}x^*, \frac{N_{tu}\theta^*}{\bar{C}_w^*}, R^*\right)$$

and for $x^* = 1$

$$\epsilon_f^* = \phi\left(N_{tu}, \frac{\theta^*}{\bar{C}_w^*}, R^*\right) \quad (11)$$

Evidently θ_d^* is not a significant parameter for $\bar{C}_w^*$ large. Also it is clear that $\bar{C}_w^*$ does not enter separately, but only in combination with time as θ^*/C_w^*. Thus the set of five independent parameters in Equation (9) is reduced to only three here.

Analog tests, as described in [1], confirmed the foregoing conclusions. For $\bar{C}_w^* > 10$, variations of 16:1 in θ_d^* had no influence on ϵ_f^*. Another series of tests, Fig. 3, over a range of $\bar{C}_w^*$ from 0 to 40, with $\theta_d^* = 1$, provided the empirical result that θ^* and $\bar{C}_w^*$ can be combined in the form $\theta^*/(1.5 + \bar{C}_w^*)$. Since for $\bar{C}_w^* > 100$

$$\frac{\theta^*}{1.5 + \bar{C}_w^*} \approx \frac{\theta^*}{\bar{C}_w^*}$$

these results support the previous conclusion. Moreover, since the analog tests were limited to $\bar{C}_w^* < 40$, this confirmation allowed a valid extrapolation of the analog results to the higher $\bar{C}_w^*$ magnitudes needed for the regenerator application ($\bar{C}_w^*$ of the order of 1000).

Fig. 4 from [1] summarizes the transient response results for the regenerator. All these curves were obtained using the electromechanical lumped-parameter analog described in [1]. A fixed magnitude of $R^* = 1$ was maintained since this condition obtains approximately in gas-turbine regenerators. The $N_{tu} = 8$ characteristic was obtained from a computer program because errors, due to the lumped-parameter nature of the analog, become excessive for $N_{tu} > 3$ with $C_{min}/C_{max} = 1$.

Unfortunately, unlike the intercooler or precooler problem to be considered later, theoretical solutions from the Equation (10) set have not been obtained for the limiting cases of $R^* = 0$ and $R^* = \infty$. While a substantial reduction from the Equation (10) set results with these restrictions, a second-order hyperbolic partial differential equation of the following form (for $R^* = 0$) remains to be solved:

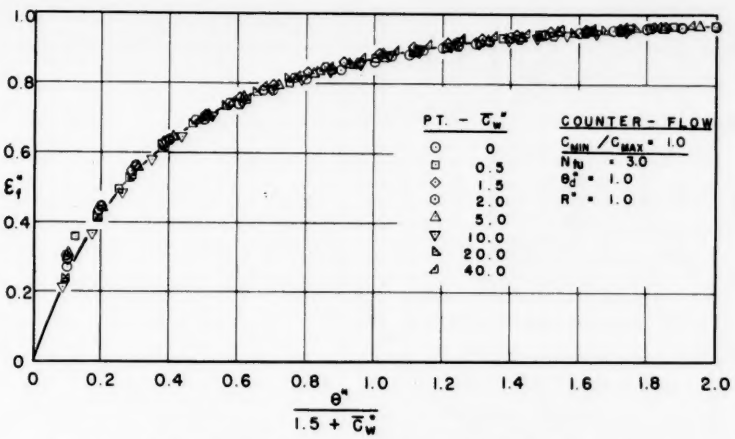

Fig. 3 Test of the ϵ_f^* correlation provided by $\theta^*/(1.5 + \bar{C}_w^*)$ for the regenerator

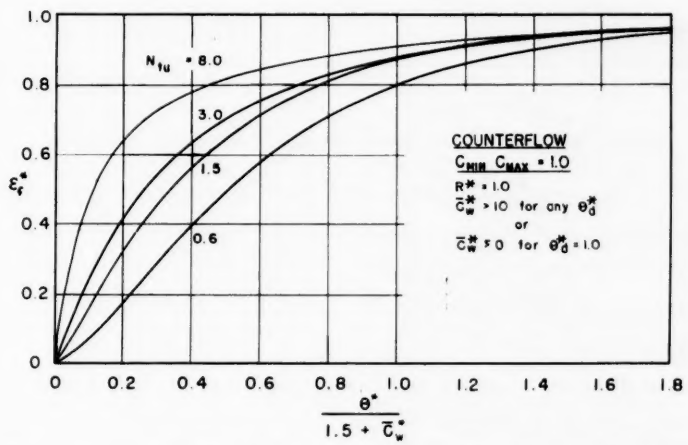

Fig. 4 Regenerator solution for problem described by Fig. 2(a), $\bar{C}_w^* > 10$. Also applicable for any $\bar{C}_w^*$ if $\theta_d^* \equiv 1$.

$$\frac{\partial^2 t_h^*}{\partial x^{*2}} + \bar{C}_w^* \frac{\partial^2 t_h^*}{\partial x^* \partial \theta^*} - N_{tu} \bar{C}_w^* \frac{\partial t_h^*}{\partial \theta^*} = 0 \qquad (12)$$

As demonstrated in [1*a*] and [1*b*], the response to a step-function change in flow rate is quite fast; 90 per cent of the new equilibrium is attained in one dwell time ($\theta_{90}^* \approx 1$). This contrasts to a $\theta_{90}^* \approx \bar{C}_w^*$ with $\bar{C}_w^* \approx 1000$, or a 90 per cent response requiring 1000 dwell times, for the step-function input of fluid temperature. Thus for most regenerator problems the assumption of virtually an instantaneous response to flow-rate changes would be valid, with major attention being directed to the much slower response due to input-fluid temperature changes.

The Gas-Turbine Intercooler and Precooler (Figs. 2*b*, 2*c*). Two characteristics of these exchangers are $C_{min}/C_{max} \approx 0$ and $\bar{C}_w \gg C_{min}(=C_h)$, of the order of 100 to 1000 fold. The first characteristic also applies to any evaporator or condenser-type heat-exchanger problem to even a better approximation than the water-cooled intercooler and precooler where $C_{min}/C_{max} \approx 0.1$ to 0.2. However, the restriction that $\bar{C}_w^* \gg 1$ only applies when the C_{min} fluid is a gas and not when it is a liquid. The solution of the problem under consideration is thus somewhat restricted, but still applicable to the air-cooled condenser and the gas-heated evaporator (e.g., convection bank in a boiler) systems as well as the indicated gas-turbine-plant exchangers.

For the current problem, since $C_{min}/C_{max} = 0$, t_c is constant and flow arrangement, e.g., counter or parallel or even crossflow, ceases to be significant. As t_c is a constant, its derivatives vanish. Under these circumstances the second of the Equation (1) set vanishes, and nondimensionalizing the remaining equations (with $C_h = C_{min}$ and $R^* = R_h/R_c$) results in the following set:

$$(t_h^* - t_w^*) = \left(\frac{R^*}{R^* + 1}\right)\left(\frac{1}{N_{tu}}\right)\left[\frac{\partial t_h^*}{\partial \theta^*} + \frac{\partial t_h^*}{\partial x^*}\right]$$

$$(t_h^* - t_w^*) - R^*(t_w^* - t_c^*) = \left(\frac{R^*}{R^* + 1}\right)\left(\frac{\bar{C}_w^*}{N_{tu}}\right)\left(\frac{\partial t_w^*}{\partial \theta^*}\right) \qquad (13a)$$

With t_c^* a specified initial condition, it is clear that at $x^* = 0$, Figs. 2(*b*) and 2(*c*), ϵ_f^* is related to $t_{h\,out}$ and

$$\epsilon_f^* = \phi(N_{tu}, \theta^*, \bar{C}_w^*, R^*) \qquad (13b)$$

The elimination of C_{min}/C_{max}, and also flow arrangement, sim-

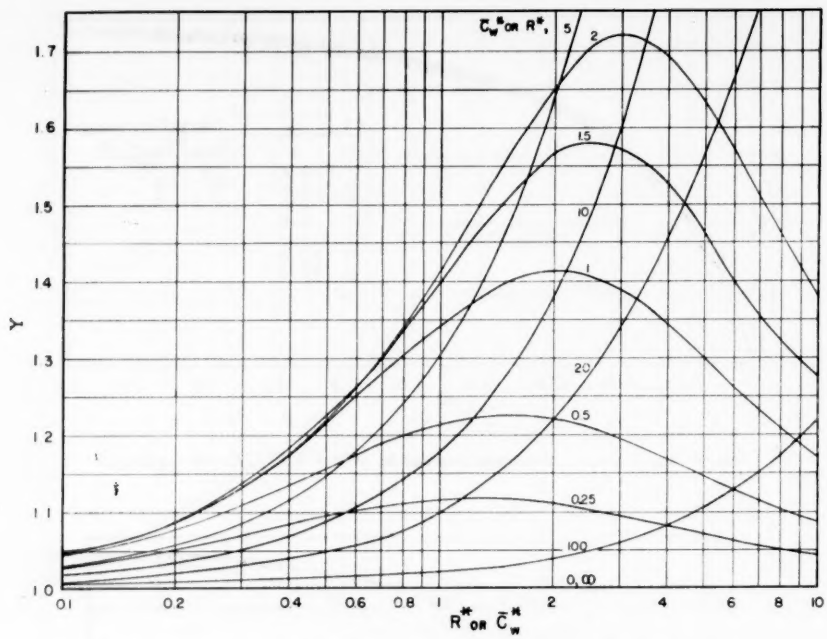

Fig. 5 $C_{min}/C_{max} = 0$ heat-exchanger solution for small times (Fig. 2b problem)

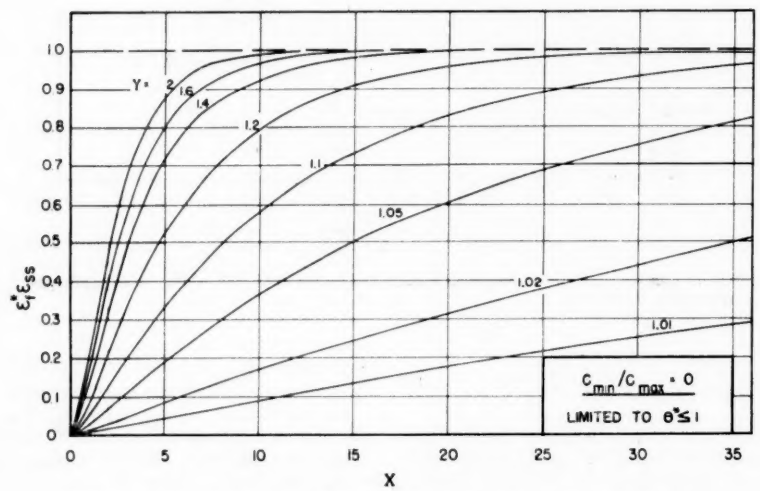

Fig. 6 $C_{min}/C_{max} = 0$ heat-exchanger solution for small times (Fig. 2b problem)

plifies this problem in comparison to the general two-fluid situation. Moreover, there are only two instead of three differential equations to work with. These reductions have allowed some success in a purely analytical attack on this problem by Rizika [5]. His solutions are for a step-function change in t_c. For small times, in the range $0 \leq \theta^* \leq 1$, calculations can be performed readily; however, for larger times the equations are much more complex and calculations are laborious. A worth-while task remains to reduce Rizika's results for $\theta^* > 1$ to a technically usable graphical form using the set of parameters indicated in Equation (13*b*). Additionally, two solutions can be obtained in a very simple form for the cases of $R^* = 0$ and $R^* = \infty$ for a step-function change in t_c, as described in Fig. 2(*b*). The simple analytical solutions will be presented first and then some analog solutions will be presented to supplement these.

Rizika's simple solution, for $0 \leq \theta^* \leq 1$, from Equation (12*a*) of [5] may be rewritten in the form

$$\epsilon_f^* \epsilon_{ss} = 1 - e^{-X}\left[Y \sinh \frac{X}{Y} + \cosh \frac{X}{Y}\right] \qquad (14)$$

with

$$\epsilon_{ss} \triangleq 1 - e^{-N_{tu}}$$

$$X \triangleq [\theta^* N_{tu}]\left[\frac{(R^*+1)}{\bar{C}_w^*}\,\frac{(R^*+1+\bar{C}_w^*)}{2R^*}\right]$$

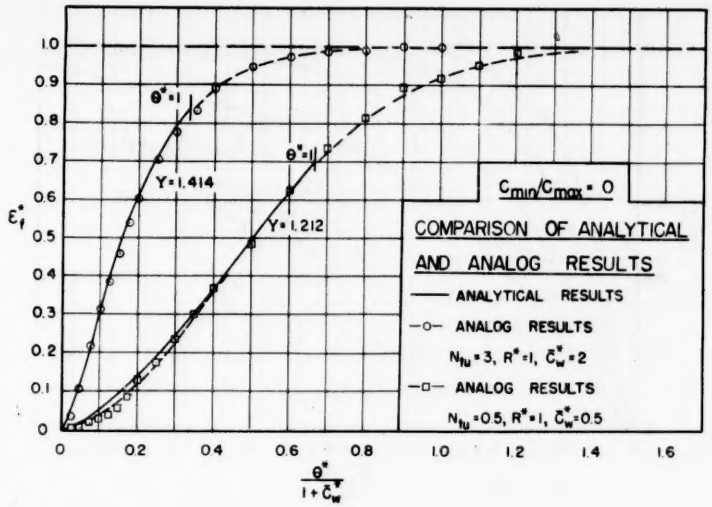

Fig. 7 Analog calibration using Equation (14) analytical solution (Fig. 2b problem)

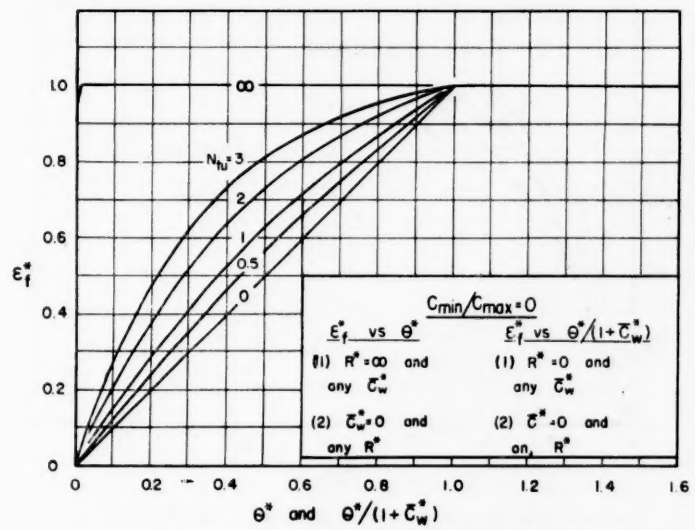

Fig. 8 Heat-exchanger solutions for $R^* = \infty$ and $R^* = 0$, Equations (15) and (16). Also applicable for any R^* if $\bar{C}_w^* = 0$ (Fig. 2b problem).

$$Y \triangleq 1 \Big/ \left[1 - \frac{\bar{C}_w^*/R^*}{\left(\frac{R^* + 1 + \bar{C}_w^*}{2R^*} \right)^2} \right]^{1/2}$$

This result is applicable to the intercooler and precooler problem shown in Fig. 2(*b*), corresponding to a step-function change in the cooling-water inlet temperature. Fig. 5 provides a ready graphical means for evaluating $Y = \phi(R^*, \bar{C}_w^*)$. Then Fig. 6 provides $\epsilon_f^* \epsilon_{ss} = \phi(X, Y)$ where X is, in effect, the time parameter. ϵ_{ss} is the steady-state effectiveness and can be evaluated readily. These graphs were used to obtain the analytical results presented in Fig. 7 as the continuous-line curves. The data points and the dashed lines are the analog results for the indicated common magnitudes of N_{tu}, R^*, $\bar{C}_w^*$. Thus Fig. 7 provides good confidence in the analog results as well as an example of the application of Equation (14).

The one severe restriction on Equation (14) is that it is limited to $\theta^* \leq 1$. Consequently it is only useful for small $\bar{C}_w^*$ magnitudes ($\bar{C}_w^* < 3$). With $\bar{C}_w^*$ of the order of 1000, as is the case for the intercooler and precooler problems, a limit of $\theta^* \leq 1$ would limit the calculable ϵ_f^* to less than 0.01. The other two simple analytical solutions to follow do not have this limitation on time, but they are restricted to $R^* = \infty$ and $R^* = 0$.

For $R^* = \infty$ with $\theta^* \leq 1$, from reference [1*a*]:

$$\left.\begin{aligned} \epsilon_f^* &= \frac{1 - e^{-N_{tu}\theta^*}}{1 - e^{-N_{tu}}} \\ \text{and with } \theta^* \geq 1 \quad & \\ \epsilon_f^* &\equiv 1 \end{aligned}\right\} \qquad (15)$$

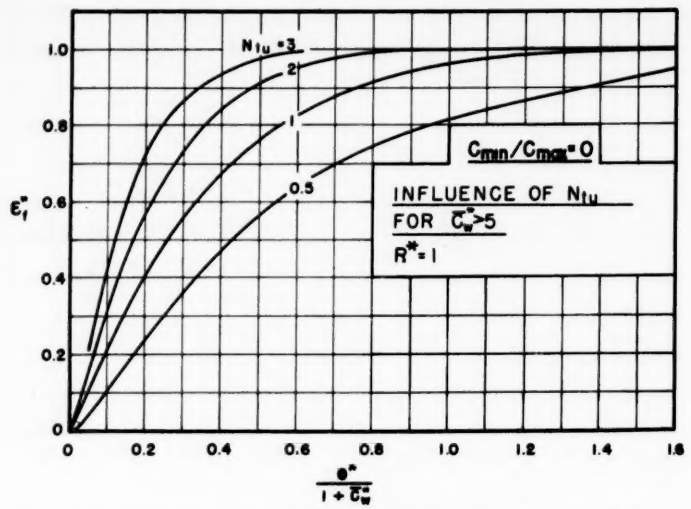

Fig. 9 Intercooler and precooler solutions for problem described by Fig. 2(*b*), $\bar{C}_w^* > 5$

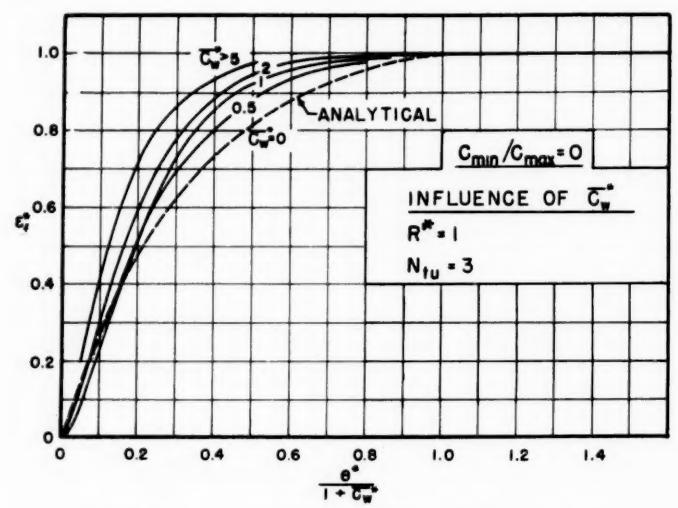

Fig. 10 $C_{min}/C_{max} = 0$ solution, influence of $\bar{C}_w^*$ (Fig. 2*b* problem)

$$\left.\begin{aligned} &\text{For } R^* = 0 \text{ with } \theta^*/(1+\bar{C}_w^*) \leqq 1 \\ &\qquad \epsilon_f^* = \frac{1 - e^{-N_{tu}[\theta^*/(1+\bar{C}_w^*)]}}{1 - e^{-N_{tu}}} \\ &\text{and with } \theta^*/(1+\bar{C}_w^*) \geqq 1 \\ &\qquad \epsilon_f^* \equiv 1 \end{aligned}\right\} \qquad (16)$$

These results are presented in Fig. 8 and are applicable to the particular intercooler and precooler problem shown in Fig. 2(*b*). It is of passing interest to note that Equations (15) and (16) or Fig. 8 provide the solution for any R^* providing $\bar{C}_w^* = 0$. Because $\bar{C}_w^* \approx 1000$ for the intercooler and precooler, this extension is not particularly useful. However, it was employed as reported in [1*a*] to provide another quite good check on the analog system in addition to that provided by Fig. 7.

Figs. 9, 10, 11, and 12 from [6] provide the results of the electromechanical analog tests for the separate influences of N_{tu}, $\bar{C}_w^*$, and R^* for the type of problem shown in Fig. 2(*b*). Additional tests, reported in [6], demonstrate convincingly that for $\bar{C}_w^* > 5$ and $R^* = 1$, $\theta^*/(1+\bar{C}_w^*)$ served as a combined time and wall-capacity-effect correlating parameter; one could anticipate this behavior from the analytical results for $\bar{C}_w^* > 0$, $R^* = 0$, Fig. 8. However, as R^* increases toward infinity, $\bar{C}_w^*$ tends to be eliminated as a significant parameter. Evidently, as R^* is increased, the lower magnitude for $\bar{C}_w^*$ increases for which $\theta^*/(1+\bar{C}_w^*)$ provides a correlation. The lack of correlation for $\bar{C}_w^* < 5$, $R^* = 1$ is evidenced in Fig. 10.

In Fig. 11 the faster response associated with large magnitudes of R^* is evident. For $R^* = \infty$ a 100 per cent response is realized in one dwell time of the gas being cooled, Fig. 8, while for $R^* = 0$, approximately $\bar{C}_w^*$ dwell times are required. This may be of the order of a 1000 dwell times for the precooler and intercooler applications under consideration. The design range of R^* is expected to be about 3 to 1, since extended surface would be incorporated on the gas side to keep R^* in this range.

In Fig. 12 an attempt is made to show some of the interesting

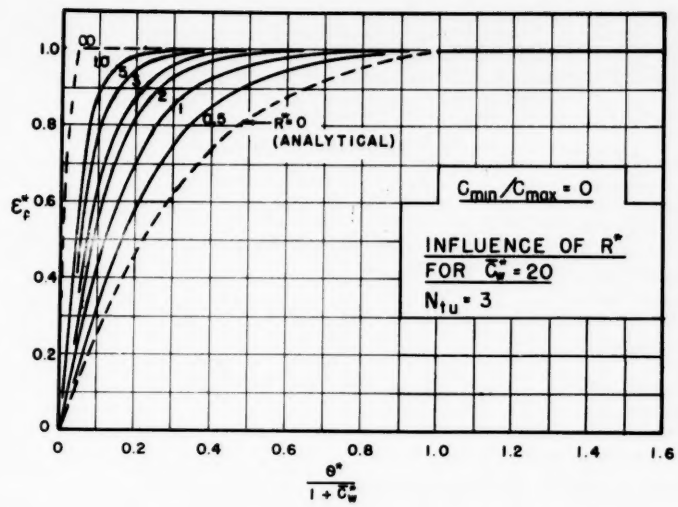

Fig. 11 $C_{min}/C_{max} = 0$ solution, influence of R^* (Fig. 2b problem)

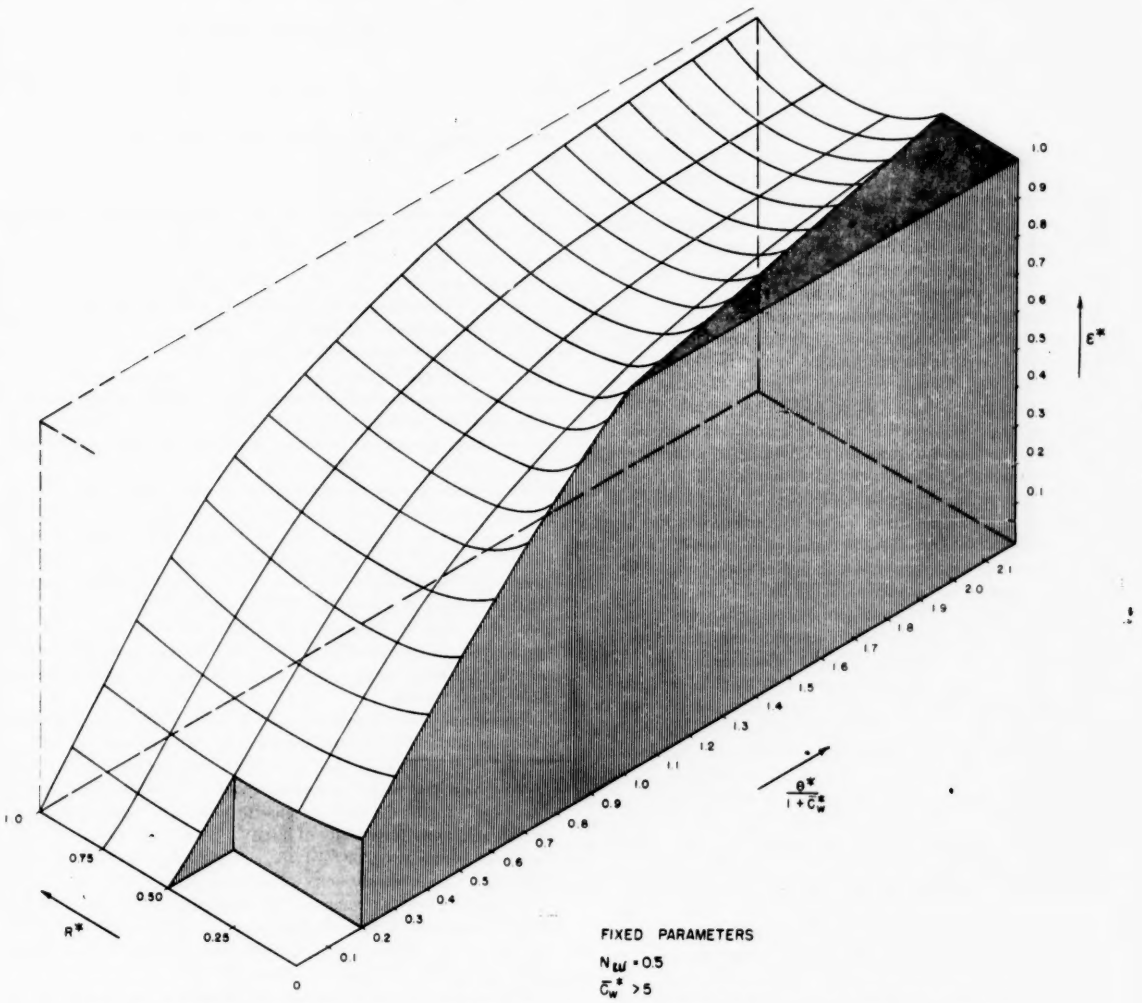

Fig. 12 $C_{min}/C_{max} = 0$ solution, influence of R^* (Fig. 2b problem) for low N_{tu} ($=0.5$) in contrast to Fig. 11 for $N_{tu} = 3$

mathematical aspects of the solution of the Equation (13) set by using a three-dimensional representation of

$$\epsilon_f^* = \phi[\theta^*/(1 + \bar{C}_w^*), R^*]$$

for a fixed N_{tu}. In the range of $R^* \leq 1$ the use of $\theta^*/(1 + \bar{C}_w^*)$ is valid even down to $\bar{C}_w^* = 5$.

The foregoing results dealt with the gas-outlet temperature response to a step-change input of the cooling-water temperature, Fig. 2(*b*). Probably this type of transient would be rare in practice in contrast to the input-response characteristic described in Fig. 2(*c*). Here the response of the outlet-gas temperature to a step change of the inlet-gas temperature is the problem under consideration. Figs. 13, 14, and 15 summarize the analog results for the influence of N_{tu}, $\bar{C}_w^*$, and R^*, respectively. For $\theta^* < 1$, $\epsilon_f^* \equiv 0$ and at $\theta^* = 1$ there is a step jump to the magnitudes shown at the zero of the $(\theta^* - 1)/(1 + \bar{C}_w^*)$ abscissa.

The selection of $(\theta^* - 1)/(1 + \bar{C}_w^*)$ as the combined time-wall-capacity parameter for these curves was conditioned by the previous experience with $\theta^*/(1 + \bar{C}_w^*)$ for the problem of the type described by Fig. 2(*b*) and by the analysis of the insulated-duct problem, to be discussed later, where $(\theta^* - 1)/\bar{C}_w^*$ turns out to be the useful parameter. Fig. 14 provides substantiation for the conclusion that when $\bar{C}_w^*$ exceeds 20 the $(\theta^* - 1)/(1 + \bar{C}_w^*)$ parameter will completely include the influence of $\bar{C}_w^*$, and therefore Fig. 13 is applicable to the precooler and intercooler situations where $\bar{C}_w^* \approx 1000$, in spite of the fact that the analog tests were conducted at a $\bar{C}_w^*$ of 20.

Fig. 15 illustrates the strong influence of R^* on the response. For $R^* = 0$ it can be shown analytically that the step change occurs at $\theta^*/(1 + \bar{C}_w^*) = 1$, or $\theta^* = (1 + \bar{C}_w^*)$, instead of at $\theta^* = 1$, as for all of the $0 < R^* \leq \infty$ characteristics. This big jump for $R^* = 0$ may be considered, however, as being a second jump, the first one occurring at $\theta^* = 1$, like the other R^* curves, but being of vanishingly small amplitude. It will be emphasized again that the design R^* magnitude for gas-turbine intercoolers and precoolers is in the range 1 to 3.

With respect to the temperature response to a flow-rate change, as in the case of the regenerator problem, analog tests demonstrate that it is virtually consummated in one dwell time, whereas 500 to 1000 dwell times are required for the response to inlet-fluid temperature changes. It is concluded, therefore, that in most practical problems, where the flow-rate changes are less than 20 per cent, the flow-rate response can be treated as occurring instantaneously and that major consideration should be directed to the very much slower response associated with input step changes in the inlet-fluid temperature. This approximation has greater validity when R^* is large and is the least valid when $R^* = 0$. For this extreme case a rough estimate indicates that the response to a flow-rate change may only be of the order of twice as fast as the response to the C_{min} fluid-inlet temperature change. A compensating feature is that even sizable flow-rate changes have only a small influence on the steady-state effectiveness and consequently only a small direct influence on outlet-fluid temperature.

The Insulated Duct (Fig. 2*d*). In this situation, for the case of a cold fluid introduced into an initially hot pipe, C_h and t_h do not exist and thus C_{min}/C_{max} vanishes. Also $R^* = R_c/R_h$ goes to ∞ corresponding to the idealized situation of perfect insulation on the outside of the pipe. Under these circumstances the first one of the Equation (1) set disappears completely and the first term on the left of the third equation is eliminated. The nondimensional differential-equation set becomes (with $\theta^* = \theta/\theta_{de}$, $N_{tu} \triangleq 1/[R_c C_c]$, and x measured in the cold-fluid flow direction)

$$\left.\begin{aligned} t_w^* - t_c^* &= \frac{1}{N_{tu}}\left[\frac{\partial t_c^*}{\partial x^*} + \frac{\partial t_c^*}{\partial \theta^*}\right] \\ t_w^* - t_c^* &= -\frac{1}{N_{tu}}\,\bar{C}_w^*\,\frac{\partial t_w^*}{\partial \theta^*} \end{aligned}\right\} \qquad (17a)$$

An analytical solution for this set of equations is available for a step-function change in t_{ci_n} and initially uniform pipe temperature [7]. It was arrived at by the following substitution of variables for θ^* and x^* in the Equation (17*a*) set:

$$\left.\begin{aligned} \tau^* &\triangleq \frac{N_{tu}}{\bar{C}_w^*}\,(\theta^* - x^*) \\ z^* &\triangleq N_{tu} x^* \end{aligned}\right\} \qquad (17b)$$

Introducing these back into the Equation (17*a*) set results in the more simple form

$$\left.\begin{aligned} t_w^* - t_c^* &= \frac{\partial t_c^*}{\partial z^*} \\ t_w^* - t_c^* &= -\frac{\partial t_w^*}{\partial \tau^*} \end{aligned}\right\} \qquad (17c)$$

and the solution can be expressed as

$$t_c^* = \phi(z^*,\ \tau^*) \qquad (18a)$$

or, alternatively, in view of the definitions of z^* and τ^*, and since $t_c^* \equiv \epsilon_f^*$ at $x^* = 1$,

$$\epsilon_f^* = \phi(z^*, \tau^*/z^*), \text{ and at } x^* = 1$$

$$\epsilon_f^* = \phi\left(N_{tu}, \frac{\theta^* - 1}{\bar{C}_w^*}\right) \qquad (18b)$$

For $\theta^* = 1$ the solution, in series form, reduces simply to

$$\epsilon_f^* = e^{-N_{tu}} \qquad (18c)$$

A solution is also available for the wall-temperature response t_w^*. At $x^* = 1$ it becomes ϵ_w^* and may be expressed as a function of N_{tu} and $(\theta^* - 1)/\bar{C}_w^*$.

These solutions for ϵ_f^* and ϵ_w^*, evaluated by a digital computer program [8], are presented graphically in terms of the $[N_{tu}, (\theta^* - 1)/\bar{C}_w^*]$ parameters in Figs. 16, 17, and 18, and also in tabular form using (z^*, τ^*) parameters, Table 1.

It is worth noting that these results are equally applicable to the problems of a hot fluid flowing in an initially cold pipe, or a cold fluid flowing in an initially hot pipe; or the parallel situation for flow through a porous matrix possessing a characterizable thermal capacity of the solid material.

To provide a sense of magnitudes in the application of these solutions to the gas-turbine problem, a hot-gas duct of 30 in. diam and 0.5 in. wall thickness, conducting air at 4 atm abs and 1300 F, has a $\bar{C}_w^* \approx 140$. The N_{tu} per foot of length is of the order of 5×10^{-3} ft^{-1} (the Stanton number divided by the hydraulic radius) and thus for a 40-ft duct length $N_{tu} \approx 0.2$. It is clear from Fig. 16 that the fluid-temperature response is of the order of 82 per cent complete in one dwell time (0.4 sec at 100 fps), whereas the 82 per cent wall-temperature response will take about 1400 dwell times.

The simple closed-form solution for ϵ_f^* at $\theta^* = 1$, Equation (18*c*), is particularly useful for locating the ordinate, at $(\theta^* - 1)/\bar{C}_w^* = 0$ on Figs. 16 and 17, for interpolating purposes.

Other Heat-Exchanger Transient Problems. To this point attention has been largely directed to gas-turbine-plant heat exchangers which are characteristically of large $\bar{C}_w^*$, and either $C_{min}/C_{max} \approx 1$ for the regenerator, or $C_{min}/C_{max} \approx 0$ for the precooler and intercooler. Since the capacity-rate-ratio range 0 to 1 encompasses all two-fluid heat exchangers, the results already presented are broadly applicable, for rough estimating purposes, when properly interpolated. The summary of solutions given in Table 2 is presented to assist the reader in this purpose.

The extension to other than step-function inputs can be accomplished readily by using the technique outlined in [1] using

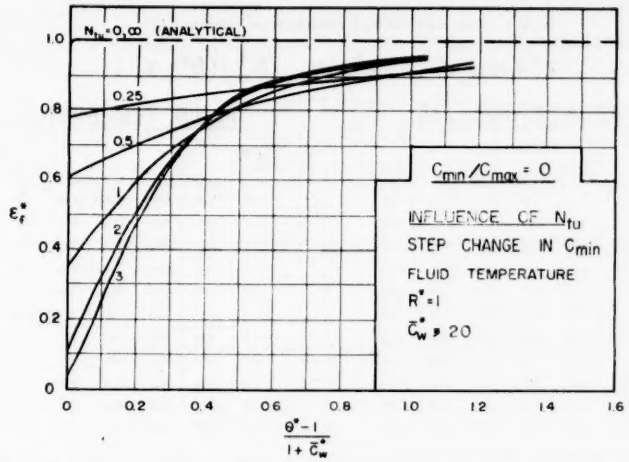

Fig. 13 Intercooler and precooler solutions for problem described by Fig. 2(c), $\bar{C}_w^* > 20$

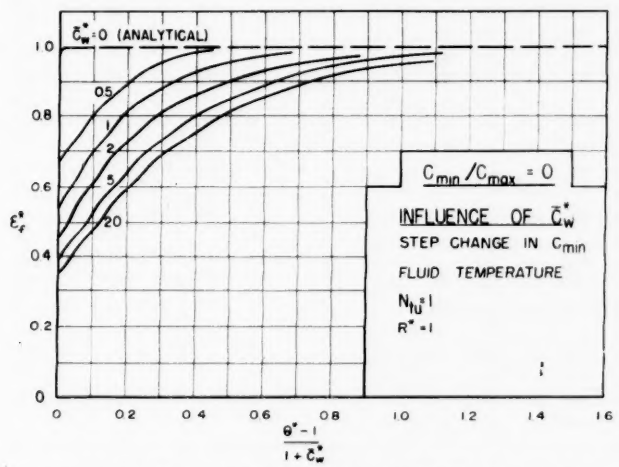

Fig. 14 $C_{min}/C_{max} = 0$ solution, influence of $\bar{C}_w^*$ (Fig. 2c problem)

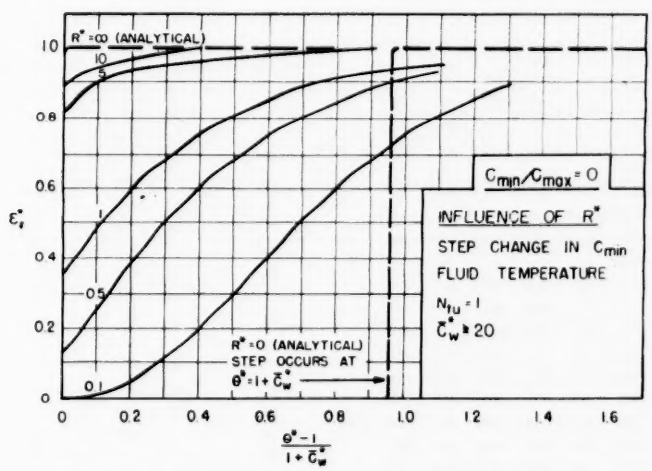

Fig. 15 $C_{min}/C_{max} = 0$ solution, influence of R^* (Fig. 2c problem)

Table 1 The insulated-duct solution from reference [8]

$$Z^* \triangleq N_{tu} x^*, \quad \tau^* = (N_{tu}/\bar{C}_w^*)(\theta^* - x^*)$$

WALL TEMPERATURE RESPONSE, $\mathcal{E}_w^*$

τ^* \ Z^*	.2	.4	.6	.8	1.0	1.2	1.4	1.6	1.8	2.0
0	0	0	0	0	0	0	0	0	0	0
.5	.337	.289	.247	.211	.181	.154	.133	.112	.096	.082
1.0	.562	.499	.442	.391	.346	.305	.269	.237	.208	.183
1.5	.712	.650	.592	.538	.488	.441	.399	.359	.323	.290
2.0	.811	.757	.705	.654	.606	.559	.515	.473	.433	.397
2.5	.876	.833	.789	.744	.700	.657	.615	.574	.534	.496
3.0	.919	.885	.850	.813	.775	.737	.698	.660	.622	.585
3.5	.947	.922	.894	.864	.833	.800	.766	.732	.698	.663
4.0	.966	.947	.926	.902	.877	.850	.821	.791	.761	.730
4.5	.978	.964	.948	.930	.910	.888	.864	.839	.813	.786
5.0	.986	.976	.964	.950	.934	.917	.898	.877	.855	.831

τ^* \ Z^*	1	2	3	4	5	6	7	8	9	10
1	.346	.183	.094	.047	.023	.011	.005	.003	.001	.001
2	.606	.397	.247	.148	.086	.049	.027	.015	.008	.004
3	.775	.585	.417	.283	.185	.118	.072	.043	.026	.015
4	.877	.730	.573	.428	.307	.213	.142	.093	.059	.037
5	.934	.831	.702	.565	.436	.325	.234	.163	.112	.074
6	.966	.898	.800	.682	.559	.442	.338	.251	.181	.128
7	.983	.940	.870	.776	.667	.555	.447	.349	.266	.197
8	.991	.966	.918	.847	.757	.656	.551	.450	.358	.278
9	.996	.981	.949	.898	.827	.741	.646	.548	.453	.366
10	.998	.989	.969	.934	.880	.811	.728	.638	.545	.455
11				.958	.919	.865	.796	.717	.631	.543
12				.974	.946	.905	.851	.784	.708	.625
13				.984	.965	.935	.893	.838	.773	.699
14				.990	.978	.956	.925	.881	.827	.763
15				.994	.986	.971	.948	.915	.871	.817
16				.997	.991	.981	.965	.940	.905	.861
17				.998	.995	.988	.976	.958	.932	.896
18				.999	.997	.992	.984	.971	.951	.924
19				.999	.998	.995	.990	.980	.966	.945

τ^* \ Z^*	12	14	16	18	20	22	24	26	28	30
2	.001	.000	.000							
4	.014	.005	.002	.000	.000	.000				
6	.060	.026	.011	.004	.002	.001	.000			
8	.155	.081	.039	.018	.008	.003	.001	.000	.000	
10	.297	.178	.099	.052	.026	.012	.005	.002	.001	.000
12	.459	.312	.196	.116	.065	.034	.017	.008	.004	.002
14	.616	.462	.324	.212	.131	.077	.043	.023	.012	.006
16	.746	.608	.464	.334	.226	.145	.088	.051	.028	.015
18	.844	.733	.602	.465	.341	.237	.157	.099	.059	.034
20	.909	.828	.721	.597	.467	.350	.248	.169	.109	.067
22	.950	.896	.815	.709	.591	.469	.355	.257	.178	.118
24	.974	.940	.883	.803	.700	.587	.473	.362	.265	.187
26	.987	.967	.930	.872	.792	.694	.583	.472	.367	.273
28	.994	.983	.960	.921	.862	.782	.687	.582	.473	.372
30	.997	.991	.978	.953	.912	.852	.774	.681	.579	.474
32	.999	.996	.988	.973	.946	.903	.843	.766	.675	.577
34		.998	.994	.985	.968	.939	.895	.834	.758	.670
36		.999	.997	.992	.982	.963	.932	.887	.827	.752
38			.999	.996	.990	.978	.958	.926	.880	.819
40			.999	.998	.995	.988	.975	.953	.919	.873
42				.999	.997	.993	.985	.971	.948	.913

FLUID TEMPERATURE RESPONSE, $\mathcal{E}_f^*$

τ^* \ Z^*	.2	.4	.6	.8	1.0	1.2	1.4	1.6	1.8	2.0
0	.819	.670	.549	.449	.368	.301	.247	.202	.165	..
.5	.885	.781	.688	.604	.530	.464	.406	.354	.309	.269
1.0	.927	.855	.785	.718	.654	.594	.539	.487	.439	.394
1.5	.953	.904	.852	.800	.748	.696	.646	.597	.551	.506
2.0	.970	.936	.899	.859	.817	.775	.731	.688	.645	.604
2.5	.981	.958	.931	.901	.869	.834	.798	.761	.723	.685
3.0	.988	.972	.953	.931	.906	.879	.849	.818	.786	.753
3.5	.992	.982	.968	.952	.933	.913	.889	.863	.836	.808
4.0	.995	.988	.979	.967	.953	.936	.918	.898	.876	.853
4.5	.997	.992	.986	.977	.967	.954	.940	.924	.906	.887
5.0	.998	.995	.990	.984	.977	.967	.956	.944	.930	.914

τ^* \ Z^*	1	2	3	4	5	6	7	8	9	10
0	.368	.135	.050	.018	.007	.002	.001	.000	.000	.000
1	.654	.394	.225	.123	.066	.034	.017	.009	.004	.002
2	.817	.604	.415	.270	.169	.102	.060	.034	.019	.011
3	.906	.753	.583	.427	.298	.201	.131	.082	.051	.031
4	.953	.852	.717	.572	.435	.319	.225	.153	.103	.066
5	.977	.914	.815	.693	.564	.441	.333	.243	.174	.120
6	.989	.951	.883	.788	.676	.558	.446	.344	.260	.190
7	.995	.973	.928	.857	.766	.662	.554	.449	.355	.273
8	.997	.985	.957	.907	.837	.749	.652	.550	.453	.363
9	.999	.992	.974	.941	.888	.819	.735	.643	.548	.455
10	.999	.996	.985	.963	.926	.872	.804	.723	.635	.546
11				.977	.951	.912	.858	.790	.713	.629
12				.986	.969	.940	.899	.844	.778	.704
13				.992	.980	.960	.930	.887	.833	.768
14				.995	.988	.974	.952	.919	.876	.822
15				.997	.993	.983	.968	.943	.910	.866
16				.998	.996	.989	.979	.961	.935	.901
17				.999	.997	.993	.986	.973	.954	.927
18					.998	.996	.991	.982	.968	.948
19					.999	.998	.994	.988	.978	.963

τ^* \ Z^*	12	14	16	18	20	22	24	26	28	30
0	.000	.000								
2	.003	.001	.000	.000						
4	.026	.010	.003	.001	.000	.000				
6	.095	.044	.019	.008	.003	.001	.000	.000		
8	.216	.118	.060	.029	.013	.006	.002	.001	.000	.000
10	.375	.237	.139	.076	.039	.019	.009	.004	.002	.001
12	.541	.384	.254	.156	.091	.050	.026	.013	.006	.003
14	.689	.538	.392	.268	.172	.104	.060	.033	.017	.009
16	.804	.677	.535	.398	.279	.185	.117	.070	.040	.022
18	.884	.788	.667	.535	.403	.289	.197	.128	.079	.047
20	.935	.869	.774	.659	.533	.408	.298	.208	.138	.088
22	.966	.923	.855	.762	.651	.531	.412	.306	.218	.148
24	.983	.957	.912	.843	.752	.645	.531	.415	.313	.226
26	.992	.977	.949	.901	.832	.743	.639	.529	.418	.319
28	.996	.988	.972	.941	.891	.822	.735	.635	.529	.420
30	.998	.994	.985	.966	.932	.882	.813	.727	.630	.527
32	.999	.997	.992	.981	.960	.925	.873	.804	.721	.626
34		.999	.996	.990	.977	.954	.917	.865	.796	.714
36		.999	.998	.995	.987	.973	.948	.910	.857	.789
38			.999	.997	.993	.984	.968	.942	.903	.849
40				.999	.996	.991	.981	.964	.936	.896
42				.999	.998	.995	.989	.978	.959	.931

Table 2 Summary of solutions

SOLUTION NO.	INDEPENDENT PARAMETERS			FIGURE REFS (Prob. Type) [Grap. Results]
	FIXED	PARTIALLY RESTRICTED	UNRESTRICTED	
1	$C_{min}/C_{max} = 1$ $R^* = 1$	$\bar{C}_w^* > 10$	θ^*, N_{tu}, θ_d^*	(2a), [4]
2	$C_{min}/C_{max} = 1$ $R^* = 1$ $\theta_d^* = 1$	-	θ^*, N_{tu}, $\bar{C}_w^*$	(2a), [4]
3	$C_{min}/C_{max} = 1$ $\bar{C}_w^* = 0$ $\theta_d^* = 1$	-	θ^*, N_{tu}	(2a), [4]
4	$C_{min}/C_{max} = 0$	$\theta^* \leq 1$	N_{tu}, $\bar{C}_w^*$, R^*	(2b), [5,6]
5	$C_{min}/C_{max} = 0$ $R^* = \infty$	-	θ^*, N_{tu}, $\bar{C}_w^*$	(2b), [8]
6	$C_{min}/C_{max} = 0$ $\bar{C}_w^* = 0$	-	θ^*, N_{tu}, R^*	(2b), [8]
7	$C_{min}/C_{max} = 0$ $R^* = 0$	-	θ^*, N_{tu}, $\bar{C}_w^*$	(2b), [8]
8	$C_{min}/C_{max} = 0$ $R^* = 1$	$\bar{C}_w^* > 5$	θ^*, N_{tu}	(2b), [9]
9	$C_{min}/C_{max} = 0$ $R^* = 1$, $N_{tu} = 3$	-	θ^*, $\bar{C}_w^*$	(2b), [10]
10	$C_{min}/C_{max} = 0$ $\bar{C}_w^* = 20$, $N_{tu} = 3$	-	θ^*, R^*	(2b), [11]
11	$C_{min}/C_{max} = 0$ $R^* = 1$	$\bar{C}_w^* > 20$	θ^*, N_{tu}	(2c), [13]
12	$C_{min}/C_{max} = 0$ $R^* = 1$, $N_{tu} = 1$	-	θ^*, $\bar{C}_w^*$	(2c), [14]
13	$C_{min}/C_{max} = 0$ $N_{tu} = 1$	$\bar{C}_w^* > 20$	θ^*, R^*	(2c), [15]
14	$C_{min}/C_{max} = 0$ $R^* = \infty$	-	θ^*, N_{tu}, $\bar{C}_w^*$	(2e), [16,17,18] See text for change in coordinates
15	-	-	θ^*, N_{tu}, $\bar{C}_w^*$	(2d), [16,17,18]

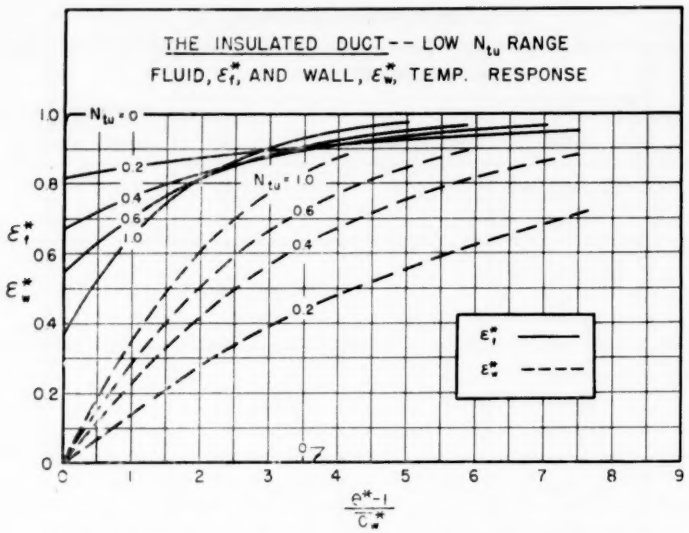

Fig. 16 Insulated-duct fluid and wall-temperature response for problem described by Fig. 2(*d*)

Duhamel's method. Also standard methods are available for obtaining approximations of the frequency response given the transient response to a step input [9].

In addition to these general considerations, it is the purpose of this section to point out some specific examples of "dividend solutions" that may be extracted from what has been presented already.

For $\bar{C}_w^* \approx 0$ and any C_{min}/C_{max}. This limiting case is of interest both from a mathematical point of view and because $\bar{C}_w^*$ is only of the order of 0.3 for a water-cooled steam condenser. The nondimensional set of differential equations paralleling the Equation (8) set becomes

$$\left.\begin{aligned}(t_h^* - t_c^*) &= \frac{1}{N_{tu}(C_{min}/C_{max})}\left[-\frac{1}{\theta_d^*}\frac{\partial t_h^*}{\partial \theta^*} + \frac{\partial t_h^*}{\partial x^*}\right] \\ (t_h^* - t_c^*) &= \frac{1}{N_{tu}}\left[\frac{\partial t_c^*}{\partial \theta^*} + \frac{\partial t_c^*}{\partial x^*}\right]\end{aligned}\right\} \quad (19)$$

Thus of the seven independent parameters of Equation (3), two are eliminated, namely, R^* and $\bar{C}_w^*$; then, for $x^* = 1$

$$\epsilon_f^* = \phi(N_{tu}, C_{min}/C_{max}, \theta^*, \theta_d^*)$$

The problem, still of considerable mathematical difficulty, is treated in [4] with the results available only in a symbolic form including integrals of exponential and Bessel functions.

Fig. 3, however, provides the analog solution for $C_{min}/C_{max} = 1$, $N_{tu} = 3$, $\theta_d^* = 1$ irrespective of R^*, since it is not a significant parameter for $\bar{C}_w^* = 0$. Only for the $\bar{C}_w^* > 0$ data points is the $R^* = 1$ test condition restrictive. Consequently, Fig. 4 must be applicable to this problem over the indicated N_{tu} range, only with the restrictions $\theta_d^* = 1$ and $C_{min}/C_{max} = 1$ (Solution 3, Table 2).

For the case of $C_{min}/C_{max} = 0$, the parameter θ_d^* ceases to be significant. Then Equations (15) and (16), with $\bar{C}_w^* = 0$, become identical and provide a solution with no restriction on R^*. Thus Fig. 8 is useful for this problem (Solution 6, Table 2). Rizika's analytical solution, Equation (14) and Figs. 5 and 6, is particularly useful in the $\bar{C}_w^* < 3$ range.

It is clear that Eigs. 4, 5, 6, and 8 brac!:et in a fairly complete manner the small $\bar{C}_w^*$ problem, with $\theta_d^* = 1$ a restriction at the $C_{min}/C_{max} = 1$ end and no restriction at the $C_{min}/C_{max} = 0$ end.

For $\bar{C}_w^* < 10$, any C_{min}/C_{max}. This problem is partially bounded by the results presented in Figs. 4 and 8. The $C_{min}/C_{max} = 1$ end is restricted to $R^* = 1$, while R^* is unrestricted for $C_{min}/C_{max} = 0$ ($0 \leq R^* \leq \infty$). Cautious interpolation for intermediate magnitudes of C_{min}/C_{max} is possible.

Results for particular values of the parameters can be obtained by the analog system, but these cannot be presented so as to cover a wide range in a compact graphical form because both R^* and θ_d^* effects need to be included.

For $C_{min}/C_{max} = 0$, $R^* = \infty$, and C_{max} Flow Cutoff (Fig. 2*e*). Figs. 16, 17, and 18, developed for the insulated-duct problem, also may be used to provide the ϵ_f^*, ϵ_w^* response of the C_{min} fluid when the "input" consists of a step reduction of the C_{max} flow to zero, as described in Fig. 2(*e*). In this extension it is necessary to replace $(\theta^* - 1)/\bar{C}_w^*$ in the abscissa of Figs. 16, 17, and 18 by $\theta^*/\bar{C}_w^*$ and evaluate the desired response $\epsilon_{f\,new}^*$ from $(\epsilon_f^* - \epsilon_{f,0}^*)/(1 - \epsilon_{f,0}^*)$, where ϵ_f^* and $\epsilon_{f,0}^*$ are obtained from the graphs.

This type of approach is also useful in the consideration of the decay cooling of a solid after electrical or nuclear heating is terminated.

Discussion

The summary of solutions in Table 2 together with the sample solutions for the regenerator problem presented in [1] should prove useful to the reader in applying the results of this work to the solution of his particular problems. It is worth while to note again in this respect that careful judgment must be exercised in any interpolations because of the large number of independent parameters involved as illustrated by Equation (3). However, for the special cases of $C_{min}/C_{max} = 0$ or unity and for $\bar{C}_w^*$ large, as is the case for gas-turbine-plant heat exchangers, coverage presented here is more complete and interpolations are less speculative. This advantage is gained because of the fortunate consolidation of θ^* and $\bar{C}_w^*$ into a single parameter when $\bar{C}_w^* > 10$.

Major attention has been given to the outlet-fluid temperature response to inlet-fluid temperature changes in contrast to the re-

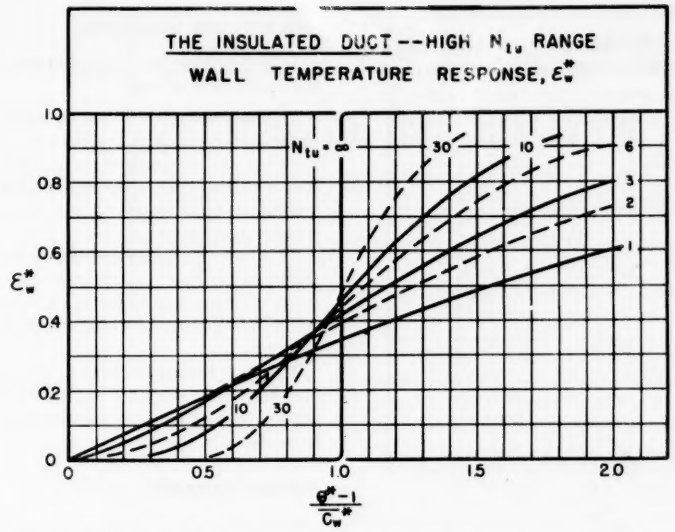

Fig. 17 Insulated-duct fluid and wall-temperature response for problem described by Fig. 2(d)

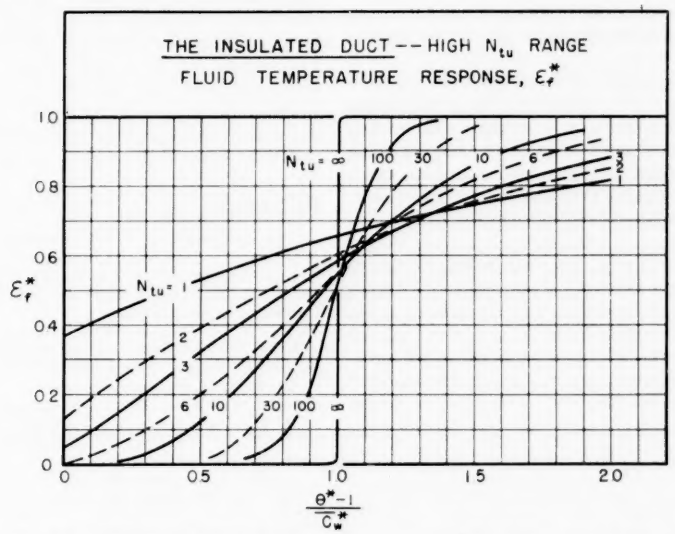

Fig. 18 Insulated-duct fluid and wall-temperature response for problem described by Fig. 2(d)

sponse to flow-rate changes. The one exception is the C_{max} flow cutoff transient described in Fig. 2(*e*). The justification for this specialization is worth repeating. Analog tests demonstrated that for $\bar{C}_w{}^*$ large, as for gas-turbine plant applications, the response to a flow-rate change was of the order of 1000 fold faster than response to a fluid-temperature change. Thus virtually instantaneous response to flow-rate changes can be assumed relative to the much slower response to fluid-temperature inputs.

Analytical methods and the analog approach employed in this program are restricted to counter and parallel-flow heat exchangers, except when $C_{min}/C_{max} = 0$, and then flow arrangement ceases to be significant.

Dusinberre [10] handles the case of crossflow by numerical methods. Tests with the electromechanical analog with counterflow remain to be accomplished. When such results are compiled possibly some general conclusions can be reached regarding the importance of flow arrangement.

The electromechanical analog used in this study simulates the heat-exchanger system of Fig. 1 by substituting for the distributed thermal capacities and resistances four discrete lumped circuits corresponding to equal increments of flow length. The simulation of fluid flow is afforded by mechanical switching which steps the lumped-fluid capacitors in discrete intervals of time. A more complete description is provided in [1*a*] and [1*b*].

Calibration of the analog was afforded by tests such as presented in Fig. 7, where the analog was set up to simulate conditions for which analytical results (Rizika's) were available. In addition to Rizika's solution, the insulated duct, the $R^* = 0$ and ∞, $C_{min}/C_{max} = 0$ solutions were employed for this purpose. The adequacy of these calibrations led to the conclusion that the

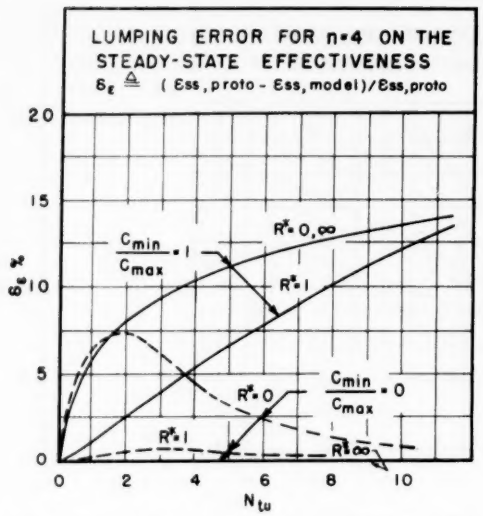

Fig. 19 Error in steady-state behavior due to lumped-parameter idealization

main experimental results as reported in Figs. 4, 9, and 13 have an uncertainty interval of the order of ±3 per cent of full scale on the ordinate.

A related inquiry to the analog-error question is the degree of correspondence between the steady-state behavior of the analog and prototype. As it is feasible to derive analytical expressions for the effectiveness of an n-lump heat exchanger corresponding to the idealization of uniform wall temperature for each lump, the question can be investigated both analytically and experimentally. Fig. 19 provides the analytical comparison. Test results support the analysis.

Much of the lumping error in ϵ_{ss}, as noted in Fig. 19, is cancelled out of the $\epsilon_f{}^*$ response because the calculation of $\epsilon_f{}^*$ from the test results includes ϵ_{ss} of the analog in the normalizing procedure. Nevertheless, it is apparent for $C_{min}/C_{max} = 1$ and $N_{tu} > 3$ that the lumped-parameter model does not provide a good representation of prototype behavior. For this reason the $N_{tu} = 8$ curve of Fig. 4 was derived from the results of a digital-computer program.

The equations leading to the results presented in Fig. 19 are presented as follows:

$$\epsilon_{ss\,model} = n\epsilon_p/[1 + (n-1)\epsilon_p] \tag{20}$$

$$\epsilon_p = \left[1\Big/\left(\frac{1}{\epsilon_c} + \frac{1}{\epsilon_h}\right)\right] \tag{21}$$

$$\left.\begin{aligned} \epsilon_c &= 1 - e^{-(N_{tu}/n)(R^*+1)/R^*} \\ \epsilon_h &= 1 - e^{-(N_{tu}/n)(R^*+1)} \end{aligned}\right\} \tag{22}$$

$$\left.\begin{aligned} \epsilon_{ss\,prototype} &= N_{tu}/(1 + N_{tu}) \quad \text{for} \quad C_{min}/C_{max} = 1 \\ &= 1 - e^{-N_{tu}} \quad \text{for} \quad C_{min}/C_{max} = 0 \end{aligned}\right\} \tag{23}$$

$$\delta_\epsilon \triangleq 1 - \frac{\epsilon_{ss\,model}}{\epsilon_{ss\,proto}} = \phi(N_{tu}, n, R^*, C_{min}/C_{max})$$

The key Equations (20) and (23) are derived in [2] and Equations (21) and (22) can be derived by elementary methods from the definition of the n-lump model where, for steady-state conditions, each wall element is at its own uniform temperature.

Summary and Conclusions

To summarize the major features of this work the following conclusions are offered:

1 The treatment of the transient response of the two-fluid heat exchanger has not yielded to a purely analytical attack. However, an electromechanical-analog approach supplemented by some analytical solutions for limiting cases has proved to be fruitful for those classes of heat exchangers characteristic of gas-turbine power plants.

2 A set of nondimensional parameters, Equations (4), is proposed for this type of problem. These equations are particularly useful since they tie directly to the set of parameters employed in describing the steady-state behavior of heat exchangers.

3 While primary consideration has been given to gas-turbine heat exchangers, the solutions presented are more generally applicable, and Table 2, the "Summary of Solutions," will prove to be useful in this respect.

Acknowledgments

S. G. Wilkes, A. L. Johnson, A. J. Oberg, and R. M. Cima, either former or current graduate students at Stanford University, contributed materially to this program. Prof. W. C. Reynolds of Stanford University directed the authors' attention to the "dividend solution" described by Fig. 2(*e*). The authors are particularly grateful to the General Motors Technical Center, Mr. Paul Vickers, and Mr. F. A. Creswick, for making available the accurate computer results of Table 1.

The work reported here is part of a heat-transfer and thermodynamics research program at Stanford University sponsored by the Office of Naval Research [Contract Nonr 225(23)].

References

1(*a*) A. L. London, A. J. Oberg, and R. M. Cima, "The Transient Response of a Two-Fluid Counter-Flow Heat Exchanger—The Gas Turbine Regenerator," TR-No. 32, Navy Department Contract Nonr 225-(23), Department of Mechanical Engineering, Stanford University, August, 1957.

1(*b*) R. M. Cima and A. L. London, "The Transient Response of a Two-Fluid Counterflow Heat Exchanger—The Gas-Turbine Regenerator," TRANS. ASME, vol. 80, 1958, p. 1169.

2 W. M. Kays and A. L. London, "Compact Heat Exchangers," first edition, National Press, Palo Alto, Calif., 1955.

3 H. M. Paynter and Y. Takahashi, "A New Method of Evaluating Dynamic Response of Counterflow and Parallel-Flow Heat Exchangers," TRANS. ASME, vol. 78, 1956, p. 749.

4 H. S. Carslaw and J. G. Jaeger, "Conduction of Heat in Solids," Oxford University Press, London, England, first edition, 1950.

5 J. W. Rizika, "Thermal Lags in Flowing Incompressible Fluid Systems Containing Heat Capacitors," TRANS. ASME, vol. 78, 1956, p. 1407.

6 F. R. Biancardi, "The Transient Response of a Condenser Using an Electrical Analog," ME 291 report, Mechanical Engineering Department Files, Stanford University, 1957–58.

7 T. E. W. Schumann, "Heat Transfer: A Liquid Flowing Through a Porous Prism," *Journal of the Franklin Institute*, vol. 208, 1929, p. 405; also "Partial Differential Equations," by H. Bateman, Dover Publications, New York, N. Y., 1944, p. 123.

8 Technical Center, Gas Turbine Division, General Motors Corporation, private communication, July, 1958.

9(*a*) H. J. Curfman, Jr., and R. A. Gardiner, "Method for Determining the Frequency Response Characteristics of an Element or System From the System Transient Output Response to a Known Input Function," NACA TR 984, 1950, pp. 651–660.

9(*b*) R. H. MacMillan, "The Frequency Response Method—A Brief Survey," edited by R. Oldenburger, The Macmillan Company, New York, N. Y., 1956, p. 613.

10 G. M. Dusinberre, "Calculation of Transients in a Cross-Flow Heat Exchanger," TRANS. ASME, series D, *Journal of Heat Transfer*, vol. 81, 1959, pp. 61–67.

HARRY KRAUS
Engineer, Westinghouse Bettis Atomic Power Division, Pittsburgh, Pa.
Assoc. Mem. ASME.

GEORGE SONNEMANN
Westinghouse Professor of Mechanical Engineering, University of Pittsburgh, Pittsburgh, Pa. Mem. ASME.

Stresses in Hollow Cylinders Due to Asymmetrical Heat Generation[1]

Equations are derived for the radial, tangential, shear, and axial stresses arising in nuclear reactor vessels, thermal shields, and so on, from internal heat generation caused by the absorption of gamma radiation. The heat generation considered behaves as a decaying exponential through the wall of the hollow cylinder and is an arbitrary function of the angle around the axis of the cylinder.

Introduction

In nuclear reactor practice, it has been found that heat is generated in the structural portions of the nuclear reactor by absorption of gamma rays which emanate from the core of the reactor. The structural members in question are generally the core barrel, the thermal shields, and the pressure vessel which surround the nuclear core. Such gamma-ray heating must be considered in the design of these members because it produces thermal stresses in them. It is a particularly serious problem with respect to the pressure vessel because the thermal stresses produced by the gamma-ray heating add to the stresses already present due to the internal pressure which acts in the vessel. The combination of these effects may result in an excessively high stress level and means must therefore be available to determine the contribution of the gamma heating to the total stress acting in the vessel.

Several investigators have addressed their attention to this problem. In 1951, J. C. Carter [1][2] found expressions for the stresses in the most common geometric shapes in which there is uniform heat generated throughout the body. Since it is agreed that the decaying exponential best describes the absorption of gamma rays in a material, F. P. Durham [2], in 1954, derived equations for both the temperature and stresses in a thin cylinder with this variation by use of a slab approximation. In 1956, H. J. Honohan [3] made a further refinement by using the temperature distribution obtained by the slab approximation in conjunction with the exact equations for the stresses in a hollow cylinder due to an axially symmetric temperature distribution. The exact solution for temperature and stresses due to the radial exponential internal heat generation in a hollow cylinder was obtained, in 1957, by Sonnemann and Davis [4].

In all of the afore-mentioned efforts, axial symmetry of the heat generation has been assumed. However, this is not the actual case because it is known that the gamma rays are not emitted uniformly around the longitudinal axis of a nuclear core. Thus it is felt that a study should be made which will take into account the angular variation of the internal heat generation as well as the radial variation. Of main interest along this line is the determination of the shear stresses set up in the structural members by gamma-ray heating, as well as the effect of the angular variation on the other stresses. To date the assumption of axial symmetry did not give rise to any shear stresses.

[1] Based on a thesis submitted by H. Kraus to the Graduate Faculty of the Schools of Engineering and Mines, University of Pittsburgh, in partial fulfillment of the requirements for the degree of Master of Science.

Contributed by the Nuclear Engineering Division of The American Society of Mechanical Engineers and presented at the Nuclear Congress, Cleveland, Ohio, April 5–10, 1959.

Note: Statements and opinions advanced in papers are to be understood as individual expressions of their authors and not those of the Society. Manuscript received at ASME Headquarters, December 12, 1958.

[2] Numbers in brackets designate References at end of paper.

Nomenclature

a = inner radius of cylinder, in.
a_n, A_n, b_n, B_n = arbitrary constants, dimensionless
c_n, C_n, d_n, D_n = arbitrary constants, dimensionless
E = modulus of elasticity, lb/in.^{2}
F_n = Airy stress function, dimensionless
$f(\theta)$ = arbitrary variation of heat generation with angle, dimensionless
G = shear modulus, lb/in.^{2}
h_n = sine transform of $f(\theta)e^{\beta_1}$, dimensionless
H_i = heat generation at inner surface, Btu/sec/in.^{3}
k = thermal conductivity, Btu/sec/in/deg F
n = index of sine series, dimensionless
r = radius to a point in the wall, in.
t = dimensionless radius
T, T', T'' = temperature difference, deg F
x, z = dummy variables appearing in integrals, dimensionless
y = radius to a point in the wall divided by the inner radius of the cylinder, dimensionless
y_0 = outer radius divided by inner radius, dimensionless
α = coefficient of thermal expansion, in/in/deg F
β = logarithmic decrement of heating, in.$^{-1}$
β_1 = logarithmic decrement times inner radius, dimensionless
$\gamma_n(t)$ = see equation (19), dimensionless
δ_n, ϵ_n, ρ_n, η_n = arbitrary constants, dimensionless
θ = angular co-ordinate, dimensionless
σ = stress, dimensionless or lb/in.^{2}
Θ = dimensionless temperature difference
λ_n = amplitude of nth term of $f(\theta)$, dimensionless
ν = Poisson's ratio, dimensionless
ξ = conversion factor, see equation (27), lb/in.^{2}

Superscripts I, II, III refer to Case I, Case II, and Case III, of the boundary conditions on temperature.
Subscripts T, S, A, R refer to dimensionless tangential, shear, axial, and radial stresses, respectively.
Subscripts $\theta\theta$, $t\theta$, zz, tt refer to dimensional tangential, shear, axial, and radial stresses, respectively.

Statement of the Problem

It is the goal of this investigation to determine the exact temperature distribution and the exact radial, axial, tangential, and shear stress distributions produced in a long, hollow; circular cylinder with internal heat generation under steady-state conditions. The heat generation will be in the form of a decaying exponential in the radial direction and an arbitrary function of the angle around the longitudinal axis of the cylinder. There will be no variation along the axis of the cylinder.

Assumptions to be used in the analysis are as follows:

1 The properties of the cylinder material are independent of temperature.

2 The cylinder material is elastic, isotropic, and homogeneous.

3 The arbitrary function of angle which describes the variation of the internal heat generation around the longitudinal axis of the cylinder will be representable by an infinite series of sine terms; i.e., the function is odd. It will be periodic in the interval from 0 to π.

4 The cylinder will be considered to be long in order to utilize the concept of plane strain. Thus the results obtained will be valid away from the ends of the long cylinder.

Three cases of boundary conditions will be used to determine the temperature distribution. These cases are described as follows:

Case I: A cylinder with equal temperatures specified on its inside and outside surfaces. This case describes the temperature conditions in the thermal shields of a nuclear reactor core, where the coolant on the inner and outer surfaces is at essentially the same temperature.

Case II: A cylinder with a specified temperature on its inside surface and insulated on the inside surface. This is a rare case which occurs only in the thimble of a test reactor.

Case III: A cylinder with a specified temperature on the inside surface and insulated on the outside surface. This case applies to reactor pressure vessels.

Stress distributions will be obtained for the usual requirement that the shear stress and the radial stress each vanish at both the inside and outside surfaces of the hollow cylinder. No pressure effects will be taken into consideration here.

Solution

Procedure. The solution of the problem is divided into two basic steps.

First, the heat-conduction equation applicable to the cylinder with internal heat generation is solved to yield the temperature distribution in the hollow cylinder.

Second, a thermo-elastic displacement potential is determined from the temperature distribution. All of the stresses acting in the cylinder are obtained from this potential by taking appropriate combinations of its derivatives. Since it is found that the shear and radial stresses obtained in this manner do not vanish at the inner and outer surfaces of the cylinder, an Airy stress function from the ordinary theory of elasticity is superimposed on the displacement potential to cause the stresses to vanish as required.

Solution of the Temperature Problem. For the cylinder with internal heat generation, the heat conduction equation is

$$\frac{\partial^2 T}{\partial r^2} + \frac{1}{r}\frac{\partial T}{\partial r} + \frac{1}{r^2}\frac{\partial^2 T}{\partial \theta^2} = -\frac{H_i}{k}\left[1 + f(\theta)\right]e^{-\beta(r-a)} \quad (1)$$

$$T = T(r, \theta) - T(a, \theta) \quad (2)$$

$$f(\theta) = \sum_{n=1}^{\infty} \lambda_n \sin n\theta \quad (3)$$

Since the boundary conditions that are to be imposed on the temperature are homogeneous, the solution of equation (1) is accomplished by superposition of the solutions of the following equations

$$\frac{\partial^2 T'}{\partial r^2} + \frac{1}{r}\frac{\partial T'}{\partial r} = -\frac{H_i}{k}e^{-\beta(r-a)} \quad (4)$$

$$\frac{\partial^2 T''}{\partial r^2} + \frac{1}{r}\frac{\partial T''}{\partial r} + \frac{1}{r^2}\frac{\partial^2 T''}{\partial \theta^2} = -\frac{H_i}{k}f(\theta)e^{-\beta(r-a)} \quad (5)$$

$$T = T'(r) + T''(r, \theta) \quad (6)$$

Sonnemann and Davis [4] have found the stresses associated with the solution of equation (4). It is the aim of the present investigation to determine the stresses associated with the solution of equation (5). To maintain consistency with the Sonnemann-Davis paper, the following dimensionless variables are introduced:

$$\Theta = \frac{T''k\beta^2}{H_i}; \quad t = \beta_1 y; \quad \beta_1 = \beta a; \quad r = ay \quad (7)$$

Upon substitution of these in equation (5), one obtains

$$\frac{\partial^2 \Theta}{\partial t^2} + \frac{1}{t}\frac{\partial \Theta}{\partial t} + \frac{1}{t^2}\frac{\partial^2 \Theta}{\partial \theta^2} = -f(\theta)e^{\beta_1}e^{-t} \quad (8)$$

Equation (8) is solved by reducing it to an equation in one variable by means of the finite Fourier sine transformation with respect to the variable θ. The transformed equation is an inhomogeneous Euler equation whose complementary solution is well known and whose particular solution is obtained by variation of parameters. Upon determination of the transformed temperature, the inversion formula for the finite Fourier sine transform is applied to yield the solution for the dimensionless temperature.

$$\Theta_1 = \frac{2}{\pi}\left\{A_1 t + B_1 t^{-1} - h_1 e^{-t}(1 + t^{-1})\right\}\sin\theta \quad (9)$$

$$\Theta_n = \frac{2}{\pi}\left\{A_n t^n + B_n t^{-n} + \frac{h_n}{2n}\left[t^n\int_t^{\infty}\frac{e^{-x}dx}{x^{n-1}} + t^{-n}\int_{\infty}^{t} e^{-x}x^{n+1}dx\right]\right\}\sin n\theta \quad (10)$$

$$\Theta = \Theta_1 + \sum_{n=2}^{\infty}\Theta_n \quad (11)$$

Here h_n is the sine transform of $f(\theta)e^{\beta_1}$ and is given by

$$h_n = \frac{\pi}{2}\lambda_n e^{\beta_1} \quad (12)$$

The arbitrary constants A_1, B_1, A_n, and B_n, appearing here, are found from the boundary conditions on the temperature. This is done in a later section.

Solution of the Stress Problem

Thermo-Elastic Displacement Potential. Goodier [5] shows that the thermo-elastic displacement potential Φ satisfies

$$\nabla^2\Phi = \frac{1+\nu}{1-\nu}\alpha T \quad (13)$$

To be consistent with the previous development, the definition of T is introduced into equation (13) to yield

$$\frac{\partial^2 \Phi'}{\partial t^2} + \frac{1}{t}\frac{\partial \Phi'}{\partial t} + \frac{1}{t^2}\frac{\partial^2 \Phi'}{\partial \theta^2} = \Theta \quad (14)$$

$$\Phi = \Phi' \frac{1+\nu}{1-\nu} \frac{\alpha H_i}{k\beta^4} \tag{15}$$

Equation (14) is solved by the same procedure as is employed in the solution for the dimensionless temperature distribution. Thus, the solution for the thermo-elastic displacement potential is

$$\Phi_1' = \frac{2}{\pi}\left\{\frac{A_1 t^3}{8} + \frac{B_1 t \ln t}{2} + C_1 t + D_1 t^{-1} - \frac{3h_1}{2}\left[e^{-t}(1+t^{-1}) - \frac{tEi(-t)}{3}\right]\right\}\sin\theta \tag{16}$$

$$\Phi_n' = \frac{2}{\pi}\left\{\frac{A_n t^{n+2}}{4(n+1)} + \frac{B_n t^{-n+2}}{4(-n+1)} + C_n t^n + D_n t^{-n} + \gamma_n(t)\right\}\sin n\theta \tag{17}$$

$$\Phi' = \Phi_1' + \sum_{n=2}^{\infty} \Phi_n' \tag{18}$$

$$\gamma_n(t) = \frac{h_n}{4n^2}\left[t^n \int_{\infty}^{t} z \int_{\infty}^{z} \frac{e^{-x}dxdz}{x^{n-1}} + t^n \int_{\infty}^{t} z^{-2n+1} \int_{\infty}^{z} e^{-x}x^{n+1}dxdz - t^{-n}\int_{\infty}^{t} z^{2n+1}\int_{z}^{\infty}\frac{e^{-x}dxdz}{x^{n-1}} - t^{-n}\int_{\infty}^{t} z\int_{\infty}^{z} e^{-x}x^{n+1}dxdz\right] \tag{19}$$

$$-Ei(-t) = \int_{t}^{\infty}\frac{e^{-x}dx}{x} \tag{20}$$

The Airy Stress Function. As explained previously, the radial and shear stresses obtained from the thermo-elastic displacement potential do not vanish at the inner and outer surfaces. Hence an Airy stress function from the ordinary theory of elasticity is superimposed upon the solution. It is the solution of the equation

$$\nabla^2\nabla^2 F = 0 \tag{21}$$

For the conditions of the problem at hand, the Airy stress function is known to be [6] for $n \geqslant 2$

$$F_n = (a_n t^{n+2} + b_n t^{-n+2} + c_n t^n + d_n t^{-n})\sin n\theta \tag{22}$$

Since linear terms of the Airy stress function do not influence the stress distribution, the first term of the Airy stress function may be written as

$$F_1 = (a_1 t^3 + d_1 t^{-1})\sin\theta \tag{23}$$

and

$$F = F_1 + \sum_{n=2}^{\infty} F_n \tag{24}$$

Determination of the Stresses From the Thermo-Elastic Displacement Potential and the Airy Stress Function. Melan and Parkus [7] show that the stresses can be obtained by taking the following derivatives of the thermo-elastic displacement potential and the Airy stress function (using the present variables)

$$\sigma_{tt} = \beta^2\left(\frac{1}{t}\frac{\partial}{\partial t} + \frac{1}{t^2}\frac{\partial^2}{\partial\theta^2}\right)(F - 2G\Phi);$$

$$\sigma_{\theta\theta} = \beta^2\frac{\partial^2}{\partial t^2}(F - 2G\Phi) \tag{25}$$

$$\sigma_{t\theta} = -\beta^2\frac{\partial}{\partial t}\left[\frac{1}{t}\frac{\partial}{\partial\theta}(F - 2G\Phi)\right];$$

$$\sigma_{zz} = \beta^2\nabla^2(F - 2G\Phi) \tag{26}$$

Now define

$$\xi = \frac{2}{\pi}\frac{E}{1-\nu}\frac{\alpha H_i}{k\beta^2} \tag{27}$$

$$\sigma_{tt} = \xi\sigma_R;\quad \sigma_{\theta\theta} = \xi\sigma_T;\quad \sigma_{t\theta} = \xi\sigma_S;\quad \sigma_{zz} = \xi\sigma_A \tag{28}$$

Upon performing the operations indicated in equations (25) and (26), one obtains the following relations for the dimensionless stresses. For $n = 1$

$$\sigma_{T_1} = \left\{\frac{2d_1}{t^3} + 6\left(a_1 - \frac{A_1}{8}\right)t - \frac{B_1}{2t} + \frac{h_1 e^{-t}}{t^3}(t^3 + 2t^2 + 3t + 3)\right\}\sin\theta \tag{29}$$

$$\sigma_{R_1} = \left\{\frac{-2d_1}{t^3} + 2\left(a_1 - \frac{A_1}{8}\right)t - \frac{B_1}{2t} - \frac{h_1 e^{-t}}{t^3}(t^2 + 3t + 3)\right\}\sin\theta \tag{30}$$

$$\sigma_{S_1} = \left\{\frac{2d_1}{t^3} - 2\left(a_1 - \frac{A_1}{8}\right)t + \frac{B_1}{2t} + \frac{h_1 e^{-t}}{t^3}(t^2 + 3t + 3)\right\}\cos\theta \tag{31}$$

$$\sigma_{A_1} = 8\nu a_1 t\sin\theta - \frac{\pi}{2}\Theta_1 \tag{32}$$

For $n \geqslant 2$

$$\sigma_{Tn} = \left\{(2+n)(1+n)\delta_n t^n + (1-n)(2-n)\epsilon_n t^{-n} + n(n-1)\rho_n t^{n-2} + n(n+1)\eta_n t^{-n-2} - \frac{h_n}{8n^2}\left[n(2+n)t^n\int_t^{\infty}\frac{e^{-x}dx}{x^{n-1}} + n(2-n)t^{-n}\int_{\infty}^{t} e^{-x}x^{n+1}dx + n^2 t^{-n-2}\int_{\infty}^{t} e^{-x}x^{n+3}dx + n^2 t^{n-2}\int_{\infty}^{t}\frac{e^{-x}dx}{x^{n-3}}\right]\right\}\sin n\theta \tag{33}$$

$$\sigma_{Rn} = \left\{(2-n)(1+n)\delta_n t^n + (1-n)(2+n)\epsilon_n t^{-n} + n(1-n)\rho_n t^{n-2} - n(n+1)\eta_n t^{-n-2} - \frac{h_n}{8n^2}\left[n(2-n)t^n\int_t^{\infty}\frac{e^{-x}dx}{x^{n-1}} + n(2+n)t^{-n}\int_{\infty}^{t} e^{-x}x^{n+1}dx - n^2 t^{-n-2}\int_{\infty}^{t} e^{-x}x^{n+3}dx - n^2 t^{n-2}\int_{\infty}^{t}\frac{e^{-x}dx}{x^{n-3}}\right]\right\}\sin n\theta \tag{34}$$

$$\sigma_{Sn} = \left\{-n(n+1)\delta_n t^n - n(1-n)\epsilon_n t^{-n} - n(n-1)\rho_n t^{n-2} + n(n+1)\eta_n t^{-n-2} + \frac{h_n}{8}\left[t^n\int_t^{\infty}\frac{e^{-x}dx}{x^{n-1}} + t^{-n}\int_{\infty}^{t} e^{-x}x^{n+1}dx + t^{n-2}\int_{\infty}^{t}\frac{e^{-x}dx}{x^{n-3}} - t^{-n-2}\int_{\infty}^{t} e^{-x}x^{n+3}dx\right]\right\}\cos n\theta \tag{35}$$

$$\sigma_{An} = 4\nu[(n+1)a_n t^n + (1-n)b_n t^{-n}]\sin n\theta - \frac{\pi}{2}\Theta_n \tag{36}$$

In these equations

$$\delta_n = a_n - \frac{A_n}{4(n+1)}; \quad \rho_n = c_n - C_n \tag{37}$$

$$\epsilon_n = b_n - \frac{B_n}{4(-n+1)}; \quad \eta_n = d_n - D_n \tag{38}$$

Finally, the total stresses acting are given by

$$\sigma_T = \sigma_{T_1} + \sum_{n=2}^{\infty} \sigma_{Tn} \tag{39}$$

$$\sigma_S = \sigma_{S_1} + \sum_{n=2}^{\infty} \sigma_{Sn} \tag{40}$$

$$\sigma_R = \sigma_{R_1} + \sum_{n=2}^{\infty} \sigma_{Rn} \tag{41}$$

$$\sigma_A = \sigma_{A_1} + \sum_{n=2}^{\infty} \sigma_{An} \tag{42}$$

It should be pointed out here that, in the event that it is known that the angular variation of the internal heat generation can be adequately described by N terms of the sine series, the infinite sums appearing in all of the preceding expressions for temperature, stress, and so forth, go over into finite sums of N terms. Furthermore, if the variation of the internal heat generation can be adequately described by a single sine term of a given n, the infinite sums go over into single terms involving the given n. For example, in a square nuclear core it is agreed that four peaks occur in the gamma heating around the periphery of the core (one peak at each corner of the square), and a rough approximation of this variation can be achieved by using $n = 4$ only.

Application of Boundary Conditions. Three cases of boundary conditions on the temperature will be considered here. Common to all of these cases is the condition that the dimensionless temperature difference, Θ, is equal to zero at the inner surface of the hollow cylinder. Applying this condition to equation (11), one obtains the following relation (for $n \geq 1$) between the arbitrary constants

$$B_n = -A_n\beta_1^{2n} - \frac{h_n}{n}\left[\beta_1^{2n}\int_{\beta_1}^{\infty}\frac{e^{-x}dx}{x^{n-1}} + \int_{\infty}^{\beta_1} e^{-x}x^{n+1}dx\right] \tag{43}$$

This relation is valid for all three cases of the boundary conditions, and all $n \geq 1$. A_n is now obtained for each of the three individual cases.

Case I: Equal temperatures on the inside and outside surfaces of the cylinder

$$A_n^{\,I} = -h_n \frac{(\beta_1 y_0)^{2n}\int_{\beta_1 y_0}^{\infty}\frac{e^{-x}dx}{x^{n-1}} + \int_{\infty}^{\beta_1 y_0} e^{-x}x^{n+1}dx - \beta_1^{2n}\int_{\beta_1}^{\infty}\frac{e^{-x}dx}{x^{n-1}} - \int_{\infty}^{\beta_1} e^{-x}x^{n+1}dx}{2n(\beta_1 y_0)^{2n}(1 - y_0^{-2n})} \tag{44}$$

Case II: Inside surface is insulated

$$A_n^{\,II} = \frac{-h_n}{2n}\int_{\beta_1}^{\infty}\frac{e^{-x}dx}{x^{n-1}} \tag{45}$$

Case III: Outside surface is insulated

$$A_n^{\,III} = -h_n \frac{(\beta_1 y_0)^{2n}\int_{\beta_1 y_0}^{\infty}\frac{e^{-x}dx}{x^{n-1}} - \int_{\infty}^{\beta_1 y_0} e^{-x}x^{n+1}dx + \beta_1^{2n}\int_{\beta_1}^{\infty}\frac{e^{-x}dx}{x^{n-1}} + \int_{\infty}^{\beta_1} e^{-x}x^{n+1}dx}{2n(\beta_1 y_0)^{2n}(1 + y_0^{-2n})} \tag{46}$$

The arbitrary constants in the stress relations are found subject to the requirement that the shear and radial stresses both vanish at the inner and outer surfaces of the cylinder. For $n = 1$ these conditions give

$$-2d_1 = \frac{B_1\beta_1^2 y_0^2}{2(1 + y_0^2)} + h_1\frac{y_0^4 e^{-\beta_1}(\beta_1^2 + 3\beta_1 + 3) - e^{-\beta_1 y_0}(\beta_1^2 y_0^2 + 3\beta_1 y_0 + 3)}{y_0^4 - 1} \tag{47}$$

$$\left(a_1 - \frac{A_1}{8}\right) = \frac{B_1}{4\beta_1^2(1 + y_0^2)} + h_1\frac{e^{-\beta_1}(\beta_1^2 + 3\beta_1 + 3) - e^{-\beta_1 y_0}(\beta_1^2 y_0^2 + 3\beta_1 y_0 + 3)}{2\beta_1^4(1 - y_0^4)} \tag{48}$$

For $n \geq 2$ the boundary conditions lead to four simultaneous equations in four unknowns. To save space, these are written

$$\begin{aligned} a_{11}\delta_n + a_{12}\epsilon_n + a_{13}\rho_n + a_{14}\eta_n &= b_1 \\ a_{21}\delta_n + a_{22}\epsilon_n + a_{23}\rho_n + a_{24}\eta_n &= b_2 \\ a_{31}\delta_n + a_{32}\epsilon_n + a_{33}\rho_n + a_{34}\eta_n &= b_3 \\ a_{41}\delta_n + a_{42}\epsilon_n + a_{43}\rho_n + a_{44}\eta_n &= b_4 \end{aligned} \tag{49}$$

Here the a_{ij} have replaced the coefficients in equations (34) and (35), and the b_i have replaced the inhomogeneous portions of the same equations. This set of simultaneous equations is solved by Cramer's Rule for every $n \geq 2$.

Results and Conclusions

Since the solutions derived in this investigation represent the stresses caused by the varying portion of the heat generation only, they do not present the whole picture of the stresses in a hollow cylinder with internal heat generation. In performing an entire stress calculation, the stresses arising from the uniform portion of the heat generation must be added to the results obtained herein. The stresses referred to are those which arise from the temperature distribution resulting from equation (4). As mentioned previously, Sonnemann and Davis [4] have solved the problem of the stresses due to the uniform heat generation. Their results are presented in the form of graphs from which the dimensionless stresses can be read directly.

Given the magnitude and distribution of the heat generation in a hollow cylinder, a stress calculation would proceed as follows:

1 A Fourier analysis is performed to determine the sine series representation of the angular variation of the internal heat generation. This may result in an infinite series, a finite series, or just one term as mentioned previously.

2 A uniform value around which the heat generation oscillates

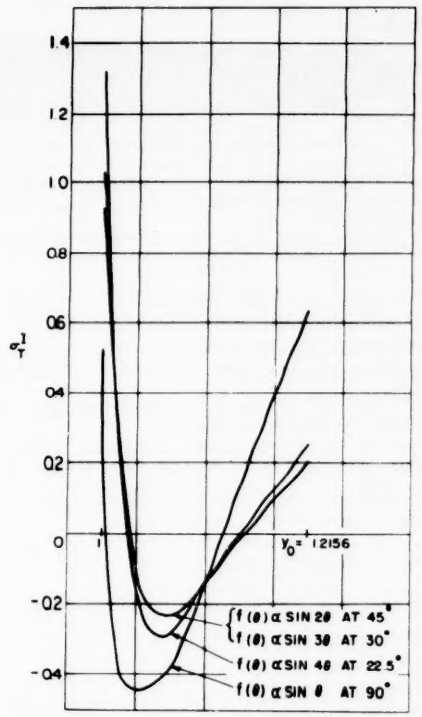

Fig. 1 Dimensionless tangential stress in a thick cylinder due to the varying portion of the heat generation only (Case I of the boundary conditions)

is determined. Using this value, the stresses due to it are determined by use of the Sonnemann-Davis paper.

3 The stresses due to the varying portion of the heat generation are found with the formulas derived in the present investigation.

4 The total stress is found by adding the stresses computed for the uniform and the varying portions of the heat generation.

Because the formulas derived herein are rather unwieldy, an IBM 704 code [8] has been written to facilitate the calculation of the temperature and stresses for any desired situation. This code was used to prepare Figs. 1 and 2 which illustrate the behavior of the dimensionless tangential and shear stresses due to the angularly varying portion of the heat generation. The stresses are shown for the location at which each achieves its maximum for the value of n involved. For simplicity, the Fourier representation of the varying portion of the heat generation has been assumed to consist of only one term of each value of n shown in the figures. Since the shears vary cosinusoidally, their maximum values occur across the wall at $\theta = 0$ deg. The tangential stresses in turn vary sinusoidally and are shown for the various angles at which they achieve their maximum values; namely, for $\theta = 90$ deg/n.

Table 1 has been prepared to compare the stresses for Case I of the boundary conditions obtained from the method of analysis described (this will be called the proposed method) and those obtained from the present method which uses the peak level of the radial exponential heat generation as a uniform value applied around the entire cylinder. In the table stresses are given for the angle and radius at which they individually achieve their maximum value. All of these maximum stress values do not occur at the same point as explained heretofore. The table is intended only to give an idea of the maximum magnitudes of the stresses

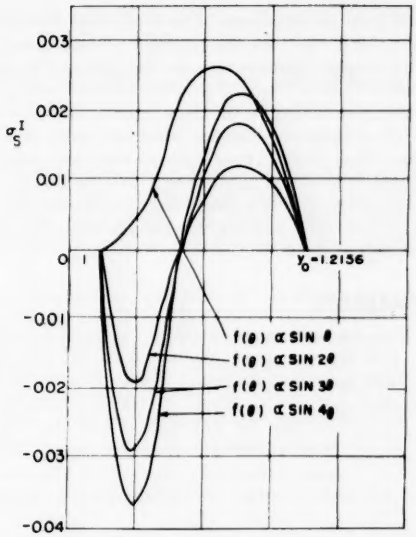

Fig. 2 Dimensionless shear stress in a thick cylinder due to the varying portion of the heat generation only (Case I of the boundary conditions)

Table 1 A comparison of stresses obtained by the present and proposed methods of analysis (Case I of the boundary conditions)

	PRESENT METHOD	PROPOSED METHOD			
MAXIMUM TANGENTIAL STRESSES IN A THICK CYLINDER ($y_0 = 1.2156$)					
STRESS	$\sigma_{\theta\theta} = 13,382$	$\sigma_{\theta\theta_1} = 13,501$	$\sigma_{\theta\theta_2} = 14,557$	$\sigma_{\theta\theta_3} = 14,547$	$\sigma_{\theta\theta_4} = 15,302$
y	1.0	1.215	1.0	1.0	1.1077
θ	all	90°	45°	30°	22.5°
MAXIMUM TANGENTIAL STRESSES IN A THIN CYLINDER ($y_0 = 1.0216$)					
STRESS	$\sigma_{\theta\theta} = 1,428$	$\sigma_{\theta\theta_1} = 1,469$	$\sigma_{\theta\theta_2} = 1,487$	$\sigma_{\theta\theta_3} = 1,472$	$\sigma_{\theta\theta_4} = 2,014$
y	1.0	1.0216	1.0	1.0216	1.0
θ	all	90°	45°	30°	22.5°
MAXIMUM SHEAR STRESSES IN A THICK CYLINDER ($y_0 = 1.2156$)					
STRESS	0	$\sigma_{t\theta_1} = 69.4$	$\sigma_{t\theta_2} = 51.5$	$\sigma_{t\theta_3} = 76.5$	$\sigma_{t\theta_4} = 96.9$
y	all	1.1077	1.0359	1.0359	1.0359
θ	all	0°	0°	0°	0°
MAXIMUM SHEAR STRESSES IN A THIN CYLINDER ($y_0 = 1.0216$)					
	0	$\sigma_{t\theta_1} = 0.448$	$\sigma_{t\theta_2} = 0.838$	$\sigma_{t\theta_3} = 1.371$	$\sigma_{t\theta_4} = 7.341$
y	all	1.018	1.0036	1.018	1.0072
θ	all	0°	0°	0°	0°

PHYSICAL DATA: $\alpha = 9.9 \times 10^{-6}$, $\kappa = 2.745 \times 10^{-4}$, $E = 25 \times 10^6$, $\nu = 0.30$, $\beta\alpha = 45$, $H_i = 0.0389$, $\lambda_1 = 0.15\ H_i$, $\lambda_2 = 0.15\ H_i$, $\lambda_3 = 0.15\ H_i$, $\lambda_4 = 0.15\ H_i$

that one is dealing with in a typical situation, and to compare the methods of analysis. To obtain information concerning the principal stresses, one must realize that at the points of maximum tangential stress (inner and outer surfaces for Case I), the shear stress is zero and at points of maximum shear, the tangential stress

is reduced from its maximum. Due to the fact that the shears are so low, their effect on the principal stresses is very slight. Hence the tangential stress remains the primary factor to be considered.

The table reveals that for the thick cylinder the present design method gives tangential stresses which are quite close to, but lower than, those obtained from the more exact proposed method. A significant difference in results arises between the two methods for the thin cylinder. For a given amplitude of variation, when n is increased, the difference between the stresses obtained by the two methods increases.

Acknowledgments

The thesis investigation on which this paper is based was carried out with the support of the Joint Westinghouse-University of Pittsburgh Fellowship Program. The authors are indebted to T. J. Lawton and K. W. Brand, of the Westinghouse Bettis Atomic Power Division, for writing the IBM 704 Code which made it possible to obtain the data presented herein. Thanks are due to B. F. Langer, of the Bettis Atomic Power Division, for his valuable help and comments during the course of the investigation

References

1 J. C. Carter, "Temperature and Stress Distribution in Spheres, Rods, Tubes, and Plates in Which the Heat Source Is Within the Boundaries of the Solids," ANL-4690, Argonne National Laboratory, Chicago, Illinois, 1951.

2 F. P. Durham, "Optimum Heat Transfer for Minimum Thermal Stress in Nuclear Reactor Shells," ASME Paper No 54—A-126.

3 H. J. Honohan, "Steady State Thermal Stress Distribution in Long Hollow Cylinders Experiencing a Radial Exponential Internal Heat Generation," Master of Science thesis, University of Pittsburgh, Pittsburgh, Pa., 1956.

4 G. Sonnemann and D. M. Davis, "Stresses in Long Thick-Walled Cylinders Caused by Pressure and Temperature," ASME Paper No. 57—A-256.

5 J. N. Goodier, "On the Integration of the Thermo-Elastic Equations," *Philosophical Magazine*, ser. 7, vol. 23, 1937, pp. 1017–1032.

6 S. Timoshenko and J. N. Goodier, "Theory of Elasticity," McGraw-Hill Book Company, Inc., New York, N. Y., second edition, 1951, p. 116.

7 E. Melan and H. Parkus, "Wärmespannungen," Springer Verlag, Vienna, Austria, 1953, p. 33.

8 K. W. Brand, H. Kraus, and T. J. Lawton, "F0010—A Two-Dimensional IBM 704 Code for the Calculation of Thermal Stresses in a Long Hollow Cylinder With Internal Heat Generation," WAPD-TM-133, Westinghouse Bettis Atomic Power Division, Pittsburgh Pa., 1958.

Journal of ENGINEERING FOR POWER

Information for Authors

• Manuscripts should be submitted in final form to the Editor. Each manuscript must be accompanied by a statement that it has not been published elsewhere nor has it been submitted for publication elsewhere. A paper which would occupy more than 8 pages of the Journal may be returned to the author for abridgment.

• The author should state his business connection, the title of his position, and his mailing address. A short abstract (50 to 100 words) should be included on the first page immediately preceding the introductory paragraph of the paper.

Three copies of the manuscript are required. One of these must be a carefully prepared printer's copy, typed in double spacing, on one side of the page only, with wide margins, on $8^1/_2$ by 11-in. opaque white paper. Mimeographed manuscripts, if prepared with exceptional care, can be accepted provided they are completely edited.

• As far as possible, all mathematical expressions should be typewritten. Greek letters and other symbols not available on the typewriter should be carefully inserted in ink. Care should be taken to distinguish between capital and lowercase letter, between zero (0) and the letter (*O*), between the numeral (1) and the letter (*l*), etc. A letter representing a vector cannot be printed with an arrow above or below it. The letter should be underscored with a single wavy line, wherever it appears in the text, to designate boldface type.

• A list of symbols carefully marked for the use of the editor (thus: κ, Greek l.c. kappa), if it has not been included in the body of the paper, should accompany the manuscript on a separate page.

• Before preparing a manuscript the author should study printed articles in the Journal, with special attention to the form and style of mathematical expressions, tables, footnotes, references, and abstract. Numbers that identify mathematical expressions should be enclosed in parentheses. Numbers that identify references at the end of the paper should be enclosed in brackets. Care should be taken to arrange all tables and mathematical expressions in such a way that they will fit into a single column when set in type. Equations that might extend beyond the width of one column (fractions that should not be broken or long expressions enclosed in parentheses) should be rephrased to go on two or more lines within column width. Fractional powers are preferred to root signs and should always be used in more elaborate formulas. The solidus should be used instead of the horizontal line for fractions wherever possible.

• A normal paper should not exceed 8 pages in the Journal. It is about 8000 words or 20 double-spaced typewritten pages exclusive of drawings. A Technical Brief should not exceed 750 words or about one page in the Journal inclusive of drawings.

• Originals and two copies of figures must accompany the manuscript. Line drawings should not be larger than $8^1/_2 \times 11$ in. and should be planned for reduction to column width. Lettering should be large enough to be clearly legible when the illustration is reduced. The originals of line drawings must be in India ink on white or pale blue tracing paper or tracing cloth. Photographs of equipment or test specimens must be glossy prints and should be used sparingly. Captions for figures should be typed double-spaced and included as the last page of the manuscript. The figure number and author's name should be written in the margin or on the back of each illustration.

• Titles of papers should be brief.

• Authors can obtain copies of the ASME Manual MS-4, "An ASME Paper," from the Editor and are urged to do so before drafting their papers in final form.

• Papers published in Journals of the Transactions of the ASME must be presented at a Meeting, either in person or by title.

• An author is entitled to 25 preprints free of charge (in the case of two authors, 15 each; three or more authors, 10 each). Larger quantities of preprints or reprints can be ordered from Editorial Department, The American Society of Mechanical Engineers, 29 West 39th Street, New York 18, N. Y. Quotations will be sent on request.

Please address all communications to:

Editor, ASME,

29 West 39th Street,

New York 18, N. Y.

ASME Publications Committee